

NANOSTRUCTURED POLYMERIC THIN FILM: HARNESS TRANSITION
BETWEEN 2D TO 3D FOR DESIGNED FUNCTIONALITIES

A Dissertation

Presented to the Faculty of the Graduate School
of Cornell University

In Partial Fulfillment of the Requirements for the Degree of
Doctor of Philosophy

by

Wei-Liang Chen

August 2018

© 2018 Wei-Liang Chen

ALL RIGHT RESERVED

NANOSTRUCTURED POLYMERIC THIN FILM: HARNESS TRANSITION
BETWEEN 2D TO 3D FOR DESIGNED FUNCTIONALITIES

Wei-Liang Chen, Ph. D.

Cornell University 2018

Polymer brushes are polymer chains tethered to a surface at sufficient coverage so that the resulting steric repulsion forces them to stretch outward. This 2D stretching of the polymer brushes gives them unique physical properties different from traditional polymer melts. Tuning of the brush configuration, especially at the nanoscale could make polymer brushes a useful functional coating in the fields like anti-fouling and lubrication which counted on their behavior at highly confined regime. Upon removal of lateral confinement through patterning, they would have quite rich response in terms of mechanical, physical properties that are distinct to their non-patterned form for the reduction of the lateral pressure. In short, the foundation of this materials then depends on the ability to harness such transition between 2D to 3D stretching which is the key for the development of advanced materials and devices for biotechnology and electronic/optical applications.

In this work, we look forward to increasing the understanding in patterned polymer brushes and it started from the neutral polymer brushes. Brush nanopatterning was conducted using orthogonal process following either top-down or bottom-up approaches with patterned lines as small as 200 nm. The pattern morphology depends not only on the wetting properties of the areas adjacent to the pattern, but also on process history to which the sample has been exposed, especially related to solvent

quality. Furthermore, we demonstrated the method to control crosslinking on the edges of the pattern and this leads to the non-ordinary stimuli-responsive behavior.

Subsequently, the stability of non-patterned and nanostructured strong polyelectrolyte brushes is studied as a function of both brush character and the properties of a contacting liquid. Nanopatterned polymer brushes proved its value in showing that the chain dynamic is also a dominant factor in brush degrafting and it should also be considered besides the reaction kinetics.

The finding inspired us to design polymer brushes with more complex configuration. To characterize them, we fabricated optical grating which have polymer brushes anchoring only on the sidewall. Such platform when working with neutral scattering should allow the reconstitution of the 3D brush profile provide more insight to complicated behavior.

The knowledge obtained was also expanded horizontally to the two different fields. For liquid crystal elastomer patterning, it managed to create micro-objects with controlled actuation motion by simply changing the direction of the patterns. On the other hand, polyelectrolyte brushes found its application in the field of biophysics where it could act as a cushion to facilitate the spontaneous formation of supported lipid bilayer with high transmembrane protein mobility.

BIOGRAPHICAL SKETCH

Wei-Liang Chen is the second son of Dr. Yuan-Fang Chen and Janq-Huey Cherng and was born in Tainan, Taiwan. At his childhood he was a curious baby and enjoyed the time of asking questions. He spent lots of time fishing at seashore and usually he earned nothing but lots of sweats on the back and sunburn. However, through these he learned the importance of patience and being not discouraged by failure which laid down the foundation of his personality. In his early school time he was always interested in subjects like physics and math which explain all phenomena in elegant ways through derivation without much memorizing. Later, his interest led him to the Chemical Engineering dept. at National Taiwan University even though chemistry was not his favorite. His study still concentrated on the theoretical and numerical modeling and this continued until his senior exchange year at University of California, Santa Barbara. At the time he was fortunate to conduct undergraduate research under the supervision of prof. Donald H. Aue, where he used molecular simulation code in one of the fastest supercomputer to calculate the thermodynamic parameters of hydrocarbons. At Cornell University, he was attracted by the nature of polymer and joined Prof. Christopher K. Ober's research group and started to work on projects about polymer brushes and its patterning. Despite the winter of Ithaca is freezing, the loneliness and difficulties on the way of his research were even more torturing. Fortunately, like Nietzsche said long ago: "*Was mich nicht umbringt, macht mich starker*", he found his path to his Ph.D. eventually. In these five year, not only did he work hard on research but also meet a amazing woman, Jing Jiang, who later became his wife on Jun 12th, 2017. His career will continue as postdoctoral researcher at University of Pennsylvania and his exploration in science is just about to begin.

Dedicated to

My dear wife, parents and siblings

You make me who I am and able to arrive here.

ACKNOWLEDGMENTS

First, I would like to thank prof. Ober for recruiting me even knowing that I did not have much experience in experiments. These years I have mentored many students and it is always hard to train a rookie from the very beginning. From him I learned the nature of a good researcher and it will be the precious of my life. I am also grateful for the intelligent people he put around me from whom I gained both valuable knowledge and friendship. I would also like to thank my committee members, prof. Lynden Archer and prof. Fernando Escobedo who are experts in polymer physics. I always enjoyed our discussion and every time they made me see that there is always possibility to make my research better. Thank for their patience in reviewing my thesis and share their brilliant ideas with me.

Next, I would like to send my regard to my collaborators. To Prof. Jürgen Rühle, Dr. Oswald Prucker and Dr. Matthias Menzel at University of Freiburg, I cannot be more thankful to the help they gave me in these years in my research project and the warm reception when I visited Germany. It is the credit of our teamwork to publish these works successfully. I wanted to specially thank to prof. Rühle for carefully editing our work and provided clear outline. To prof. Rudolf Zentel and David Ditter, thank you for allowing me to use orthogonal process in your materials which turned out to be awesome actuation objects. To prof. Susan Daniel and Han-Yuan Liu, thank for your trust in me and polymer brushes. Our collaboration proved that true scientists could think of awesome idea even in the moment of coffee chat. To prof. Kirby and Pranav Sundaram, thank for the great work in biosensor project. To prof. Anthony Ryan, prof. Richard Jones, prof. Rana Ashkar, Dr. Andrew Parnell, Bras Wim, I appreciate your inputs in designing the platform for neutron characterization and I hope it will be a great success.

In addition, I appreciated the staffs at CNF, CCMR and NBTC, especially Garry

Bordonaro, Vince Genova, Christopher Martin, Michael Skvarla, John Treichler, Aaron Windsor, Teresa Porri and Donald Tennant. I could not be familiar with nanofabrication without their kind guidance. With more than one thousand hour spent in the cleanroom, your help save not only my time but also my research funding. I would like to acknowledge also Dr. John Defranco at Orthogonal Inc., for providing suggestion and materials for orthogonal process and Dr. Michael Brazil at Vergason Technology, Inc. for giving me opportunity to explore the mechanism of thin film cracking.

I gratefully acknowledge the help from Ober research group members, both previous and present ones. Dr. David Calabrese was my first mentor here who taught me all the synthesis techniques needed for the polymer brushes. His strict lecture built a strong foundation in my knowledge and I will always be grateful for that. I learned how to effectively use AFM from prof. Clemens Liedel and it turned out to be my most reliable tool. Prof. Myungwoong Kim helped me a lot in my Q exam and shared his knowledge with me generously. Dr. Ihsan Amin has inspiring science spirit and helped me to figure out the effective way for the brush synthesis and characterization. Dr. Hong Xu for helping me to build DFT modeling and countless inputs. I enjoyed constant discussion and fun from group members especially Roselynn Cordero, Yiren Zhang, Ziwei Liu, Hai Tran, Amanda Leonardi, Kazuki Kazahara, Dr. Jing Jiang, prof. Lijie Dong and Chengjian Shi. Your company made my days in Ober group and I will never forget these days we spent together. Special thank to my best apprentice, Michael Edward Klaczko, your feedback ignited my passion in teaching back and your contribution to process development is remarkable.

I would like to express my appreciation to my friends who helped me a lot especially: Dr. Po-Cheng Chen, Dr. Chih-Yun Hsia, Dr. Cheng-Yang Chung, Dr. Henry Chu, Dr. Hung-Lung Hu, Dr. Chun-Ti Chang, Dr. Kai-Yuan Chen, Katherine

Tung, Endian Wang, Han-Yuan Liu, Ding-Yuan Kuo, Rohit Singh, Shih-Hao Tseng, Kevin Lee, Hsien-Lien Huang, Da-Jun Fu, Yi-An Yang Chengyu Liu. I cannot image how my life would be without your support at then.

Finally, I would like to thank my dear wife, Jing Jiang, who is considerate all the time and forgive me for being too busy in my research. Her support is always powerful and makes me a better man. Thank to my parents for shaping my personality and make me dare to chase this big goal in front of me disregard of difficulties. Encouragement from you always supports me against the odds. My cousin, Wei-Chin Chen shared his interests with me and during this years it was him who kept my interesting part alive. I am so grateful to everything I experienced in Cornell and all these things make me the one holding this Ph.D. degree. I will honor this degree by making more contribution to the science community and this is happening only because every love, assurance and encouragement I received from you.

TABLE OF CONTENTS

BIOGRAPHICAL SKETCH	iii
DEDICATION	iv
ACKNOWLEDGEMENTS	v
TABLE OF CONTENTS	viii
LIST OF FIGURES	xi
LIST OF SCHEMES	xviii
LIST OF TABLES	xviii
LIST OF ABBREVIATIONS	xix
CHAPTER 1: Fundamental Structure of Polymer Brushes and the Resulting Properties.	1
CHAPTER 2: Patterning Process Development for Polymer Brushes.	65
CHAPTER 3: Morphology of Nanostructured Polymer Brushes Dependent on Production and Treatment	108
CHAPTER 4: Reduced Lateral Confinement and Its Effect on Stability in Patterned Strong Polyelectrolyte Brushes.	145
CHAPTER 5: Entropic Death of Non-Patterned and Nanostructured Polyelectrolyte Brushes.	178
CHAPTER 6: Toward a platform for comprehensive polymer brush characterization with neutron and laser scattering	214
CHAPTER 7: Conclusion and Outlook	239

LIST OF FIGURES

Figure 1.1 Scheme of scaling laws of polymer brushes under different conditions.	2
Figure 1.2 Chain segmental density $\varphi(z)$ and free-end distribution $\epsilon(z)$ functions.	9
Figure 1.3 Mushroom to brush transition of PAAm brushes at different grafting densities.	11
Figure 1.4. Transition of PMMA brushes from semi-dilute brush region to concentrated brush state as $\sigma > 0.4 \text{ nm}^{-2}$ when good solvent, acetone was applied.	13
Figure 1.5 Free chain-end distribution profiles as determined by different fits of the experimental neutron reflectivity curves.	16
Figure 1.6 Brush entanglement areal density as function of normalized grafting density.	18
Figure 1.7 PEB phase diagram under different conditions.	20
Figure 1.8 Wet thickness at pH = 5.8 for PAA brushes as a function of the grafting density and ionic strength of the aqueous solution in the (a) osmotic brush (O δ B) regime and (b) the salted brush (SB) regime.	24
Figure 1.9 Swollen thickness of PMeVP brush as a function of different salt concentration.	26
Figure 1.10 a), b) Structure of two complexes between di-valent ions and PMAA brushes. c) Swelling properties of PMAA brushes at different metal	28

ion $\text{Me}(\text{NO})_3$ concentrations. d) Simulated swelling properties of PEBs with different grafting densities in trivalent ion added medium.

Figure 1.11 Segmental density profile of PEB with multivalent ions added. 31

Figure 1.12 Schematic Description of the Fabrication of Nanopatterned PMEO₂MA Brushes. 38

Figure 1.13. I) Fabrication process for top-down patterned brushes for the detection of vapor organic compounds(VOC). II) AFM scan and III) Photographic images. 41

Figure 1.14. Rescaled height and width as a function of reduced stripe width for polymer brushes with different molecular weights and grafting densities. 43

Figure 2.1 E-beam direct patterning results. a) SEM images of 1 - 0.15 μm line patterns of free PVP/PSS. b) AFM images of patterned 150 nm PDMAEMA brush lines. 78

Figure 2.2 Results of E-beam lithography patterning on initiator. a) AFM scan on trenches made of PMMA brushes grown on patterned initiator. b) Relative thickness of the PMMA brush in the trench as a function of the exposure dose. 79

Figure 2.3 Patterns of the OSCoR4000 and 3 different polymer films with their chemical structures shown. 80

Figure 2.4 SEM images of E-beam lithography patterning of OSCoR 4000 on different substrate. 82

Figure 2.5 Multilayer film quality evaluation under optical microscope after 88

PAB with the different film combinations.

- Figure 2.6** E-beam lithography patterning result of the PMMA brush with combination A. Results after development, stripping and acetone immersion are displayed. a) 150 nm trench AFM scan top-down view and b) cross-sectional view. c) Optical microscope images taken in AFM. **90**
- Figure 2.7** E-beam lithography patterning result of the PMMA brush with combination B. **91**
- Figure 2.8** E-beam lithographic evaluation of the combination: PMMA polymer brush/ CYTOP/ ZEP520. **92**
- Figure 2.9** Patterning results fabricated with Brush/CYTOP/BARC/UV210. **94**
- Figure 2.10** Bottom-up patterning a) process flow and b) the results with different fillers. **96**
- Figure 2.11** Patterned PMeVP brushes made of substrates with different initiator deposition time. **98**
- Figure 3.1.** radical-chain polymerization and the monomers used for synthesis of the polymer brushes. **120**
- Figure 3.2.** AFM height profiles of dry nanostructured PtBuMA brushes measured perpendicular to the brush line direction showing the transition from a quasi-two to a quasi-three dimensional system and the lens-like morphology. **122**
- Figure 3.3.** Plots of the maximum height h_{\max} (a), the maximum width w_{\max} (b), and the cross section integral A (c) as a function of the pattern size Δ of dry bottom-up PtBuMA nanobrushes grown in a single experiment after immersion in toluene (■) and in methanol (□). Theoretical lines based on the **124**

corresponding conditions are also presented in (a) and (b) as a comparison.	
Figure 3.4. AFM height profiles of the 0.4 μm Δ line showing an example of the change of the dry PtBuMA NPBs morphology after immersing it in methanol.	126
Figure 3.5. Aspect ratios of the patterned PtBuMA brush lines as a function of Δ respectively Δ/h_0 for the inset graph.	128
Figure 3.6. Plots of the maximum height h_{max} (a) and the maximum width w_{max} (b) as a function of the pattern size Δ of dry BU P(tBuMA-co-MABP) nanobrushes from a single experiment after immersion in toluene (■) and in methanol (□).	131
Figure 3.7. AFM height profiles of dry TD PtBuMA brush. a) after manufacturing process, b) after immersion in toluene and c) after immersion in methanol.	132
Figure 3.8. Plots of the maximum height h_{max} (a), the maximum width w_{max} (b) and the cross section integral A (c) as a function of the pattern size Δ of dry top-down patterned PtBuMA nanobrushes.	133
Figure 3.9. Dry brush morphology of TD patterned PMeVP brushes. a) Evolution of dry morphology of patterned PVP brush. b) Degrafted brush cross-sectional morphology at different pattern sizes. c) Suggested mechanism for brush degrafting in water.	135
Figure 4.1. Schematic description of brush relaxation under different conditions.	149

Figure 4.2. a) FTIR spectra of PMETAC brushes at different stages. b) PMETAC brushes degrafting kinetics with different initiators. c) PMETAC brushes degrafting kinetics at different temperatures and d) with different pH buffers.	155
Figure 4.3 AFM scan cross-section images of top-down patterned PMMA brush. [Δ = a) 225, b) 600, c) 1000 nm]	159
Figure 4.4 Comparison of AFM measured morphologies between TD and BU patterned PMMA brushes.	161
Figure 4.5 Characterization of degrafting condition of PMETAC brushes by comparing dry cross-sectional area ratio versus the pattern sizes for different processes.	164
Figure 4.6 AFM dry cross-sectional image of the 1 μ m PMETAC brush pattern before and after degrafting at RT in water for different processes.	164
Figure 4.7 Scheme for the polymer brush relaxation under reduced lateral confinement.	166
Figure 4.S1. NMR spectrum of the reaction solution of PMETAC brushes.	169
Figure 4.S2. Uncorrected degrafting trend for the TD and the M. TD patterned brushes.	170
Figure 4.S3. Dry AFM cross-sectional images of the top-down patterned PMETAC brushes degrafting in water at different temperatures.	171
Figure 5.1: Synthesis route for cationic polyelectrolyte brush (poly[4-vinyl-N-methylpyridinium] iodide).	187

Figure 5.2: Degrafting behavior of PMeVP brushes at different degrees of charging and external salt concentrations.	190
Figure 5.3: Degrafting behavior of PMeVP brushes at different solvent temperatures.	194
Figure 5.4: Degrafting behavior of strong polyelectrolyte PMeVP brushes ($M_n = 650 \cdot 10^3 \text{ g} \cdot \text{mol}^{-1}$; PDI = 1.67) with different grafting densities.	195
Figure 5.5: Degrafting behavior of nanostructured PMeVP brushes with different pattern sizes at different temperatures.	197
Figure 5.6: Degrafting behavior of nanostructured PMeVP brushes. a) The NPBs have been exposed to water with different KI salt concentrations. b) The NPBs have been exposed to water in different ways for overall 3 h at 0 °C: ■ (1*3 h); and ● (6*0.5 h).	199
Figure 5.7: a) Sketch illustration the influence of the osmotic shock. b) Illustration depicting the number of entanglements as a function of the pattern size. c) Depiction of the influence of the pyridinium-iodide interactions on the intermolecular structure of the PEB chains.	205
Figure 5.8: Degrafting behavior of high molecular weight, neutral PVP and low molecular weight, polyelectrolyte PMeVP nanobrushes monitored using the relative dry cross section integral as a function of the pattern size. The NPBs have been exposed to good solvents at different temperatures for different periods of time.	206
Figure 6.1. PDMAEMA brushes dry thickness as function of polymerization time.	225

Figure 6.2. fabrication process of the transmission platform.	227
Figure 6.3. Pictures of the platforms. a) platform with substrate bending, only part of the wafer was exposure properly. b) platform with particles and stitch line. c) platform with all improving process conducted.	229
Figure 6.4. Optical characterization setup and the resulting diffraction signals.	230
Figure 6.5. fabrication process of reflective platform on silicon. ALD: atomic layer deposition. RIE: reactive ion etching.	232
Figure 6.6 SEM pictures of the platform during the fabrication process.	233
Figure 6.7. SEM images of the grating after etching with BOE 30:1.	234
Figure 6.8. SEM images of the grating with PDMAEMA brushes grown on the gratings in Figure 6.7. Scale bar: 200 nm.	235
Figure 6.9. SEM images of the PDMAEMA brushes grown on grating made of 10 nm SiO ₂ and 15 nm Cr.	236
Figure 7.1 LCE formulation used as patterning subject.	244
Figure 7.2 Fabrication process and result for the patterned LCE free films.	245
Figure 7.3 Thermal actuation motion of patterned LCE.	247
Figure 7.4. Detection mechanism for the proposed immunosensor.	248
Figure 7.5. Process flow for the fabrication of the biosensor platform and the picture of the platform taken with fluorescent microscope.	250
Figure 7.6. Proposed design for the photo-cleavable polymer brushes as SLB cushion.	252

LIST OF SCHEMES

Scheme 2.1 Finalized processes for fabrication of patterned polymer brushes	99
--	-----------

LIST OF TABLES

Table 1.1 Summary of studies of degrafting phenomena in polymer brushes	35
Table 2.1 Photolithographic evaluation results and corresponding parameters for synthesized fluoropolymer photoresist.	83
Table 2.2 Summary of multilayer patterning process testing results.	86
Table 3.1. XPS elemental analysis data of TD patterned PtBuMA and PVP films.	136
Table 5.1: Reaction rates of bond scission for PMeVP brushes.	193
Table 6.1. Measured parameters of two different samples with PDMAEMA brushes. Values reported are grating density (chains/ nm ²) / PDI.	226
Table 6.2. Values for neutron scattering-related parameters of the substrates.	231

LIST OF ABBREVIATIONS

A_i : initial dry brush cross-sectional area
 A_o : dry brush cross-sectional area after the exposure procedure
 A_{rel} : relative brush cross-sectional area in degrafting process.
 A : pre-exponential factor in Arrhenius equation
 a : Monomer diameter
 C_s : Concentration of salt/electrolyte
 E_a : activation energy
 f : Fraction of changed monomers / average degree of ionization
 F : Total Free energy
 F_{el} : Elastic energy of entropic spring
 F_{int} : Exclude volume repulsion between segments, internal energy of the system
 h : Film(brush) thickness
 k : reaction rate
 k_B : Boltzmann constant
 N : Number of monomers in polymer
 N_e : Entanglement degree of polymerization
 R : gas constant
 R_g : Radius of gyration
 T : Temperature
 v : Exclude volume
 w : Width of the patterned brushes
 Δ : Pattern Size of the patterned brushes
 λ_G : Guoy-Chapman length
 ϵ_r : Relative dielectric constant
 σ : Grafting density(number of chains per area)
 θ : Theta solvent(or refer to theta solvent quality)
 φ : Polymer segmental density
 ϵ : Chain free-end distribution function
 Σ : Reduced grafting density ($\sigma\pi R_g^2$)
 Ω : Number of entanglements per unit area
 τ : Terminal disentanglement time
AFM: Atomic force microscopy
APDMES: 3-aminopropyldimethylethoxysilane
APTES: (3-aminopropyl)triethoxysilane
ATRP: atom transfer radical polymerization
BARC: Bottom Anti-Reflective Coating.
BIBB: α -bromoisobutyryl bromide
BOE: buffered oxide etch
BU: Bottom-up (patterning)
CuCRP: Cu(0)-meditated controlled radical polymerization.
DCM: Dichloromethane
DFT: Density Functional Theory
DFTB: Density-Functional Tight-Binding

DMF: Dimethyl formamide
 DMSO: Dimethyl sulfoxide
 DUV: Deep ultraviolet light
 EBL: E-beam lithography
 FOTS: (1H,1H,2H,2H-Perfluorooctyl)trichlorosilane
 FTIR: Fourier Transform Infrared
 GPC: Gel permeation chromatography
 HFE: Hydrofluoroether
 HSQ: hydrogen silsesquioxane
 LCE: liquid crystal elastomers
 LCST: Lower Critical Solution Temperature
 LED: Light-emitting diode
 MABP: 4-(methacryloyloxy)benzophenone
 MD: Molecular Dynamics
 MEMS: MicroElectrical Mechanical Systems
 MIBK: methyl isobutyl ketone.
 MPB: microstructured polymer brush
 M.TD: Modified top-down (patterning)
 NEMS: NanoElectrical Mechanical Systems
 NPB: nanopatterned polymer brush (nanostructured polymer brush)
 NR: Neutron reflectivity
 PAA: Poly (acrylic acid)
 PAB: Post-application Bake.
 PAAm: Polyacrylamide
 PDI: polydispersity index
 PDMAEMA: Poly(2-dimethylaminoethyl methacrylate)
 PDMS: polydimethylsiloxane
 PEB: polyelectrolyte brush (or post-exposure bake)
 PEDOT: poly(3,4-ethylenedioxythiophene): poly(styrene sulfonate)
 PEGf: 2-[methoxy(polyethylenoxy)propyl]trichlorosilane
 PEHMA: poly(2-ethylhexyl methacrylate)
 PEL: polyelectrolyte
 PESS: poly(ethyl *p*-vinylbenzenesulfonate)
 PHEMA: poly(2-hydroxyethyl methacrylate)
 PAA: Poly (acrylic acid)
 PAB: post-application bake
 PAN: Polyacrylonitrile
 PBS: phosphate buffered saline
 PCSMA: poly(cysteine methacrylate)
 PDFMA: Poly(1H,1H,2H,2H-heptadecafluorodecyl methacrylate)
 PDMA: poly(N,N-dimethylacrylamide)
 PDMAEMA: poly(2-(dimethylamino)ethyl methacrylate)
 PMAETAI: poly[(2-(Methacryloyloxy)Ethyl) Trimethylammonium Iodide]
 PMDETA: N,N,N',N',N''-pentamethyldiethylenetriamine
 PMETAC: poly[(2-(Methacryloyloxy)Ethyl) Trimethylammonium Chloride]

PMAA: poly(methyl methacrylic acid)
PMEO₂MA: Poly(2-(2-methoxyethoxy)ethyl methacrylate)
PMeVP: poly(N-methyl-4-vinylpyridinium iodide)
PMMA: polymethyl methacrylate
PNIPAM: poly(*N*-isopropylacrylamide)
POEGMA: poly(oligo(ethylene glycol) methacrylate)
POEGMEMA: poly[oligo(ethylene glycol) methyl ether methacrylate]
PPEGMA: poly(polyethylene glycol) methacrylate
PS: polystyrene
PSS: poly(styrenesulfonate, sodium salt)
PTFE: polytetrafluoroethylene
SFA: surface force apparatus
P2VP: poly 2-vinylpyridine
PVP: poly 4-vinylpyridine
RCP: radical chain polymerization
RT: room temperature
SAM: self-assembled monolayer
SEM: scanning electron microscopy.
SLB: supported lipid bilayer
SLD: scattering length density
SRIE: strong reactive ion etching (used in chapter 3 for oxygen RIE)
TBAF: tetrabutylammonium fluoride
TD: top-down (patterning)
TEA: triethylamine
TFT: thin film transistor
THF: tetrahydrofuran
TMC: trimethylchloride
QCM-D: Quartz Crystal Microbalance with Dissipation
WRIE: weak reactive ion etching (used in chapter 3 for oxygen RIE)
XPS: x-ray photoelectron spectroscopy

CHAPTER 1

Fundamental Structure of Polymer Brushes and their Resulting Properties

Abstract

Polymer brushes are materials made of densely tethered polymer chains with one end attached to a surface or interface. This arrangement imparts them invaluable properties in a range of application fields such as lubrication, anti-fouling and biomimetic. As more and more applications rely on polymer brushes, the importance of a fundamental understanding of brush structure becomes higher as well. This chapter starts with a survey of fundamental properties of the polymer brushes and focuses on the change of the swelling properties of the polymer brushes as a function of the surrounding and intrinsic parameters.

As a member of the polymeric material family, tuning brush morphologies may be achieved through changing molecular weight, solvent quality as well as brush grafting density which is a unique handle only for brushes. More tuning flexibility can be obtained when charges are present on polymer chains, which makes them polyelectrolyte brushes. Different behaviors of these polymer brushes are shown in Figure 1.1 with corresponding equation for the scaling behavior of t . In the end, the change of brush structure under patterning conditions will be addressed and which acts as a novel tool to tailor their properties by allowing lateral stretching.

*Portions are excerpted from W-L. Chen, R. Cordero, H. Tran and C. K. Ober. 50th

Anniversary Perspective: Polymer Brushes: Novel Surfaces for Future Materials.

Macromolecules, 2017, 50 (11), pp 4089–4113. Copyright © 2017 American

Chemical Society.

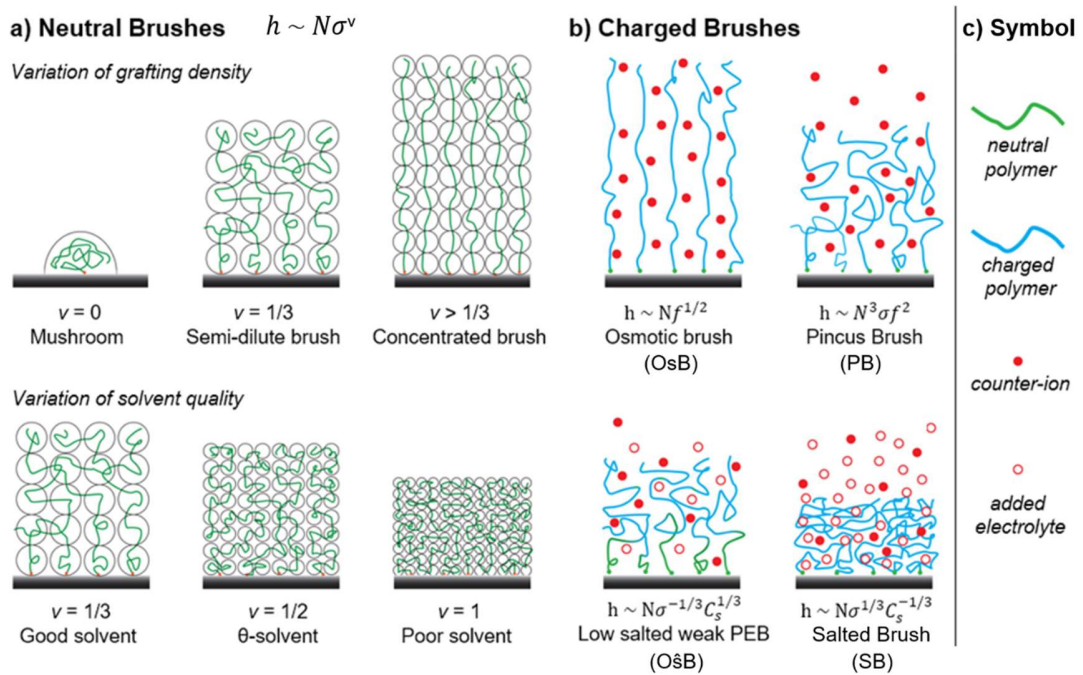


Figure 1.1 Scheme of scaling laws of polymer brushes under different conditions. a) Neutral brushes with general scaling law $h \sim N\sigma^v$ with variation of v for different conditions. b) Scaling laws for charged brushes under different conditions. c) symbols for the scheme.

1.1 Neutral brushes

1.1.1 Theoretical Understanding

A fundamental understanding of brush structure was first derived in the work of Alexander.¹ Compared to uniformly absorbed polymers, which have a film thickness h smaller than the free polymer radius of gyration R_g ,² Alexander noticed that the thickness of end-absorbed polymers could have the distinct behavior at increased grafting density where the chain-chain interaction dominates. The distance between tethering points is smaller than the polymer stretching distance and it reflects the start of the interaction between grafted chains. Following the “Flory argument”, Alexander derived the brush conformation by a balance between elastic energy of entropic spring,

F_{el} and excluded volume repulsion between segments, F_{int} (internal energy of the system). Polymer chains are considered as ideal and elastic energy approximated as a quadratic end-to-end distance, which is represented by a brush film thickness. The excluded volume originates from uniformly distributed monomer segments and is proportional to its volume fraction. The total free energy of a single polymer chain in the brush $F = F_{el} + F_{int}$ then could be written as:

$$F = k_B T \left[\frac{3h^2}{2Na^2} + \frac{vN^2\sigma}{h} \right] \quad (1)$$

Here a is the monomer diameter, v is the excluded volume and σ is the grafting density (number of chains per area). By minimization of total free energy, the thickness of a polymer brush could be obtained:

$$h \sim N(\sigma v)^{1/3} \quad (2)$$

A similar relationship was obtained by de Gennes through simple scaling analysis where polymers in the brush were considered as a series of tension blobs and their steric interaction determines the conformation of the brushes.³ This leads the correlation length of polymer chains in the brush to be the distance between grafting points, which equals to $\sigma^{-1/2}$ and is the same in the work of Alexander.¹ This description is then referred to as Alexander – de Gennes brush and it is the most fundamental model of the brush. One important difference of the polymer brushes is

that the brush dimension is proportional to N instead of $N^{1/2}$ in its free form. For the chains in the brush, their length could be much larger than R_g due to steric deformation and this leads to properties distinct from free polymers. Also, it could be noticed that the dependence on the excluded volume is also stronger compared to free polymer ($1/5$) since now polymer chains ‘feel’ more strongly the presence of the other chains. This leads to a higher sensitivity to the surrounding stimuli and is a fundamental reason why polymer brushes could be a better stimuli-responsive material.

Through similar ideas, the thickness scaling law for polymer brushes in theta solvents and poor solvents have also been derived.^{4,5} The power law exponent of the grafting density on thickness increases from $1/3$ to $1/2$ to 1 as the solvent quality decreases from good to Θ to poor. In contrast, the dependence on the molecular weight remains constant at N . Similar increases on this dependence could be obtained when the grafting density is further increased from moderate grafting density to high grafting density. At high surface coverage, the excluded-volume effect between segments are fully screened out like concentrated polymer solutions and higher order interactions become important. The thickness scaling relationship of the brush could have higher power law exponent dependence than $1/3$ and it could be even up to 1 .⁶⁻⁸

The Alexander – de Gennes brush model also provides a picture of the brush segment density along the vertical distance from the surface $\varphi(z)$. Segment density of the model could be described as follows: (All properties have been normalized to the monomer size, a)³

$$\varphi(z) \sim \begin{cases} \sigma(z/a)^{2/3} & a < z < \sigma^{-1/2} \\ \sigma^{2/3} & \sigma^{-1/2} \leq z \leq h \end{cases} \quad (3)$$

Above brush thickness h the brush segment density drops quickly to zero. The segment density reaches a plateau when $z > \sigma^{-1/2}$ and equals the density of the tension blob. However, this result is later found to be inaccurate due to the oversimplification of the brush structures. In the model, polymer chains are assumed to stretch out uniformly and their free-ends located at the most outer edge. In fact, the optimum state of a brush allows polymer chain ends to be buried inside without penalty in free energy. Heath and Scheutjens *et al.*⁹ first showed that the polymer brush segment density is a parabola and the chain ends distribute over the entire height of the polymer brush rather than focus on the top. This phenomenon is later explained thoroughly by Milner *et al.*¹⁰⁻¹², Skvortsov *et al.*¹³ and Zhulina *et al.*¹⁴ independently in different works and later referred as a “Parabolic Brush”. The paragraph below is a brief description based on the self-consistent field (SCF) method of Milner.

The expression of the brush total free energy can be treated in a similar way to before, but now the excluded volume is considered as the sum of effects of segment density.

$$F = \sum_{i=1}^K \int_0^N dn \left[\frac{1}{2} \left(\frac{d\vec{r}_i}{dn} \right)^2 \right] + \frac{1}{2} v \int dV \varphi^2(\vec{r}) \quad (4)$$

In this system, each grafted chain i is represented as a set of N monomer coordinates $\vec{r}_i(n)$, with $n=0, 1, \dots, N$. and K is the total number of chains. The free energy for

addition of a single chain in the system could then be expressed by Eq. 5 by setting potential energy as $U(\vec{r}) = -v\varphi(\vec{r})$.

$$\Delta F_i = \int dn \left[\frac{1}{2} \left(\frac{d\vec{r}_i}{dn} \right)^2 \right] - \int dn U(\vec{r}) \quad (5)$$

The mean field potential energy approximation is valid based on the fact that each chain should “feel” the existence of the other chains before itself due to the dense tethering. Eq. (5) is similar to the path integral for one particle motion in quantum mechanics by treating $\vec{r}(n)$ as the position of particle at time n . Subsequently, condition $\vec{r}_i(N) = 0$ is set for the end grated chains which applies no limitation on the positions of free ends.

In the particle system, these conditions together mean that no matter where the particle starts its motion, in the end they would have to reach the surface at the same time N . To fit the conditions, the potential energy $U(\vec{r})$ would then have the form $U(\vec{r}) \propto z^2$ which equals to the potential of harmonic oscillator. Since $U(\vec{r}) = -v\varphi(\vec{r})$, the segment density profile is a parabola which could be found out to be

$$\varphi(z) = v^{-1}(A(h) - Bz^2), z \geq 0 \quad (6)$$

where $B = \frac{\pi^2}{8N^2}, A(h) = \frac{N\sigma v}{h} + \frac{Bh^3}{3}$

The coefficient B was derived from the fact that each particle should arrive at the surface at the same time N , while $A(h)$ was derived from the mass balance, $N\sigma = \int_0^h \varphi(z) dz$.

The last piece of the brush structure left in the model is the chain free-end distribution. Derivation of the chains' free-end distribution $\epsilon(z)$ should start from the fact that the local segments density $\varphi(z)$ is contributed from the polymer chains whose free-end lies above z . Here $dz(n; z)/dn$ is the function refers to the velocity at z of a particle which began at ρ .

$$\varphi(z) = \int_z^h \frac{dn}{dz(z; \rho)} \epsilon(\rho) d\rho \quad (7)$$

Based on the result of Semenov *et al.*¹⁵ which was used for chain free-end distribution of the block copolymer in a melted micelle, the condition used in Eq. A3 in their work has to be changed to Eq. 7 here due to the varying segmental density. A similar solution could be derived if free energy, F shown in Eq. 4 is minimized with the conditions of Eq. 7 and Eq. 8 through indefinite Lagrange multipliers:^{16,17}

$$\int_0^\rho \frac{dn}{dz(z; \rho)} dz = N \quad (8)$$

It then could be shown that the function $dz(z; \rho)/dn$ has the form of $[G(\rho) - G(z)]^{1/2}$ with G an unknown function. Eq. 8 could now be written in the following form by assuming a new function $f(G) = \frac{dz}{dG}$.

$$\int_{G(0)}^{G(\rho)} \frac{f(G)}{[G(\rho) - G(z)]^{\frac{1}{2}}} dG(z) = N \quad (9)$$

This equation is a classic Abel integral equation with solvable $f(G)$,¹⁸ which leads $z(z; \rho)/dn$ to be the following form:

$$z(z; \rho)/dn = \pi(\rho^2 - z^2)^{\frac{1}{2}}/2N \quad (10)$$

By setting two additional parameters, $t = (\rho/h)^2$, $u = (z/h)^2$ and inserting Eq. 10 into Eq. 7, another solvable generalized Abel integral equation could be obtained:¹⁹

$$\int_u^1 \frac{g(t)dt}{(t-u)^{\frac{1}{2}}} = \frac{(A(h) - Bz^2)}{v} \quad (11)$$

where $g(t) = \frac{N\epsilon(\rho)}{\pi\rho^{d-2}}$, the coefficient d is dependent on the power of z on the right-hand side. This could lead to the final form of chain free-end distribution:¹⁰

$$\epsilon(\rho) = \frac{(2B)^{\frac{3}{2}}}{\pi v} \left[2z(h^2 - z^2)^{\frac{1}{2}} + \left(\frac{A}{B} - h^2\right)(h^2 - z^2)^{-\frac{1}{2}} \right] \quad (12)$$

As could be seen in the equation, when the brushes are under no external force, $h = A/B$ and only first term contributes to the distribution of the chain free-end. A comparison between two different brushes is shown in Figure 1.2. Compared to an Alexander – de Gennes brush where segment density is constant, brushes with parabolic segment density profile would have more excluded volume repulsion in the deeper layers. The equilibrium chain conformation is determined by the trade-off

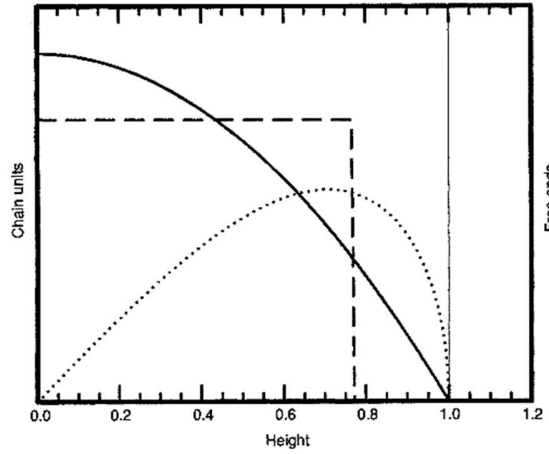


Figure 1.2 Chain segmental density $\varphi(z)$ and free-end distribution $\epsilon(z)$ functions, x-axis is normalized to the height of parabolic brush while y-axis is normalized to the segmental density of Alexander – de Gennes brush. Dashed line: $\varphi(z)$ for Alexander – de Gennes brush. Solid line: $\varphi(z)$ for Parabolic Brush. Dotted line: $\epsilon(z)$ for Parabolic Brush without external force. Reprinted from ref. 20 with permission from American Association for the Advancement of Science.

between excluded repulsion (maximum at low z) and chain entropic stretching (maximum at high z). More detailed comparisons between the step-like brush and parabolic brush have been discussed in other literature²⁰ and will not be addressed here.

1.1.2 Experimental Study

In theory, the transition from a low grafting density “mushroom” state to a “brush” state happens when the reduced grafting density, $\Sigma = \sigma\pi R_g^2$ is greater than one. However different experimental studies showed different conclusions in terms of the starting of the strong stretching and the breadth of the transition zone between the two states. In the study of Kent *et al.*²¹, diblock copolymer polystyrene-*b*-poly(dimethylsiloxane) (PS-*b*-PDMS) was chosen to form brushes on the interface of a Langmuir trough. It was shown that even at a value of $\Sigma = 12$ the strong stretching limit was not achieved and the dependence of the exponential order of N, σ on h was less than the one in Eq. 2. On the other hand, Wu *et al.* studied the transition of the brush thickness with poly(acrylamide) (PAAm) brushes grown on the grafting density gradient.²² PAAm brushes showed a sharp transition at the $\Sigma \sim 6$ where the thickness scaling changed from σ to $\sigma^{1/3}$ (Figure 1.3). Interestingly, water contact angle was measured on the same brushes and it showed a broader crossover region between two states which fits better to theoretical prediction.²³ Another study of Zheng *et al.* conducted experiments with crystalline-amorphous diblock copolymers which used a PS block as brush and a crystalline block as solid base.²⁴ The brushes showed a transition starting from $\Sigma \sim 3.7$ to 14.3. It was then concluded that $\Sigma > 5$ is a general

standard to define the brush state.²⁵ Nevertheless, this guideline is not accurate for the semi-flexible brushes which have been predicted to be quite different from the general rule of flexible brushes. It has been observed on semi-flexible polymer brushes with threshold of mushroom to brush transition at $\Sigma < 1$.²⁶

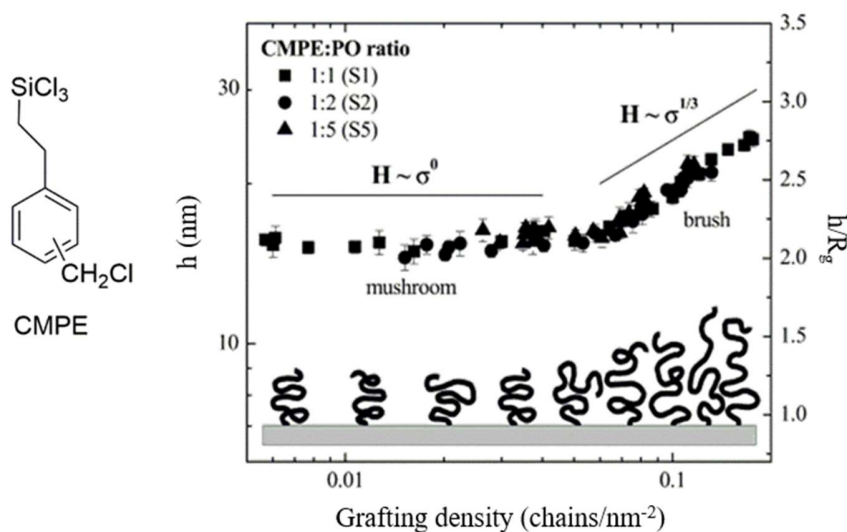


Figure 1.3 Mushroom to brush transition of PAAM brushes at different grafting densities. 1-trichlorosilyl-2-(m/p-chloromethylphenyl) ethane (CMPE)/paraffin Oil(PO) mixture was used to tune brush grafting density through vapor deposition. Reproduced from ref. 22 with permission from American Chemistry Society.

The swelling properties of polymer brush, $h \sim N$, was first reported by Hadziioannou and Tirrell *et al.*^{27,28} with a surface-adsorbed PS brush. Thickness dependence on the grafting density for a good solvent, $h \sim \sigma^{1/3}$ was later observed through different techniques including ellipsometry^{29,30}, neutron reflectivity³¹, surface force apparatus

(SFA)³² and atomic force microscopy (AFM).^{22,33} Early studies generally used brushes made of “grafting to” techniques which places limitation on brush grafting density. With the advance of polymerization techniques, polymer brushes with high grafting density are synthesized and they were proven to be different from its low grafting density analog. In the work of Yamamoto *et al.* it was found that the power law exponent of thickness scaling $h \sim \sigma^v$ of polymethyl methacrylate (PMMA) brush changed gently from 1/3 to 2/5 from low to high grafting density ($\sigma > 0.4 \text{ nm}^{-2}$).^{33,34} The increase of power law exponent v to 2/5 was also observed in the study of Wu *et al.*²² and then explored systematically in the study of Moh *et al* (Figure 1.4).³⁰ In their study, PMMA brushes with at most $\sigma = 0.8 \text{ nm}^{-2}$ have been synthesized and also showed an increase of v starting at $\sigma = 0.4 \text{ nm}^{-2}$. It was concluded that $0.8 < v < 1.3$ for $\sigma > 0.7 \text{ nm}^{-2}$ which is consistent with theoretical scaling of $v = 1$ at high grafting density.^{7,8} PMMA brushes were also tested in different solvent conditions changing from good to Θ to poor by varying the composition of an acetone/methanol mixture. At medium grafting density ($\sigma < 0.4 \text{ nm}^{-2}$), the exponential dependence increased as the solvent quality decreased but collapsed to a single dependence with $v = 0.8$ at high grafting density which is the same dependence as the one in pure methanol. The reason why $v = 0.8$ at poor solvent brush and high σ brush was the “self-solvent” effect since a polymer is a Θ solvent for itself and this became obvious at high polymer concentration. However, this scaling relationship is different from the one shown earlier in the study of Auroy *et al.*³¹ where $v = 1$ under poor solvent conditions. This could be possibly due to the difference in the grafting techniques and substrates used for the experiments. Nonetheless, it could be observed that the scaling exponent of the brush thickness v increases as either increasing

grafting density or decreased the solvent quality. Such similar trends could be explained by the fact that they both change with the extent of chain overlap in a similar way which determines the scaling behavior.

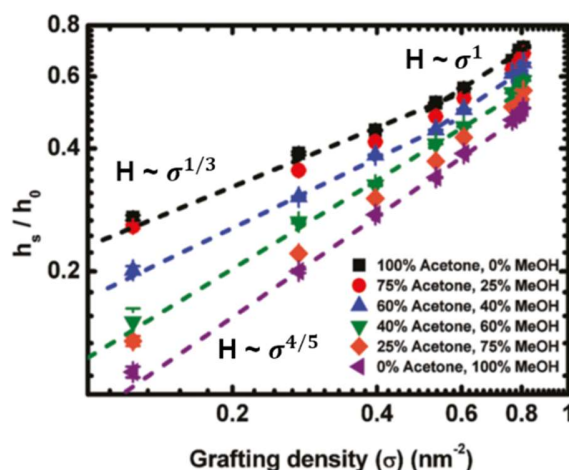


Figure 1.4. Transition of PMMA brushes from semi-dilute brush region to concentrated brush state as $\sigma > 0.4 \text{ nm}^{-2}$ when good solvent, acetone was applied. Such transition was not observed in methanol immersion where scaling remained constant as $\sigma^{4/5}$. Reproduced from ref. 30 with permission from American Chemistry Society.

The detailed structure of polymer brushes determines their fundamental behavior and is the key for their engineering. Neutron reflectivity(NR) is one of the major tools for this purpose since it allows characterization of the specific deuterated part. Although initial studies used brushes made by “grafting from” techniques which did not reach the strongly stretched region, a parabolic-like profile of the brush segmental density was observed where $\Sigma < 12$.^{21,35-37} The profile of the strongly stretched polymer brush was not observed until the study of Levicky *et al.* where $\Sigma_{max} = 28$ for

polystyrene-*b*-poly(2-vinylpyridine) (PS-*b*-P2VP) adsorbed brushes.³⁸ One of the most interesting observations was that polymer segment density became flatter as Σ increased in the strongly stretched region, which could be explained by the fact that at larger Σ the increased entropy penalty caused chains to be redistributed to the bulk. Such a penalty was not observed at the transition region where the higher Σ could only increase segmental density rather than flattening.³⁷ Furthermore, it was observed that the segment density more closely resembled the step-like profile at higher Σ , which was predicted for the Alexander-de Gennes brush. On the other hand, with a change of solvent quality the brush shrank and the average segmental density increased due to the magnified chain overlap. Surprisingly the profile was the flattest at good solvent quality and the roundest at medium solvent quality which showed the importance of solvent quality as a handle to control brush behavior. Another handle that provides the unique segmental density for brushes is dispersity. R uhe *et al.* showed that polymer brushes with high dispersity synthesized by free-radical polymerization (FRP) have exponential decay segmental density profiles.²⁹ By the application of a special setting³⁹, ellipsometry probed the segmental density profile of the poly(4-vinylpyridine), (PVP), brushes directly without deuterium and the result fits the theoretical prediction of Milner *et al.*¹² Since such a profile was not observed in the PS brushes synthesized by the same method but with lower molecular weight⁴⁰, high molecular weight is another condition for the appearance of an exponential decay segmental density profile.

A few more complicated properties of polymer brushes which required more complex NR setups have been probed in recent years. First, for parabolic brushes, free chain

ends are distributed within the brushes rather than all on the top layer. It was investigated by Spiliopoulos *et al.*⁴¹ by diblock copolymer of deuterated PS and virgin PS (dPS-*b*-PS) which was non-deuterated only at last 16 % of the free end. The free, non-deuterated chain ends could then be distinguished in a sea of deuterated substrates. The result derived from low grafting density polymer brushes with $\Sigma = 6$, fit well to theoretical predications of parabolic brushes as shown in Figure 1.1. However, by using a different model the NR data could also generate another set of better fitted profiles with more free chain-ends on the top layer (Figure 1.5). This could possibly be caused by a transition state between brush and mushroom where the sample was situated that made both profile fitting possible. Further measurement on brushes with higher grafting density should help to solve the dilemma. Second, in another study of Abbott *et al.*⁴², the segmental density profile was studied with mechanical pressure present. The pressure needed to change the segmental density profile (from parabolic profile in swollen state to step-like profile in collapsed state) predicted by the SCF theory was more than one order of magnitude greater than experiment result. Experimentally only ~1 bar was needed to change the shape from parabolic to step-like and this magnitude was also observed in other studies.^{43,44} The result suggested that the osmotic pressure does not act the same as the mechanical pressure in the brush structure and it's still unclear how those two parameters interact. Third, post-polymerization efficiency of the polymer brushes was also probed by Schüwer *et al.* who used deuterated amino acid with different sizes to react with pre-activated poly(2-hydroxyethyl methacrylate)(PHEMA) polymer brushes at different grafting densities and the reaction efficiency was monitored by increased neutron

density.⁴⁵ It was shown that only the top 25% of the brush was reacted at the highest grafting density for the larger amino acid. Even though this result suggests that post-polymerization modification is not a good strategy to create homogeneously modified dense brushes, the possibility of direct site-specific modification on the other hand could be valuable for other purposes.

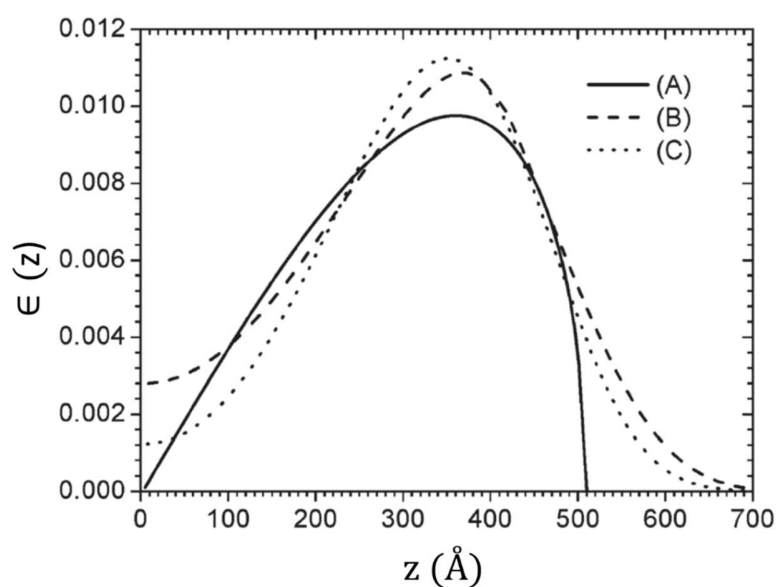


Figure 1.5 Free chain-end distribution profiles as determined by different fits of the experimental neutron reflectivity curves: A: SCF theory $z(1 - z)^{0.5}$; B: Modified SCF theory, $c + z^n(1 - z)^{0.5}$; C: $c + z^n e^{-azx}$. Weighted squared differences: A: 0.936, B: 0.802, C:0.824. Here a, c, n, x are modeling fitting parameters. Reproduced from ref. 41 with permission from American Chemistry Society.

1.1.3 Entanglement in Polymer Brushes

As a polymeric material, polymer brushes are expected to have entanglements just like the others.⁴⁶ Ruths *et al.* conducted SFA studies of PS brushes grafted on the both side

of a gap⁴⁷ Surprisingly, brush stretching became less/ lower when the brushes were left at the largest compression for an hour. Since the disentanglement time estimated based on the brush parameters was up to hours, it was concluded that stretching was hindered by the entangled conformation. In addition, even with molecular weight $\sim 10^6$, the number of entanglements in the brushes was approximated to be only 3-5 per polymer chain. This behavior could be the reason why such effects were not observed in other SFA studies with shorter polymer chains. Kenji *et al.* also showed the intramolecular entanglements within the PMMA brushes. It was shown that the compressibility of the PMMA brushes was smaller than that of spin-coated PMMA films. By comparing the brushes to the polymeric network with similar extents of stretching, the number of entanglements was calculated to be 2/3 of the PMMA melt, due to low chain overlap in the brush conformation. Although both experiments showed the resulting effects of brush entanglement, the relationship between grafting density, molecular weight and the number of entanglements is still ambiguous to people in the field. Robert *et al.* later with molecular simulation showed the scaling law for the number of entanglements(Ω) per unit area in the brushes versus grafting density to be $\Omega \propto \sigma^{1.78}$ for good solvent and $\Omega \propto \sigma^{1.50}$ for θ -solvent (Figure 1.6).⁴⁸ Although such scaling fits well with the thickness scaling law ($\sigma^{1/3}$, $\sigma^{1/2}$) when $\varphi^2 h$ was used to evaluate Ω , further experimental work is still needed to prove the validity of the law. Similarly, the effect of entanglement on chain dynamics has also been studied by simulation and the disentanglement time has been evaluated in the work of Lang *et al.* to be $\tau \propto \left(\frac{N}{g}\right)^3 \exp\left(\frac{N}{N_e}\right)$ where N_e is the degree of entanglement of polymerization in the brush and g is the size of the tension

blob which is proportional to $\sigma^{-1/2\nu} a^{-1/\nu}$ ($\nu = 0.588$ in good solvent and 0.5 for θ -solvent). Compared to the general polymer melt disentanglement time ($\tau \propto (N/N_e)^3$ for Rouse model), the dependence on chain length is stronger. Similar exponential proportionality has been also shown in other brush penetration experiments.^{49,50} Such phenomena originate from the restricted arm retraction dynamics, which means the center of mass could not move until the polymer chain retracts back from the top. This behavior is similar to the relaxation of branched polymers which was developed the earliest by De Gennes and later used on the explanation of brush dynamic.⁵¹⁻⁵³

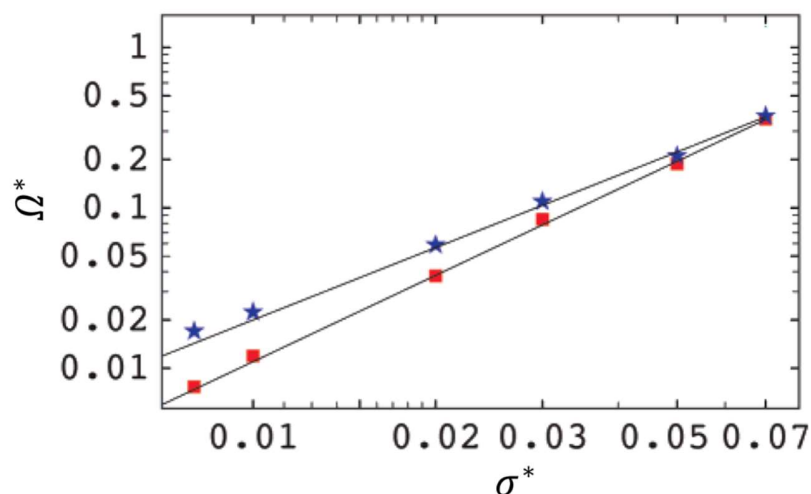


Figure 1.6 Brush entanglement areal density as function of normalized grafting density. Blue star: θ -solvent. Red square: good solvent. Reproduced from ref. 48 with permission from American Chemistry Society.

1.2 Charged Brushes

Charged brushes (referred as polyelectrolyte brush, PEB) have distinct properties compared to their neutral counterparts. In short, additional interactions due to charges

on the chain would have to be considered and this increases the complexity of a PEB structure. Additionally, interactions are greatly different when the surroundings of the PEB is changed. One of the most studied conditions is the addition of electrolyte since it can not only alter the osmotic pressure but also interaction between ions. If the charges on the brush are not permanently associated with certain chemical groups, pH value/salt concentration of its surroundings control the charge ratio and determine their behavior. Such PEBs are referred to as “weak” polyelectrolyte brushes and they have more tunable properties compared to “strong” polyelectrolyte brushes whose charges are associated with strong acid/base groups. Theoretical understanding has been flourishing since the pioneering work of Pincus⁵⁴ but many theories failed when compared to experimental results. For that aspect, this section will focus mainly on the experimental observations of PEBs and the following paragraph is only a brief description of PEB theory. More detailed reviews on PEBs’ theory can be found in other recently published reviews.^{16,55,56}

1.2.1 Theory of Charged Brushes

Figure 1.7 shows the phase diagram of PEB swelling developed by Zhulina *et al.* which managed to describe most observed cases.⁵⁷ A schematic description may be found in Figure 1.1. For the electrolyte-free case (middle diagram), at low dissociation level f , the grafted polymer changes from grafted individual neutral coils (NC) into neutral brushes (NB) as the grafting density increases. For charged polymer brushes, since both inter- and intra-chain repulsive forces increase as f rises, it also makes the state of loose grafted polyelectrolyte transit from NC to Isolated Stick(IS) and then to Oriented Stick

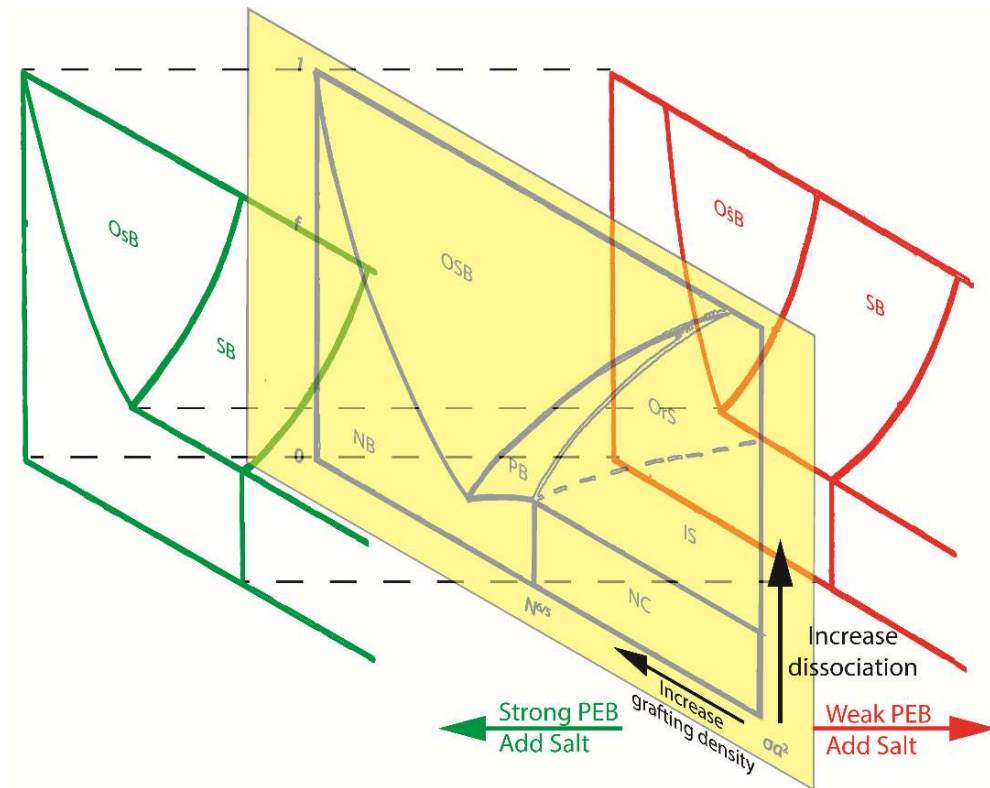


Figure 1.7 PEB phase diagram under different conditions. Black: PEB with no salt added. Green: strong PEB with moderate salt added. Red: weak PEB with moderate salt added. Reproduced ref. 57 with permission from American Chemistry Society.

(OrS) in the progress. Furthermore, the critical grafting density of the mushroom-brush transition also becomes lower. Once inter-chain repulsive force is strong enough, the grafted chains would transit into the brush state called “Pincus Brushes” (PB). PB features the low electrostatic potential which is not strong enough to confine all counterions within the brush and leaves a charged internal state as shown in Figure 1.1. The resulting electrostatic repulsion makes chains stretch more than those in neutral conditions. For PB, the characteristic distribution length of the counterions, the Guoy-

Chapman length ($\lambda_G = \frac{\epsilon_r k_B T}{\sigma f N e^2}$) is therefore larger than the PB brush thickness which could be expressed as follows:

$$h \sim N^3 \sigma f^2 \quad (13)$$

The strength of the electrostatic field increases as the increase of grafting density and extent of dissociation, leading to a decrease of λ_G . When the electrostatic force is strong enough, all counterions are retained in the brush structure and the brush is virtually electroneutral. The increased osmotic pressure within the brush induces strong stretching of the chains and such PEBs are called ‘Osmotic Brushes’(OsB).⁵⁴

The equation for OsB is expressed as:

$$h \sim N f^{1/2} \quad (14)$$

The addition of electrolytes to the PEBs turns them into so called “Salted Brushes” (SB) where the charges are screened. Theory suggests that the transformation happens when the outer electrolyte concentration equals that inside the PEB layer where the osmotic pressure is decreased by penetration of electrolytes.⁵⁴ The scaling of SB is expressed by Eq. 15 and is the same for both strong and weak PEBs.

$$h \sim N \sigma^{1/3} C_s^{-1/3} \quad (15)$$

Here C_s is the concentration of added salt and the threshold of the transition is derived to be at $C_s = \varphi f$. For strong PEBs, the transition between SB and OsB is clearly defined since the extent of dissociation is irrelevant to the salt concentration. For weak PEBs the added salt could increase the extent of dissociation by replacing the associated counterions on the polyelectrolyte chains, which would decrease the concentration of counterions in the brush and thus drive the equilibrium to the right hand side and facilitate dissociation. Theoretical scaling of dissociation is $f \sim (C_s/\sigma)^{2/3}$. Therefore, before the concentration of the salt is enough to penetrate into the PEB and screen the electrostatic interaction, the increased C_s could actually increase the stretching level of the PEB rather than decrease it due to the enhanced electrostatic repulsion between dissociated charges on the chains. The brushes in such state are referred as “O \hat{S} B” to distinguish it from OsB of strong PEBs and the thickness scaling is the following:

$$h \sim N\sigma^{-1/3}C_s^{1/3} \quad (16)$$

One final remark from the diagram is that the PEBs become NB again as the grafting density increases and the transition happens earlier when salt is added. This is because the excluded volume repulsion becomes dominating at high σ values and the balance based again on the steric repulsion and the chain spring recovering force which could be written as Eq. 1.⁵⁸ Naturally, the transition happens earlier for weak PEBs since the electrostatic force is weaker.

1.2.2 Experimental study on Swelling Properties

Swelling properties of the strong PEBs are quite unique among all the other types of brushes. Results from different groups have confirmed that the wet thickness of strong

PEBs, (e.g. PMeVP synthesized by free-radical polymerization) is independent of the grafting density and only proportional to the molecular weight and the square root of the fraction of charged monomers, f .^{29,59,60} Such brushes could be referred to OsB as described in Eq. (14).

Weak PEBs behave in a rather complicated manner since now the charges could be altered in different environments. R uhe *et al.*^{61,39} showed that pH could affect the swelling of a poly(methacrylic acid) (PMAA) brush by affecting its degree of dissociation. The swelling thickness could increase up to 100 times compared to the dry state at pH 10 (20 nm to 2 μ m). Later, Wu *et al.*⁶² conducted experiments on weak PEBs made of poly(acrylic acid) (PAA) and it was found out that the wet thickness versus grafting density behaved similar to neutral brush with power law exponent dependence which was opposite to the prediction of mean field theory (O B, Eq. 16).⁵⁷ As shown in Figure 1.8, wet thickness of the PAA brushes in both O B and SB regimes have similar grafting density power exponents dependence of 1/3. Similar behavior was observed by Lego *et al.*⁶³ and it was suggested that it might originate from low dissociation level for polymers in the brush state as observed in other studies.⁶⁴⁻⁶⁶ The same mechanism was not only predicted by theory^{67,68} but also contributes to the inhomogeneous ionization along the brush. Such behavior is similar to what has been found by Dong *et al.* who

showed that PMAA & PAA brushes have a higher dissociation constant at the surface by comparing pH changes derived from titration and FTIR studies.⁶⁸

1.2.3 Interaction with monovalent electrolytes

Experimental demonstrations have been provided by studies regarding scaling of brush thickness of strong PEBs in solvents of different ion strengths.

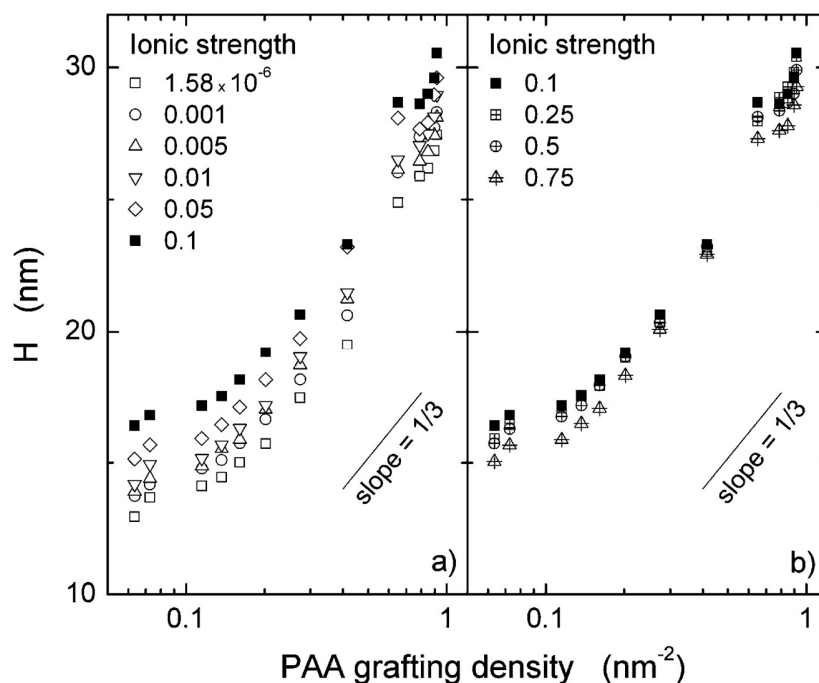


Figure 1.8 Wet thickness at pH = 5.8 for PAA brushes ($M_n = 48000$ g/mol) as a function of the grafting density and ionic strength of the aqueous solution in the (a) osmotic brush (O&B) regime and (b) the salted brush (SB) regime. The symbols represent different ionic strength values. Reproduced from ref. 63 with permission from American Chemistry Society.

Poly(styrenesulfonate, sodium salt) (PSS) brushes were tested at different electrolyte

concentrations and their thickness scaling power exponent was determined to be -0.27 by NR measurement⁵⁹ and -1/3 for SFA measurement⁶⁰. Such deviation could originate from the difference in the measurement technique since brushes were in contact with each other at the time of measurement. Furthermore, a SFA measured force profile fit the theory except for the high compression region where ion concentration inside the brushes was not predicted precisely. The -1/3 power exponent was also obtained by Biesalski *et al.* with cationic poly(N-methyl-4-vinylpyridinium iodide) (PMeVP) brushes and halogen ions.⁶⁹ Interestingly, when the ions were changed from chloride to bromide to iodide, deviation from scaling prediction occurred and even reswelled at high concentrations of iodide. (Figure 1.9c) It was explained as the result of special complex formation between the brush and highly polarizable iodide ions which changed from the neutral state to dissoluble, negatively charged state at higher iodide concentration. Such results were not observed with either chloride or bromide ions as shown in Figure 1.9.

Weak PEBs behaved the same as strong PEBs in the Salted Brush regime. Eq. 15 has been proven in the experimental studies of PAA⁶² and PMAA^{61,70} brushes. Also, weak PEBs behaved as predicted in Eq. 16 at low electrolyte concentration and the sensitivity of the swelling change decreased as either pH values increased or grafting density decreased.^{61,62,70} Similarly, as can be seen in Figure 1.8b, Wu *et al.* showed the slope of the PAA brushes increase at higher salt concentration and the wet thickness decreases.⁶² These could both be explained by the fact that electrolyte gets into the brushes easily at lower grafting density. As electrolyte concentration increases, charge screening starts to

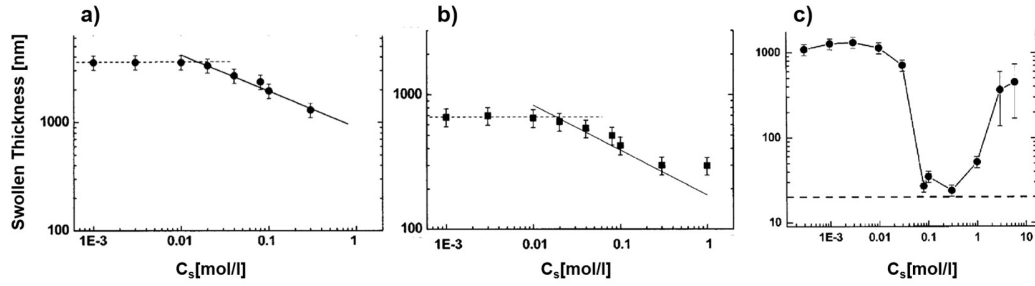


Figure 1.9 Swollen thickness of PMeVP brush as a function of different salt concentration. a) NaCl was used, dry thickness 62 nm. b) KBr was used, dry thickness 21 nm. The solid lines qualitatively represent the scaling law as predicted by mean-field theory, Eq. 15. c) KI was used. Dashed line represents dry thickness 20 nm. Reproduced from ref. 69 with permission from American Institute of Physics.

dominate at $C_{s,max}$ where weak PEBs reach their maximum thickness. This maximum value, $C_{s,max}$ is proportional to the grafting density ($C_{s,max} \sim \sigma$) as predicted⁶⁶ but its value could be lower due to counter-ion condensation.⁶⁰ An interesting aspect of Eq. 14 is that the thickness is a decreasing function of grafting density^{72,73} but it has not yet been observed experimentally. At low salt concentration, the thickness of PAA brushes is proportional to the grafting density but with completely different scaling exponent of $1/3$.⁶²

Lego *et al.* showed that PAA brushes have a unique thickness scaling at pH 9. The power exponent for grafting density increased from 0.87 to 0.96 rather than $1/3$ as the salt concentration increased from 0 to 1×10^{-3} M. In addition, in the Salted Brush regime, it has been shown that $h \sim \sigma^{1.09} C_s^{-0.21}$ and such scaling is different from previous studies.⁷⁴ This was close to the scaling of the Pincus Brush as expressed in Eq. 13.⁵⁴

Although the Pincus Brush has long been developed, very few studies use it due to its narrow regime and complexity. It remains unclear why their brushes behaved like Pincus Brushes rather than those reported in other studies.

1.2.4 Interaction with multivalent electrolytes

Multivalent electrolytes induce completely different structural changes in PEBs depending on their own specific ionic properties. Due to their ability to form complex crosslinks, nature uses them when additional stability is needed.^{77,78} Konradi and R  he on the other hand have conducted a series of studies on weak PEBs, PMAA interacting with multivalent ions.^{75,73} Using FTIR, the relationship between grafting density, complexation and dissociation was quantitatively studied. As the grafting density increased, the degree of complexation decreased as did the level of dissociation. Two geometries of complexation (chelated bidentate/bridging bidentate, Figure 1.10a&b) were observed in PMAA brushes and the amount of complexation showed different dependence on the grafting density. Different ions had different coordination preferences and thus swelling properties. Through comparison with FTIR spectra, it was shown that Cu^{2+} bridging bidentate links could collapse at very low ion concentration of 10^{-6} M and Al^{3+} could induce even stronger collapse at the same concentration. Only alkaline-earth metal ions could reswell the network at high ion concentration similar to the case of PMeVP brushes with iodide ion.⁶⁹ Such trends also followed the reverse order of the ion radius, where $\text{Sr}^{2+} > \text{Ca}^{2+} > \text{Mg}^{2+}$ as shown in Figure 1.10c and is the result of charge inversion. Unexpectedly, the collapse of brushes with Cu^{2+} or Al^{3+} was weaker than the collapse with alkaline-earth metals due to the higher hydrophilicity of

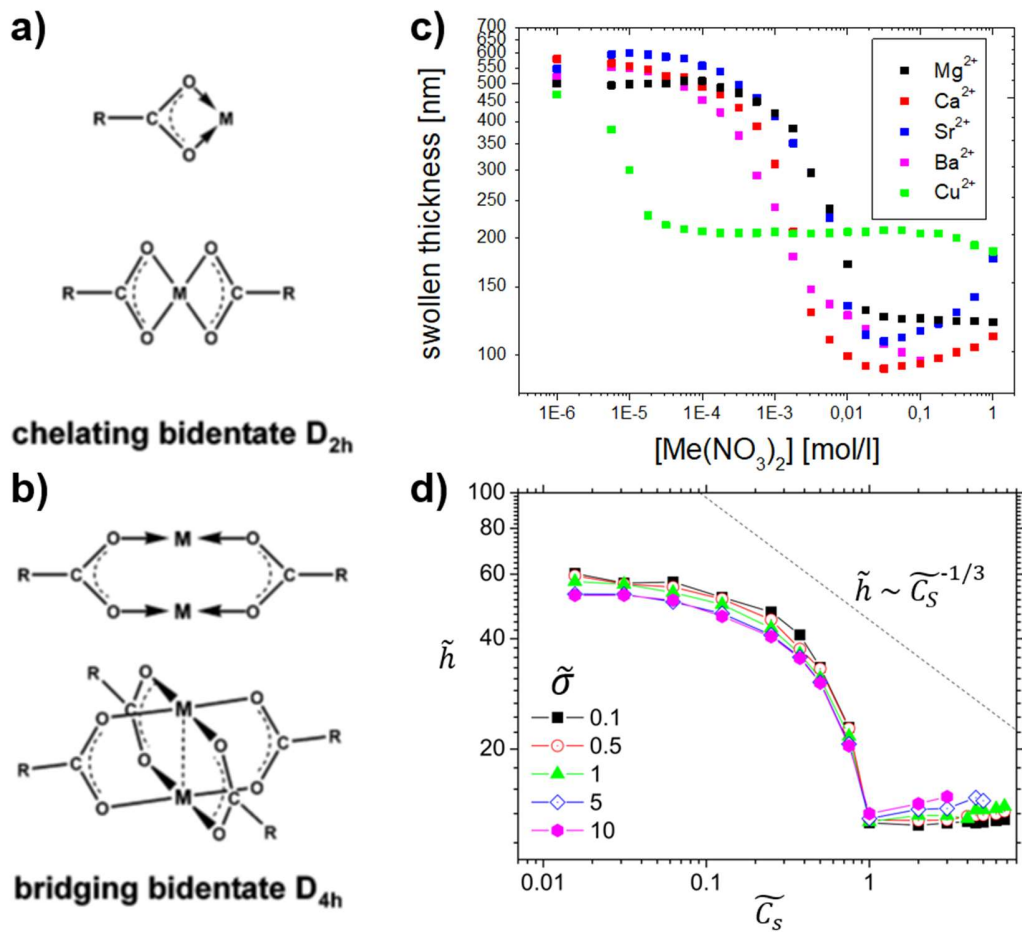


Figure 1.10 a), b) Structure of two complexes between di-valent ions and PMAA brushes. c) Swelling properties of PMAA brushes at different metal ion $Me(NO_3)_3$ concentrations. d) Simulated swelling properties of PEBs with different grafting densities in trivalent ion added medium. Wet thickness, grafting density and salt concentration are expressed in normalized values. $\tilde{C}_s = 1$ is the concentration of ion in the PEB system. Reproduced from ref. 73, 75, 76 with permission from American Chemistry Society and Elsevier.

result observed by Tirrell *et al.* with the same metal ions.⁷⁹ With a proper model, Gupta *et al.* managed to show the similar reswelling for trivalent ions added to a PEB by Langevin dynamics simulation (Figure 1.10d).⁷⁶ Furthermore, it showed that reswelling is stronger at higher grafting density due to the stronger electrostatic repulsion but further experimental proof is still needed.

Tirrell and coworkers conducted studies with PSS brushes soaked in metal ions with different charges at fixed ionic strength.⁷⁹⁻⁸³ Compared to the situation with only monovalent ions, di- or trivalent ions can induce stronger collapse in the SB regime as a result of lower osmotic pressure, and the process happens at lower ion concentration. These multivalent ions may be released only at high monovalent ion concentration. Since the amount of complexation of $\text{Ru}(\text{NH}_3)_6^{3+}$ in PEBs could be quantified by cyclic voltametry (CV), it was confirmed that additional collapse of the brushes was induced by the complexation of $\text{Ru}(\text{NH}_3)_6^{3+}$ and the mechanism of complexation was different at different total ionic strength. At high total ionic strength (SB regime), high concentrations of monovalent ions competed with the trivalent ion and the complexation thus built on the kinetic equilibrium between ions. In contrast, at low total ionic strength, trivalent ions diffused easily into brushes without much competition and achieved saturation. The maximum uptake of the trivalent ion was seen to decrease with an increase in total ionic strength.

Another interesting finding is the appearance of attractive forces between brushes in SFA experiments with brushes on both sides of a gap. CV experiments confirmed ion complexation and brush attraction. Such results were solely observed for multivalent ions ($\text{Ru}(\text{NH}_3)_6^{3+}$ / La^{3+} / Al^{3+} / Ca^{2+}) but not for monovalent ions. The attractive force

induced by La^{3+} could be so strong that the force-distance curve “jump-in” occurred at a shorter distance without increase of compressive force during a compression experiment. By comparing the attractive forces between trivalent ions, it was concluded that $\text{La}^{3+} > \text{Al}^{3+} > \text{Ru}(\text{NH}_3)_6^{3+}$. This trend followed the reverse order of their hydration radius. They pointed out the importance of hydration and charge density in complexation attraction. In addition, such interactions were not observed for brushes at high grafting density with Y^{3+} due to the reduction of chain interpenetration.

The complexation induced structural change was characterized by Yu *et al.* (Figure 1.11a).⁸³ A segmental density profile transition was observed on PSS brushes to evolve from a parabolic form to a Gaussian form when certain multivalent ions were used ($\text{Ca}^{2+}/\text{Ba}^{2+}/\text{Y}^{3+}$), in contrast to the general condition of monovalent ions and Mg^{2+} .^{84,85} The Gaussian-like form was believed to be caused by crosslinking of PSS segments by the multivalent ions which not only give rise to geometric constraints to the chain segments but also effectively decreases the solvent quality and caused the formation of micelle-like structure as described theoretically by Zulina *et al.*⁸⁶ Simulations using Molecular Dynamics (MD) and Density Functional Theory (DFT) have already predicted similar transitions when multivalent ions are added.^{76,87–89} Nevertheless, the physical meaning of the double peak segment density profiles in Ba^{2+} loaded sample was not explained clearly by the authors, although this self-organizing behavior has also been shown in the simulation results at either low temperature⁸⁷ or high grafting density.⁹⁰ Only Jiang *et al.* claimed that the origin of layer-by-layer like structure is due to the energy minimization of complexes. As shown in Figure 1.11b, the complexes formed by polymer chains and trivalent ions have net local charge and

the interaction energy between these complexes force them to separate to reach a minimized energy. This behavior was shown to be more obvious when the size of the ions increases, which fits the experimental result where only the largest ion, Ba^{2+} showed layered structure.⁹⁰

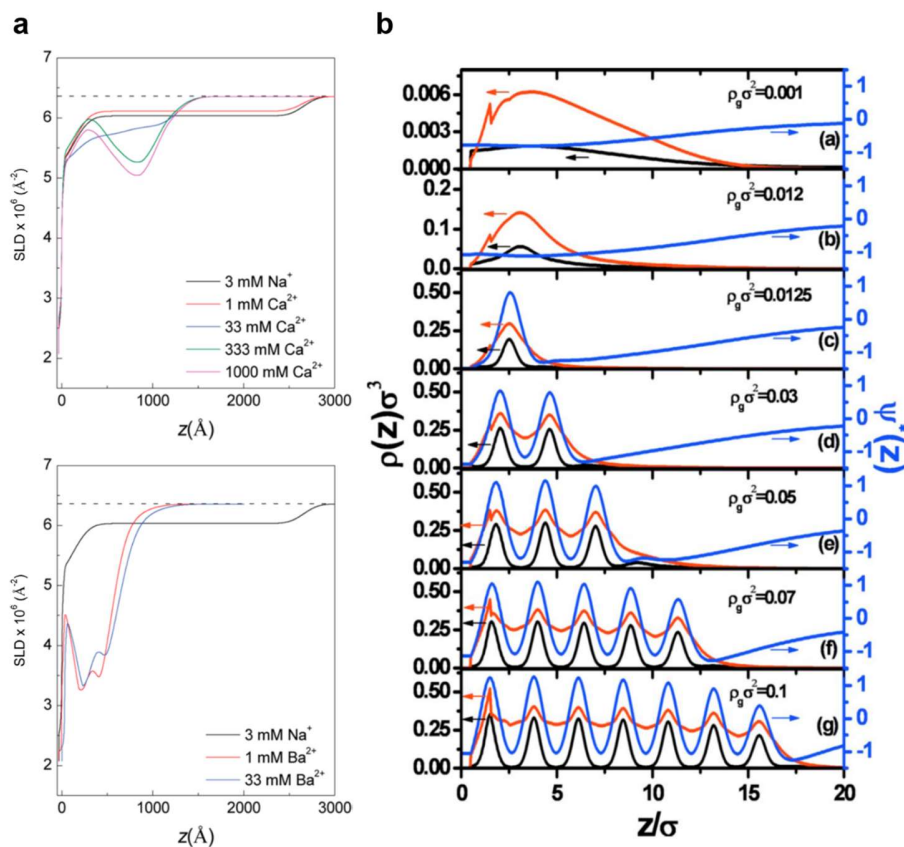


Figure 1.11 Segmental density profile of PEB with multivalent ions added. a) NR scattering length density (SLD) profile of PSS brush with dry thickness 28 nm. SLD is proportional to the local segmental density of polymer. b) Simulation segmental density profiles of counterions (black), polymers (red) in left Y axis, and mean electrostatic potential (blue) in right Y axis in PEBs at different grafting densities. Trivalent cation was used as added ion in model. ρ_g : grafting density, ρ : segment density, σ : unit length in model, Ψ : electrostatic potential. Reproduced from ref. 83, 90

with permission from American Chemistry Society and American Institute of Physics. Quartz Crystal Microbalance with dissipation (QCM-D) studies have also been applied as a useful way to explore the dynamics of PEB complexation. Liu and coworkers characterized the conformations of PSS brushes under complexation by monitoring brush changes.^{91,92} Charge inversion was also observed when Cs^+ , Ca^{2+} and La^{3+} were used as added ions and the reswelling induced by La^{3+} was stronger. Inhomogeneous structures were formed only when multivalent ions were added, and it could be due to incomplete complexation. The study also showed that the hydration level of PEB increases even with dilute salt solution ($<10^{-2}$ M) and leads to a thickness increase for strong PEBs, which is different from the mechanism of weak PEBs. Meanwhile, Che *et al.* proposed that it is caused by the breaking of dipole-dipole interactions with penetration of the ions. In the end it makes a strong PEB thicker, less dense and softer at low salt concentration by breaking physical crosslinks.⁹³ Together with other studies the big picture of brush complexation has been understood much in past years. It could be anticipated that in the future, studies with combination of QCM-D, FTIR, SFA results will continue to offer a better picture of the complete mechanism and structure of PEB complexation.

1.3 Stability of Polymer Brushes

The swelling of polymer brushes depends in very subtle ways on the nature of both the medium and the brush structure as discussed in previous sections. Such morphological variability of the polymer brushes is one of the most important advantages of polymer brushes compared to the other materials. Besides, the linkage

between polymer chains and the interface is generally made of covalent bonds which are quite stable in most of the conditions of human living. However, in 2008 Tugulu *et al.* showed that the poly(oligo(ethylene glycol) methacrylate)(PPEGMA₅₂₆, suffix for monomer molecular weight in g/mol) brushes could delaminate from covalently bonded SiO_x substrate when immersed in cell culture medium. The brush film started to peel off like crosslinked polymeric film buckling under compressive stress⁹⁴ as time passes and full detachment could happen within a day.⁹⁵ Since the crosslinking of the PPEGMA brushes could happen naturally through auto-oxidation during synthesis, this is possible. Interestingly, it was found that crosslinking of the brushes(with oligo(ethylene glycol) dimethacrylate as monomer) did not prevent detachment and the brushes did not detach in water. This observation led to the conclusion that the complexation between poly(ethylene glycol) and metal ions in the cell culture medium was a major reason for enhanced swelling and subsequent degrafting. Since lowering grafting density could effectively increase brush stability, it was claimed that the degrafting mechanism should be similar to the one reported by Sheiko *et al.* that the bottle brushes structure concentrated the force on the backbone and led to C-C bond scission.⁹⁶ Further study by Paripovic and Klok demonstrated that increasing hydrophobicity at the linkage is an effective strategy to increase the stability of the brushes against degrafting.⁹⁷ This could be achieved by either adding additional hydrophobic block at the bottom or increasing the length of the carbon spacer in the initiator, which could survive at least 3 days in aqueous solution with pH = 12. The most recent study from the same group confirmed that both siloxane groups and ester/amide linkages contribute to the degrafting process of polymer brushes by using initiators with only a single group present at a time.⁹⁸

Similar peel-off degrafting phenomena have also been observed by Zhang *et al.* with carboxylated poly(OEGMA₅₂₆-*r*-HEMA) brushes grafted on a QCM-D substrate. When the brushes were transferred from water to phosphate buffered saline(PBS), the brush film peeled off from the QCM surface only when the dry thickness of the brushes was more than 75 nm.⁹⁹ The critical thickness of the degrafting could be varied based on the metals which the thiol bonded to, and it increased with the increase of binding energy. It was subsequently defined to be ~250 nm in terms of wet thickness and the brush degrafting could be achieved by tuning either pH, ion concentration and grafting density irrelevant of chemical composition or structure.^{100,101} In conclusion, the degrafting mechanism depends purely on the mechanochemistry of the Au-S bond but it remains unknown if an ester linkage also contributes.

Nevertheless, Simancus in 2011 in her thesis first reported that the PMeVP brushes could lose most of the brush material even with only water immersion at room temperature.¹⁰² This phenomenon was quite interesting since the greatest tension experienced in a polymer chain of the brushes should be no more than 10 pN based on the theory¹⁰³ and experiment.^{33,34} Unlike tension experienced in bottle brushes(nN level)^{96,103}, this level is much less than the force needed to facilitate the breaking of the covalent bond which is 500 pN.¹⁰⁴ On the other hand, the free energy of a polymer chain in swollen polymer brushes, for example a chain extended to 0.7 of its contour length,

Polymer	Initiators	Comment on stability	Ref:
POEGMA ₅₂₆ PHEMA		<1 days in cell culture medium, Buckling like degrafting	95
Carboxylated poly(OEGMA ₅₂₆ - <i>r</i> -HEMA)		Immediately in PBS, degrafting happened only when $h_{wet} > 250$ nm. Degrafting happened on Au-S only	98 99 100
PEHMA PHEMA PMAA POEGMA ₃₆₀ POEGMEMA ₃₀₀ PEHMA- <i>b</i> -PMAA PMMA- <i>b</i> -PMAA		Additional PMMA/PEHMA block could prevent degrafting. Initiator with higher hydrophobicity could increase stability.	97
POEGMA ₃₆₀ POEGMEMA ₃₀₀		All brushes degrafted in cell culture medium. No obvious difference could be observed in the stability between brushes with different initiators.	98
PMeVP		Lost all materials in room temperature water immersion in 2 h	102
PMAA		Stability of ester-linked brushes are weaker against hydrolysis than amide-linked brushes.	103 105
PDMA		Neutral brushes degrafted faster at higher grafting density and molecular weight.	104

Table 1.1 Summary of studies of degrafting phenomena in polymer brushes. PEHMA: poly(2-ethylhexyl methacrylate), POEGMEMA: poly[oligo(ethylene glycol) methyl ether methacrylate].

per bond and is considerably less than the bond energies which are generally more than 300 kJ/mol. Bond homolysis is not possible in the context and other mechanism must be considered.

In subsequent years, more literature came to point to the same conclusion that the polymer brushes are not as stable as expected before. Galvin *et al.* studied the addition of monovalent cations to a PMAA in an aqueous environment which leads initially to stronger swelling as the salt concentration increases. Nonetheless, the authors only proved that the linkage(ester/amide) determines the stability of the PMAA brushes based on the hydrolysis stability, namely, the brushes with amide-linked initiator is more stable than the one with ester-linked initiator¹⁰⁶ This is different from what's observed by Ataman *et al.* where they showed not much difference in degrafting of bottle brushes.⁹⁸ The addition of more salt then leads to a maximum in swelling after which it decreases. These results can be explained by an initially increasing dissociation of the acid groups and a later dominating shielding of the charges, which renders the brush less charged. Melzak *et al.* have studied poly(N,N-dimethylacrylamide)(PDMA) brushes under basic conditions and showed an accelerated degrafting rate at either higher molecular weight or grafting density.¹⁰⁷ This result is surprising since the accelerating effect of the molecular weight was more prominent than grafting density. In another study, Borozenko monitored the effect of pH and temperature on the degrafting behavior of polyacrylic acid using fluorescence methods.¹⁰⁸ Only with added NaCl and a pH > 9.5 was brush scission observed. Furthermore, there are two other works which reported the degrafting of the strong PEB¹⁰⁹ and the zwitterionic brushes.¹¹⁰ It was revealed that the degrafting of poly[(2-(methacryloyloxy)ethyl)

trimethylammonium iodide] (PMETAI) and poly(2-(dimethylamino)ethyl methacrylate) (PDMAEMA) brushes are due to the hydrolysis of an ester linkage in the initiator only and siloxane is not involved. The study on zwitterionic brushes – poly(cysteine methacrylate)(PCSMA) brushes did not focus on the degrafting phenomena therefore no further detail could be solicited. Table 1 summarizes current studies on the degrafting phenomena in polymer brushes. It could be seen that most studies focus on neutral or weakly charged polymer brushes.

1.4 Patterned Polymer Brushes

1.4.1 Fabrication of Patterned Polymer Brushes.

Patterned brushes are useful in many applications when the specific dimension is needed to create specific functions. Patterned brushes due to their surface-attached properties could have unique responsive properties compared to other patterned polymers. Generally patterned brushes are created by either “bottom-up” or “top-down” and they have their own distinct advantages.

The “bottom-up” patterning process creates patterned moieties first and then polymer is grown upon them. Since polymer growth is the last step, contamination is reduced to a minimum. UV photolithography was used by Dong *et al.* to create patterned photoresist as the templates for initiator back-filling at the sub- μm level^{111,112}. The patterned brushes showed good biocompatibility and promising results as a platform for either immobilization of protein or directed growth of neural cells. Similar patterning processes have later been applied using e-beam lithography(EBL) and the pattern size was further reduced to 200 nm by Chen *et al.*¹¹³ EBL was also used by Jonas *et al.* to

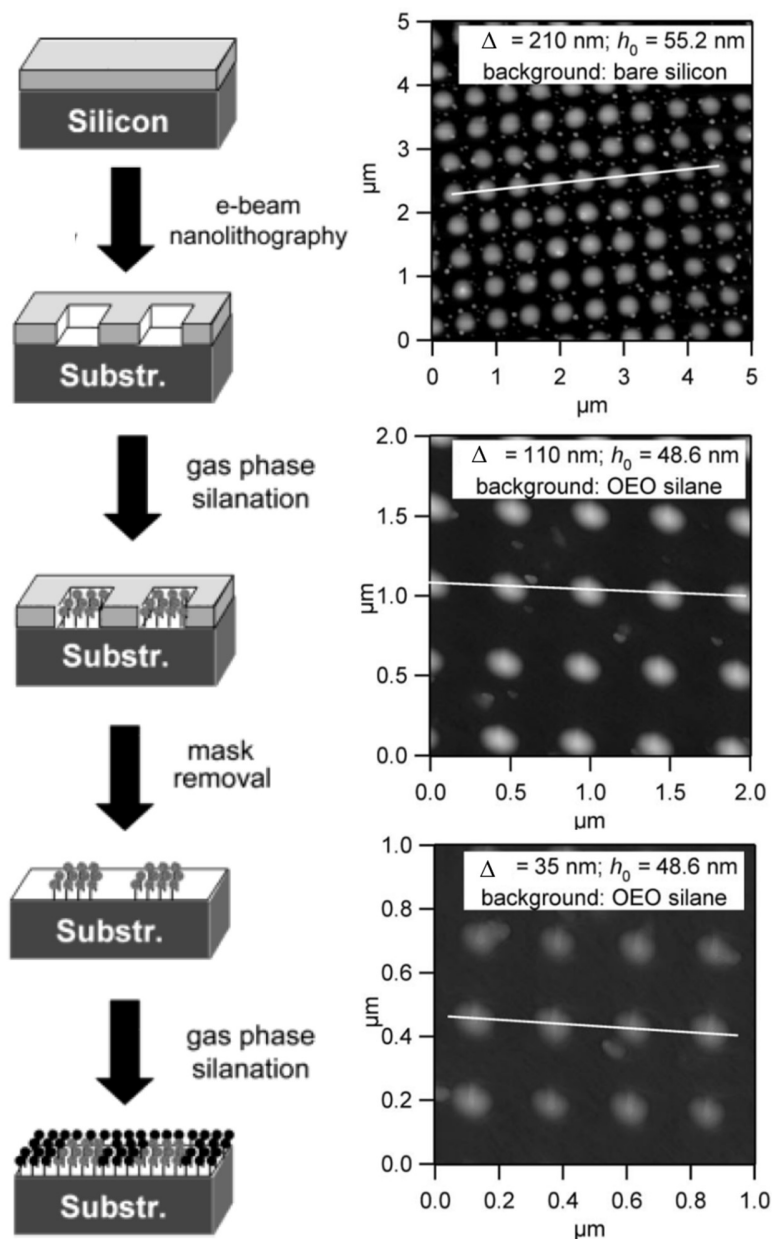


Figure 1.12 Schematic Description and AFM scanning results of the Fabrication of Nanopatterned PMEO₂MA Brushes. Δ : pattern sizes. h_0 : Non-patterned brush height. OEO: oligo(ethylene oxide) Reproduced from ref. 114, 115 with permission from American Chemistry Society.

create patterned poly(2-(2-methoxyethoxy)ethyl methacrylate)(PMEO₂MA) down to 20 nm by back-filling vapor initiator. (Figure 1.12)^{114,115} Another study by Zauscher *et al.*

deposited a thin gold film to create chemical contrast as sites for the growth of patterned brushes.¹¹⁶ However, the presence of an additional gold layer could not trouble for the fundamental study of latter process integration. Even without photoresist, direct initiator removal could be done with UV interferometric lithography¹¹⁷ and EBL¹¹⁸ to reach nano-scale pattern dimensions. But patterns made by UV interferometric lithography would have a grafting density gradient in the pattern due to the nature of technique. In addition, pre-filled small molecules could also be patterned as a template for following pattern formation. With the lithography process, those small molecules could be either removed to expose reaction sites with an AFM tip^{119,120} or directly reacted to form chemical groups for grafting/chain growth.^{121–123} Jordan *et al.* fabricated patterned templates on a surface with EBL which created thin layers of hydrocarbon (<2 nm) for the later initiator grafting.^{124,125} This process has the advantage that no prior preparation is needed. Control of the initiator grafting density is possible through the change of the lithographic parameters.^{119,120,124} On the other hand, initiators could be directly grafted by microcontact printing to create patterned initiators at the μm level with low cost¹²⁶. Another unique patterning process uses light-mediated polymerization which permits reaction only in the light-exposed area and permits chances to more complex patterning.^{127–129} It has been proven that this could be used to form patterned di-block copolymer brushes with the poly(2-(methylthio)ethyl methacrylate) as a first block grown on the entire surface and poly(2,2,2-trifluoroethyl methacrylate) as a second block grown on selected areas.¹²⁹ Furthermore, with the control of light energy, a polymer brush gradient was also shown to be possible.¹²⁸

“Top-down” patterning processes in contrast created patterns on pre-synthesized polymer brushes directly. Rastogi *et al.* firstly noticed that the possibility of using EBL to directly pattern certain methacrylate brushes. It has been shown that the solvent used to remove degraded brushes were quite important since poor choice of solvent could dissolve polymer too much and deteriorate the pattern profile¹³⁰ In further study, by the application of supercritical carbon dioxide, a broadening of the line was reduced from 88% to 56% compared to the tetrahydrofuran(THF) development.¹³¹ Furthermore, it has been proven that EBL could create nanochannel PS-*b*-PMMA diblock copolymer brushes due to specific degradation of PMMA blocks.¹³² A few more general methods were developed by design of brush initiators. Two different UV-cleavable initiators were developed and the brushes grown on them were successfully patterned to give patterns with μm scale features.^{133,134} With the same idea, cleavable groups could be combined into a functional group and used to create chemical contrast after UV exposure.¹³⁵ Although no further attempt was made, patterns of sub- μm level should be possible with an appropriate photolithography tool. With high enough energy(75W lamp for 300 sec), poly(*N*-isopropylacrylamide (PNIPAM) brushes have been directly removed with UV lithography.¹³⁶ However, this technique is very chemistry dependent and no nanopattern can be achieved with such strong exposures. Other than those lithography-based methods, AFM was adapted by Chi *et al.* to create patterned brushes by direct scratching and lines with 100 nm resolution were obtained.¹³⁷ Traditional ideas of the semiconductor industry which transfers lithographic patterns through oxygen plasma has also been applied to create patterned brushes by Chen *et al.*¹³⁸ With designed grafting patterns, patterned brushes showed colorimetric signals due to changes of the

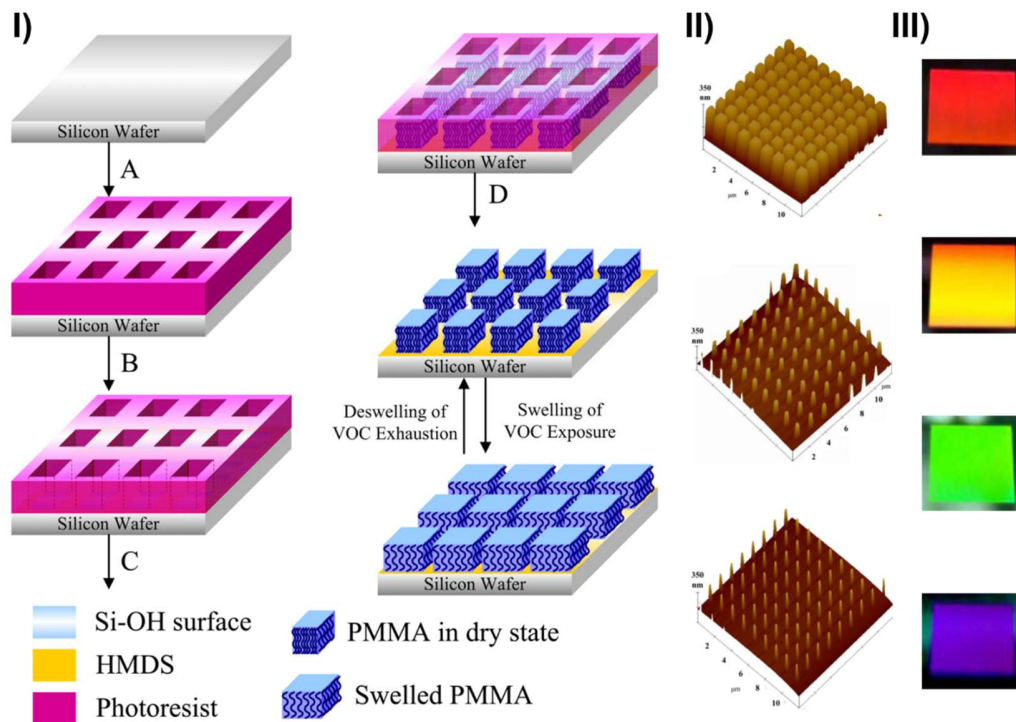


Figure 1.13. I) Fabrication process for top-down patterned brushes for the detection of vapor organic compounds(VOC). A): Coat hexamethyldisilazane(HMDS) and then EBL pattern. B) Oxygen plasma treatment to remove exposed HMDS. C) surface-initiated polymerization to grow PMMA brushes. D) Solvent treatment to remove photoresist. The behavior of the patterns under different solvent treatments (solvent quality decreased from top to bottom) are shown in II) AFM scan and III) Photographic images. Reproduced from ref. 142 with permission from American Institute of Physics.

brush morphologies and this idea gave rise to a series of different sensors based on patterned brushes. As for now, patterned brushes have been used for thermal sensors with PNIPAM brushes¹³⁹, pH sensors with poly(2-dimethylaminoethyl methacrylate) (PDMAEMA) brushes^{138,140}, copper sensors with polyacrylonitrile(PAN) brushes¹⁴¹ and

organic solvent sensors with PMMA brushes(Figure 1.13).¹⁴² All these sensors could conduct reversible morphological changes under differently designed conditions and they all benefited from the fact that the morphological change of polymer brushes is more sensitive to environmental stimuli. Since all processes could be modified to work with standard semiconductor fabrication technologies, these top-down patterned polymer brushes could be easily put into mass production.

1.4.2 Fundamental understanding of patterned polymer brushes

The 2D stretching nature of the polymer brushes is due to the presence of neighboring polymer chains. When these chains are removed, the polymer chains are no longer forced to stretch upward, and they could freely explore the free space nearby.

In the end the patterned brushes will become an already stretched, lens-like shape and their thickness decreases from the center of the patterns.^{143,144} Patra *et al.* are the first to try explaining the theoretical behavior of line patterned brushes with an MD model.¹⁴³ It was found that the scaling law for the center thickness of patterned brushes still follows the one for non-patterned brushes(Eq. 2). After normalization with non-patterned brush thickness, the decrease of the center thickness could all be described with one uniform function of the pattern size Δ and size of the chain(contour length, proportional to N), $\tilde{h}(\frac{\Delta}{N})$. As shown in Figure 1.14, the beginning of the center thickness decrease, happens at $\frac{\Delta}{N} \sim 4$ and marks the transition from 2D stretching to 3D stretching, where the center steric repulsion is not strong enough to hold it as before. On the other hand, the extra width of the pattern w_{ex} (amount of brush extends over the edge of the

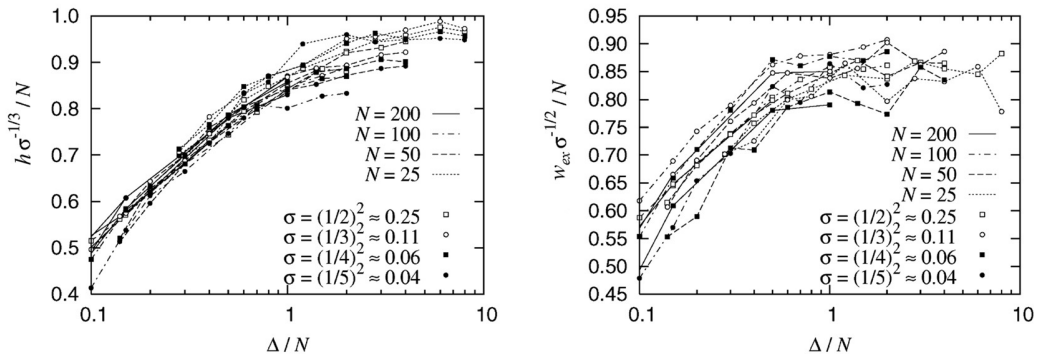


Figure 1.14. Rescaled height (left) and width (right) as a function of reduced stripe width for polymer brushes with different molecular weights and grafting densities. Here all the numbers are normalized to the size of the coarse-grained monomer size. Reprinted from ref. 143 with permission from American Chemistry Society.

stripe on each side) is proportional to the $N\sigma^{1/2}$ instead and follow another uniform function, $\tilde{w}(\frac{\Delta}{N})$. The authors claimed that the additional increase of the w_{ex} with σ is due to the inclination of the chains since polymer chains are pushed farther at higher grafting density. The scaling law was later partly proven experimentally by Lee *et al.* by measuring the dry morphology of patterned PNIPAM brushes with AFM.¹⁴⁴ However, due to the difference of the environment (dry vs. wet) and the lack of precise measurement on grafting density, only qualitative agreement could be achieved under certain assumptions. The dry morphology of patterned brushes was then studied further by Huck *et al.*¹¹⁵ It was showed that since a larger fraction of the brushes interact with free, hydrophilic space nearby as Δ shrinks, PMEO₂MA, PNIPAM brush thickness decreases more than the model which counts only entropy effects. For PS brushes the thickness was higher due to the unfavorable hydrophilic/hydrophobic interaction.¹⁴⁵ Quantitative agreement between the model and experimental data could be achieved.

Also, the thermoresponsive behavior of PNIPAM brushes was studied later in patterned form. It was surprising to see that the responsiveness, defined by the center thickness ratio in the wet state over dry state, was the largest for the smallest patterns. Also, the transition at low critical solution temperature(LCST) became broader as a decrease of pattern size. This could be understood with the reference to the fact that the LCST of the PNIPAM brushes decreases with the lowered grafting density and the responsiveness is the highest for the medium grafting density.^{146,147} Smaller patterns are composed of less stretched polymer chains with different tension from center to the edge. Because of it, those less stretched chains could respond further to stimuli at lower LCST while the more stretched chains would do the opposite. As mentioned previously, the change from free polymer to the polymer brush form amplifies the morphology change due to dense grafting. However, since the ‘real’ entropy spring resistance force increases faster than linear proportionality(which is the ideal condition in Eq. 1)¹⁰⁵, overstretched chains in brushes of higher grafting density would have only limited response to stimuli. Solvent induced morphological change on patterned brushes was also studied in both simulation¹⁴⁸ and experiments.^{113,149,150} However, the morphological change result was completely opposite between them and needs further investigation. Interestingly, until now there is only work discussing the behavior of patterned PEB. The patterned random copolymer PEB, PNIPAM-*r*-PMAA. Since patterned PEB had 40 nm gold on the bottom layer, only wet thickness comparison was done under different pH and salt conditions. The PEB showed a larger thickness at larger patterns when using pH and monovalent salt as stimuli.¹⁵¹ In the swollen state, pH = 9.0 and 0 – 0.02 M potassium chloride (KCl), the larger patterns have higher thickness. On the contrary, at both pH =

4.0 and 0.2 M KCl solutions, the thickness of all patterns was the same due to the collapse of PEB. This is interesting since the scaling of the thickness along patterns of different sizes should still exist at either SB (when using salt as stimuli) or neutral brush in poor solvent (when using pH as stimuli). This could be due to the decrease of the threshold for 2D to 3D stretching

to even smaller pattern sizes than what's reported in the literature.

1.5 Summary

Following the understanding of polymer brushes, increasing numbers of novel applications make use of their novel stimuli-responsive properties and their special mechanical behaviors due to steric repulsion. The transition of stretching of polymer brushes in small patterns showed promising tunable behavior as complex nanomaterials especially suitable for the micro/nano-electromechanical systems (MEMS/NEMS). However, in order to fully utilize those properties, two issues have to be solved beforehand. First, the understanding on the behavior of the patterned brushes are still quite poor. Most of the studies provide only qualitative comparison and focus on the morphology of neutral brushes and many of the results are contradictory. In addition, there are only few reports that have studied patterned PEBs which have a better response due to the presence of the charges. Second, the stability issue, even though it has been solved to some extent, has not yet been well explained, especially considering the origin of chain scission. For bottle brushes it is easily understood that the tension focused on the origin could trigger the bond scission, but the situation gets more complex in the normal brush form. Also, some other aspects of polymers such as entanglement and

chain dynamic have not been considered yet in the degrafting phenomena. If the degrafting is absolutely caused by physical chain swelling, those physical factors should also be included in the discussion.

To tackle those issues mentioned above, a series of investigations were conducted. Chapter 2 describes the development of different patterning processes based on fluorinated materials in order to achieve process orthogonality. Two application-orientated prototypes biosensors and liquid crystal actuators are then fabricated based on this technique. Chapter 3 describes the investigation of morphological behavior of the patterned neutral brushes. Through solvent treatment and surface modification, the morphology of the patterned brushes is studied in detail and this could be the foundation of future device design. The stability issue of the polyelectrolyte brushes is discussed in Chapter 4 and 5 with two different polymer brushes. In chapter 4, short chain, high grafting density poly[(2-(methacryloyloxy)ethyl) trimethylammonium chloride] (PMETAC) brushes were synthesized and test in patterned form. It was found that as the pattern size shrinks the stability increases as a result of the enhanced free stretching on the edge of the pattern. However, for brushes with long chains, low grafting density PMeVP brushes showed completely opposite trends during the degrafting test. In subsequent investigations shown in Chapter 5, with our collaborators we proved that the stability of the brushes is also determined by physical factors such as crosslinking, entanglement and chain dynamics. A model combining all these parameters could predict the degrafting trend of the brushes successfully.

Chapter 6 on the other hand focuses on the fabrication of silicon grafting that would allow the polymer brushes to grow on the sidewall only. This special design could allow

simultaneous neutron and laser scattering characterizations possible and provide precious information in both macroscopy and nanoscopy. Finally, Chapter 7 discusses the future of polymer brushes as a next-generation material and a specific example which produces a biomimetic surface coating will be presented.

REFERENCES

1. Adsorption of chain molecules with a polar head a scaling description. *J. Phys.* **38**, 983–987 (1977).
2. Scaling theory of polymer adsorption. *J. Phys.* **37**, 1445–1452 (1976).
3. Conformations of Polymers Attached to an Interface. *Macromolecules* **13**, 1069–1075 (1980).
4. Collapse of grafted chains in poor solvents. *J. Phys.* **49**, 547–550 (1988).
5. Halperin, A. & Zhulina, E. B. Stretching Polymer Brushes in Poor Solvents. *Macromolecules* **24**, 5393–5397 (1991).
6. Birshtein, T. M. & Zhulina, E. B. Conformations of star-branched macromolecules. *Polymer* **25**, 1453–1461 (1984).
7. Zhulina, E. B., Borisov, O. V., Pryamitsyn, V. A. & Birshtein, T. M. Coil-Globule Type Transitions in Polymers. 1. Collapse of Layers of Grafted Polymer Chains. *Macromolecules* **24**, 140–149 (1991).
8. Polymer brush at high coverage. *Macromolecules* **24**, 4981–4982 (1991).

9. Configuration of terminally attached chains at the solid/solvent interface: self-consistent field theory and a Monte Carlo model. *Macromolecules* **20**, 1692–1696 (1987).
10. Milner, S. T., Witten, T. A. & Cates, M. E. Theory of the Grafted Polymer Brush. *Macromolecules* **21**, 2610–2619 (1988).
11. Milner, S. T. Compressing Polymer “Brushes”: a Quantitative Comparison of Theory and Experiment. *EPL Europhys. Lett.* **7**, 695 (1988).
12. Milner, S. T., Witten, T. A. & Cates, M. E. Effects of Polydispersity in the End-Grafted Polymer Brush. *Macromolecules* **22**, 853–861 (1989).
13. Structure of densely grafted polymeric monolayers. *Polym. Sci. USSR* **30**, 1706–1715 (1988).
14. To the theory of superstructures in concentrated solutions of block copolymers. *Polym. Sci. USSR* **31**, 196–205 (1989).
15. Semenov, A. N. Contribution to the theory of microphase layering in block-copolymer melts. *Zh Eksp Teor Fiz* **88**, 1242–1256 (1985).
16. Polyelectrolyte brushes: theory, modelling, synthesis and applications. *Soft Matter* **11**, 8550–8583 (2015).
17. Zhulina, E. B. & Borisov, O. V. Structure and interaction of weakly charged polyelectrolyte brushes: Self-consistent field theory. *J. Chem. Phys.* **107**, 5952–5967 (1997).

18. Barsanti L., G. P. *Second edition*. (2014). doi:10.1007/s007690000247
19. Huang, L., Huang, Y. & Li, X. F. Approximate solution of Abel integral equation. *Comput. Math. Appl.* **56**, 1748–1757 (2008).
20. Polymer Brushes. *Science* **251**, 905–914 (1991).
21. A quantitative study of tethered chains in various solution conditions using Langmuir diblock copolymer monolayers. *Macromol. Rapid Commun.* **21**, 243–270 (2000).
22. Formation and Properties of Anchored Polymers with a Gradual Variation of Grafting Densities on Flat Substrates. *Macromolecules* **36**, 2448–2453 (2003).
23. On the Structure and Pressure of Tethered Polymer Layers in Good Solvent. *Macromolecules* **28**, 3197–3204 (1995).
24. Onsets of Tethered Chain Overcrowding and Highly Stretched Brush Regime via Crystalline–Amorphous Diblock Copolymers. *Macromolecules* **39**, 641–650 (2006).
25. Brittain, W. J. & Minko, S. A structural definition of polymer brushes. *J. Polym. Sci. Part Polym. Chem.* **45**, 3505–3512 (2007).
26. Observing the Mushroom-to-Brush Transition for Kinesin Proteins. *Langmuir* **29**, 15142–15145 (2013).
27. Forces between surfaces of block copolymers adsorbed on mica. *J. Am. Chem. Soc.* **108**, 2869–2876 (1986).

28. Polymeric amphiphiles at solid-fluid interfaces: Forces between layers of adsorbed block copolymers. *Proc. Natl. Acad. Sci.* **84**, 4725–4728 (1987).
29. Scaling Laws for the Swelling of Neutral and Charged Polymer Brushes in Good Solvents. *Macromolecules* **35**, 499–507 (2002).
30. Solvent Quality Effects on Scaling Behavior of Poly(methyl methacrylate) Brushes in the Moderate- and High-Density Regimes. *Langmuir* **27**, 3698–3702 (2011).
31. Characterization of the brush regime for grafted polymer layers at the solid-liquid interface. *Phys. Rev. Lett.* **66**, 719 (1991).
32. Surface force measurements of polystyrene-block-poly (ethylene oxide) adsorbed from a nonselective solvent on mica. *Macromolecules* **24**, 3383–3387 (1991).
33. Surface Interaction Forces of Well-Defined, High-Density Polymer Brushes Studied by Atomic Force Microscopy. 2. Effect of Graft Density. *Macromolecules* **33**, 5608–5612 (2000).
34. Surface Interaction Forces of Well-Defined, High-Density Polymer Brushes Studied by Atomic Force Microscopy. 1. Effect of Chain Length. *Macromolecules* **33**, 5602–5607 (2000).
35. Neutron reflectivity studies of polymers adsorbed on mica from solution. *Macromolecules* **24**, 94–98 (1991).

36. Determination of end-adsorbed polymer density profiles by neutron reflectometry. *Macromolecules* **25**, 434–439 (1992).
37. Structure of bimodal polymer brushes in a good solvent by neutron reflectivity. *Macromolecules* **29**, 2843–2849 (1996).
38. Concentration profiles in densely tethered polymer brushes. *Macromolecules* **31**, 3731–3734 (1998).
39. Segment density profiles of polyelectrolyte brushes determined by Fourier transform ellipsometry. *J. Chem. Phys.* **111**, 7029 (1999).
40. On the swelling behavior of linear end-grafted polystyrene in methanol/toluene mixtures. *Colloid Polym. Sci.* **282**, 939–945 (2004).
41. Neutron Reflectivity Study of Free-End Distribution in Polymer Brushes. *Macromolecules* **42**, 6209–6214 (2009).
42. Is Osmotic Pressure Relevant in the Mechanical Confinement of a Polymer Brush? *Macromolecules* **48**, 2224–2234 (2015).
43. Measurement of forces in symmetric and asymmetric interactions between diblock copolymer layers adsorbed on mica. *Macromolecules* **26**, 6455–6466 (1993).
44. Relationship between Interfacial Forces Measured by Colloid-Probe Atomic Force Microscopy and Protein Resistance of Poly(ethylene glycol)-Grafted Poly(L-lysine) Adlayers on Niobia Surfaces. *Langmuir* **21**, 6508–6520 (2005).

45. Neutron Reflectivity Study on the Postpolymerization Modification of Poly(2-hydroxyethyl methacrylate) Brushes. *Macromolecules* **44**, 6868–6874 (2011).
46. Critical dynamics of a polymer chain in a grafted monolayer. *Macromolecules* **24**, 1549–1553 (1991).
47. Repulsive Forces and Relaxation on Compression of Entangled, Polydisperse Polystyrene Brushes. *Macromolecules* **33**, 3860–3870 (2000).
48. Entanglements of an End-Grafted Polymer Brush in a Polymeric Matrix. *Macromolecules* **40**, 8389–8395 (2007).
49. Chennevière, A. *et al.* Quantitative analysis of interdigitation kinetics between a polymer melt and a polymer brush. *Macromolecules* **46**, 6955–6962 (2013).
50. Geoghegan, M. *et al.* The kinetics of penetration of grafted polymers into a network. *Macromolecules* **32**, 5106–5114 (1999).
51. De Gennes, P. & De Gennes, P. G. Reptation of stars. *J. Phys.* **36**, 1199–1203 (1975).
52. Klein, J. Dynamics of Entangled Linear, Branched, and Cyclic Polymers. *Macromol. Mol Cryst Liq Cryst Polym Prepr Am Chem SOC Div Polym Chem Anal. Polym. Syst. Burk Allen N Eds Appl. Sci. X-Ray Diffr. Methods Polym. Sci. J Org Chem* **193435**, 105–118 (1986).

53. Witten, T. A., Leibler, L. & Pincus, P. A. Stress Relaxation in the Lamellar Copolymer Mesophase. *Macromolecules* **23**, 824–829 (1990).
54. Colloid stabilization with grafted polyelectrolytes. *Macromolecules* **24**, 2912–2919 (1991).
55. Polyelectrolyte brushes. *Curr. Opin. Colloid Interface Sci.* **11**, 316–323 (2006).
56. Theoretical Approaches to Neutral and Charged Polymer Brushes. in **198**, 149–183 (Springer-Verlag, 2006).
57. Zhulina, E. B., Birshtein, T. M. & Borisov, O. V. Theory of Ionizable Polymer Brushes. *Macromolecules* **28**, 1491–1499 (1995).
58. Borisov, V., Zhulina, E. B. & Birshtein, T. M. Diagram of the States of a Grafted Polyelectrolyte Layer. 9
59. Determination of the Structure of Polyelectrolyte Brushes. *Macromolecules* **32**, 8952–8964 (1999).
60. A Study of Polyelectrolyte Brushes Formed from Adsorption of Amphiphilic Diblock Copolymers Using the Surface Forces Apparatus. *Macromolecules* **35**, 9480–9486 (2002).
61. Synthesis and swelling behavior of a weak polyacid brush. *J. Chem. Phys.* **117**, 4988–4994 (2002).

62. Behavior of surface-anchored poly (acrylic acid) brushes with grafting density gradients on solid substrates: 1. Experiment. *Macromolecules* **40**, 8756–8764 (2007).
63. Lego, B., Skene, W. G. & Giasson, S. Swelling Study of Responsive Polyelectrolyte Brushes Grafted from Mica Substrates: Effect of pH, Salt, and Grafting Density. *Macromolecules* **43**, 4384–4393 (2010).
64. Biesalski, M., Johannsmann, D. & R uhe, J. Synthesis and swelling behavior of a weak polyacid brush. *J. Chem. Phys.* **117**, 4988–4994 (2002).
65. Zhang, H. & R uhe, J. Swelling of Poly(methacrylic acid) Brushes: Influence of Monovalent Salts in the Environment. *Macromolecules* **38**, 4855–4860 (2005).
66. Wu, T. *et al.* Behavior of surface-anchored poly (acrylic acid) brushes with grafting density gradients on solid substrates: 1. Experiment. *Macromolecules* **40**, 8756–8764 (2007).
67. Zhulina, E. B., Birshtein, T. M. & Borisov, O. V. Theory of ionizable polymer brushes. *Macromolecules* **28**, 1491–1499 (1995).
68. Dong, R., Lindau, M. & Ober, C. K. Dissociation Behavior of Weak Polyelectrolyte Brushes on a Planar Surface. *Langmuir* **25**, 4774–4779 (2009).
69. Electrolyte-induced collapse of a polyelectrolyte brush. *J. Chem. Phys.* **120**, 8807 (2004).

70. Swelling of Poly(methacrylic acid) Brushes: Influence of Monovalent Salts in the Environment. *Macromolecules* **38**, 4855–4860 (2005).
71. On the theory of grafted weak polyacids. *Macromolecules* **27**, 3087–3093 (1994).
72. Polyacrylic acid brushes: surface pressure and salt-induced swelling. *Langmuir* **16**, 8324–8333 (2000).
73. Interaction of Poly(methacrylic acid) Brushes with Metal Ions: An Infrared Investigation. *Macromolecules* **37**, 6954–6961 (2004).
74. Swelling Study of Responsive Polyelectrolyte Brushes Grafted from Mica Substrates: Effect of pH, Salt, and Grafting Density. *Macromolecules* **43**, 4384–4393 (2010).
75. Interaction of Poly(methacrylic acid) Brushes with Metal Ions: Swelling Properties. *Macromolecules* **38**, 4345–4354 (2005).
76. Gupta, V. S. & Hsiao, P.-Y. Polyelectrolyte brushes in monovalent and multivalent salt solutions. *Polymer* **55**, 2900–2912 (2014).
77. Polymer physics of the cytoskeleton. *Curr. Opin. Solid State Mater. Sci.* **15**, 177–182 (2011).
78. Specificity of metal ion cross-linking in marine mussel adhesives. *Chem. Commun.* **0**, 1672–1673 (2003).

79. Polyelectrolyte Brushes at Interfaces: Properties, Structure and Interactions. (2005).
80. Brushes of strong polyelectrolytes in mixed mono- and tri-valent ionic media at fixed total ionic strengths. *Soft Matter* **9**, 10458 (2013).
81. Reversible Adhesion with Polyelectrolyte Brushes Tailored via the Uptake and Release of Trivalent Lanthanum Ions. *J. Phys. Chem. C* **119**, 14805–14814 (2015).
82. The effect of multivalent counterions to the structure of highly dense polystyrene sulfonate brushes. *Polymer* **98**, 448–453 (2016).
83. Structure of Polyelectrolyte Brushes in the Presence of Multivalent Counterions. *Macromolecules* **49**, 5609–5617 (2016).
84. X-ray Reflectivity Study of the Effect of Ion Species on Nanostructure and Its Transition of Poly(styrenesulfonate) Brush at the Air/Water Interface. *Chem. Lett.* **41**, 1060–1062 (2012).
85. Structure and Collapse of a Surface-Grown Strong Polyelectrolyte Brush on Sapphire. *Langmuir* **28**, 3187–3193 (2012).
86. Zhulina, E., Singh, C. & Balazs, A. C. Behavior of tethered polyelectrolytes in poor solvents. *J. Chem. Phys.* **108**, 1175–1183 (1998).

87. He, G.-L., Merlitz, H. & Sommer, J.-U. Molecular dynamics simulations of polyelectrolyte brushes under poor solvent conditions: Origins of bundle formation. *J. Chem. Phys.* **140**, 104911 (2014).
88. Carrillo, J.-M. Y. & Dobrynin, A. V. Morphologies of Planar Polyelectrolyte Brushes in a Poor Solvent: Molecular Dynamics Simulations and Scaling Analysis. *Langmuir* **25**, 13158–13168 (2009).
89. Jiang, T. & Wu, J. Ionic Effects in Collapse of Polyelectrolyte Brushes. *J. Phys. Chem. B* **112**, 7713–7720 (2008).
90. Jiang, T. & Wu, J. Self-organization of multivalent counterions in polyelectrolyte brushes. *J. Chem. Phys.* **129**, 084903 (2008).
91. Reentrant behavior of grafted poly(sodium styrenesulfonate) chains investigated with a quartz crystal microbalance. *Phys Chem Chem Phys* **13**, 2880–2886 (2011).
92. Cation-Specific Conformational Behavior of Polyelectrolyte Brushes: From Aqueous to Nonaqueous Solvent. *Langmuir* **30**, 12850–12859 (2014).
93. Chu, X., Yang, J., Liu, G. & Zhao, J. Swelling enhancement of polyelectrolyte brushes induced by external ions. *Soft Matter* **10**, 5568 (2014).
94. Edmondson, S., Frieda, K., Comrie, J. E., Onck, P. R. & Huck, W. T. S. Buckling in Quasi-2D Polymers. *Adv. Mater.* **18**, 724–728 (2006).

95. Tugulu, S. & Klok, H.-A. Stability and Nonfouling Properties of Poly(poly(ethylene glycol) methacrylate) Brushes under Cell Culture Conditions. *Biomacromolecules* **9**, 906–912 (2008).
96. Sheiko, S. S. *et al.* Adsorption-induced scission of carbon–carbon bonds. *Nature* **440**, 191–194 (2006).
97. Paripovic, D. & Klok, H.-A. Improving the Stability in Aqueous Media of Polymer Brushes Grafted from Silicon Oxide Substrates by Surface-Initiated Atom Transfer Radical Polymerization. *Macromol. Chem. Phys.* **212**, 950–958 (2011).
98. Ataman, N. C. & Klok, H.-A. Degrafting of Poly(poly(ethylene glycol) methacrylate) Brushes from Planar and Spherical Silicon Substrates. *Macromolecules* **49**, 9035–9047 (2016).
99. Zhang, Y., He, J., Zhu, Y., Chen, H. & Ma, H. Directly observed Au–S bond breakage due to swelling of the anchored polyelectrolyte. *Chem. Commun.* **47**, 1190 (2011).
100. Zhang, Y. *et al.* Predicting Au–S bond breakage from the swelling behavior of surface tethered polyelectrolytes. *Soft Matter* **7**, 11496–11500 (2011).
101. Lv, B. *et al.* Molecular Composition, Grafting Density and Film Area Affect the Swelling-Induced Au–S Bond Breakage. *ACS Appl. Mater. Interfaces* **6**, 8313–8319 (2014).

102. Kimberly Simancas, Margrit Zacharias, Jürgen Rühle, Gerard Urban & Holger Reinecke. Entropic death of polyelectrolyte brushes: chain stretching, bond scission and surfactant complexation. (University of Freiburg, IMTEK, 2011).
103. Sheiko, S. S., Panyukov, S. & Rubinstein, M. Bond Tension in Tethered Macromolecules. *Macromolecules* **44**, 4520–4529 (2011).
104. Akbulatov, S., Tian, Y., Kapustin, E. & Boulatov, R. Model Studies of the Kinetics of Ester Hydrolysis under Stretching Force. *Angew. Chem. Int. Ed.* **52**, 6992–6995 (2013).
105. Rubinstein, M. & Colby, R. H. *Polymer Physics*. (OUP Oxford, 2003).
106. Galvin, C. J., Bain, E. D., Henke, A. & Genzer, J. Instability of Surface-Grafted Weak Polyacid Brushes on Flat Substrates. *Macromolecules* 150803081219001 (2015). doi:10.1021/acs.macromol.5b01289
107. Melzak, K. A., Yu, K., Bo, D., Kizhakkedathu, J. N. & Toca-Herrera, J. L. Chain Length and Grafting Density Dependent Enhancement in the Hydrolysis of Ester-Linked Polymer Brushes. *Langmuir* **31**, 6463–6470 (2015).
108. Borozenko, O. *et al.* Monitoring in Real-Time the Degrafting of Covalently Attached Fluorescent Polymer Brushes Grafted to Silica Substrates—Effects of pH and Salt. *Macromolecules* **44**, 8177–8184 (2011).
109. Bain, E. D. *et al.* Surface-Initiated Polymerization by Means of Novel, Stable, Non-Ester-Based Radical Initiator. *Macromolecules* **45**, 3802–3815 (2012).

110. Alswieleh, A. M. *et al.* Zwitterionic Poly(amino acid methacrylate) Brushes. *J. Am. Chem. Soc.* **136**, 9404–9413 (2014).
111. Patterned Biofunctional Poly(acrylic acid) Brushes on Silicon Surfaces. *Biomacromolecules* **8**, 3082–3092 (2007).
112. Biomimetic Polymer Brushes Containing Tethered Acetylcholine Analogs for Protein and Hippocampal Neuronal Cell Patterning. *Biomacromolecules* **14**, 529–537 (2013).
113. Chen, J.-K., Hsieh, C.-Y., Huang, C.-F. & Li, P. Characterization of patterned poly(methyl methacrylate) brushes under various structures upon solvent immersion. *J. Colloid Interface Sci.* **338**, 428–434 (2009).
114. Binary Nanopatterned Surfaces Prepared from Silane Monolayers. *Nano Lett.* **4**, 365–371 (2004).
115. Chain Entropy and Wetting Energy Control the Shape of Nanopatterned Polymer Brushes. *Macromolecules* **41**, 6859–6863 (2008).
116. Surface-Initiated Polymerization on Nanopatterns Fabricated by Electron-Beam Lithography. *Adv. Mater.* **16**, 2141–2145 (2004).
117. Yu, Q. *et al.* Nanopatterned polymer brushes as switchable bioactive interfaces. *Nanoscale* **5**, 3632 (2013).

118. Maeng, I. S. & Park, J. W. Patterning on Self-Assembled Monolayers by Low-Energy Electron-Beam Irradiation and its Vertical Amplification with Atom Transfer Radical Polymerization. *Langmuir* **19**, 4519–4522 (2003).
119. Fabrication of Stimulus-Responsive Nanopatterned Polymer Brushes by Scanning-Probe Lithography. *Nano Lett.* **4**, 373–376 (2004).
120. Programming nanostructures of polymer brushes by dip-pen nanodisplacement lithography (DNL). *Nanoscale* **2**, 2614 (2010).
121. Surface-Initiated Polymerization on Self-Assembled Monolayers: Amplification of Patterns on the Micrometer and Nanometer Scale. *Angew. Chem. Int. Ed.* **42**, 559–563 (2003).
122. Nanopatterned Polymer Brushes by Combining AFM Anodization Lithography with Ring-Opening Metathesis Polymerization in the Liquid and Vapor Phase. *Small* **2**, 848–853 (2006).
123. Nanostructured Polymer Brushes. *Small* **3**, 459–465 (2007).
124. Engineered Polymer Brushes by Carbon Templating. *Adv. Mater.* **21**, 2921–2925 (2009).
125. Structured Polymer Brushes on Silicon Carbide. *Chem. Mater.* **22**, 272–278 (2010).

126. Variable adhesion of micropatterned thermoresponsive polymer brushes: AFM investigations of poly (N-isopropylacrylamide) brushes prepared by surface-initiated polymerizations. *Adv. Mater.* **14**, 1130 (2002).
127. Microstructuring of molecularly thin polymer layers by photolithography. *Adv. Mater.* **10**, 1073–1077 (1998).
128. Fabrication of Complex Three-Dimensional Polymer Brush Nanostructures through Light-Mediated Living Radical Polymerization. *Angew. Chem. Int. Ed.* **52**, 6844–6848 (2013).
129. Simple Benchtop Approach to Polymer Brush Nanostructures Using Visible-Light-Mediated Metal-Free Atom Transfer Radical Polymerization. *ACS Macro Lett.* **5**, 258–262 (2016).
130. Direct Patterning of Intrinsically Electron Beam Sensitive Polymer Brushes. *ACS Nano* **4**, 771–780 (2010).
131. Development of a Directly Patterned Low-Surface-Energy Polymer Brush in Supercritical Carbon Dioxide. *ACS Appl. Mater. Interfaces* **1**, 2013–2020 (2009).
132. Patterning of Polymer Brushes. A Direct Approach to Complex, Sub-Surface Structures. *Nano Lett.* **10**, 3873–3879 (2010).

133. Photo-cleavable anti-fouling polymer brushes: A simple and versatile platform for multicomponent protein patterning. *Polymer* **54**, 1762–1767 (2013).
134. Patterning of photocleavable zwitterionic polymer brush fabricated on silicon wafer. *Colloids Surf. B Biointerfaces* **123**, 878–886 (2014).
135. Photo-switchable polyelectrolyte brush for dual protein patterning. *J. Mater. Chem.* **21**, 13789 (2011).
136. Mandal, K., Balland, M. & Bureau, L. Thermoresponsive Micropatterned Substrates for Single Cell Studies. *PLoS ONE* **7**, e37548 (2012).
137. Structured Polymer Brushes by AFM Lithography. *Small* **5**, 919–923 (2009).
138. Chen, J.-K. & Bai, B.-J. pH-Switchable Optical Properties of the One-Dimensional Periodic Grating of Tethered Poly(2-dimethylaminoethyl methacrylate) Brushes on a Silicon Surface. *J. Phys. Chem. C* **115**, 21341–21350 (2011).
139. Chen, J.-K., Wang, J.-H., Cheng, C.-C. & Chang, J.-Y. Reversibly Thermoswitchable Two-Dimensional Periodic Gratings Prepared from Tethered Poly(*N*-isopropylacrylamide) on Silicon Surfaces. *ACS Appl. Mater. Interfaces* **5**, 2959–2966 (2013).

140. Chen, J.-K., Pai, P.-C., Chang, J.-Y. & Fan, S.-K. pH-Responsive One-Dimensional Periodic Relief Grating of Polymer Brush–Gold Nanoassemblies on Silicon Surface. *ACS Appl. Mater. Interfaces* **4**, 1935–1947 (2012).
141. Zeng, J.-R., Cheng, C.-C., Chang, C.-J., Huang, C.-H. & Chen, J.-K. Fabrication of two-dimensional photonic crystals of tethered polyvinyltetrazole on silicon surfaces for visualization in Cu²⁺ ion sensing. *Dyes Pigments* **139**, 300–309 (2017).
142. Chen, J.-K., Wang, J.-H., Cheng, C.-C., Chang, J.-Y. & Chang, F.-C. Polarity-indicative two-dimensional periodic relief gratings of tethered poly(methyl methacrylate) on silicon surfaces for visualization in volatile organic compound sensing. *Appl. Phys. Lett.* **102**, 151906 (2013).
143. Simulation of Grafted Polymers on Nanopatterned Surfaces. *Nano Lett.* **6**, 133–137 (2006).
144. Scaling Behavior of Nanopatterned Polymer Brushes. *Small* **3**, 63–66 (2007).
145. Steenackers, M. *et al.* Morphology Control of Structured Polymer Brushes. *Small* **3**, 1764–1773 (2007).
146. Mendez, S., Curro, J. G., McCoy, J. D. & Lopez, G. P. Computational Modeling of the Temperature-Induced Structural Changes of Tethered Poly(*N*-isopropylacrylamide) with Self-Consistent Field Theory. *Macromolecules* **38**, 174–181 (2005).

147. Yim, H. *et al.* Effects of Grafting Density and Molecular Weight on the Temperature-Dependent Conformational Change of Poly(*N*-isopropylacrylamide) Grafted Chains in Water. *Macromolecules* **39**, 3420–3426 (2006).
148. Koutsioubas, A. G. & Vanakaras, A. G. Polymer Brushes on Periodically Nanopatterned Surfaces. *Langmuir* **24**, 13717–13722 (2008).
149. Chen, J.-K. *et al.* Using Solvent Immersion to Fabricate Variably Patterned Poly(methyl methacrylate) Brushes on Silicon Surfaces. *Macromolecules* **41**, 8729–8736 (2008).
150. Chen, J.-K. & Chen, T.-Y. Fabrication of high-aspect-ratio poly(2-hydroxyethyl methacrylate) brushes patterned on silica surfaces by very-large-scale integration process. *J. Colloid Interface Sci.* **355**, 359–367 (2011).
151. Kaholek, M. *et al.* Weak Polyelectrolyte Brush Arrays Fabricated by Combining Electron-Beam Lithography with Surface-Initiated Photopolymerization. *Chem. Mater.* **18**, 3660–3664 (2006).
152. Paik, M. PATTERNING AND CHARACTERIZATION APPROACHES OF POLYMER THIN FILMS. (Cornell University, 2010).

CHAPTER 2

Patterning Process Development for Polymer Brushes

Abstract

This chapter describes the development of selected patterning processes with the goal of producing patterned polymer brushes with neither damage nor contaminant with dimensions smaller than 200 nm. Direct Electron-beam (E-beam) writing and fluorinated photoresists were tested but they showed limitations in the fabrication of damage free patterns. On the other hand, an orthogonal patterning process was also tested. Such processing may be beneficial since any contaminant could either lower the performance of the device or add difficulties to multilayer integration. To make a general orthogonal process suitable for all organic materials, a few material combinations were screened and the final process was made with CYTOP due to its low thermal expansion and permeability which leads to mechanical compatibility. CYTOP allows brush patterning through both bottom-up and top-down methods with the same process condition. Furthermore, it also makes the inclusion of hard mask materials possible which can break the limitation of pattern thickness. In all, the developed orthogonal processes with DUV photolithography proved its versatility and robustness for the patterning of the polymer brushes and other organic materials.

2.1 Introduction

Patterning of the organic materials has been a great interest following the development of the organic electronics including, but not limited to, light-emitting diodes (LED), thin field-effect transistors (TFT), sensors, photovoltaics and memory.¹⁻⁴ Compared to traditional hard material based electronics, the advantage of organic materials in electronics is the freedom to tailor their properties based on the knowledge

built by organic chemists in hundreds of years.⁵ However, the processing of these organic materials with conventional photolithography often adversely affects the quality in each step including the use of solvents (i.e. spin coating/ development/lift-off).⁶ Since the foundation of the hard materials processing in the semiconductor industry lays on the insolubility of the hard materials, finding specific solvent/organic material combination with *orthogonality* means minimal modification in an existing process and therefore most favored for the least cost.⁷ The basic orthogonal solvent could be a hydrophilic solvent in processing a hydrophobic film and *vice versa*. Although a strategy based on hydrophobic/hydrophilic immiscibility has been demonstrated in multilayer light-emitting diodes⁸ and patterned devices^{6,9}, the strategy needs to consider the polarity for the processed materials which adds additional limitation to the process.

A more general orthogonal patterning process has been developed in our group since 2008 based on fluorinated photoresist and hydrofluoroether(HFE).¹⁰ Fluorinated materials are naturally suitable for or due to the low adhesion and immiscibility regardless the polarity of the patterned subject. The only interactions that could exist between fluorinated materials and others are polar and dispersive forces based on the significant dipole moment of the C-F bond. However, the special helical configuration of a perfluorinated hydrocarbon segment makes the C-F dipoles cancel out each other and prevent the central carbon from nucleophilic attack, which in turn reduces the polar interaction.¹¹ Furthermore, dispersive interaction is also low for the small electronic cloud of the fluorine leading to significant reduced polarizability. The sufficiently different intermolecular interactions also make fluorinated solvent a separate phase in either aqueous or organic solvents.¹² Utilizing these properties, our group fabricated a series of contaminant free organic electronic devices based on perfluorinated materials.^{10,13,14} Furthermore, it allows the lateral integration through repeated photolithography/material deposition/lift-off cycles.¹⁵ These demonstrated results led to

the foundation of Orthogonal Inc. which focuses on the production of various commercial orthogonal photoresists. One of its products, OSCoR4000 has proven its ability in fabrication of flexible organic electrochemical transistors and organic LEDs.^{16,17}

Besides a fluorinated photoresist, other perfluorinated materials could be used as sacrificial layer (SL) between a top photoresist and a bottom subject to reach the same orthogonality as a fluorinated photoresist. A commercially available fluorinated polymer, CYTOP, has been used to fabricate both μm level patterns with UV photolithography¹⁸ and nm level patterns with E-beam lithography¹⁹ with the commercial resist on top. For its excellent electrical and coating properties, it has been used as part of organic electronics design including TFT, LED and inverter²⁰⁻²² Likewise, our group also demonstrated the excellence of poly(1H,1H,2H,2H-heptadecafluorodecyl methacrylate) (PDFMA) as SL to enable both subtractive and additive patterning on organic materials with UV photolithography.²³ In addition, orthogonal patterning on biomolecules has also been demonstrated using PDFMA as nanoimprint resist to avoid damage from UV exposure and solvent treatment.²⁴

Polymer brushes as organic materials could be patterned through either similar top-down processes as mentioned above or bottom-up processes which synthesizes the polymer brushes on a pre-patterned template. Bottom-up processing could easily fabricate patterned polymer brushes down to nm level since the pre-patterning is conducted on hard material.²⁵⁻²⁷ However, as mentioned in chapter 1 the bottom-up patterned brushes form already relaxed profile rather than the perpendicular one in photolithography.²⁸ Such profiles could be detrimental to device integration especially with hard materials. Patterned brushes with perpendicular profiles have been fabricated through direct E-beam patterning in our group taking advantage of the chain-scission reaction of the methacrylate polymer under E-beam exposure.²⁹ Nonetheless, the

reaction mechanism is determined by chemical structure of the polymer and patterning is only possible for polymers with dominating chain scission reaction under E-beam exposure.

In this chapter, our goal is to develop an undamaged, contaminant-free patterning process for the both charged and non-charged polymer brushes in order to better probe their properties under reduced confinement. The presence of the neighboring polymer chains is the reason why polymer brushes stretch away from the surface and experience tension. Once those neighboring chains are removed, polymer brushes should relax from their high tension state to relaxed state as what's observed in HF lift-off experiment.³⁰ A perpendicular profile is therefore required for the patterns since it could preserve the tension accumulation during the polymerization and allow us to observe the stress relaxation process during the solvent treatment. For that, a variety of different patterning processes were evaluated and a process based on CYTOP as SL and DUV photolithography was chosen in the end. This process, although it still induces minor structural modification on the sidewall of the patterns, leads to the least damages compared to the others. A bottom-up patterning process based on CYTOP is also demonstrated which will be used as a complementary process in later chapters for the study of patterned polymer brushes.

2.2 Experimental Section

Materials. Allylamine, anhydrous toluene, (3-aminopropyl)triethoxysilane, α -bromo-isobutyryl bromide (BIBB), chlorodimethylsilane, dimethyl sulfoxide (DMSO), hydrazine, hydrochloric acid, inhibitor remover (for removing hydroquinone and monomethyl ether hydroquinone), magnesium sulfate, [2-methacryloyloxy)ethyl]trimethylammonium chloride (80% in water) (MAETAC), methyl methacrylate (MMA), Pt on activated carbon (10 wt %), triethylamine,

N,N,N',N',N''-pentamethyldiethylenetriamine (PMDETA), potassium hydroxide, pyridine, sodium chloride, sodium phosphate dibasic heptahydrate, sodium phosphate monobasic monohydrate, anhydrous triethylamine (TEA), PVP (M_w=65000), PSS (M_w = 70000), (1H,1H,2H,2H-perfluorooctyl)trichlorosilane (FOTS), trimethylchlorosilane were purchased from Sigma Aldrich and used without further purification unless stated otherwise. Monomers were passed through inhibitor remover to remove the inhibitor before use. CYTOP fluoropolymer was purchased from BELLEX International Corporation. Deionized water (DI water) with a resistivity of 18.2 MΩ · cm at 25°C was obtained from Millipore's Milli-Q Synthesis A10 system. Copper tape (882-L copper) with 88.9 μm copper film was from Lamart Co. XR-1541-002 resist (hydrogen silsesquioxane, HSQ 2 mol% solution) was purchased from Dow Corning. All the other solvents were purchased from Fisher Scientific.

Mono-functional silane initiator synthesis and liquid phase immobilization. First, 2-bromo-2-methyl-N-allylpropanamide and chlorodimethylsilane were synthesized by published procedures and used subsequently as reactants.¹ Hydrosilylation was carried out using another literature procedure to obtain mono-functional ATRP initiator, 2-bromo-2-methyl-N-{3-[chloro(dimethyl)silyl]-propyl}propanamide.^{31,32} Wafer pieces were cleaned repetitively with dichloromethane (DCM) and DI water rinse and then dried with nitrogen. Wafers were then oxidized using a Harrick Plasma Cleaner for ten minutes. Moisture was further removed by 10 minutes 110 °C oven baking. In a glove box, the wafer pieces were immersed in a toluene solution of the initiator (10 mM) and pyridine (0.5 mM) for a given time at room temperature. The substrates were then removed from the solution and washed with DI water, and DCM sequentially and sonicated for ten minutes in DCM. Wafers were given a final rinse of dichloromethane and blown dry under nitrogen gas.

Multi-functional silane initiator synthesis and vapor phase immobilization. Wafer cleaning and oxidation processes remained the same as in the previous procedure. Clean, oxidized, moisture free wafer pieces were then exposed to 3-aminopropyl triethoxysilane vapor under reduced pressure in a glass chamber containing liquid (3-aminopropyl)triethoxysilane pumped down to a desired pressure and then sealed. Pressure was kept at 1 Torr for 2 h and then annealed for a further 30 minutes at 110 °C. The pieces were then put into a Schlenk flask and purged with three vacuum evacuating/argon back-filling cycles. Anhydrous DCM (30mL), anhydrous TEA (0.6mL), BIBB (0.6 mL) were added in this order and left to stand overnight. The pieces were then taken out of the flask, washed with acetone, ethanol, and DI water sequentially and blown dry under nitrogen gas.

Polymer brush synthesis. Polymerization was conducted by first preparing the set-up as shown in the literature³³. A glass slide was cut into pieces with a size corresponding to the initiator-deposited piece. The glass piece was then coated with copper tape to be the metal catalyst source. This taped glass piece was then clamped face-to-face together with initiator-deposited wafer pieces by the copper clamp. The distance between the pieces was separated by a PTFE spacer with $d = 0.5$ mm. The set-up was then put into containers with different reaction conditions to produce the different brushes.

PDMAEMA polymerization A solution of 1 mL DMAEMA, 1 mL H₂O, 18.4 μ L PMDETA in combination was used and the polymerization was conducted at room temperature for a predetermined time. Afterwards the wafer pieces were taken out, rinsed with ethanol before being blown dry with nitrogen.

PMMA polymerization. Solution of 2 mL MMA, 1 mL DMSO, 36 μ L PMDETA, 1.5mL hydrazine combination was used and the polymerization was conducted at room temperature for a given time. Afterwards the wafer pieces were removed, rinsed

with DCM and sonicated in DCM for 10 minutes before being blown dry with nitrogen.

PMETAC polymerization. A solution of 2 mL MAETAC, 2 mL DI water, 1 mL methanol, 36 μ L PMDETA, 2.5mL hydrazine were combined and the polymerization was conducted at 60 °C for a given time. Afterwards the wafer pieces were taken out and rinsed with ice cold DI water before being blown dry with nitrogen.

PVP polymerization. A solution of 2 ml VP, 3 ml DMSO, 36 μ l N,N,N',N',N''-pentamethyldiethylenetriamine, and 2.5 ml hydrazine were heated at 80 °C for a given time. Afterwards the wafer pieces were taken out and rinsed with ethanol before being blown dry with nitrogen.

Reactive ion etching (RIE) conditions. RIE was conducted on a Oxford PlasmaLab 80+ RIE system with the following parameters: O₂ flow rate, 50 sccm at a RF power of 75 W. Pressure started at 50 mTorr then decreased to 20 mTorr in 6 sec and stayed at 20 mTorr; DC bias minimum was 5V.

For the SiO₂, the following conditions were used: CF₄ 30 sccm, Forward power 150 w, DC bias 73V

E-beam lithography E-beam lithography was conducted with JEOL-9500 under the conditions: 100 kV, 500 pA, aperture 60. Doses were varied as described in the text.

Direct E-beam lithography patterning Filtered PSS solution in water and PVP solution in ethanol were used to cast films by spin coating. A PSS film was subject to a post-application bake (PAB) step at 90 °C for 5 minutes while PVP was PAB at 90 °C for 1 min. After E-beam exposure, the PSS film was developed in water for 2 sec while the PVP film was developed in DMF for 15 sec. N₂ flow was then used to dry the film.

For PDMAEMA brushes, it was developed in isopropanol (IPA) for 90 sec before being dried in N₂ flow.

For direct patterning on \initiator, a film covered with ATRP initiator made of a multifunctional silane initiator was subjected to E-beam lithography and the PMMA polymerization was conducted to derive the patterned PMMA brushes.

Fluorinated resist patterning

Free polymer films were prepared with PMMA in anisole, poly(t-butyl methacrylate)(PtBuMA) in chloroform and poly(ethyl p-vinylbenzene sulfonate) (PESS) in cyclohexane by spin-coating. PESS was synthesized based on published procedures.³⁴ PAB conditions: PMMA, 170 °C for 1 min, PtBuMA, 90 °C for 2 minutes, PESS, 90 °C for 2 minutes.

Diluted OSCoR4000 was spin coated and PAB at 90 °C for 1 min with enough thickness to protect an underlayer polymer film. After exposure, it was then subjected to a post-exposure bake (PEB) step at 90 °C for 1 min and developed with developer103 for 1 min before spin drying. RIE was used to the transfer pattern down to the polymer film. The OSCoR4000 was stripped with stripper700 for 2 minutes before spinning dry. E-beam lithography patterned samples were processed with the same conditions.

A random copolymer fluorinated photoresist composed of 2-nitrobenzyl methacrylate (N monomer) and 3,3,4,4,5,5,6,6,7,7,8,8,9,9,10,10,10-heptadecafluorodecyl meth-acrylate (F monomer) was synthesized based on a published procedure.¹³ ¹H-NMR was conducted with 1:1(v/v) CDCl₃ + CFCl₃ to check the resulting monomer ratio in the polymer. 3 photoresists with ratios(F/N) were derived and developed for different times as shown below. HFE-7600 was used as a

photoresist solvent and HFE-7200 was used as developer. PAB: 110 °C for 1 min, PEB: 110 °C for 1 min.

Ratio of monomer in polymer(F/N)	2.295	2.75	3.455
Development time	7 minutes	50 seconds	50 seconds

For OSCoR5001, it was spin coated on a PMMA brush and PAB at 90 °C for 1 min. After exposure, it was then PEB at 90 °C for 1 min and developed with developer100 for 80 sec before spinning dry.

Multilayer patterning process

The following are standard conditions unless mentioned otherwise in the text.

Deposition of the SiO₂ was conducted on CVC SC4500 E-gun Evaporation system with deposition rate ~ 0.1 nm/sec probed by QCM. Temperature of the substrate was monitored, and it was always below 25 °C during the process.

Pattern transfer through SiO₂ was achieved by RIE with CF₄ gas while other pattern transfer was all made using oxygen gas.

The BARC used was DUV-252 anti-reflective coating (Brewer Science) with PAB at 90 °C for 30 seconds and then 185 °C for 1 min.

Hydrogen silsesquioxane (HSQ): PAB at 150 °C for 2 minutes.

UV210 (Shipley): PAB at 135 °C for 1 minute, PEB at 135 °C for 1 minute.

Developed in MIF-726 (AZ Electronic Materials) for 1 min.

ZEP520: PAB at 120 °C for 2 minutes. Development: Either in hexyl acetate for 2 min or in n-amyl acetate for 45 seconds, then methyl isobutyl ketone (MIBK):IPA(1:3) for 30 seconds and finally in IPA for 30 seconds.

CYTOP Top-down patterning process. Top-down patterning processing started with spin-coating three layers on the polymer brush with individual post-application baking conditions. CYTOP was coated first and PAB treated at 110 °C, 5 minutes, ramped to 150 °C in 5 minutes, held at 150 °C for 5 minutes, ramped to 185 °C in 5 minutes, and held at 185 °C for 6 minutes. Following the first CYTOP coating, it was subject to RIE etching for 5 seconds in order to create a hydrophilic surface for subsequent material deposition.

For E-beam lithography patterning, ZEP520 resist was then coated using the same conditions previously mentioned and developed in hexyl acetate for 1 min at 0 °C then blow dry with N₂. Pattern transfer was done using RIE. The pieces were then soaked in stirring hydrofluoroether NOVEC 7300 (3M) at 50 °C overnight and rinsed with NOVEC 7300 repetitively. Afterwards, pieces were blown dry with nitrogen gas. A stability test was conducted by soaking patterned samples in acetone for 4 hours and then drying in nitrogen.

For DUV top-down patterning process, the 2nd layer was a DUV-252 anti-reflective coating layer (Brewer Science) with PAB at 90 °C for 30 seconds and 185 °C for 1 min. The 3rd layer was UV210 DUV photoresist with PAB at 135 °C for 1 min. DUV photolithography patterning was then conducted on an ASML 300 DUV stepper. The sample was then subjected to PAB at 135 °C for 1min and development with MIF-726 developer for 1 min and spun to dry. 50 to 0.2 μm line patterns were created on the photoresist. Pattern transfer was conducted by RIE and the lift-off was conducted the same as for E-beam lithography patterning.

CYTOP Bottom-up patterning process. The bottom-up process was similar to the TD process. The Si wafer was cleaned with SC-2 process (soaked in solution made of HCl:H₂O₂:water = 2:2:1, volume ratio) for 2 h, then rinsed with DI water and dried with nitrogen gas. The patterned CYTOP polymer film on the cleaned wafer was

treated in the same way as the TD process. The initiator was deposited by the same methods (no further wafer oxidation needed) as before and the CYTOP was removed afterward to obtain a wafer with initiator pattern. Bottom-up patterned brushes were then fabricated by subsequent polymerization on the wafer with the initiator pattern.

Deposition of surface fillers. For 2-[methoxy(polyethylenoxy)propyl]trichlorosilane (PEGf), Deposition of fillers on the surface was done by using MVD 100 molecular vapor deposition tool (SPTS technology). Briefly, a silicon wafer (cleaned as before) was cleaned with RF plasma for 60 seconds in the MVD 100. PEGf vapor was injected and vented for 4 cycles and followed by water vapor condensation. This big cycle was then conducted again and a wait of 15 min to finish deposition.

For FOTS and TMC, solution deposition was used on a cleaned silicon wafer. After RF plasma cleaning for 7 min, the wafer was then left in toluene solution overnight with 10 mM filler compound and 5mM TEA in a glovebox. After deposition it was rinsed with toluene and methanol before being blown dry in nitrogen.

After that, the static water contact angle was measured for 3 times at different places to confirm the success deposition. The value of averaged water contact angles of filler deposited surfaces are: FOTS: $109.98 \pm 3.96^\circ$ / PEGf: $53.45 \pm 2.67^\circ$ / TMC: $90.68 \pm 2.75^\circ$.

Characterization. Patterns were characterized using a Zeiss Supra/Ultra SEM and Veeco Icon AFM. Thicknesses of the non-patterned polymer brushes were measured using an imaging ellipsometer – a Nanofilm Ep3 with a 532 nm laser at 50-60° angle of incidence. A Cauchy model (Cauchy layer/silicon substrate) was used to fit the data, in which the Cauchy layer was representative of the polymer brush. AppNANO ACCESS-NC tapping mode silicon cantilever were used to acquire topographic

images in air at room temperature. An Olympus MX50 optical microscope was used to take images at larger scales.

Hydrogen nuclear magnetic resonance spectroscopy (NMR) spectra were recorded on Varian Gemini 400 MHz spectrometer.

2.3 Results and Discussion

2.3.1 Direct electron beam lithography patterning

Electron beam lithography, due to its ability to create a pattern with the highest resolution, was chosen first to create patterned brushes for subsequent testing. Two preliminary tests were conducted on free PVP and PSS which were subsequently developed by corresponding good solvent, DMF and water. Unsurprisingly they both showed crosslinking after exposure to E-beam which eliminates their possibility to form undamaged patterned brushes. In addition, they both suffer from the adhesion issue and became patchy during development. Figure 2.1a showed the best patterning result of two polymers and it suggested that the test should be conducted with polymer brushes rather than free polymer. The pattern is designed to have lines ranging from 15 nm to several μm in order to test the limit of the resolution. Since our group has already shown the direct E-beam patterning of a series of methacrylate-based polymer brushes, subsequently PDMAEMA brushes were selected due to their methacrylate structure and the ease of forming polyelectrolyte through quaternization reaction.

E-beam doses ranging from 50 - 1200 $\mu\text{C}/\text{cm}^2$ were used to induce chain-scission reaction in the exposed area because the highest dose reported to pattern brushes was 1060.8 $\mu\text{C}/\text{cm}^2$ with the same patterning tool, JEOL 9500.³⁵ A PDMAEMA brush whose initial thickness = 120 nm was synthesized on a silicon wafer by modified Cu(0)-mediated controlled radical polymerization(CuCRP) with copper tape and hydrazine as reducing agent.³³ After E-beam exposure, the patterned PDMAEMA

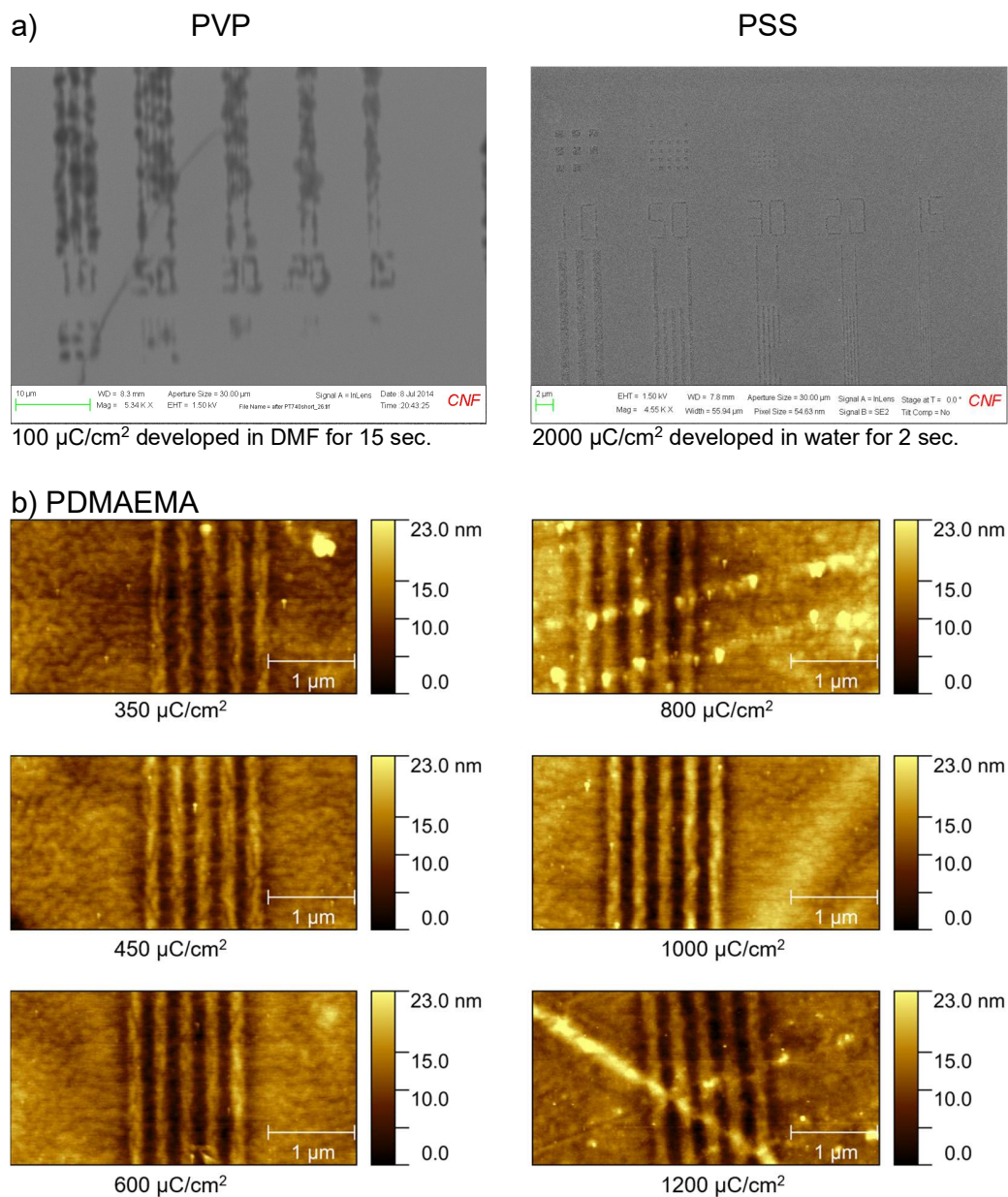


Figure 2.1 E-beam direct patterning results. a) SEM images of 1 - 0.15 μm line patterns of free PVP/PSS. b) AFM images of patterned 150 nm PDMAEMA brush lines.

brushes were developed in IPA for 90 sec and dried with nitrogen flow. The dry patterns were then measured with an AFM and compared.

The patterning results are shown in Figure 2.1b. It was expected that the optimal dose should appear in the range chosen and the pattern starts to appear under an optical microscope when the dose is $350 \mu\text{C}/\text{cm}^2$. Unfortunately, even at the maximum dose of $1200 \mu\text{C}/\text{cm}^2$ there is only a 13.9 nm gap as characterized by AFM. Although it is possible to remove the material completely with prolonged E-beam exposure, such low E-beam sensitivity makes massive production of the samples expensive and unrealistic. It has already taken 30 minutes for a single pattern with $1200 \mu\text{C}/\text{cm}^2$ and it could take at least 5 times longer for complete patterning. On the other hand, since there are no obvious differences in patterning between high and low doses, it is also possible that E-beam exposure would actually induce crosslinking in the PDMAEMA brushes as happens with PS brushes.³⁶ Together, these results mean that there is only a limited set of conditions under which E-beam lithography is a good choice to directly pattern polymer brushes.

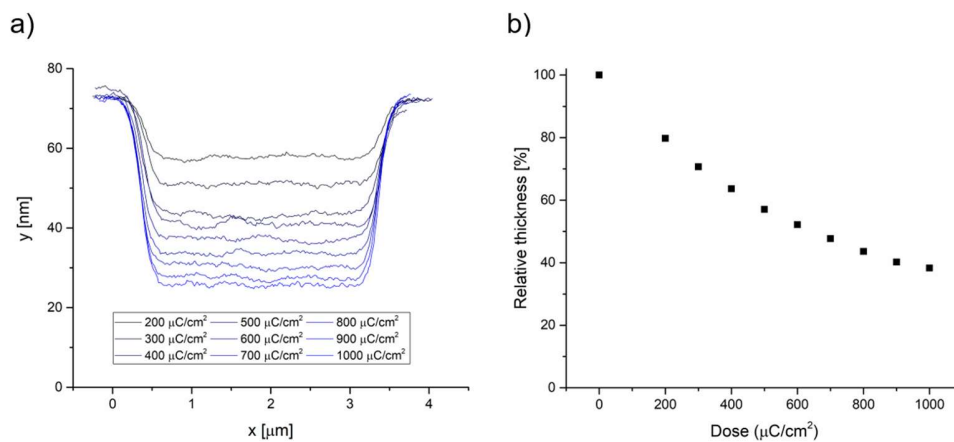


Figure 2.2 Results of E-beam lithography patterning on initiator. E-beam doses ranged from $200 - 1000 \mu\text{C}/\text{cm}^2$. a) AFM scan on trenches made of PMMA brushes grown on patterned initiator. b) Relative thickness of the PMMA brush in the trench as a function of the exposure dose.

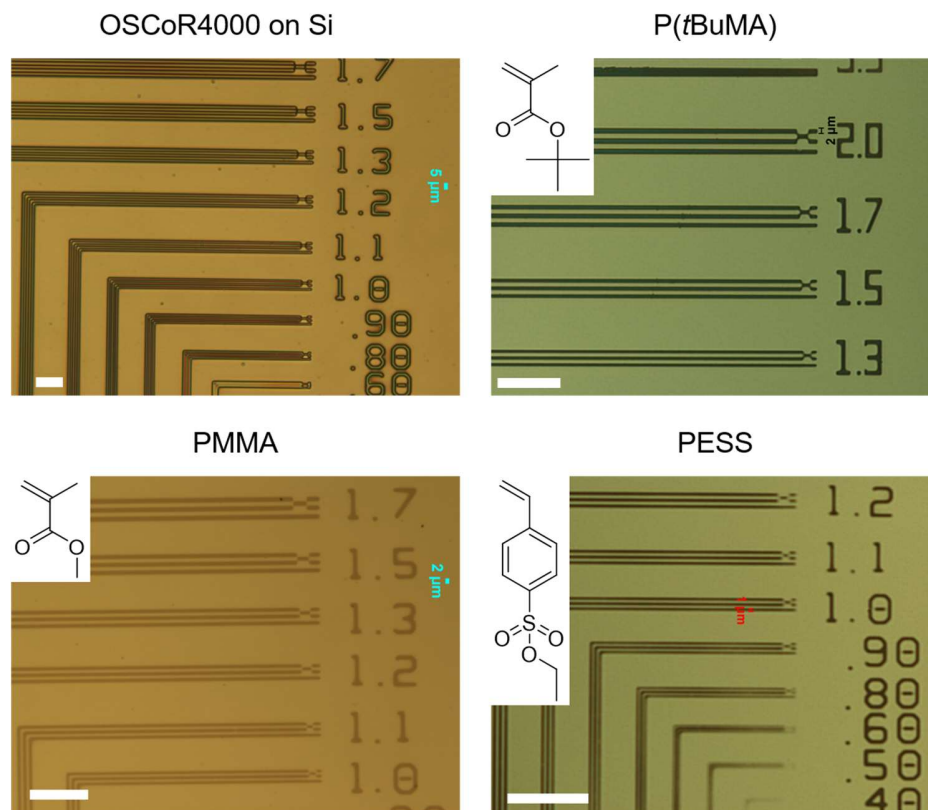


Figure 2.3 Patterns of the OSCoR4000 and 3 different polymer films with their chemical structures shown. After photolithography, OSCoR4000 patterns were transfer through RIE and stripped away in the end. White scale bar is 20 μm .

In addition to direct patterning, E-beam lithography has also been proven to cleave reactive bromide groups from a self-assembled monolayer (SAM) surface to create patterned initiator and subsequently patterned polymer brushes. In the work of Maeng *et al.* the substrates were exposed at 1.0 KeV by scanning electron microscopy (SEM) for 1h to create finely defined patterns.^{37,38} Although the reaction mechanism could be different due to the difference in the accelerating voltage between SEM and an E-beam lithography tool, it should take a shorter time for E-beam lithography to provide the same exposure dose on the substrate to define the pattern (~ 100 times faster for E-beam lithography tool). Doses ranging from 200 - 1000 $\mu\text{C}/\text{cm}^2$ were selected for tests

to keep the process efficiency on the initiator film made of APTES and BIBB. The exposed substrate was then used as a base and 73.4 nm thick PMMA brush was synthesized on it through CuCRP. To show the cleavage efficiency, 3 μm trench patterns were measured with AFM and the relative thickness in the exposed region is presented in Figure 2.2a. Obviously, as the dose increases the trench becomes deeper, which indicates that a larger fraction of the reactive bromine group is cleaved from the surface. Nevertheless, the dose needed to completely remove the initiator is more than 3000 $\mu\text{C}/\text{cm}^2$ based on the trend shown in Figure 2.2b. The long exposure time is still a problem even if cleavage is only needed for monolayer on the surface.

2.3.2 Fluorinated resist patterning

E-beam direct patterning methods have the advantage of simplified process which leads to reduced contamination and defects. However, the reaction upon E-beam exposure depends on the chemistry of the molecules used in the polymer brushes and this make it an inherently poor choice for general patterning processes. Fluorinated photoresist on the other hand is a good choice to reach process orthogonality since the adhesion between fluorinated materials and others are always low due to the inert nature of fluorine-containing compounds. The first testing photoresist focused on a commercial fluorinated photoresist, OSCoR4000 which showed good performance in patterning acid polymers, poly(3,4-ethylenedioxythiophene): poly(styrene sulfonate)(PEDOT:PSS).¹⁶

To check if the performance changes on the polymer, three different free polymer films were chosen for pattern testing: PMMA, PtBuMA and PESS. PMMA is one of the most fundamental polymers in the brush field while the other two polymers could be converted to polyelectrolyte brushes, PMAA and PSS, through deprotection of terminal aliphatic groups.^{34,39} After forming the patterns through photolithography, patterns were then transferred to the polymer films through oxygen plasma reactive

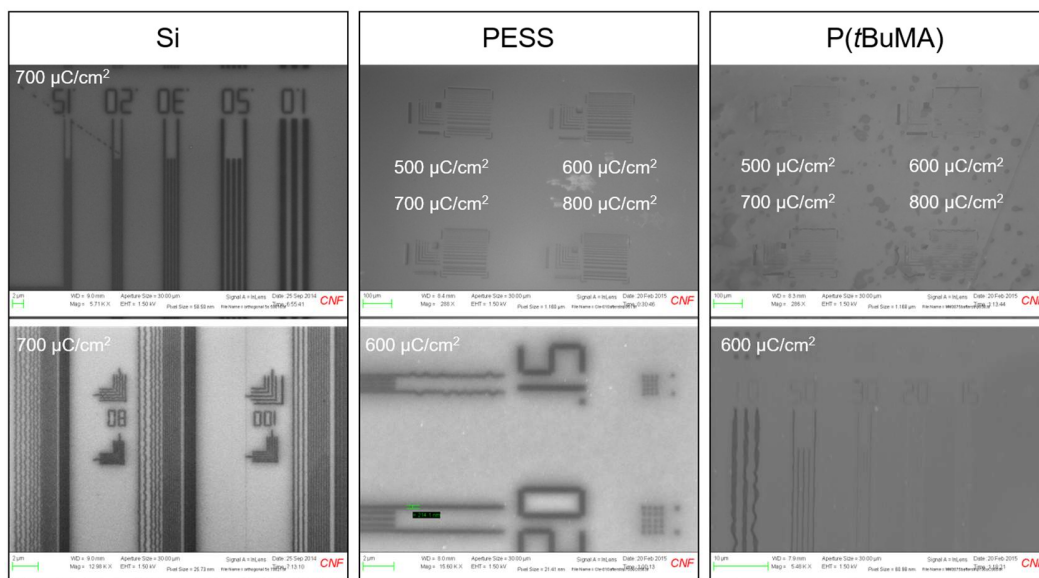


Figure 2.4 SEM images of E-beam lithography patterning of OSCoR 4000 on different substrate. For PESS and P(*t*BuMA) images shown are after photoresist lift-off.

ion etching. In the end the residual OSCoR4000 was stripped with the fluorinated solvent. Since polymer have different etch rates, the film thicknesses and exposure doses were chosen separately so that the covered area is completely protected. The patterning results are shown in Figure 2.3. With the ABM contact aligner, the best resolution of the OSCoR4000 on silicon wafer is $\sim 1 \mu\text{m}$ for 1:1 line:space pattern and the resolution does not change when using different polymers as an underlayer. Furthermore, profilometer measurements confirmed that the thickness of the polymer patterns remained the same as the initial film thickness. To improve resolution, E-beam lithography was then chosen to pattern the OSCoR4000 and the pattern results are shown in Figure 2.4. The optimal E-beam dose for OSCoR4000 on a silicon wafer is $700 \mu\text{C}/\text{cm}^2$ and the best resolution is 100 nm line. With smaller patterns it could be observed that they start to have snake-like wrinkled shape which wiggles normal to the direction of the line patterns. The reason for the appearance of this shape is because

photoresist overswells during the development step and accumulates residual compressive stress in the patterns which could only be subsequently relaxed by wiggling since patterns are constrained to the substrate.^{40,41} This problem could be solved by reduce film swelling through changing developer or photoresist composition

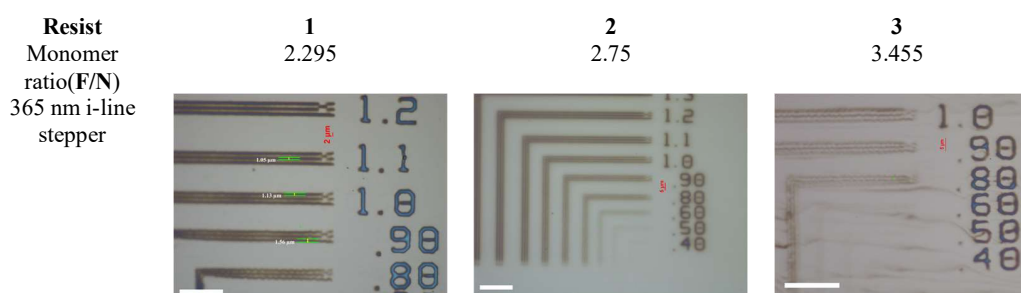


Table 2.1 Photolithographic evaluation results and corresponding parameters for synthesized fluoropolymer photoresist. Scale bar: 20 μm .

but 100 nm is enough for current requirement.

When the OSCoR4000 was used to pattern polymers, the best resolution decreased to 200 nm for PESS sample, even though from previous experiment we know that the PESS could crosslink under the exposure of the E-beam, it is very insensitive and dose below 1500 $\mu\text{C}/\text{cm}^2$ is not high enough to induce any observable crosslinking. At 600 $\mu\text{C}/\text{cm}^2$ it could form well defined 200 nm line patterns as shown in the SEM scan. However, it was found that the thickness of the patterns increases by ~ 20 nm as the dose of E-beam raises to 800 $\mu\text{C}/\text{cm}^2$. It suggests that the photoresist forms undefined chemical bonds with the PESS due to the E-beam exposure since it was not observed in photolithography patterned samples. Similarly, for P(*t*BuMA) polymer films, the lift-off of the photoresist apparently failed as the residue of the photoresist is still observable. Since the minimum dose required to form good patterns is 600 $\mu\text{C}/\text{cm}^2$

and still the residue remained, E-beam patterning with OSCoR4000 photoresist was not selected for later processing.

In our group, sub 100 nm E-beam lithography patterns have been made with two different fluorinated photoresists based on either polymethacrylate¹³ or resorcinarene.¹⁴ Through further optimization it would be possible to have fluorinated photoresist with better performance. Since the resorcinarene-based fluorinated photoresist has its patterning mechanism based on acid catalysis(chemically amplified resist), its lithographic performance could be adversely affected by the presence of the acid underlayer.⁴² Although successful acid polymer film patterning has been shown under proper conditions¹⁴, it could increase the difficulty for process optimization. For that, random copolymer fluorinated resist composed of 2-nitrobenzyl methacrylate(*N monomer*) and 3,3,4,4,5,5,6,6,7,7,8,8,9,9,10,10,10-heptafluorodecyl methacrylate(*F monomer*) was synthesized based on a published procedure.¹³ Three different monomer ratios were chosen to synthesize photoresist and the best patterning results on a silicon substrate with ABM contact aligner and i-line stepper are shown in Table 2.1.¹³ The ABM contact aligner was used first with a 254 nm filter for testing. The sensitivity of the photoresist increases following a decrease of the *F/N* ratio while all patterns have the best resolution at $\sim 1.1 \mu\text{m}$. Though the performance could possibly be further improved, the patterns all showed wrinkled lines in the μm level patterns which behaved worse than OSCoR4000. This could also mean that the wrinkle effect could happen at larger pattern size under E-beam exposure for the synthesized photoresist. For that, we decided to seek other solutions.

At this stage, both E-beam lithography negative tone photoresist and self-synthesized fluorine photoresists have proved to be inadequate for patterning organic materials. Although positive tone fluorinated E-beam resist has been shown by our group before, it is not an optimized product and may still have other potential issues.²³

Photolithography is then naturally a preferred choice. Compared to UV photolithography, DUV photolithography at 248 nm could achieve better resolution which might suit our needs. With the kind help from Orthogonal Inc. the newly developed orthogonal photoresist suitable for DUV exposure, OSCoR5001 was selected to test. In Figure 2.4a. we could see the dose test on a silicon wafer has quite good results with 238 nm resolution achieved at 19 mJ/cm². However, in the following test when the patterns were formed on PMMA polymer brushes, the profile became more rounded rather than ideal rectangular profile (Figure 2.4b). It may be that the photoresist adheres stronger on PMMA than on a silicon wafer which prevents the complete dissolution of the edge materials. Furthermore, the bubble-like shapes observed after the development suggests that the heating process was too harsh for the materials and it did not have enough time for vapor to diffuse out. Changing doses does not improve the photoresist profile as shown in Figure 2.4c that the profile replicates itself along different doses.

In short, the fluorinated photoresist has advantages in terms of low adhesion force. Nonetheless, the only available DUV fluorinated photoresist still has performance complications associated with interfacial interactions and even a PMMA surface could produce deteriorated resolution. To overcome this issue, it's better to have one uniform underlayer for the patterning material which guarantees the performing consistency is independent of the patterned substrate. This leads us to explore multilayer processing as the patterning strategy.

2.3.3 Multilayer patterning process

Multilayer patterning has been one of the successful industrial fabrication strategies when a single material layer could not meet the requirement for a given process. For example, a Bottom Anti-Reflective Coating (BARC) is generally coated right

underneath a photoresist to prevent light scattering from the substrate in photolithography.⁴³ A conductive layer lies under the E-beam resist and prevents charging and proximity effects on a surface in E-beam lithography which reduces deflection of E-beam.^{44,45} In addition, a ‘hard mask’ layer is often used when the patterned resist alone could not stand up to the etching chemistry. Chromium is a common choice for silicon etching since a common etchant for silicon – fluorine vapor - is not reactive with chromium at all.⁴⁶ The same idea can be applied for using silicon dioxide as hard mask on organic materials.⁴⁷ Sometimes due to the nature of the resist, an additional underlayer such as PMMA is coated underneath a resist as a sacrificial layer to enhance lift-off.^{48,49}

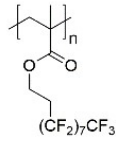
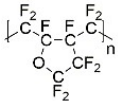
	SL	<i>OSCoR4000</i>	<i>PDFMA</i>	<i>CYTOP</i>
Top film				
Photoresist		Film dissolved	Cracked during development	✓
SiO ₂ \ Photoresist		SiO ₂ buckled at high temperature.	SiO ₂ buckled at high temperature.	N/A
HSQ \ Photoresist		HSQ cracked	HSQ cracked	✓

Table 2.2 Summary of multilayer patterning process testing results. Photoresists were always used with BARC underneath it. Chemical structures of the sacrificial layers are presents except for OSCoR4000 for commercial reason. SiO₂ was deposited through E-beam evaporation. HSQ: hydrogen silsesquioxane.

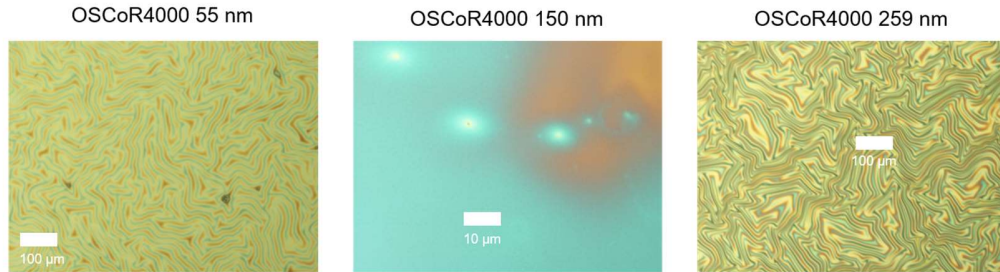
2.3.3.1 Preliminary experiments

In our group, parylene-C and PDFMA have been used as sacrificial layers to reach orthogonal patterning on the organic materials.^{23,24,50} Since lift-off in the Parylene-C process relies on the mechanical peel-off it is sometimes problematic and not preferred. Instead, fluorinated materials which could be dissolved by hydrofluoroethers (HFE) showed no intermixing on polymer films are therefore favored.⁵¹ Other than PDFMA, CYTOP is another widely-applied fluorinated polymeric SL which has been used to fabricate several OLEDs and was therefore chosen.^{18,21} The multilayer combinations and their corresponding test results are briefly described in Table 2.2 and will be discussed in below.

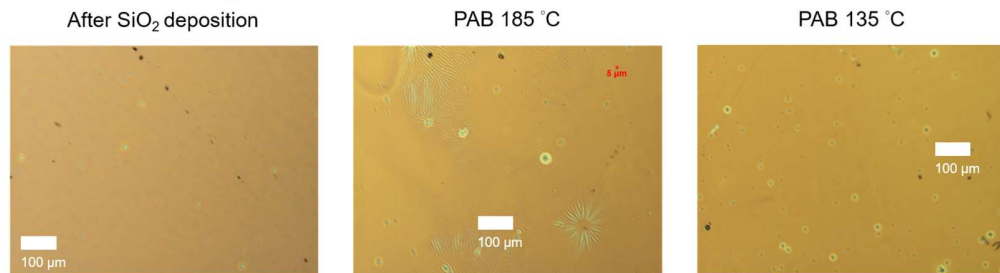
To begin with, direct photoresist coating on a film of OSCoR4000 failed since it dissolved during the coating process. The non-fluorinated component in the OSCoR4000 made it soluble in normal organic solvent used for photoresist coating. A spin-on glass material – hydrogen silsesquioxane (HSQ) was explored then as an interfacial material between photoresist and substrate since it has been shown to form good layers on PMMA.⁴⁸ In addition it could effectively reduce the thickness of the photoresist needed for its high etch resistance in oxygen plasma and lead to better resolution. Although the results showed that the HSQ could form thin films on the OSCoR4000 when the spinning started right after the addition of the tiny fluid, the high solubility of the OSCoR4000 in the solvent used for HSQ - MIBK, leads to the intermixing of the film during a post-application bake (PAB) step. The resulting film has the properties of both silicon dioxide and fluorinated polymer which could not be dissolved again through HFE. The solubility issue was then solved by utilization of E-beam evaporation for its dry nature. With only 20 nm of evaporated SiO₂, the film quality is good enough to both adhere on the fluorinated film and allow BARC to stay on.

Nevertheless, a dilemma appeared when trying to process the SiO₂ included process.

a) PMMA\OSCoR4000\SiO₂\BARC\photoresist



b) PMMA\OSCoR4000\SiO₂



c) PMMA\PDFMA\Top layers

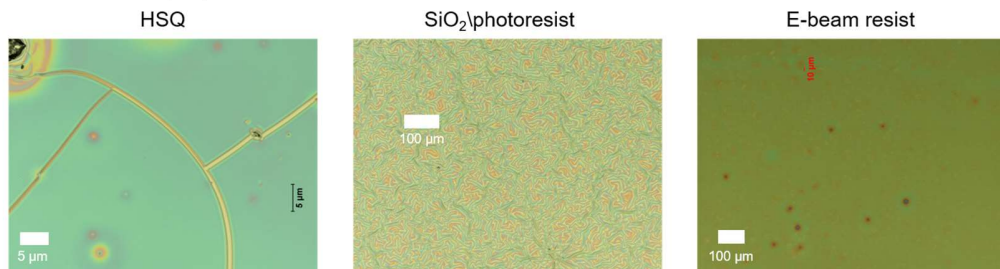


Figure 2.5 Multilayer film quality evaluation under optical microscope after PAB

with the film combinations shown. SiO₂ was kept as 20 nm in all process. a)

Images were taken after the coating of the photoresist(UV210). Baking condition:

OSCoR4000: 185°C 1 min\ BARC: 90°C, 30 sec then 185 °C, 1min\ UV210:

135°C 1min. b) Images taken after deposition of SiO₂ and the following thermal

treatment. Thickness of OSCoR4000 was 150 nm with the same baking condition.

c) PDFMA SL testing results with different top layers. Baking condition: HSQ:

170C, 4 min\ Photoresist: 120 °C, 1min\E-beam resist: 120 °C, 5min.

It was found out that after the deposition of the SiO₂, the surface became frosted in the subsequent baking process for drying of the BARC and photoresist. A series of baking conditions were then investigated to improve the quality of the film. Three multilayer samples with different OSCoR4000 thicknesses varying between 55 - 259 nm were made and tested with the PAB temperature 185 °C, the lowest temperature required for BARC processing. In Figure 2.5a the optical microscope images showed that the SiO₂ under the BARC and photoresist buckled seriously except for the sample with medium SL thickness. The same phenomena could also be observed when other hard materials like metal are deposited on a soft material.⁵²⁻⁵⁴ Generally the buckling originates from the compressive residual stress accumulated in the cooling process after the deposition due to the difference of the thermal contraction rate and is detrimental to subsequent processing. However, the situation is a little different here because the buckling happened during the heating process. The formation of buckling is triggered by the softening of the polymeric film which then forms the compliant film morphology to release the stress.

The reason for the different results observed maybe that the thin SL is not enough to isolate thermal expansion/contraction from under a PMMA layer while thick SL on the other hand has too strong thermal sensitivity. However, when focusing on the film quality right after deposition of SiO₂, it could be seen that the mini-buckling still appears after baking solely at 185°C for 1 minute (Figure 2.5b). On the contrary, film quality is better when baking was only 135°C for 1 minute which makes the E-beam resist as the only choice.

Another candidate, PDFMA was also tested as a SL for the patterning process. Due to its low adhesion nature, the spin-coating of the other material on PDFMA requires a short oxygen plasma pre-treatment to increase the interfacial interaction between PDFMA and the film above it. An HSQ coating was successful but the cracking is still

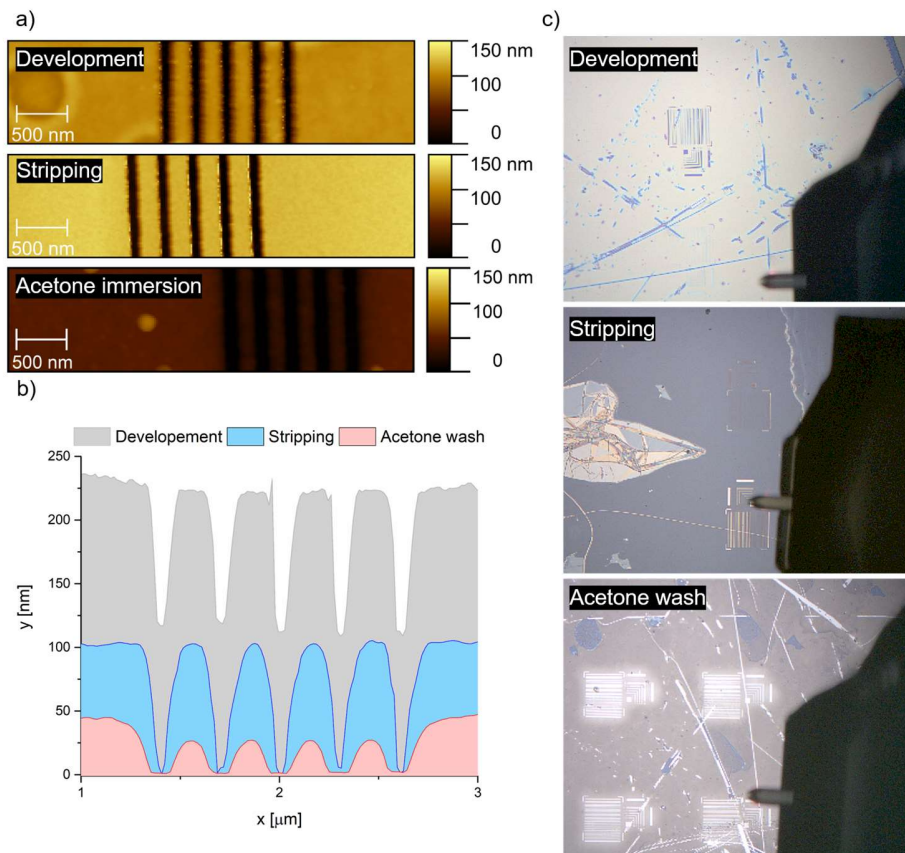


Figure 2.6 E-beam lithography patterning result of the PMMA brush with combination A. Results after development, stripping and acetone immersion are displayed. a) 150 nm trench AFM scan top-down view and b) cross-sectional view. c) Optical microscope images taken in AFM.

observable after the PAB step. Since DUV photolithography would require higher temperatures, HSQ is not a proper hard mask material on PDFMA. The formation of cracks on the surface demonstrates that the adhesion between PDFMA and HSQ is stronger and that leads to film cracking instead of buckling.^{54,55} For the SiO₂, again the thermal expansion mismatch makes it crack much easier at even 120 °C. Since PDFMA does not work well at high PAB temperature, E-beam resist ZEP520 was chosen and the coated film showed good quality.

For the next step, we tested the lithography performance of two multilayer combinations: A: PMMA/OSCoR4000/SiO₂/ZEP520. B: PMMA/PDFMA/ZEP520. The results for combination A are shown in Figure 2.6. After E-beam lithography, the patterns look good on the largest dose applied – 50 $\mu\text{C}/\text{cm}^2$. The pattern was transferred successfully to the bottom PMMA brush layer through RIE process and the top materials were lifted-off. The resulting pattern could preserve the profile of the resist without solvent-induced relaxation. An acetone bath was then applied to test the pattern integrity. After immersion overnight, an AFM scan showed that the pattern degraded to 1/4 of its original volume and it could be caused by thermal degradation during the deposition of SiO₂. It was also proven when comparing the optical image before and after acetone wash, that the color of the non-patterned area changed from blue (~100 nm) to light brown (<50 nm). This phenomenon tells us that, even though the bulk substrate temperature never went above 21°C during the deposition process as

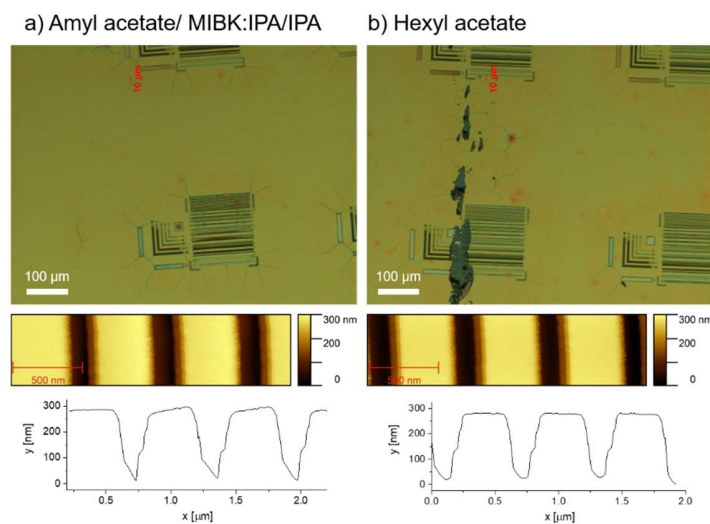


Figure 2.7 E-beam lithography patterning result of the PMMA brush with combination B. a) and b) were developed with two different developers. 300 nm 1:1 line:space pattern AFM scans and optical microscope images are displayed.

measured by the thermocouple in the instrument, in the nano-scale the SL surface still experienced high temperature caused by the evaporated material. The melting temperature of silicon oxide, at the evaporation deposition pressure 10^{-6} Torr, is above $750\text{ }^{\circ}\text{C}^{56,57}$. This is well above the thermal degradation temperature for polymers which makes them into chain fragments and ultimately becomes soluble.

Similar E-beam lithography testing was also conducted for combination B and the cracking of the film could be observed using optical microscopy as shown in Figure 2.7. Further AFM scans proved that it was caused by the dissolution of the PDFMA SL because the trench depth greater than the initial thickness of the E-beam resist (ZEP520, 150 nm). The reason for this is because PDFMA undergoes chain scission during exposure by the E-beam at doses below $500\text{ }\mu\text{C}/\text{cm}^2$ which was proven before

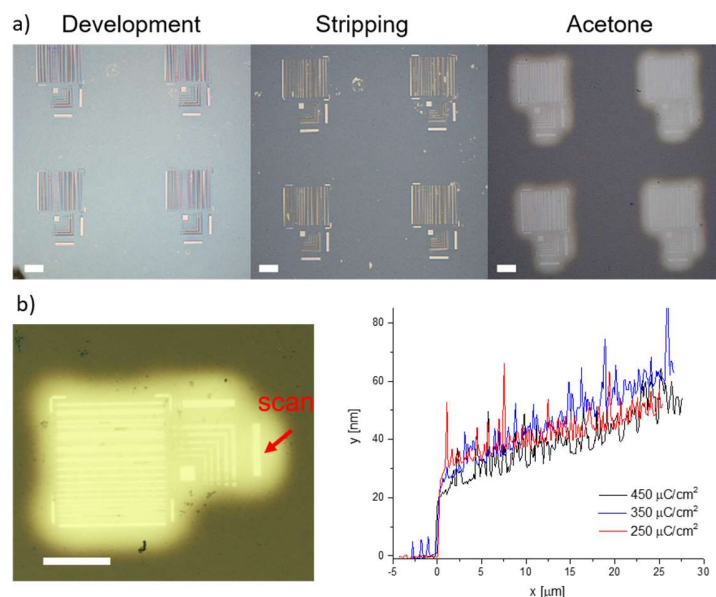


Figure 2.8 E-beam lithographic evaluation of the combination: PMMA polymer brush/ CYTOP/ ZEP520. a) optical microscopic images of the process after different steps. b) AFM scans on the big trenches exposed with different E-beam doses. Scale bar: 100 μm .

in our group.²³ In addition, since the resulting chain fragments are still highly fluorinated, there is not much difference between the patterns after different developing processes with different polarity because solubility of fluorinated material remains nearly the same in all solvents. Based on the same mechanism, the formation of cracking should be due to the penetration of the solvent through the patterned area which leads to the delamination of PDFMA.

2.3.3.2 CYTOP top-down patterning process

Both OSCoR4000 and PDFMA based processes suffer significantly from thermal mismatch which is due to the flexible nature of the methacrylate backbone. To ensure better process compatibility, a fluorinated material with a coefficient of thermal expansion like that of hard material is more preferred. In such a context, another commercially available fluorinated polymer CYTOP was chosen for its low thermal expansion and good chemical resistance.

E-beam lithography was selected first to fabricate nm patterns with a CYTOP layer as a SL which has been proven by Jungho *et al.*¹⁹ The results after each step are shown in Figure 2.8a. With ZEP520 as E-beam resist, the pattern was fabricated successfully on the PMMA/CYTOP/ZEP520 combinations without any film cracking observed. Next RIE processing also managed to transfer pattern to the PMMA polymer brush layer and the lift-off was performed well. However, in the integrity test (acetone immersion for 4 hours), a serious problem showed up that not only the patterned area, but also the area nearby all had decreased thickness as a cloud surrounding the pattern could be observed after acetone wash. Since PMMA could have chain scission reaction upon exposure to the E-beam, this could be possible. But surprisingly even though the dose used for PMMA as E-beam resist is above 800 $\mu\text{C}/\text{cm}^2$, it still lost > 50% of the materials at the edge of the patterns (original thickness is 85 nm) under

250 $\mu\text{C}/\text{cm}^2$ used for the ZEP520 resist as shown in Figure 2.8b and the loss increased with the increase of the used dose. AFM characterization also showed that such thickness decrease effects could go until at least 30 μm away from the patterned area.

A DUV lithography process was also conducted with CYTOP as SL. With their better thermal expansion property, HSQ and BARC films performed well on PMMA/CYTOP combinations and later the DUV photolithography process came out well also. Figure 2.9 showed that at the smallest 225 nm patterned PMMA brushes could be formed. After acetone immersion, the non-patterned area could still retain its original thickness while there was still $\sim 50\%$ materials lost on the patterns. Since

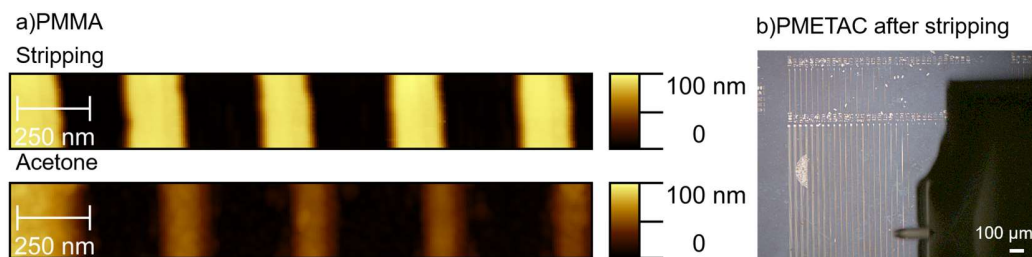


Figure 2.9 Patterns fabricated with top-layers: CYTOP/BARC/UV210. a): AFM scan on PMMA polymer brush 225 nm line pattern. After stripping, sample was soaked into acetone wash to test the integrity of the patterns. b): Optical microscope image on patterned PMETAC brushes after lift-off.

PMMA is insensitive to DUV, the degradation of the PMMA during the acetone immersion must be caused by the RIE which created detached, soluble fragments in the process. These phenomena have been investigated in more detail and will be reported in later chapters. The advantage of the CYTOP process is proven by patterning highly swollen polyelectrolyte brushes of PMETAC. Figure 2.9b showed that successful patterning could be done without any damage on the surface. A HSQ

based CYTOP top-down process was later used to pattern thick liquid crystal elastomer films and will be discussed in later chapters.

2.3.3.3 CYTOP Bottom-up patterning process

Since the top-down process could produce unavoidable modification of the patterned polymer brushes, focus was then shifted to the development of the bottom-up patterning process. The bottom-up patterning process has polymer synthesis as a final step and it could therefore avoid contamination in the process. Our group has already fabricated bottom-up patterned polymer brushes to the μm level by patterning of the initiators.⁵⁸ With a similar approach, bottom-up patterned brushes were fabricated by first patterning the filler-deposited surface with CYTOP/photoresist assembly to expose fresh reactive sites for initiator and then depositing initiator. The process flow and the patterning results are shown in Figure 2.10. Pre-filling the reactive hydroxyl regions on the silicon should effectively prevent the deposition of initiator which were diffused through CYTOP. Compared to the sample without any filler, patterned PMMA polymer brushes made on the substrate with filler, 2-[methoxy(polyethylenoxy)propyl]trichlorosilane(PEGf), not only fail prevent deposition (still some brushes grown on the filled area), but it also had more brushes grown on the area away from the pattern than close to the pattern. The protection of silicon from initiator deposition is stronger when using trimethylchloride (TMC) and strongest when using (1H,1H,2H,2H-Perfluorooctyl)trichlorosilane (FOTS) as filler. This could be due to the fact that the thickness of the FOTS filler, 8.27 nm is higher than the other two fillers (PEGf: 1.81 nm, TMC: 0.33 nm). Obviously, thickness is not the only reason determining the blocking effect since TMC has better blocking effect than PEGf. The presence of multi-chloride groups in PEGf indicates that they might still be present on the surface in the form of reactive hydroxy groups which could be

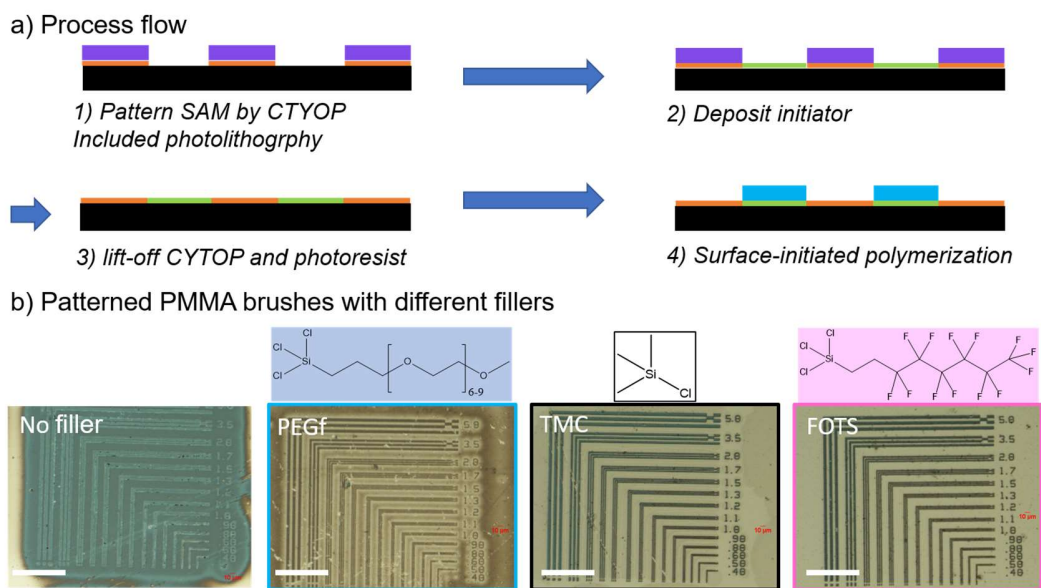


Figure 2.10 Bottom-up patterning a) process flow and b) the results with different fillers. PMMA is used as polymer for the growth of the brushes. Scale bar: 100 μm . The chemical structures of the fillers are shown above the optical microscopy images. Thickness of the fillers: PEGf: 1.81 nm/ TMC: 0.33 nm/ FOTS: 8.27 nm.

the anchor for the initiators. In the end this decreases the blocking efficiency of PEGf while the TMC simply could not fill the surface completely. The presence of the fluorinated group could also be helpful in blocking due to its immiscibility in both hydrophobic/hydrophilic phases.

Another method was also applied and we managed to fabricate bottom-up patterned polymer brushes. Since the diffusion of the initiator is detrimental to the pattern definition, deposition of the initiator was conducted at different time to tell the diffusion rate of the initiators. Figure 2.11 showed the optical microscope images of a 1 μm line made of PMeVP brushes grown on the samples with different initiator deposition times of 0.5/1/3/5 hours. The fabrication process is the same as Figure 2.10a but no filler was used. It can be seen that even with 0.5 hour deposition time, the effect of initiator diffusion is still observable as the line width expands beyond 1 μm .

Furthermore, it has thinner brushes grown on the center of the pattern compared to its surrounding based on the color of the patterns. It was found out that this is due to loss of activity in the center, as shown in another study that the surface energy of the plasma activated silicon surface decreased upon longer exposure to the air.⁵⁹ The CYTOP covered area, on the other hand is less exposed and therefore more reactive and leads to more initiator deposition and then polymer brushes grown on. A gentle plasma cleaning process was then applied to re-activate the exposed area before initiator deposition and the result showed that with 0.5 hour initiator deposition time it has the best pattern without line width expansion.

However, decreased deposition time also leads to reduced grafting density as proven in the work of Lego *et al.*⁶⁰ Compared to the overnight initiator deposited polymer brush, the grafting density reduced to ~0.5 of the grafting density by comparing the thickness of the polymer brushes. For that, we also tried to deposit initiator through 2-step reaction by first evaporating (3-aminopropyl)trimethoxysilane (APTES) on the silicon surface and then reacting it with α -bromoisobutyryl bromide (BIBB). The density of the gas is a lot less compared to the liquid, as is its diffusion coefficient. Taking advantage of it, patterned polymer brushes with grafting densities the same as the non-patterned area are obtained. By using DUV photolithography, bottom-up patterned polymer brushes could achieve line resolution smaller than 200 nm (initiator deposition area).

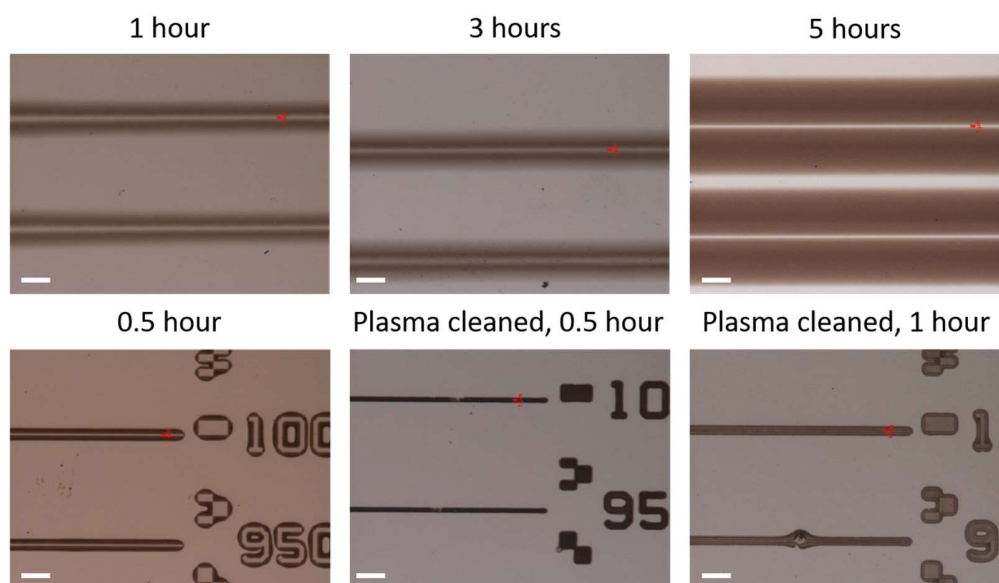


Figure 2.11 Patterned PMeVP brushes made of substrates with different initiator deposition time. Two of which were subject to plasma cleaning process before the deposition.

The free growth condition of the bottom-up patterned brushes makes its resulting morphology an already relaxed one which is different from the perpendicular profile in the top-down patterned polymer brushes. The difference in morphology makes the direct comparison to top-down patterned brushes challenging and the relaxed profile is not preferred for integration in electronic devices. We have tried to fabricate bottom-up patterned, unrelaxed polymer brushes by growing the polymer brushes before the lift-off of CYTOP. Nonetheless, a major problem showed-up that the polymer chains of the brushes penetrated into the CYTOP during the polymerization process and made lift-off impossible. For the future, a patterned template made of fluorinated materials that could have an on-demand degradation reaction which is non-destructive to the polymer brushes could be ideal because small molecules would not entangled with polymer brushes.

Bottom-up patterning process

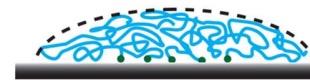
1) Form pattern through DUV photolithography on CYTOP



2) Deposit initiator and use HFE to lift-off

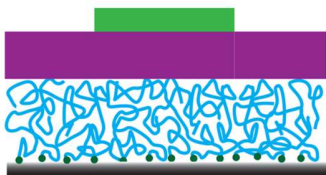


3) Surface-initiated Polymerization

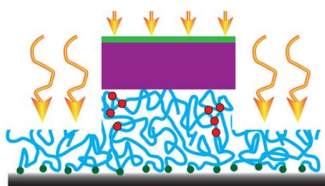


Top-down patterning process

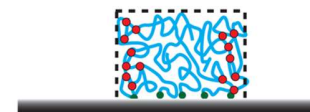
1) Form pattern through DUV photolithography



2) RIE pattern transfer



3) Use HFE to lift-off



Scheme 2.1 Finalized processes for fabrication of patterned polymer brushes

2.4 Conclusion

In the chapter, we fabricated patterned polymer brushes made by different methods and their properties are compared. Our target was to make sub 200 nm patterns without any damage to the structures of the polymer. Although E-beam lithography is one of the most widely used processes to fabricate sub-100 nm feature in academia, the vulnerable property of polymers under E-beam exposure together with wide-ranging back-scattering makes it unfavorable in the context here. DUV photolithography combined with an orthogonal photoresist is another powerful combination using the low adhesion/immiscibility of fluorinated materials and provides a basis for clean patterns together with the low sensitivity of polymer to DUV radiation reduces the chance of brush damage. However, the varying interaction between surfaces and the photoresist could be detrimental and increases the difficulty for process optimization. A more general way to pattern organic materials is then developed based on multilayer processing with a fluorinated sacrificial layer. With the continuous underlayer beneath the photoresist layer, the performance of photolithography could be guaranteed. CYTOP, with a lower thermal expansion and

low permeability, was chosen as sacrificial layer. Both top-down and bottom-up patterning processing is available and will be used as fundamental processes in subsequent chapters (Scheme 2.1).

REFERENCES

- (1) Horowitz, G. Organic Field-Effect Transistors. *Adv. Mater.* **1998**, *10*(5), 365–377.
- (2) Chiu, Y.-C.; Shih, C.-C.; Chen, W.-C. Nonvolatile Memories Using the Electrets of Conjugated Rod-Coil Block Copolymer and Its Nanocomposite with Single Wall Carbon Nanotubes. *J Mater Chem C* **2014**.
- (3) Sekitani, T.; Yokota, T.; Zschieschang, U.; Klauk, H.; Bauer, S.; Takeuchi, K.; Takamiya, M.; Sakurai, T.; Someya, T. Organic Nonvolatile Memory Transistors for Flexible Sensor Arrays. *Science* **2009**, *326*(5959), 1516–1519.
- (4) Cao, Y.; Steigerwald, M. L.; Nuckolls, C.; Guo, X. Current Trends in Shrinking the Channel Length of Organic Transistors Down to the Nanoscale. *Adv. Mater.* **2010**, *22*(1), 20–32.
- (5) Clayden, J. *Organic Chemistry*, 2nd ed.; Oxford University Press: Oxford, 2012.

- (6) Huang, J.; Xia, R.; Kim, Y.; Wang, X.; Dane, J.; Hofmann, O.; Mosley, A.; Mello, A. J. de; Mello, J. C. de; Bradley, D. D. C. Patterning of Organic Devices by Interlayer Lithography. *J. Mater. Chem.* **2007**, *17*(11), 1043–1049.
- (7) Meerholz, K. Device Physics: Enlightening Solutions. *Nature* **2005**, *437* (7057), 327–328.
- (8) Gong, X.; Wang, S.; Moses, D.; Bazan, G. C.; Heeger, A. J. Multilayer Polymer Light-Emitting Diodes: White-Light Emission with High Efficiency. *Adv. Mater.* **2005**, *17*(17), 2053–2058.
- (9) Balocco, C.; Majewski, L. A.; Song, A. M. Non-Destructive Patterning of Conducting-Polymer Devices Using Subtractive Photolithography. *Org. Electron.* **2006**, *7*(6), 500–507.
- (10) Zakhidov, A. A.; Lee, J.-K.; Fong, H. H.; DeFranco, J. A.; Chatzichristidi, M.; Taylor, P. G.; Ober, C. K.; Malliaras, G. G. Hydrofluoroethers as Orthogonal Solvents for the Chemical Processing of Organic Electronic Materials. *Adv. Mater.* **2008**, *20*(18), 3481–3484.
- (11) Kirsch, P. *Modern Fluoroorganic Chemistry*. 316.
- (12) Horvath, I. T.; Rabai, J. Facile Catalyst Separation Without Water: Fluorous Biphasic Hydroformylation of Olefins. *Science* **1994**, *266*(5182), 72–75.
- (13) Taylor, P. G.; Lee, J.-K.; Zakhidov, A. A.; Chatzichristidi, M.; Fong, H. H.; DeFranco, J. A.; Malliaras, G. G.; Ober, C. K. Orthogonal Patterning of

- PEDOT:PSS for Organic Electronics Using Hydrofluoroether Solvents. *Adv. Mater.* **2009**, *21* (22), 2314–2317.
- (14) Lee, J.-K.; Chatzichristidi, M.; Zakhidov, A. A.; Taylor, P. G.; DeFranco, J. A.; Hwang, H. S.; Fong, H. H.; Holmes, A. B.; Malliaras, G. G.; Ober, C. K. Acid-Sensitive Semiperfluoroalkyl Resorcinarene: An Imaging Material for Organic Electronics. *J. Am. Chem. Soc.* **2008**, *130* (35), 11564–11565.
- (15) Zakhidov, A. A.; Lee, J.-K.; DeFranco, J. A.; Fong, H. H.; Taylor, P. G.; Chatzichristidi, M.; Ober, C. K.; Malliaras, G. G. Orthogonal Processing: A New Strategy for Organic Electronics. *Chem. Sci.* **2011**, *2* (6), 1178.
- (16) Zhang, S.; Hubis, E.; Girard, C.; Kumar, P.; DeFranco, J.; Cicoira, F. Water Stability and Orthogonal Patterning of Flexible Micro-Electrochemical Transistors on Plastic. *J. Mater. Chem. C* **2016**, *4* (7), 1382–1385.
- (17) Ouyang, S.; Xie, Y.; Wang, D.; Zhu, D.; Xu, X.; Tan, T.; DeFranco, J.; Fong, H. H. Photolithographic Patterning of Highly Conductive PEDOT:PSS and Its Application in Organic Light-Emitting Diodes. *J. Polym. Sci. Part B Polym. Phys.* **2014**, *52* (18), 1221–1226.
- (18) Chang, J.-F.; Gwinner, M. C.; Caironi, M.; Sakanoue, T.; Sirringhaus, H. Conjugated-Polymer-Based Lateral Heterostructures Defined by High-Resolution Photolithography. *Adv. Funct. Mater.* **2010**, *20* (17), 2825–2832.

- (19) Park, J.; Ho, J.; Yun, H.; Park, M.; Lee, J. H.; Seo, M.; Campbell, E. E. B.; Lee, C.; Pyo, S.; Lee, S. W. Direct Top-down Fabrication of Nanoscale Electrodes for Organic Semiconductors Using Fluoropolymer Resists. *Appl. Phys. A* **2013**, *111* (4), 1051–1056.
- (20) Huang, W.; Besar, K.; LeCover, R.; Dulloor, P.; Sinha, J.; Martínez Hardigree, J. F.; Pick, C.; Swavola, J.; Everett, A. D.; Frechette, J.; et al. Label-Free Brain Injury Biomarker Detection Based on Highly Sensitive Large Area Organic Thin Film Transistor with Hybrid Coupling Layer. *Chem Sci* **2014**, *5* (1), 416–426.
- (21) Dhar, B. M.; Kini, G. S.; Xia, G.; Jung, B. J.; Markovic, N.; Katz, H. E. Field-Effect-Tuned Lateral Organic Diodes. *Proc. Natl. Acad. Sci.* **2010**, *107*(9), 3972–3976.
- (22) Dhar, B. M.; Özgün, R.; Jung, B. J.; Katz, H. E.; Andreou, A. G. Optimum Bias of CMOS Organic Field Effect Transistor Inverter through Threshold Adjustment of Both P-and n-Type Devices. *Electron. Lett.* **2010**, *46* (19), 1335–1336.
- (23) Newby, C. NOVEL APPLICATIONS OF FLUOROPOLYMERS IN SOLUTION-PROCESSED ELECTRONICS. Ph.D. Thesis, Cornell University, 2014.

- (24) Midthun, K. M.; Taylor, P. G.; Newby, C.; Chatzichristidi, M.; Petrou, P. S.; Lee, J.-K.; Kakabakos, S. E.; Baird, B. A.; Ober, C. K. Orthogonal Patterning of Multiple Biomolecules Using an Organic Fluorinated Resist and Imprint Lithography. *Biomacromolecules* **2013**, *14* (4), 993–1002.
- (25) Ejaz, M.; Yamamoto, S.; Tsujii, Y.; Fukuda, T. Fabrication of Patterned High-Density Polymer Graft Surfaces. 1. Amplification of Phase-Separated Morphology of Organosilane Blend Monolayer by Surface-Initiated Atom Transfer Radical Polymerization. *Macromolecules* **2002**, *35* (4), 1412–1418.
- (26) Chen, J.-K.; Hsieh, C.-Y.; Huang, C.-F.; Li, P.-M.; Kuo, S.-W.; Chang, F.-C. Using Solvent Immersion to Fabricate Variably Patterned Poly(Methyl Methacrylate) Brushes on Silicon Surfaces. *Macromolecules* **2008**, *41* (22), 8729–8736.
- (27) Ahn, S. J.; Kaholek, M.; Lee, W.-K.; LaMattina, B.; LaBean, T. H.; Zauscher, S. Surface-Initiated Polymerization on Nanopatterns Fabricated by Electron-Beam Lithography. *Adv. Mater.* **2004**, *16* (23–24), 2141–2145.
- (28) Lee, W.-K.; Patra, M.; Linse, P.; Zauscher, S. Scaling Behavior of Nanopatterned Polymer Brushes. *Small* **2007**, *3* (1), 63–66.
- (29) Rastogi, A.; Paik, M. Y.; Tanaka, M.; Ober, C. K. Direct Patterning of Intrinsically Electron Beam Sensitive Polymer Brushes. *ACS Nano* **2010**, *4* (2), 771–780.

- (30) Welch, M. E.; Ober, C. K. Characterization of Polymer Brush Membranes via HF Etch Liftoff Technique. *ACS Macro Lett.* **2013**, *2* (3), 241–245.
- (31) KOEPEL, R. R.; RUSSELL, A. J.; RAVIKUMAR, T. United States Patent Application: 0090074709 - METHODS, DEVICES AND SYSTEMS FOR BIOCIDAL SURFACE ACTIVITY. 20090074709, A1.
- (32) Ramakrishnan, A.; Dhamodharan, R.; Rhe, J. Controlled Growth of PMMA Brushes on Silicon Surfaces at Room Temperature. *Macromol. Rapid Commun.* **2002**, *23* (10–11), 612–616.
- (33) Zhang, T.; Du, Y.; Mller, F.; Amin, I.; Jordan, R. Surface-Initiated Cu(0) Mediated Controlled Radical Polymerization (SI-CuCRP) Using a Copper Plate. *Polym Chem* **2015**, *6* (14), 2726–2733.
- (34) Woeste, G.; Meyer, W. H.; Wegner, G. Copolymers of Ethyl P-Vinylbenzenesulfonate for the Preparation of Polyelectrolytes of Reproducible Ion Content. *Makromol. Chem.* **1993**, *194* (4), 1237–1248.
- (35) Paik, M. PATTERNING AND CHARACTERIZATION APPROACHES OF POLYMER THIN FILMS. Ph.D. Thesis, Cornell University, 2010.
- (36) Paik, M. Y.; Xu, Y.; Rastogi, A.; Tanaka, M.; Yi, Y.; Ober, C. K. Patterning of Polymer Brushes. A Direct Approach to Complex, Sub-Surface Structures. *Nano Lett.* **2010**, *10* (10), 3873–3879.

- (37) Maeng, I. S.; Park, J. W. Patterning on Self-Assembled Monolayers by Low-Energy Electron-Beam Irradiation and Its Vertical Amplification with Atom Transfer Radical Polymerization. *Langmuir* **2003**, *19*(10), 4519–4522.
- (38) Maeng, I. S.; Park, J. W. Formation of a Rectangular Poly(Methyl Methacrylate) Micropattern onto a Polystyrene Brush with Use of ATRP and Electron Beam Irradiation. *Langmuir* **2003**, *19*(23), 9973–9976.
- (39) Grant, D. H.; Grassie, N. The Thermal Decomposition of Poly(t-Butyl Methacrylate). *Polymer* **1960**, *1*, 445–455.
- (40) Stafford, C. M.; Vogt, B. D.; Harrison, C.; Julthongpiput, D.; Huang, R. Elastic Moduli of Ultrathin Amorphous Polymer Films. *Macromolecules* **2006**, *39*(15), 5095–5099.
- (41) Lawson, R. A.; Frommhold, A.; Yang, D.; Robinson, A. P. G. Chapter 8 - Negative-Tone Organic Molecular Resists. In *Frontiers of Nanoscience*; Robinson, A., Lawson, R., Eds.; Materials and Processes for Next Generation Lithography; Elsevier, 2016; Vol. 11, pp 223–317.
- (42) Lee, J.-K.; Chatzichristidi, M.; Zakhidov, A. A.; Hwang, H. S.; Schwartz, E. L.; Sha, J.; Taylor, P. G.; Fong, H. H.; DeFranco, J. A.; Murotani, E.; et al. Acid-Diffusion Behaviour in Organic Thin Films and Its Effect on Patterning. *J. Mater. Chem.* **2009**, *19*(19), 2986.

- (43) Weimer, M.; Wang, Y.; Neef, C. J.; Claypool, J.; Edwards, K.; Zu, Z. Materials for and Performance of Multilayer Lithography Schemes. In *Advanced Lithography*; International Society for Optics and Photonics, 2007; pp 65192S–65192S.
- (44) Sundaram, V. M.; Wen, S.-B. An Easy Method to Perform E-Beam Negative Tone Lift-off Fabrication on Dielectric Material with a Sandwiched Conducting Polymer Layer. *J. Micromechanics Microengineering* **2011**, *21* (6), 065021.
- (45) Angelopoulos, M. Conducting Polymers in Microelectronics. *IBM J. Res. Dev.* **2001**, *45* (1), 57–75.
- (46) Peng, W.; Chen, Y.; Ai, W.; Zhang, D.; Song, H.; Xiong, H.; Huang, P. CMOS-Compatible Fabrication for Photonic Crystal-Based Nanofluidic Structure. *Nanoscale Res. Lett.* **2017**, *12* (1).
- (47) Nojiri, K. *Dry Etching Technology for Semiconductors*; Springer International Publishing: Cham, 2015.
- (48) Rommel, M.; Nilsson, B.; Jedrasik, P.; Bonanni, V.; Dmitriev, A.; Weis, J. Sub-10 Nm Resolution after Lift-off Using HSQ/PMMA Double Layer Resist. *Microelectron. Eng.* **2013**, *110*, 123–125.

- (49) Yang, H.; Jin, A.; Luo, Q.; Li, J.; Gu, C.; Cui, Z. Electron Beam Lithography of HSQ/PMMA Bilayer Resists for Negative Tone Lift-off Process. *Microelectron. Eng.* **2008**, *85* (5–6), 814–817.
- (50) DeFranco, J. A.; Schmidt, B. S.; Lipson, M.; Malliaras, G. G. Photolithographic Patterning of Organic Electronic Materials. *Org. Electron.* **2006**, *7*(1), 22–28.
- (51) Newby, C.; Lee, J.-K.; Ober, C. K. The Solvent Problem: Redissolution of Macromolecules in Solution-Processed Organic Electronics. *Macromol. Res.* **2013**, *21* (3), 248–256.
- (52) Bowden, N.; Brittain, S.; Evans, A. G.; Hutchinson, J. W.; Whitesides, G. M. Spontaneous Formation of Ordered Structures in Thin films of Metals Supported on an Elastomeric Polymer. **1998**, *393*, 4.
- (53) *Metallization of Polymers 2*; Springer: Place of publication not identified, 2012.
- (54) Maji, D.; Das, S. Analysis of Plasma-Induced Morphological Changes in Sputtered Thin Films over Compliant Elastomer. *J. Phys. Appl. Phys.* **2014**, *47* (10), 105401.
- (55) Jia, Z.; Peng, C.; Lou, J.; Li, T. A Map of Competing Buckling-Driven Failure Modes of Substrate-Supported Thin Brittle Films. *Thin Solid Films* **2012**, *520* (21), 6576–6580.

- (56) Ferguson, F. T.; Nuth, J. A. Vapor Pressure of Silicon Monoxide. *J. Chem. Eng. Data* **2008**, *53* (12), 2824–2832.
- (57) Kurt J. Lesker Company. Material Deposition Chart.
https://www.lesker.com/newweb/deposition_materials/materialdepositionchart.cfm?pgid=0#s.
- (58) Dong, R.; Krishnan, S.; Baird, B. A.; Lindau, M.; Ober, C. K. Patterned Biofunctional Poly(Acrylic Acid) Brushes on Silicon Surfaces.
Biomacromolecules **2007**, *8* (10), 3082–3092.
- (59) Kaya, S.; Rajan, P.; Dasari, H.; Ingram, D. C.; Jadwisienczak, W.; Rahman, F. A Systematic Study of Plasma Activation of Silicon Surfaces for Self Assembly.
ACS Appl. Mater. Interfaces **2015**, *7* (45), 25024–25031.
- (60) Lego, B.; François, M.; Skene, W. G.; Giasson, S. Polymer Brush Covalently Attached to OH-Functionalized Mica Surface via Surface-Initiated ATRP: Control of Grafting Density and Polymer Chain Length. *Langmuir* **2009**, *25* (9), 5313–5321.

CHAPTER 3

Morphology of Nanostructured Polymer Brushes Dependent on Production and Treatment

Abstract

The morphology of top-down and bottom-up nanostructured neutral brushes is studied as a function of the production process and the quality of solvent to which the brushes have been exposed. Neutral brushes of poly(*tert*-butyl methacrylate) (*PtBuMA*) were grafted from the substrate by surface initiated radical-chain polymerization (SI-RCP). Brush patterning was conducted using deep ultraviolet (DUV) photolithography following either top-down (TD) or bottom-up (BU) approaches with patterned lines as small as 200 nm. The resulting brushes were immersed in toluene or methanol and the change of morphology of the dried brushes was monitored using tapping mode atomic force microscopy (AFM). TD nanostructured polymer brushes (NPBs) exhibit a box-like and BU generated brushes a lens-like shape directly after the production process. We show that the pattern width for the BU brushed depends not only on the wetting properties of the areas adjacent to the pattern, but also on the process history to which the sample has been exposed, especially the solvent quality. Furthermore we show that TD NPBs are crosslinked on the edges of the pattern because of the high energy process conditions during brush patterning and study the behavior of the thus obtained structures.

*Reproduced with permission from Chen, W.-L.; Menzel, M.; Prucker, O.; Wang E.; Ober, C. K.; R uhe, J. Morphology of Nanostructured Polymer Brushes Dependent on Production and Treatment. *Macromolecules* 2017, 50, 4715–4724.
Copyright 2017 American Chemical Society

Introduction

Polymer brushes are polymer chains tethered by one end to the surface of a solid with a high grafting density so that the polymer chains stretch away from the surface.¹⁻³ They can be used to introduce tailor-made surface characteristics including anti-fouling behavior,^{4,5} transport-enhancement^{6,7} or stimuli-responsive properties^{8,9}. Besides the unique properties of the different polymer brushes, it has become more and more important to locally control those properties by patterning of the brushes.¹⁰ In particular, nanostructured polymer brushes (NPBs) have proven to show extraordinary characteristics. The NPBs have pattern sizes comparable to molecular size or rather the contour length of the surface attached chains^{11,12}. NPBs show unique properties at the nanoscale¹³ and are the key for the development of advanced materials and devices for biotechnology¹⁴ and electronic/optical applications.^{15,16} When moving from microstructured brushes (where the pattern size is small but still large compared to molecular dimensions) to their nanostructured peers, important changes occur in the physics of the system. To understand these differences it is necessary to look at the edges of the pattern. For both micro- and nanostructured brushes chains tethered to the surface such an edge can fan out into areas where no surface-bound molecules are present. This way the brush molecules can relax some of the stress causing them to stretch. However, they cannot reach too far out into the free area nearby as they are still bound to the surface with one end. For microstructured brushes such edge effects affect only a small portion of all chains, namely those close to the edge of the pattern. However, upon decreasing the dimension of the patterns the relative proportion of such chains compared to the total number of chains contained in

the structure increases and when the pattern sizes reach the contour length of the surface-bound polymer chains a transition occurs from a 2D system which can swell only in one dimension to a 3D system which can practically swell in all three dimensions. This gives rise to a scaling behavior, where the brush height (in solution) is directly correlated with the pattern size.

Patra *et al.*^{13,17} were one of the first, who studied theoretically the scaling behavior of NPBs in good solvent as a function of the pattern size, molecular weight and graft density of the brushes. They have shown that the brush height increases very strongly with pattern size until it reaches the dimension of the contour length. Beyond this size, the brush height no longer varies with pattern size. They have complemented these theoretical studies with bottom up generated poly(N-isopropylacrylamide) (PNIPAM) brushes attached to small gold islands. They showed that the height of brushes synthesized under identical reaction conditions is significantly larger on nanopatterns with larger feature sizes compared to their smaller peers demonstrating a good correlation between theory and experiment.

Koutsioubas and Vanakaras have simulated the behavior of NPBs in solvents of varying solvent quality.¹⁸ They have found that under poor solvent conditions, the brush shrinks to a ball-like structure, which is distinctively different from the lenslike structure observed in a good solvent.

Jonas *et al.* investigated the influence of wetting energy of a substrate on the morphology of bottom up generated poly(2-(2-methoxyethoxy)ethyl methacrylate) (PMEO₂MA) polymer brush nanodroplets on silicon wafers.¹⁹⁻²¹ A model based on a 'Flory argument' was developed to calculate the theoretical morphology of NPBs,

where each polymer brush chain is treated as a vector with one end grafted on the surface and the other end stretched out and every vector has the same volume. The model successfully predicted the experimental results of PMEO2MA brushes on substrates with different surface energies and showed the wetting of the substrate leads to a decrease of the brush height in the nanostructured regime.

In a study by Chen *et al.* the shape of dry NPBs after solvent immersion was reported.²²⁻²⁴ They showed that for poly(methyl methacrylate) (PMMA) and poly(2-hydroxyethyl methacrylate) (PHEMA) the aspect ratio of the dry brush after immersion in a good solvent is higher than after immersion in a poor solvent. However, these results are a little difficult to compare to the work of Patras^{13,17} and Jonas²⁰, because Chen *et al.* exposed their brushes to quite strong ultrasound, which might lead to degrafting of some of the chains.²⁵ To explain the pattern size dependence they proposed that a change from brush to mushroom like regime occurs. Looking into the NPB generation, many investigations have been reported within the last decade to improve the manufacturing process of such systems.^{11,12,15} They can be categorized into two different lines: On the one hand there is the indirect or bottom-up (BU) approach in which the surface bound initiators are patterned and serve as a template to graft polymer chains from the surface during surface initiated polymerization (SIP).^{13,21,26,27} On the other hand there is the direct patterning or top-down (TD) approach in which the pattern is directly written on the surface of the pre-synthesized polymer brush. Materials are either removed mechanically²⁸ or degrafted by high energy irradiation²⁹. Although the direct writing step in TD process might

induce certain irreversible chemical/physical modification on the pre-synthesized polymer brushes²⁸⁻³⁰, it grants a flexible choice for application integration.

While for both top down and bottom up processes exemplary systems have been studied, a complete picture of the relationship between morphology and nanostructuring process is still lacking, because for the implementation of the different brush nanostructuring methods in the publications so far different polymers and different substrate materials have been used and it is difficult to compare systems generated with one process with a chemically different system by another process. Thus it might prove difficult to understand what is inherent to the processing and what is inherent to the physicochemistry of the brushes.

Motivated by such a situation, the present experimental work investigates the different morphologies of BU and TD patterned high molecular weight PtBuMA brushes with feature sizes in the range of the brush's contour length as a function of their production and development process. The growth by surface initiated radical-chain polymerization (SI-RCP) of high molecular weight polymer brushes on silicon is performed as reported previously,³¹ as was the nanopatterning by deep ultraviolet (DUV) photolithography to get BU and TD NPBs.³⁰ Such specific TD process was chosen for its high compatibility with industrial nanofabrication process which is generally available nowadays. The morphology of the thus obtained dry NPBs is studied by tapping mode AFM directly after manufacturing and immersion in solvents of different quality. The investigation enables a closer look on the impact of the production method on the NPBs morphology and properties.

Experimental Section

Materials. Silicon wafers (Si-Mat Silicon Materials) $600 \pm 15 \mu\text{m}$ thick, 125 ± 0.2 mm diameter and $\langle 100 \rangle \pm 0.5^\circ$ orientation with a native silicon oxide layer of ≈ 2 nm. tert-Butyl methacrylate (tBuMA) and 4-vinylpyridine (VP) were chromatographically purified over ALOX B, distilled in vacuum from copper(I) chloride and stored under nitrogen at -21°C . Toluene was distilled under a nitrogen atmosphere from a sodium alloy using benzophenone as an indicator. CYTOP fluoropolymer was purchased from BELLEX international incorporation. PtBuMA free polymer was purchased from Scientific Polymer Products, Inc. ($M_n = 1.26 \cdot 10^5 \text{ g}\cdot\text{mol}^{-1}$, PDI = 1.75). PVP free polymer was purchased from Sigma-Aldrich® ($M_n = 2.78 \cdot 10^4 \text{ g}\cdot\text{mol}^{-1}$, PDI = 1.86). All other solvents and chemicals were used as received from Sigma-Aldrich®.

Characterization. NMR spectra were recorded on a Bruker Avance 250 MHz spectrometer using CDCl_3 as the solvent. The molar masses were determined by GPC on an Agilent 1100 Series from PSS using THF as the eluent. The equipment was calibrated with narrow molecular weight PMMA standards. The AFM was equipped with a NanoWizard® head and controller from JPK. All AFM images were collected in the tapping mode (AC mode) using a SPM ACL-W probe from AppNano with a spring constant of 49 Nm^{-1} and a resonance frequency of 200 kHz. SEM images were taken on LEO 1550 field emission scanning electron microscope system. FT-IR spectra were measured at ATR-mode using Thermo Scientific Nicolet iZ10 FTIR with 4 cm^{-1} resolution and 128 scans. X-ray photoelectron spectroscopy (XPS) measurements were performed with a Surface Science SSX-100 spectrometer using a monochromatic Al $K\alpha$ source (1486.6 eV). Non-linear least squares curve fitting was

applied to high resolution spectra, using CasaXPS software. For the TD patterned film, XPS data are shown after removal of the CYTOP signals. The removal was based on the elemental ratio of CYTOP and the corrected ratio of the film materials could then be derived.

Top-Down Patterning Process. TD patterning process started with spin-coating three layers on the polymer brush with individual post-application baking (PAB) condition. CYTOP was coated first and PAB at 110 °C 5 min, ramped to 150 °C in 5 min, stayed at 150 °C for 5 min, ramped to 185 °C in 5 min, stay at 185 °C for 6 min. Following the first CYTOP coating, it was subject to RIE with Oxford PlasmaLab 80+ RIE system for 5 sec in order to create hydrophilic surface for subsequent material deposition. 2nd layer was XHRiC-16 anti-reflective coating layer (Brewer Science) with PAB at 175 °C for 1 min. 3rd layer was OiR-620 photoresist (FUJIFILM) with PAB at 90°C for 1 min. Photolithography patterning was then conducted on GCA Autostep 200 DSW i-line Wafer Stepper. The sample was then subject to post exposure bake (PEB) at 115 °C for 1 min before developing with MIF-726 (AZ Electronic Materials) developer for 1 min and spun to dry. 50 to 0.4 µm line patterns were created on the photoresist. Pattern was transferred by RIE process. The thickness of the layers were designed so that the residual materials contained on CYTOP and its thickness was > 700 nm. The design ensured the successful removal of the residual materials since the residual CYTOP had enough fraction of material intact. The pieces were then soaked in stirring hydrofluoroether, NovecTM-7300 at 50 °C overnight and rinsed with NovecTM-7300 repetitively. Afterward, pieces were blown dry with nitrogen gas.

Bottom-Up Patterning Process. BU process was similar to the TD process and modified based on previous published procedure.^{27,30} Wafer was cleaned with SC-2 process (soaked in solution made of HCl/H₂O₂/water (2/2/1 v/v/v)) for 2 h, then rinsed with DI water and dried with nitrogen gas. The patterned CYTOP polymer film on the cleaned wafer was conducted in the same way as the TD process but with different lithographic materials. On CYTOP, first layer was a spin-coated DUV-252 anti-reflective coating layer (Brewer Science) with PAB at 90 °C for 30 sec and 185 °C for 1 min. 2nd layer was a spin-coated UV 210 DUV photoresist (Shipley) with PAB at 135 °C for 1 min. Deep-UV photolithography patterning was then conducted on ASML 300 DUV stepper. The sample was then subject to PEB at 135°C for 1 min before developing with MIF-726 (AZ Electronic Materials) developer for 1 min and spun to dry. 50 μm to 0.2 μm line patterns were created on the photoresist. The pattern transfer was done with RIE process. The initiator was deposited in the same method (no wafer oxidation needed) as before and the CYTOP was removed afterward to obtain wafer with initiator pattern. BU patterned brushes were then fabricated by subsequent polymerization on the wafer with initiator pattern.

Immobilization of the Initiator on the Si Surface. The bottom-up template was cut in (2 x 6) cm² pieces and then flushed with nitrogen to remove all debris of silicon from the surface. For the top-down approach two sides polished silicon wafers were cut in (2 x 6) cm² pieces, flushed with nitrogen to remove all debris, soaked in H₂O/HCl conc./H₂O₂ (2/2/1 v/v/v) for 4 h and then rinsed with methanol and toluene. Substrates were placed in a Schlenk tube and left on vacuum overnight to remove all oxygen.

Immobilization of the initiator was done according to Rhe *et al.*²⁸ Substrates were placed in a Schlenk tube and fully covered with dried toluene and 3 ml of the initiator solution. 2-3 drops of dried trimethylamine were also added as a catalyst for the reaction. The Schlenk tube was placed in a dark place and the reaction mixture was stirred at room temperature for 24 h (top-down approach) or 1 h (bottom-up approach). Prior to polymerization, each substrate was carefully washed with toluene and methanol to remove physisorbed initiator and trimethylamine. The bottom-up template was additionally stirred in hydrofluoroether (NovecTM-7300) overnight. Substrates were then placed in flat Schlenk tubes and dried in vacuum overnight before polymerization.

Surface Initiated Radical-Chain Polymerization.

PtBuMA Brush. Distilled tBuMA and dry toluene were poured under nitrogen into flat Schlenk tubes containing the cleaned and dried substrate. The flasks were hermetically closed and the content was degassed by repeated freeze-thaw cycles. Flasks were filled with nitrogen and placed in a thermostat at 60.0 ± 0.1 °C for a specific time. After polymerization, wafers were rinsed and extracted overnight in toluene to remove all physisorbed polymer. Not attached polymer in solution was precipitated in methanol, filtered and dried under reduced pressure for characterization.

PVP Brush. Distilled VP and DMF were poured under nitrogen into flat Schlenk tubes containing the cleaned and dried substrate. The flasks were hermetically closed and the content was degassed by repeated freeze-thaw cycles. Flasks were filled with nitrogen and placed in a thermostat at 60.0 ± 0.1 °C for a specific time. After

polymerization, wafers were rinsed and extracted overnight in methanol to remove all physisorbed polymer. Not attached polymer in solution was precipitated in toluene, filtered and dried under reduced pressure for characterization.

Immersion Procedure. Samples of patterned brush or spincoated polymer with a dimension of (0.7 x 0.7) cm² was placed in a Schlenk tube and dried under reduced pressure for 2 h. 5 ml of solvent was poured under nitrogen into the Schlenk tube. After 2 h the brush was rinsed with solvent and dried under reduced pressure for characterization.

Patterning of a Spin-coated Free Polymer Layer and Dissolving.

PtBuMA. Solutions of free PtBuMA in chloroform were used for spin coating on silicon wafer and subject to PAB at 135 °C for 1 min, and then 185° C for 5 min. After coating, the PtBuMA film was subject to TD process to create patterns. To remove the unmodified polymer, patterned film was put into 50 °C THF stirring bath for 2 h. The film was then dried in vacuum overnight.

PVP. Solutions of free PVP in dimethyl formamide (DMF) were used for spin coating on silicon wafer and subject to PAB at 90 °C for 2 min, and then 185 °C for 5 min. After coating, the PVP film was subject to TD process to create patterns. To remove the unmodified polymer, the patterned film was placed into 50 °C DMF stirring bath for 3 h. The film was then dried in vacuum overnight.

Results and Discussion

Patterning Process. The key idea of this study was to fabricate indirectly (BU) and directly (TD) patterned polymer brushes prepared from the same monomer and initiator having nearly identical chain length and graft density to allow a consistent

comparison. The patterning processes used are the same as in scheme 2.1 and the chemical structure of the polymer brushes are shown in Figure 3.1. For both approaches the first main step was the coating of CYTOP, a fluoropolymer, onto either a silicon wafer (BU) or a homogenous polymer brush (TD). The use of a fluoropolymer avoids any swelling of the surface-attached layers or any intermixing.³² After that, a series of photolithographic materials was coated and the patterns were created by DUV photolithography. In case of the TD approach the patterns on the resist were transferred to the CYTOP layer and the polymer brush layer by the RIE process where the high energy species (ions, radicals) in the plasma lead to chain fragmentation of the polymer.

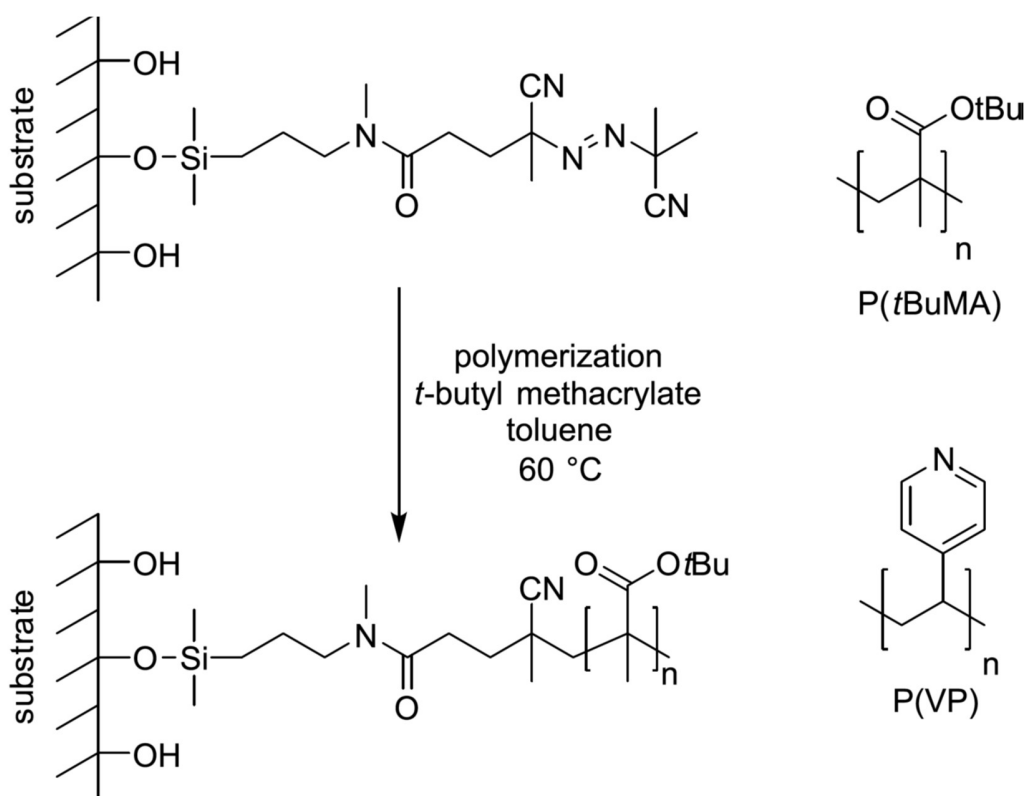


Figure 3.1. radical-chain polymerization and the monomers used for synthesis of the polymer brushes.

Bottom-Up Patterned Nanobrush. To prepare the BU patterned polymer brushes, we first patterned a CYTOP™ film functioning as a template by DUV photolithography. The pattern transfer was done by reactive ion etching (RIE) to form an array of trenches ranging from 0.2 μm to 50 μm in width. The silicon substrate was then functionalized with the azo initiator silane in toluene. A reaction time of only 1 h was chosen to prevent creeping of the initiator under the CYTOP film. In a next step the CYTOP layer was lifted off while stirred in hydrofluoroether overnight. The PtBuMA brush was then grown from the azo initiator-covered regions in toluene by radical-chain polymerization (RCP) similar to the work of Prucker and R  he³¹. When the CYTOPTM film was not removed before brush growth, it was observed that the fluoropolymer could not be completely removed in the end, presumably through chain transfer and follow up reaction across the brush- fluoropolymer interface. The reason why we have decided to use RCP brushes for our study is that this method generally allows the generation of very high molecular weight brush molecules in many cases of more than 106 g*mol⁻¹. Therefore the contour length is in the range of several microns, so that in all of the samples with the smaller pattern sizes the size is equal or smaller than the contour length. The supernatant solution was poured into excess of methanol to precipitate the nonattached polymer. The molecular weight of the non-bonded polymer was determined by GPC and taken as representative of the molecular weight of the polymer brush.³³ The silicon wafer was then further extracted in toluene using a soxhlet extractor equipment. Each wafer supports the complete range of line sizes to ensure that there are no differences in polymerization conditions and the distances between the lines were chosen large enough to avoid an overlap of patterns.

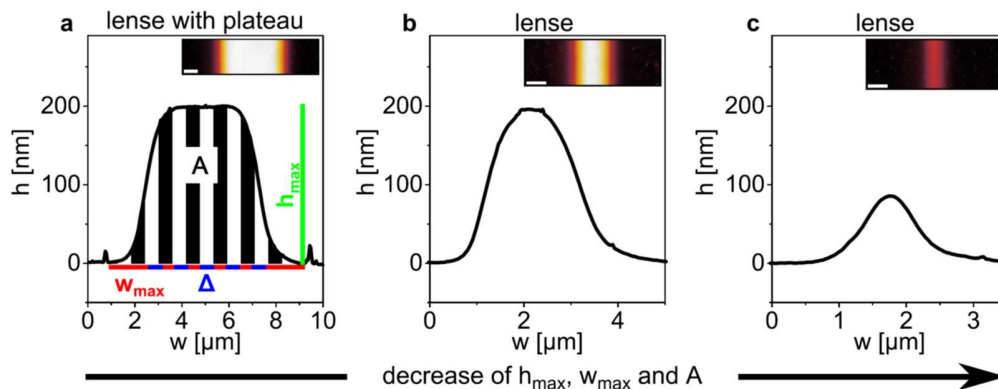


Figure 3.2. AFM height profiles of dry nanostructured PtBuMA brushes measured perpendicular to the brush line direction showing the transition from a quasi-two to a quasi-three dimensional system and the lens-like morphology. In profile a) are the characteristic dimensions illustrated. The pattern sizes are a) 5, b) 2 and c) 0.4 μm . Inset figures are the AFM top-down views of the brushes with scale bar for 1 μm .

The dry patterned PtBuMA brushes were analyzed using tapping mode atomic force microscopy (AFM) in air. Figure 3.2 shows the height profiles of the polymer brush lines with pattern sizes of 5, 2 and 0.4 μm measured perpendicular to the line direction. The characteristic dimensions are the maximum height h_{max} , maximum width w_{max} and the integral A of the patterned brush line cross section as well as the pattern size Δ , which describes the width of the initiator-covered, respectively, polymer grafted region. All these parameters are illustrated in Figure 3.2a. On the one hand the profiles illustrate that h_{max} , w_{max} and A are decreasing with decreasing pattern size and on the other hand they show the transition from a quasi-two dimensional to a three dimensional system. The quasi two dimensional system is

present where the line profile shows a plateau at the center of the pattern. In this system h_{\max} reaches the dimension of a homogenous brush layer and the edge area or rather excess width is small compared to Δ (Figure 3.2a). We will call such systems microstructured polymer brushes (MPBs) or rather microbrushes. A quasi-three-dimensional system is obtained where h_{\max} decreases in comparison to the homogeneous brush and the height profile shows a lens-like shape (Figure 3.2b and 2c). The lenslike shape results from several causes. The first is that the excess width reaches the dimension of Δ and the polymer chains at the periphery of the line become more important to the overall behavior of the NPB. At the edge of the pattern the chains have more space available and can stretch horizontally into the polymer-free areas along the surface. As the chains at the edge fan out the chains at the center can also relax. If the pattern size is small enough compared to the chain length this results in a decreasing of the brush height and a lens-like morphology. When the drying process is fast and no further rearrangement of the polymer chains occurs, this will also result in a lenslike morphology in the dry state. We will call those nanopatterned polymer brushes (NPBs) or rather nanobrushes.

In the experiments shown in Figure 3.3 the maximum height h_{\max} of the brush lines decreased from 255 to 65 nm with decreasing pattern size Δ from 50 to 0.2 μm . The plot shows that the transition point from the quasi-two to the quasi-three dimensional system is at around $\Delta \approx 3 \mu\text{m}$. This value is slightly less than the contour length of the polymer chains which is for the high molecular weight material ($DP \approx 13000$) approximately 3.2 μm . Accordingly, the transition from the micro- to nanobrush regime occurs when pattern size and contour length are close to each other.

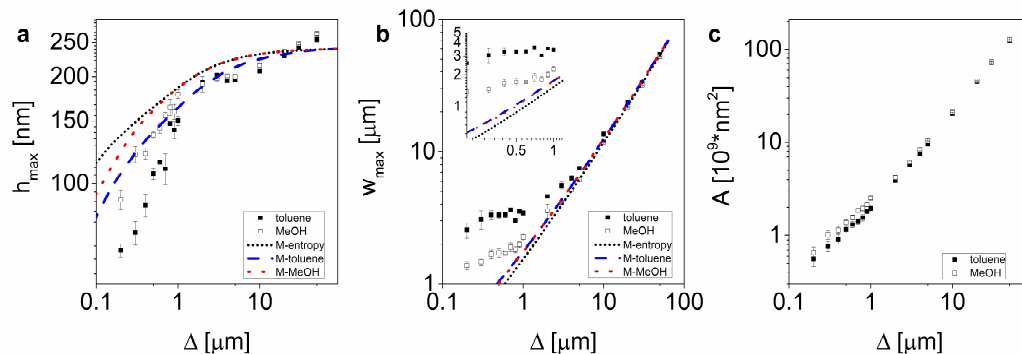


Figure 3.3. Plots of the maximum height h_{\max} (a), the maximum width w_{\max} (b), and the cross section integral A (c) as a function of the pattern size Δ of dry bottom-up PtBuMA nanobrushes grown in a single experiment after immersion in toluene (■) and in methanol (□). The data were obtained by tapping mode AFM. The dotted lines are guidelines for the eye. Theoretical lines based on the corresponding conditions are also presented in (a) and (b) as a comparison. The entropy line was obtained without including surface wetting effect while the other two were obtained by combination of the wetting energies measured experimentally.

At these pattern sizes the slope of the height/size relationship changes. At very small pattern sizes the maximum height increases strongly with pattern size (i.e. between 0.2 and 1 μm pattern size the height increases from almost 0 to about 180 nm), while for larger structures it remains almost constant (between 1 and 50 μm it increases only from about 190 to 220 nm). The plot of the height integral A as a function of Δ is shown in Figure 3.3c. This cross-sectional integral was calculated by integration of the height profile, which was measured using AFM perpendicular to the brush line

direction. The integral scales as expected linearly with the pattern size ($A \propto \Delta$). This relation can be derived from

$$l \cdot A = \Gamma \cdot l \cdot \Delta \cdot M_n \cdot \rho^{-1} \quad (3.1)$$

where l is the length and A is the cross sectional area of the brush line. Γ is the grafting density and Δ the width of the initiator covered region. M_n and ρ are the molecular weight and the density of the polymer, respectively. That the integral of the profile is proportional to the pattern width indicates that the SI-RCP process is not affected by the pattern size. The result is in agreement with the work of Jonas *et al.*²⁰, who have observed the same scaling behavior for atom-transfer radical polymerization grown poly-2-(2-methoxyethoxy) ethyl methacrylate) (PMEO₂MA) NPB.

However, upon closer inspection of the data it is observed that the solvent from which the NPB is dried has a strong influence on the morphology scaling, at least for small pattern sizes. We found that the shape of the height profile or rather the brush's morphology was affected by whether it had been immersed in a good (toluene) or a non-solvent (methanol) before drying and analysis. When the brush is dried from toluene solution the lens-shape is much flatter (i.e. wider and less high) than when the same brush dried from methanol solution.

Figure 3.4 displays the morphology of a PtBuMA nanobrush line pattern as a function of solvent exposure. After the PtBuMA brush synthesis the wafer was extracted in toluene to remove all unattached polymer chains and dried under vacuum. The dry nanobrush profile was measured using tapping mode AFM and showed a smooth lenslike morphology. However, when the nanostructured PtBuMA brush was immersed in methanol, dried and again analyzed by AFM the morphology of the brush

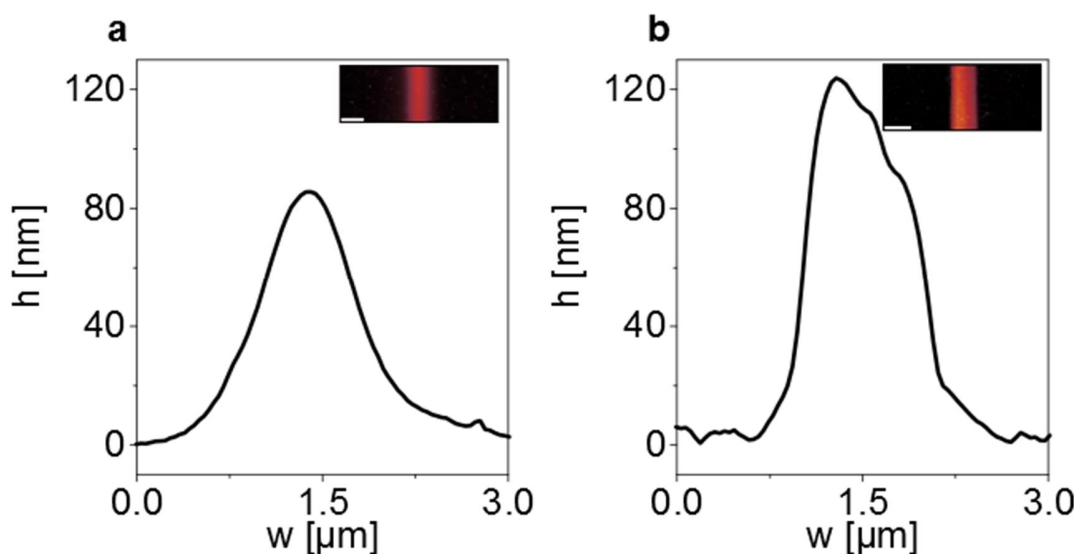


Figure 3.4. AFM height profiles of the 0.4 μm Δ line showing an example of the change of the dry PtBuMA NPBs morphology after immersing it in methanol. Profile a) displays the dried brush after extraction with toluene and b) displays the dried brush after immersion in methanol. Inset figures are the AFM top-down views of the brush with scale bar for 1 μm .

line had changed (Figure 3.4b). The same effect could also be observed with SEM (Figure 3.S1). The width of the brush lines decreased and the height increased (but the volume stayed the same). This effect was most obviously observable for the smaller pattern sizes where the patterned brush or rather NPB shows a quasi-three dimensional behavior, but it had no influence on the basic h_{max} as a function of Δ behavior as shown in Figure 3.3.

The morphological change can be explained, when first the situation of the brush in solvent is viewed. When the brush is exposed to a good solvent, the chains at the edge of the pattern fan out quite strongly into the polymer free solution next to the pattern. Upon drying they collapse and form a dry film with a morphology with a lenslike

shape. When a bad solvent is used, this fanning out is strongly reduced and the spreading of the polymer outside of the pattern becomes much weaker. Accordingly, in the good solvent case the pattern height is much lower than in the bad solvent case. Although w_{\max} and h_{\max} change A stays the same as shown in Figure 3.3c, which indicates that there is no degrafting or chemical reaction happening.

The observed scaling behavior of NPBs as a function of solvent quality has been simulated by Koutsioubas and Vanakaras for brushes in contact with solvent.¹⁸

Although in contrast to this work we monitor the NPB's dry state morphology, the comparison might be useful. It was found that in agreement with our findings the lateral expansion of the brush decreases with decreasing solvent quality and in contrast to our findings the vertical expansion of the brush decreases with decreasing solvent quality as well.¹⁸ Such difference could originate from the model used in the simulations and its limited accuracy for poor solvent conditions where the brush chains are "crystallizing" instead of remaining in the amorphous state.^{34,35}

Additionally, the simulations do not take wetting effects into consideration which are quite important for dry nanobrushes. Still, the simulations illustrate quite nicely how important the solvent-polymer interaction is for the shape of NPBs.

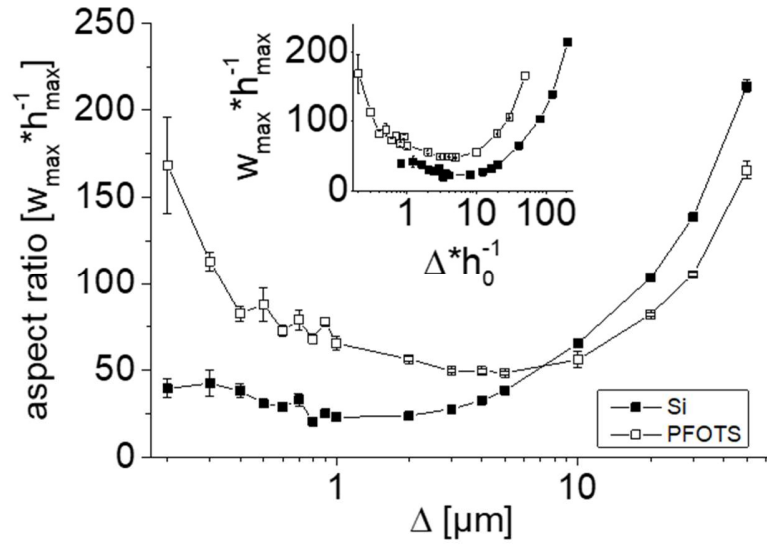


Figure 3.5. Aspect ratios of the patterned PtBuMA brush lines as a function of Δ respectively Δ/h_0 for the inset graph. ■ are the data of brushes grown on Si substrate and □ are the data of brushes grown on FOTS modified substrate

In general, the experiments described here are in good agreement with those published by Jonas *et al.* who describe how chain entropy and wetting energy control the morphology of dry NPBs.^{20,21} They observed that if the bare surface next to the pattern is readily wetted by the polymer constituting the brush, the pattern becomes wider and h_{\max} smaller in the nanobrush regime and that non-wetting surfaces cause narrower and higher features. To elucidate the influence of the surface energy of the substrate on the NPB we modified the substrate's surface absent brushes with perfluorooctyl-trichlorosilane (FOTS) and compared the aspect ratios (w_{\max}/h_{\max}) of both brushes with each other. This is the inverse situation as the work of Jonas *et al.* who grew different polymer brushes on the same surface. In Figure 3.5 the aspect ratio is shown as a function of Δ and the inset graph shows the aspect ratio as a function of the

normalized Δ (Δ/h_0 with h_0 = nonpatterned brush height).^{13,20} The data shows that the morphology of the patterned brushes are changed with decreasing Δ , because of the transition from the micro- to nanobrush regime and the changes in the wetting energy. In the microbrush regime ($\Delta/h_0 \geq 10$) the aspect ratio is dominated by w_{\max} as h_{\max} is reaching its maximum value and essentially scales linearly with Δ . In this regime the morphology is independent of the pattern size and wetting. At smaller Δ ($10 \geq \Delta/h_0$) the patterned brushes are in the nanobrush regime. Here the brushes assume a wetting dominated lens-shaped morphology and h_{\max} of the lens is directly correlated with Δ which leads to an increasing of the aspect ratio in which this effect gets more obvious for even smaller Δ . The situation is in general for both the silicon and the fluorinated surfaces similar. But as there is less interaction between the fluorinated surface and the polymer brush chains they can more easily expand along the surface, which leads to an overall higher aspect ratio of the polymer brushes compared to those grown on regular silicon surface.

However, according to our findings, for a quantitative description not only pattern size and wetting situation must be considered, but also the solvent quality of the solvent to which the brush has been exposed. A good solvent (e.g. toluene in this case) will induce a stronger expansion of the brush along the surface, than a bad solvent (in this case methanol). Accordingly the pattern size will be larger in the first case. To elucidate the influence of the surface wetting, theoretical curves were calculated for a situation where next to the brush the silicon substrate was unmodified. As input to these calculations the surface tension of a non-patterned polymer brush prepared under the same conditions as the patterned samples was measured after solvent

immersion.^{2,35} The interfacial interaction was calculated based on this data and the results of these simulations are shown in Figure 3.3 where it becomes obvious that h_{\max} decreases as the pattern size Δ shrinks due to increased surface wetting. In addition, due to the stronger surface wetting, h_{\max} is after toluene immersion smaller than the one after methanol immersion.

Nevertheless, it becomes also obvious that only a qualitative fit was achieved when the theoretical values were compared to the experimental data, especially in the nanobrush regime where h_{\max} is smaller and w_{\max} larger than expected. One possible explanation for this is that the drying of the swollen brush is too fast for the chains to reorganize from their conformation in solvents and arrange themselves completely according to the wetting thermodynamics. In the end they are frozen in a non-equilibrium state and cover the surface to a larger extent than they would do at equilibrium. This assumption is supported by the fact that especially shows a strong deviation between theory and experiment which could be attributed to a faster drying at the edge of the brushes.

Similar tests have been done with the FOTS modified substrate next a polymer brush pattern, which exhibited a quantitatively related behavior (see supporting information).

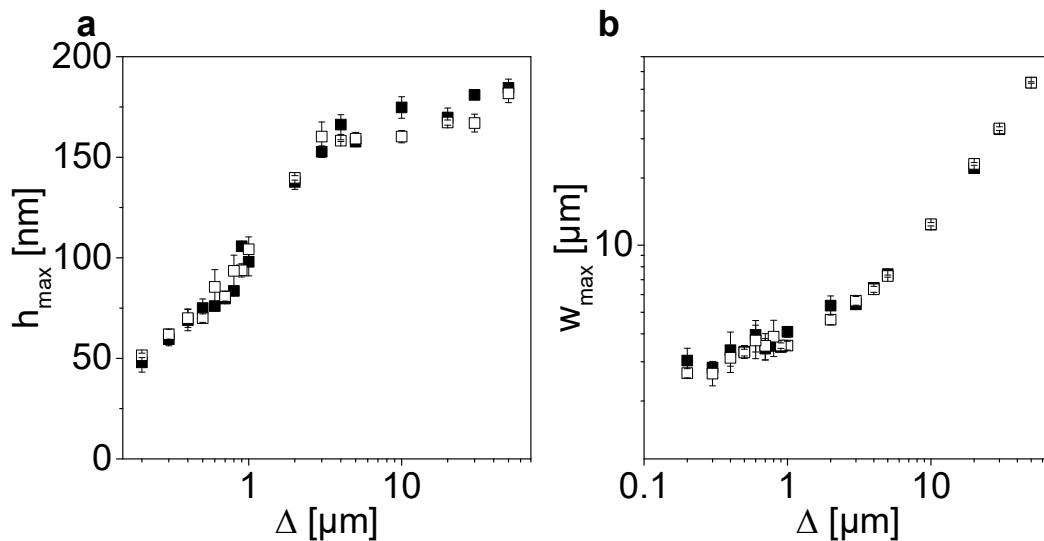


Figure 3.6. Plots of the maximum height h_{\max} (a) and the maximum width w_{\max} (b) as a function of the pattern size Δ of dry BU P(tBuMA-co-MABP) nanobrushes from a single experiment after immersion in toluene (■) and in methanol (□). The data were collected by tapping mode AFM.

The fact that the width and height of the pattern changes depending on the environment to which the sample has been exposed, could have detrimental effects in applications where such surfaces are exposed to strongly changing environments. Such undesired changes in the morphology can be completely prevented by chemical crosslinking of the polymer chains forming the brush. To demonstrate this we have grown BU patterned poly(tert-butyl methacrylate-co-4-methacryloyl-oxy-benzophenone) (P[tBuMA-co-MABP]) copolymer brushes in the same way as the PtBuMA brushes described above. The benzophenone units built into the forming copolymer can be photoactivated during UV exposure to crosslink the polymer structures in the dry, glassy state. The crosslinking leads to an immobilization of the chains and a

conservation of the brush line shape upon solvent exposure regardless of the solvent quality (Figure 3.6).

Top-Down Patterned Nanobrush. TD patterning of brush layer was conducted on both neutral and charged polymer brushes with a modified orthogonal process.³⁷ To this, a CYTOP film was spin-coated on the pre-synthesized non-patterned PtBuMA brushes ($M_n = 2.0 \cdot 10^6 \text{ g} \cdot \text{mol}^{-1}$) as a protective layer which isolate the brushes in the following process. Subsequent short oxygen-plasma etching was used to modify the CYTOP surface in order to allow the following coating of the photoresist material. The pattern formation on the brush followed the steps in BU process and the residual materials were removed by hydrofluoroether wash. In contrast to patterns derived

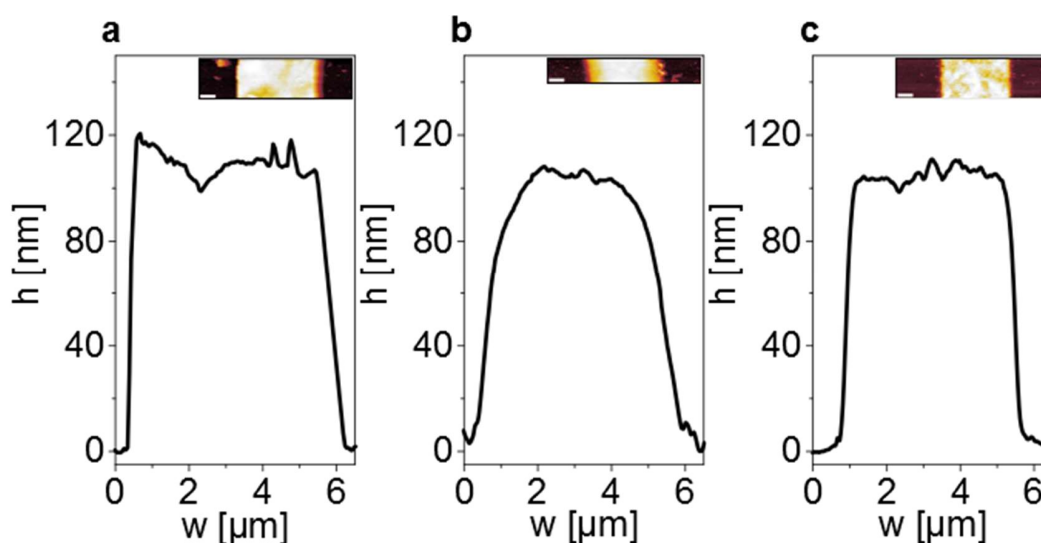


Figure 3.7. AFM height profiles of dry TD PtBuMA brush. a) after manufacturing process, b) after immersion in toluene and c) after immersion in methanol. The profiles show the morphology change from box-like to lens-like shape and back as a function of solvent quality. Inset figures are the AFM top-down views of the brushes with scale bar for 1 μm .

from the BU process consisting of solvent swollen, i.e. relaxed brushes, the orthogonal process created patterned brushes with a box-like shape as shown in Figure 3.7a.

Figure 3.8a shows the maximum height versus pattern size of the TD patterned brushes. It can be seen that after the process the thickness did not change as the pattern size decreased, thus proving successful orthogonal patterning.

Similar solvent immersion tests as for the BU patterned brushes were conducted on the TD patterned brushes in order to study how morphological changes are affected by the way the brushes are generated. Figure 3.8 shows the pattern dimensions maximum height (h_{\max}), maximum width (w_{\max}) and AFM cross sectional area (A) as a function of the pattern size (Δ). The decrease of the value of A of the patterns after immersion in toluene indicates some loss of material (Figure 3.8c). The material loss could be attributed to the extraction of the untethered polymer fragments left in the film after

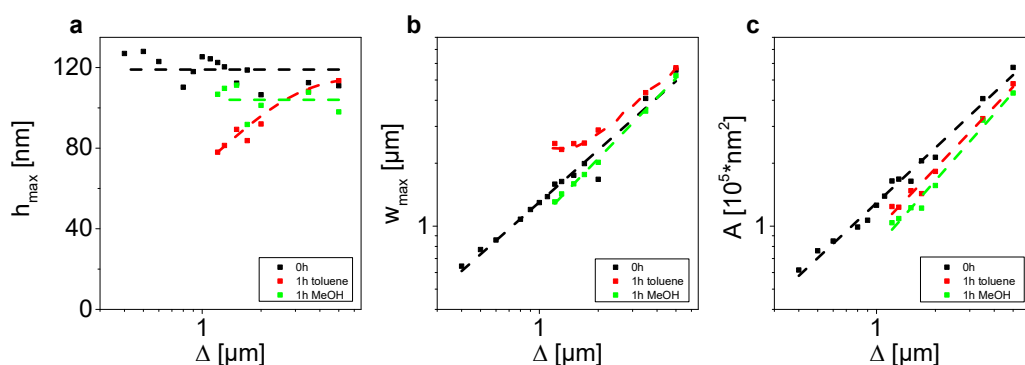


Figure 3.8. Plots of the maximum height h_{\max} (a), the maximum width w_{\max} (b) and the cross section integral A (c) as a function of the pattern size Δ of dry top-down patterned PtBuMA nanobrushes in a single experiment after patterning (■), immersion in toluene (■) and in methanol (■). The data were received by tapping mode AFM. The dash lines are guidelines for the eye.

the RIE process. The height h_{\max} as a function of pattern width Δ showed a trend similar to the BU patterned PtBuMA nanobrushes, i.e. lens-shaped structures with a width higher than the original pattern were observed. Interestingly, after soaking in methanol and drying, it was observed that the shape of patterns returned back to the box-like profile similar to the morphology directly obtained after the patterning process.

This behavior was independent of the size of the pattern. Because such phenomena were not observable for BU patterned brushes it must be caused by the TD patterning process. A possible explanation for this behavior is that the plasma process induces crosslinking of the polymer at the edges of the pattern through formation of additional covalent bonds.³⁸⁻⁴¹ Such crosslinked fraction of the pattern show a rubberlike behavior, i.e. when they are deformed and the forces which cause them to deform are removed, they will return to their original shape. Thus strong swelling of the system will cause the system to deform and this deformation is 'frozen in' by drying. However, if the system is given a chance to relax it will attain again the original shape. The reason why the shape-memory effect is only observed for bad solvents must be that a good solvent penetrates into the structure and swells it completely while a non-solvent interacts only with the surface of the pattern and allows the subchains of the network in the crosslinked edges to return to their original conformation. To prove this assumption, TD patterned poly(4-vinylpyridine) (PVP) brushes ($M_n = 4.6 \cdot 10^6 \text{ g} \cdot \text{mol}^{-1}$) were fabricated. The resulting neutral PVP brushes were then converted to strong polyelectrolyte brushes (PEBs) through quarternization of the

pyridinium ring using methyl iodide to yield poly(4-methyl-vinylpyridinium iodide) (PMeVP).

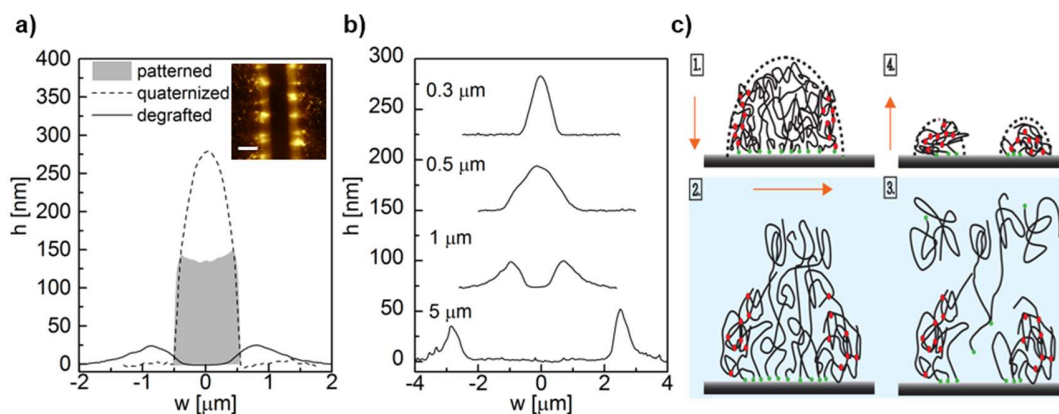


Figure 3.9. Dry brush morphology of TD patterned PMeVP brushes. a) Evolution of dry morphology of 1 μm patterned PVP brush after patterning, quaternization and degrafting in the water. Inset figure is the AFM top-down view of the brush after degrafting with scale bar for 1 μm . b) Degrafted brush cross-sectional morphology at different pattern sizes. c) Suggested mechanism for brush degrafting in water. The crosslinking on the sidewall not only limited the vertical stretching of the quaternized brush but also stabilized the material.

Such brushes become less stable against chain fragmentation and degrafting ('entropic death').⁴²⁻⁴⁵ If the brush would be crosslinked at the edge of the patterns and exposed to water, which causes some loss of the brush chains by degrafting, there should be more material remaining from the edge of the pattern than from the middle section as the crosslinking enhances the stability. In Figure 3.9a and 3.9b, the results of such experiments on patterned PVP brushes and their subsequent morphologies are shown. During quaternization the mass of the PVP increases by more than a factor of 2 as the molecular weight of the vinylpyridine repeat unit ($M_{VP} = 106 \text{ g}\cdot\text{mol}^{-1}$) increased due

to the uptake of the methyl iodide ($M_{MeVP} = 242 \text{ g} \cdot \text{mol}^{-1}$). Accordingly, the aspect ratio of the film increased quite strongly (Figure 3.9a). For wide pattern sizes ($\Delta > 1 \mu\text{m}$) after degrafting in water at room temperature, only the edge materials of the patterns were left. (Figure 3.9a and 3.9b) The smaller the pattern sizes became, the closer the two rims got and for pattern sizes smaller than $0.5 \mu\text{m}$ they merged together forming only one single structure. Additionally, it should be noted, that the material remaining on the surface after degrafting independent of the pattern size and thus independent of the initial mass of the brush. All these findings are a strong evidence of crosslinking at the pattern edges in the TD process, which hinders the lateral expansion and made material present at these edges more stable (Figure 3.9c).

polymer film	C (atom-%)	O (atom-%)	N (atom-%)	C/O
PtBuMA	80.69	19.31	0.00	4.18
Patterned PtBuMA	75.99	24.01	0.00	3.17
PVP	89.36	0.00	10.64	-
Patterned PVP	77.66	13.25	9.09	5.86

Table 3.1. XPS elemental analysis data of TD patterned PtBuMA and PVP films showing the increase of carbon/oxygen ratio after RIE process caused by crosslinking reaction.

Due to the strong osmotic pressure in the brush and the extremely strong stretching of the polymer chains the PEBs were easy to degraft and the material left over on the pattern edges could be characterized by XPS. They showed a considerable amount of

oxygen to be present in the film due to oxidation after the RIE. Such an analysis could not be done on the more stable, neutral PtBuMA brushes. To conduct experiments on neutral polymers patterned by a top-down approach, spin-coated samples of free PtBuMA were fabricated and subject to the same TD process conditions and subsequently carefully extracted. It was shown, that also in this case some material could not be washed away and a similar morphology as in the patterned PEBs, was obtained. These crosslinked materials were also subjected to detailed chemical characterization. Table 3.1 shows the XPS elemental analysis results of material stemming from the pattern edges. Compared to the original PtBuMA, the patterned TD PtBuMA showed a significant increase of the oxygen content of the material indicating the formation of additional oxygen-containing functional groups at the edge. In the ATR-FTIR spectrum (Figure 3.S7) of the leftover edge material the formation of the ketone and ester groups and C-C bonds could be observed together with disappearance of tert-butyl and original carbonyl groups. Formation of new oxygen containing groups must be more than the loss of the old one based on an increase of the C/O ratio derived from XPS study. It is then concluded that the crosslinking is composed of C-C or C-O-C bonds formed during the RIE process. Similar effects could be observed on TD patterned free PVP film (see supporting information) and its elemental analysis is included in Table 3.1.

Conclusion

The morphologies of dry nanopatterned polymer brushes, generated by bottom-up or top-down approaches depend quite strongly on how the nanoscale pattern have been generated. Even when the two processes use the same monomer and the same initiator

and one would assume at first sight that that the chemistry and physics of the systems are identical, the obtained nanostructures will have strongly differing morphologies. In the TD approach the polymer brush layer is directly patterned by degradation of the polymer chains in the illuminated part of the sample. During this etching process the high energy imparted into the film causes scission of carbon-carbon bonds and the generation of highly reactive species which induce a local crosslinking of the polymer brush chains at the edge of the pattern. This crosslinking of the polymer at the sidewalls of the pattern determines the dry brush morphology after immersion into a solvent and they exhibit a box-like shape. Even after solvent exposure the pattern edges remain sharp and steep. Treatment with a good solvent and drying leads to an expansion of the structures to a more lens-like shape while a short treatment with a poor or non-solvent leads to the recovery of the box-like morphology. This crosslinking at the pattern edges has also consequences on the stability of the system. When some of the chains are degrafted this occurs preferentially in the center of the nanostructure and the crosslinked sidewalls remain more or less unchanged. As a consequence of this, when the pattern is large enough, after degrafting polymer remains only at both former edges of the pattern. In contrast to this, when the pattern are small, the whole polymer material in the pattern becomes crosslinked and only one narrow and high structure is observed and less degrafting occurs. Thus in TD nanopatterned brushes the morphology is to a significant extent determined by the RIE-induced crosslinking. As a consequence, nanobrushes obtained by this technique are actually nanobrush networks, in microbrushes the edges of the pattern obtained by

this technique are always rather sharp while the polymer chains in the center of such structure have still brushlike properties.

In contrast to this, when the initiator layer is patterned, complete chains grow during the brush formation process. The polymer chains at the edge of the pattern can expand into the polymer free space and upon drying wet the surface of the substrate next to the polymer grafted areas. The extent of this wetting process depends on the surface tension of the surface next to the pattern, which can be controlled by modification with a self-assembled monolayer of a silane. When the polymer in the nano-pattern is dried several possible morphologies can be obtained depending on surface tension, the solvent quality and the wetting properties of the substrate. Immersing the polymer brush in good solvent leads to the relaxation of the brush chains at the periphery of the pattern while exposure to a bad or non-solvent allows this only to a much lesser extent. When a brush exposed to good solvent is dried the expansion causes (depending on the surface chemistry adjacent to the pattern) a relatively strong wetting of the substrate and the typical lens-shaped morphologies commonly observed for nanostructured brushes is obtained. In contrast to this the treatment with non-solvent leads to much lower wetting, increased height of the dry brush and much sharper pattern.

In summary, the question which morphology will be observed when a nanoscale patterned brush is generated is quite complex and depends strongly on the sample history and the finer details of sample generation. The resulting knowledge for controlling the nano-morphology of patterned polymer brushes might help in future to improve the design of more sophisticated brush based materials.

Acknowledgement

We want to thank Natalia Schatz for GPC measurements, Cory Bethrant for AFM measurement and our co-workers Wenqing Yan and Britta Knäbel for her enthusiastic support.

This work made use of several facilities at Cornell University. 1) Cornell NanoScale Facility, a member of the National Nanotechnology Coordinated Infrastructure (NCI), which is supported by the National Science Foundation (Grant ECCS-1542081). 2) Cornell Center for Materials Research Shared Facilities, which are supported through the NSF MRSEC program (DMR-1120296). 3) Nanobiotechnology Center shared research facilities at Cornell. 4) The Center for Nanomaterials Engineering & Technology.

We would like to acknowledge the great opinions on etching condition from Cornell CNF staff Vince Genova. Also we would like to thank Malcolm Thomas for helping us measuring samples on SEM at Cornell CCMR.

REFERENCES

- (1) Milner, S. T. *Polymer Brushes*. *Science* 1991, 251 (4996), 905–914.
- (2) Brittain, W. J.; Minko, S. A Structural Definition of Polymer Brushes. *J. Polym. Sci. Part Polym. Chem.* 2007, 45 (16), 3505–3512 DOI: 10.1002/pola.22180.
- (3) Brittain, W.; Advincula, R.; Rühle, J.; Caster, K. *Polymer Brushes*; 2004.
- (4) Yang, W. J.; Neoh, K.-G.; Kang, E.-T.; Teo, S. L.-M.; Rittschof, D. *Polymer Brush Coatings for Combating Marine Biofouling*. *Prog. Polym. Sci.* 2014, 39 (5), 1017–1042 DOI: 10.1016/j.progpolymsci.2014.02.002.

- (5) Meng, J.; Cao, Z.; Ni, L.; Zhang, Y.; Wang, X.; Zhang, X.; Liu, E. A Novel Salt-Responsive TFC RO Membrane Having Superior Antifouling and Easy-Cleaning Properties. *J. Membr. Sci.* 2014, 461, 123–129 DOI: 10.1016/j.memsci.2014.03.017.
- (6) Whiting, G. L.; Snaith, H. J.; Khodabakhsh, S.; Andreasen, J. W.; Breiby, D. W.; Nielsen, M. M.; Greenham, N. C.; Friend, R. H.; Huck, W. T. S. Enhancement of Charge-Transport Characteristics in Polymeric Films Using Polymer Brushes. *Nano Lett.* 2006, 6 (3), 573–578 DOI: 10.1021/nl051803t.
- (7) Bai, H.; Zhang, H.; He, Y.; Liu, J.; Zhang, B.; Wang, J. Enhanced Proton Conduction of Chitosan Membrane Enabled by Halloysite Nanotubes Bearing Sulfonate Polyelectrolyte Brushes. *J. Membr. Sci.* 2014, 454, 220–232 DOI: 10.1016/j.memsci.2013.12.005.
- (8) de Groot, G. W.; Santonicola, M. G.; Sugihara, K.; Zambelli, T.; Reimhult, E.; Vörös, J.; Vancso, G. J. Switching Transport through Nanopores with PH-Responsive Polymer Brushes for Controlled Ion Permeability. *ACS Appl. Mater. Interfaces* 2013, 5 (4), 1400–1407 DOI: 10.1021/am302820y.
- (9) Li, Z.; Wang, H.; Song, X.; Yan, J.; Hu, H.; Yu, B. Dual-Responsive Polymer Brushes as an Electrochemical Logic Gate. *J. Electroanal. Chem.* 2014, 719, 7–13 DOI: 10.1016/j.jelechem.2014.01.030.
- (10) Welch, M. E.; Ober, C. K. Responsive and Patterned Polymer Brushes. *J. Polym. Sci. Part B Polym. Phys.* 2013, 51 (20), 1457–1472 DOI: 10.1002/polb.23356.
- (11) Olivier, A.; Meyer, F.; Raquez, J.-M.; Damman, P.; Dubois, P. Surface-Initiated Controlled Polymerization as a Convenient Method for Designing Functional Polymer Brushes: From Self-Assembled Monolayers to Patterned Surfaces. *Prog. Polym. Sci.* 2012, 37 (1), 157–181 DOI: 10.1016/j.progpolymsci.2011.06.002.
- (12) Chen, T.; Amin, I.; Jordan, R. Patterned Polymer Brushes. *Chem. Soc. Rev.* 2012, 41 (8), 3280 DOI: 10.1039/c2cs15225h.

- (13) Lee, W.-K.; Patra, M.; Linse, P.; Zauscher, S. Scaling Behavior of Nanopatterned Polymer Brushes. *Small* 2007, 3 (1), 63–66 DOI: 10.1002/smll.200600414.
- (14) Yu, Q.; K. Ista, L.; P. López, G. Nanopatterned Antimicrobial Enzymatic Surfaces Combining Biocidal and Fouling Release Properties. *Nanoscale* 2014, 6 (9), 4750–4757 DOI: 10.1039/C3NR06497B.
- (15) Yu, Q.; Ista, L. K.; Gu, R.; Zauscher, S.; López, G. P. Nanopatterned Polymer Brushes: Conformation, Fabrication and Applications. *Nanoscale* 2016, 8 (2), 680–700 DOI: 10.1039/C5NR07107K.
- (16) Zhou, G.-Y.; Lee, A.-W.; Chang, J.-Y.; Huang, C.-H.; Chen, J.-K. Fabrication of Metamaterial Absorber Using Polymer Brush – Gold Nanoassemblies for Visualizing the Reversible PH-Responsiveness. *J. Mater. Chem. C* 2014, 2 (39), 8226–8234 DOI: 10.1039/C4TC01380H.
- (17) Patra, M.; Linse, P. Simulation of Grafted Polymers on Nanopatterned Surfaces. *Nano Lett.* 2006, 6 (1), 133–137 DOI: 10.1021/nl051611y.
- (18) Koutsioubas, A. G.; Vanakaras, A. G. Polymer Brushes on Periodically Nanopatterned Surfaces. *Langmuir* 2008, 24 (23), 13717–13722 DOI: 10.1021/la802536v.
- (19) Jonas, A. M.; Glinel, K.; Oren, R.; Nysten, B.; Huck, W. T. S. Thermo-Responsive Polymer Brushes with Tunable Collapse Temperatures in the Physiological Range. *Macromolecules* 2007, 40 (13), 4403–4405 DOI: 10.1021/ma070897l.
- (20) Jonas, A. M.; Hu, Z.; Glinel, K.; Huck, W. T. S. Chain Entropy and Wetting Energy Control the Shape of Nanopatterned Polymer Brushes. *Macromolecules* 2008, 41 (19), 6859–6863 DOI: 10.1021/ma801584k.

- (21) Jonas, A. M.; Hu, Z.; Glinel, K.; Huck, W. T. S. Effect of Nanoconfinement on the Collapse Transition of Responsive Polymer Brushes. *Nano Lett.* 2008, 8 (11), 3819–3824 DOI: 10.1021/nl802152q.
- (22) Chen, J.-K.; Hsieh, C.-Y.; Huang, C.-F.; Li, P.-M.; Kuo, S.-W.; Chang, F.-C. Using Solvent Immersion to Fabricate Variably Patterned Poly(Methyl Methacrylate) Brushes on Silicon Surfaces. *Macromolecules* 2008, 41 (22), 8729–8736 DOI: 10.1021/ma801127m.
- (23) Chen, J.-K.; Hsieh, C.-Y.; Huang, C.-F.; Li, P. Characterization of Patterned Poly(Methyl Methacrylate) Brushes under Various Structures upon Solvent Immersion. *J. Colloid Interface Sci.* 2009, 338 (2), 428–434 DOI: 10.1016/j.jcis.2009.06.040.
- (24) Chen, J.-K.; Chen, T.-Y. Fabrication of High-Aspect-Ratio Poly(2-Hydroxyethyl Methacrylate) Brushes Patterned on Silica Surfaces by Very-Large-Scale Integration Process. *J. Colloid Interface Sci.* 2011, 355 (2), 359–367 DOI: 10.1016/j.jcis.2010.12.012.
- (25) Riesz, P.; Kondo, T. Free Radical Formation Induced by Ultrasound and Its Biological Implications. *Free Radic. Biol. Med.* 1992, 13 (3), 247–270.
- (26) Prucker, O.; Schimmel, M.; Tovar, G.; Knoll, W.; R uhe, J. Microstructuring of Molecularly Thin Polymer Layers by Photolithography. *Adv. Mater.* 1998, 10 (14), 1073–1077.
- (27) Dong, R.; Krishnan, S.; Baird, B. A.; Lindau, M.; Ober, C. K. Patterned Biofunctional Poly(Acrylic Acid) Brushes on Silicon Surfaces. *Biomacromolecules* 2007, 8 (10), 3082–3092 DOI: 10.1021/bm700493v.
- (28) Hirtz, M.; Brinks, M. K.; Miele, S.; Studer, A.; Fuchs, H.; Chi, L. Structured Polymer Brushes by AFM Lithography. *Small* 2009, 5 (8), 919–923 DOI: 10.1002/sml.200801339.

- (29) Rastogi, A.; Paik, M. Y.; Tanaka, M.; Ober, C. K. Direct Patterning of Intrinsically Electron Beam Sensitive Polymer Brushes. *ACS Nano* 2010, 4 (2), 771–780 DOI: 10.1021/nn901344u.
- (30) Chen, W.-L.; Menzel, M.; Watanabe, T.; Prucker, O.; Rühle, J.; Ober, C. K. Reduced Lateral Confinement and Its Effect on Stability in Patterned Strong Polyelectrolyte Brushes. *Langmuir* 2017 DOI: 10.1021/acs.langmuir.7b00165.
- (31) Prucker, O.; Rühle, J. Synthesis of Poly (Styrene) Monolayers Attached to High Surface Area Silica Gels through Self-Assembled Monolayers of Azo Initiators. *Macromolecules* 1998, 31 (3), 592–601.
- (32) Taylor, P. G.; Lee, J.-K.; Zakhidov, A. A.; Hwang, H. S.; DeFranco, J. A.; Fong, H. H.; Chatzichristidi, M.; Murotani, E.; Malliaras, G. G.; Ober, C. K. Orthogonal Lithography for Organic Electronics; 2010; Vol. 7639, p 76390Z–76390Z–8.
- (33) Biesalski, M.; Rühle, J. Scaling Laws for the Swelling of Neutral and Charged Polymer Brushes in Good Solvents. *Macromolecules* 2002, 35 (2), 499–507 DOI: 10.1021/ma001776n.
- (34) Lai, P.-Y.; Binder, K. Structure and Dynamics of Grafted Polymer Layers: A Monte Carlo Simulation. *J. Chem. Phys.* 1991, 95 (12), 9288 DOI: 10.1063/1.461158.
- (35) Lai, P.-Y.; Binder, K. Structure and Dynamics of Polymer Brushes near the Θ Point: A Monte Carlo Simulation. *J. Chem. Phys.* 1992, 97 (1), 586 DOI: 10.1063/1.463554.
- (36) Wu, T.; Efimenko, K.; Vlček, P.; Šubr, V.; Genzer, J. Formation and Properties of Anchored Polymers with a Gradual Variation of Grafting Densities on Flat Substrates. *Macromolecules* 2003, 36 (7), 2448–2453 DOI: 10.1021/ma0257189.
- (37) Chang, J.-F.; Gwinner, M. C.; Caironi, M.; Sakanoue, T.; Siringhaus, H. Conjugated-Polymer-Based Lateral Heterostructures Defined by High-Resolution

Photolithography. *Adv. Funct. Mater.* 2010, 20 (17), 2825–2832 DOI:

10.1002/adfm.201000436.

(38) Chai, J.; Lu, F.; Li, B.; Kwok, D. Y. Wettability Interpretation of Oxygen Plasma Modified Poly(Methyl Methacrylate). *Langmuir* 2004, 20 (25), 10919–10927 DOI: 10.1021/la048947s.

(39) Claes, M.; Le, Q.; Kesters, E.; Lux, M.; Urionabarrenetxea, A.; Vereecke, G.; Mertens, P.; Carleer, R.; Adriaensens, P. All-Wet Strip Approaches for Post-Etch Photoresist Layers After Low-K Patterning; ECS, 2007; Vol. 11, pp 177–187.

(40) Ting, Y.-H.; Park, S.-M.; Liu, C.-C.; Liu, X.; Himpsel, F. J.; Nealey, P. F.; Wendt, A. E. Plasma Etch Removal of Poly(Methyl Methacrylate) in Block Copolymer Lithography. *J. Vac. Sci. Technol. B Microelectron. Nanometer Struct.* 2008, 26 (5), 1684 DOI: 10.1116/1.2966433.

(41) Ting, Y.-H.; Liu, C.-C.; Park, S.-M.; Jiang, H.; Nealey, P. F.; Wendt, A. E. Surface Roughening of Polystyrene and Poly(Methyl Methacrylate) in Ar/O₂ Plasma Etching. *Polymers* 2010, 2 (4), 649–663 DOI: 10.3390/polym2040649.

(42) Simancas, K. Entropic Death of Polyelectrolyte Brushes: Chain Stretching, Bond Scission and Surfactant Complexation. PhD Dissertation, University of Freiburg, IMTEK, 2011.

(43) Bain, E. D.; Dawes, K.; Özçam, A. E.; Hu, X.; Gorman, C. B.; Šrogl, J.; Genzer, J. Surface-Initiated Polymerization by Means of Novel, Stable, Non-Ester-Based Radical Initiator. *Macromolecules* 2012, 45 (9), 3802–3815 DOI: 10.1021/ma300491e.

(44) Galvin, C. J.; Bain, E. D.; Henke, A.; Genzer, J. Instability of Surface-Grafted Weak Polyacid Brushes on Flat Substrates. *Macromolecules* 2015, 150803081219001 DOI: 10.1021/acs.macromol.5b01289.

(45) Klok, H.-A.; Genzer, J. Expanding the Polymer Mechanochemistry Toolbox through Surface-Initiated Polymerization. *ACS Macro Lett.* 2015, 4 (6), 636–639
DOI: 10.1021/acsmacrolett.5b00295.

CHAPTER 4

Reduced lateral confinement and its effect on stability in patterned strong polyelectrolyte brushes*

Abstract

The stability of strong polyelectrolyte brushes was studied in the bulk and in patterned structures. Thick polyelectrolyte brushes of poly([(2-methacryloyloxy)ethyl]trimethylammonium chloride) (PMETAC) with thicknesses > 100 nm were synthesized by Cu(0)-mediated controlled radical polymerization (CuCRP). Brush patterning was conducted using deep-UV photolithography by means of either a top-down (TD) or bottom-up (BU) method with features as small as 200 nm. Brushes were soaked in water with a range of pH or temperature conditions and the hydrolysis was monitored through dry state ellipsometry and AFM measurements. BU patterns showed reduced degrafting for smaller patterns, which was attributed to increased stress relaxation at such dimensions. In contrast to the already relaxed BU patterned brush, a TD patterned brush possesses perpendicular structures, which result from the use of orthogonal lithography. It was found that the TD process induces crosslinking on the sidewall, which subsequently fortifies the sidewall materials. This modification of the polymer brushes hindered the stress relaxation of the patterns and the degrafting trends became irrelevant to the pattern sizes. With proper tuning, the

*Reproduced with permission from Chen, W.-L.; Menzel, M.; Watanabe, T.; Prucker, O.; R uhe, J.; Ober, C. K. Reduced Lateral Confinement and Its Effect on Stability in Patterned Strong Polyelectrolyte Brushes. *Langmuir* 2017, 33 (13), 3296–3303. Copyright 2017 American Chemical Society

crosslinking on the sidewall could be minimized and the degrafting trends were again relaxation–dependent

Introduction

The polymer brushes reported in this study are materials composed of polymers with one end tethered to a surface with a high graft density. By using different polymer compositions, they can be used as anti-fouling¹, transport-enhancing², or stimuli-responsive^{3,4} materials, for example. While there are many possible applications, stability of the high grafting density polymer brush is critical. A growing number of reports^{5–14} show that polymer brushes may be unstable under relatively mild conditions even with surface attachment. For example, poly(methacrylic acid) brushes may degraft from a surface in 37 °C water and only 20% of the material is left after 48 h⁸. Recently it has been concluded that the degrafting of the polymer brush is due to mechano-facilitated hydrolysis, which means degradation of molecules upon application of the mechanical force.¹⁵ Compared to a normal polymeric melt film, polymer brushes experience stronger tension on the tethering unit due to the close proximity of the polymer chains to the grafting sites.¹⁶ It has been experimentally proven that increasing grafting density can directly enhance the degrafting of a polymer brush.¹² Polyelectrolyte brushes (PEB) can be subjected to strong stretching in aqueous solvent which can induce aggressive degrafting.¹³

Although some research has been done, only a few studies have investigated the stability of strong PEBs, which are subject to very strong stretching of the polymer chains.^{17–19} Strong PEBs tested previously were either too thin or on a spherical substrate which does not induce such strong stretching.²⁰ This means the time scale for the survival of strong, thick polyelectrolyte brushes has not yet been fully explored. In addition, further questions were raised about how to alleviate degrafting. Considering

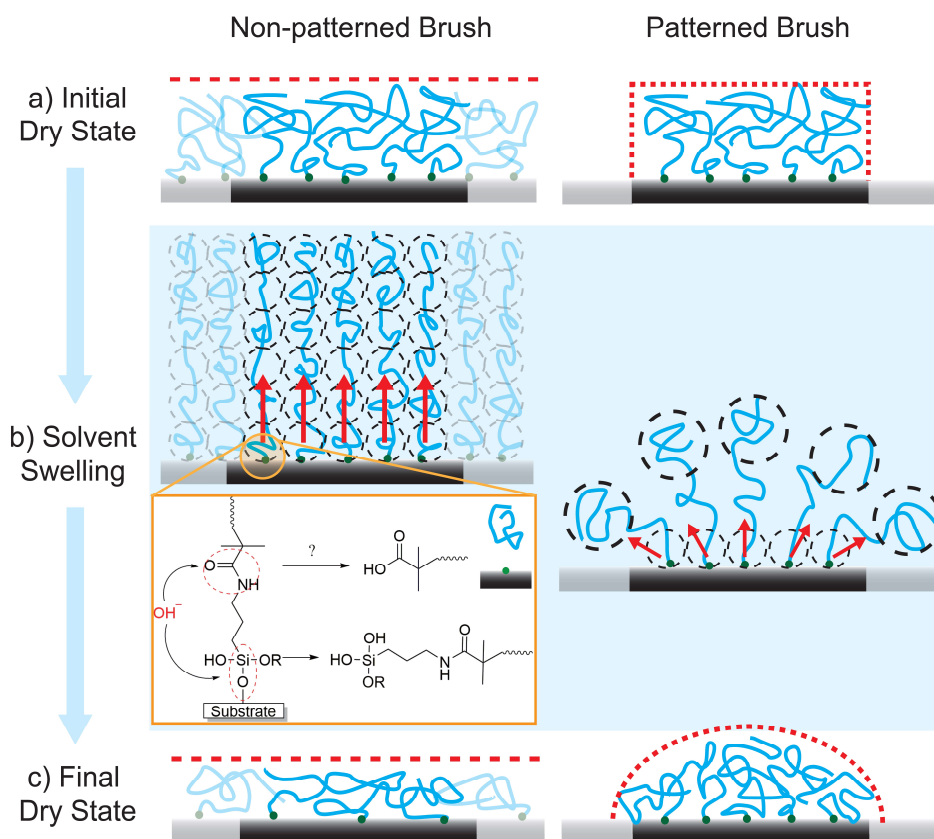


Figure 4.1. Schematic description of brush relaxation under different conditions. Patterned brushes should have more room for stress relaxation than non-patterned brushes. As a result, the extent of degrafting of the patterned brushes should be less.

the origin of the degrafting process, exploring degrafting in nanopatterned brushes might be helpful. A nanopatterned brush (brush confined within separate well defined regions with no brush) having a lateral dimension similar to brush thickness could provide for significant lateral stress relaxation.²¹ Since reduction of tension also means reduction of the brush thickness, the brushes should be more stable when patterned as shown in Figure 4.1. Furthermore, the grafting density and molecular weight have been proven to have important effects on degrafting due to the increase of the lateral

pressure.¹² The exact relationship between lateral pressure and degrafting kinetics are still unclear. The results of patterned PEB stability experiments should provide more understanding of such phenomena and help in the derivation of theory.

For those reasons, here we report the synthesis of thick poly([2-methacryloyloxy)ethyl]trimethylammonium chloride) (PMETAC) brushes and an experimental study of brush stability. PMETAC brushes are strong PEBs where the charge density on the chains does not depend on the environment. We demonstrate that degrafting of a strong PEB could be distinctly different from either a neutral polymer brush or weak PEB. To prove our hypothesis, a patterned brush with lateral dimensions down to the sub μm level was fabricated with both top-down (TD) and bottom-up (BU) methods. First, patterned neutral poly(methyl methacrylate) brushes were fabricated to provide a better understanding of the process and then the PMETAC brushes were grown as shown in Figure 4.2a. We proved that both TD and BU patterned brushes have less degrafting at smaller pattern sizes and this is a first proof of increasing brush stability by controlling lateral confinement.

Experimental section

Materials. Allylamine, anhydrous toluene, (3-aminopropyl)triethoxysilane, α -bromoisobutyryl bromide (BIBB), chlorodimethylsilane, dimethyl sulfoxide (DMSO), hydrazine, hydrochloric acid, inhibitor remover (for removing hydroquinone and monomethyl ether hydroquinone), magnesium sulfate, [2-methacryloyloxy)ethyl]trimethylammonium chloride(80% in water) (MAETAC), methyl methacrylate(MMA), Pt on activated carbon (10 wt %), triethylamine, N,N,N',N',N''-pentamethyldiethylenetriamine (PMDETA), potassium hydroxide,

pyridine, sodium chloride, sodium phosphate dibasic heptahydrate, sodium phosphate monobasic monohydrate, anhydrous triethylamine (TEA), were purchased from Sigma Aldrich and used without purification unless stated otherwise. MAETAC and MMA were passed through inhibitor remover to remove the inhibitor before use. CYTOP fluoropolymer was purchased from BELLEX international incorporation. Deionized water (DI water) with a resistivity of $18.2 \text{ M}\Omega \cdot \text{cm}$ at 25°C was obtained from Millipore's Milli-Q Synthesis A10 system. Copper tape (882-L COPPER) with $88.9 \mu\text{m}$ copper film was from Lamart Co. All the other solvents were purchased from Fisher Scientific.

Mono-functional silane initiator synthesis and immobilization. First, 2-bromo-2-methyl-N-allylpropanamide and chlorodimethylsilane was synthesized by published procedure and used as subsequent reactant.¹ Following hydrosilylation was carried out using another literature procedure to obtain mono-functional ATRP initiator, 2-bromo-2-methyl-N-{3-[chloro(dimethyl)silyl]-propyl}propanamide.^{22,23} Wafer pieces were cleaned with repetitively dichloromethane (DCM) and DI water rinsing and then dried with nitrogen. Wafers were then oxidized using a Harrick Plasma Cleaner for ten minutes. Moisture was further removed by 10 min 110°C oven baking. In a glove box, the wafer pieces were immersed in a toluene solution of the initiator (10 mM) and pyridine (0.5 mM) overnight at room temperature. The substrates were then removed from the solution and washed with DI water, and DCM sequentially and sonicated for ten minutes in DCM. Wafers were given a final rinse of dichloromethane and blown dry under nitrogen gas.

Multi-functional silane initiator synthesis and immobilization. Wafer cleaning and oxidation processes remained the same as in the previous section. Clean, oxidized, moisture free wafer pieces were then exposed to 3-aminopropyl triethoxysilane vapor under reduced pressure (in a glass chamber containing liquid (3-

aminopropyl)triethoxysilane pumped down desired pressure and then sealed. Pressure was 1 Torr for 1.8 nm APTES layer and 0.3 Torr for 14 nm APTES layer) for 2 h and then annealed for a further 30 min at 110°C. The pieces were then put into a Schlenk flask and purged with three vacuum evacuating / argon back-filling cycles. Anhydrous DCM (30mL), anhydrous TEA (0.6mL), BIBB(0.6 mL) were add in order and left to stand for overnight. The pieces were then taken out of flask, washed with acetone, ethanol, DI water sequentially and blown dry under nitrogen gas.

Polymer brush synthesis. Polymerization was conducted by first preparing the set-up as shown in the literature²⁴. Glass slide was cut into piece with the size corresponding to the initiator-deposited piece. Glass piece was then coated with copper tape to be the catalyst source. This taped glass piece was then clamped face-to-face together with initiator-deposited wafer pieces by copper clamp. The distance between the pieces was separated by Teflon spacer with $d = 0.5$ mm. The set-up was then put into different conditions for the different brushes.

PMMA polymerization. Solution of 2 mL MMA, 1 mL DMSO, 36 μ L PMDETA, 1.5mL hydrazine combination was used and the polymerization was conducted at room temperature for 2 h. Afterward the wafer pieces were taken out, rinsed with DCM and sonicated in DCM for 10 min before nitrogen blown dry.

PMETAC polymerization. Solution of 2 mL MAETAC, 2 mL DI water, 1 mL methanol, 36 μ L PMDETA, 2.5mL hydrazine combination was used and the polymerization was conducted at 60 °C for 3 h. Afterward the wafer pieces were taken out and rinsed with iced DI water before nitrogen blown dry. To collect the monomer / polymer mixture for later NMR characterization, the reacted solution was collected and passed through aluminum oxide column to remove any Cu containing complex. Solvent was removed by evaporation at 50 °C and the remaining materials were subject to NMR characterization.

Reactive ion etching (RIE) condition. RIE was conducted by Oxford PlasmaLab 80+ RIE system. Two setting (referred as strong reactive ion etching (SRIE) and weak reactive ion etching (SRIE) hereafter) were used in this study and the setting details are listed below. Generally SRIE has faster etching rate and stronger lateral damage, which may damage the profile of the pattern. On the other hand the WRIE provide slower and gentle process with more anisotropic etching. However, WRIE created more crosslinking on the edge materials.

SRIE: O₂ flow rate 50 sccm at a RF power of 150 W and a pressure of 60 mTorr.

WRIE: O₂ flow rate 50 sccm at a RF power of 75 W. Pressure started at 50 mTorr then decreased to 20 mTorr in 6 sec and stayed at 20 mTorr, DC bias minimum was 5V.

Top-down patterning process. Top-down (TD) patterning process started with spin-coating three layers on the polymer brush with individual post-application baking (PAB) condition. CYTOP was coated first and PAB at 110 °C 5 min, ramped to 150 °C in 5 min, stayed at 150 °C for 5 min, ramped to 185 °C in 5 min, stay at 185 °C for 6 min. Following the first CYTOP coating, it was subject to SRIE for 5 sec in order to create hydrophilic surface for subsequent material deposition. 2nd layer was DUV-252 anti-reflective coating layer (Brewer Science) with PAB at 90 °C for 30 sec and 185°C for 1 min. 3rd layer was UV 210 DUV photoresist (Shipley) with PAB at 135°C for 1 min. Deep-UV photolithography patterning was then conducted on ASML 300 DUV stepper. The sample was then subject to post-application bake at 135 °C for 1min and developed with MIF-726 (AZ Electronic Materials) developer for 1 min and spun to dry. 50 to 0.2 μ m line patterns were created on the photoresist. Pattern transfer was conducted by either SRIE or WRIE based on the process. For the TD patterning on PMETAC and PMMA brushes, WRIE were used, while SRIE was used for modified top-down process on PMETAC brushes in order to reduce crosslinking on the edge

materials. The pieces were then soaked in stirring hydrofluoroether NOVEC 7300 (3M) at 50 °C overnight and rinsed with NOVEC 7300 repetitively. Afterward, pieces were blown dry with nitrogen gas.

Bottom-up patterning process. Bottom-up(BU) process was similar to the TD process. Wafer was cleaned with SC-2 process (soaked in solution made of HCl:H₂O₂:water = 2:2:1, volume ratio) for 2 h, then rinsed with DI water and dried with nitrogen gas. The patterned CYTOP polymer film on the cleaned wafer was conducted in the same way as the TD process. The initiator was deposited in the same method (no wafer oxidation needed) as before and the CYTOP was removed afterward to obtain wafer with initiator pattern. BU patterned brushes were then fabricated by subsequent polymerization on the wafer with initiator pattern.

Solvent immersion degrafting experiment. Buffer solutions with strengths of 10 mM were prepared using sodium phosphate salts and adjusted to pH 4 and 9 using minute quantities of HCl and KOH. The pH of each buffer was measured using a VWR symphony SB70P pH meter. The parent polymer brush samples were segmented into different pieces specimens and placed individually into glass vials containing selected solution. The vials were then sealed and maintained at controlled temperature in oil bath for the duration of the degradation. After a certain incubation time the samples were removed, rinsed briefly with water, dried in vacuum for more than 2 h and then subjected to further characterization. For PMMA brushes, after selected solvent bath, it was rinsed with the selected solvent again and then dried in vacuum.

Results and Discussion

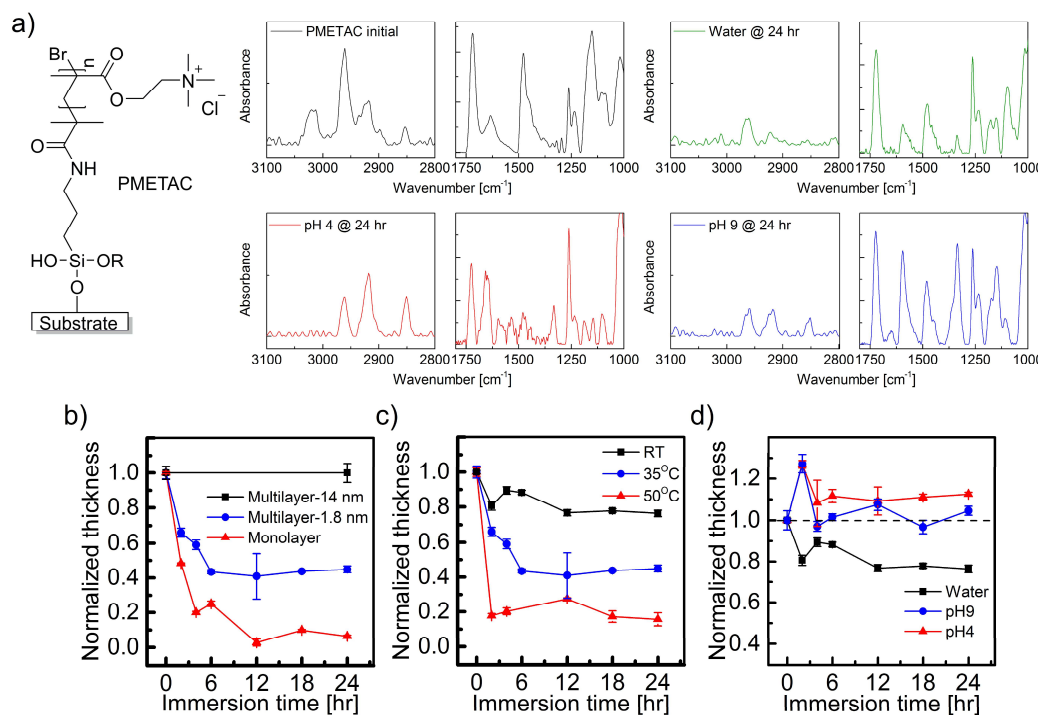


Figure 4.2. a) FTIR spectra of PMETAC brushes at different stages (original / after water bath 24 h / after pH 4 bath 24 h / after pH 9 bath 24 h. Insert figures show the detailed look at alkyl region. b) PMETAC brushes degrafting kinetics in water with different initiator layer thicknesses at 35 °C c) PMETAC brushes with 1.8 nm initiator thickness degrafting kinetics in water at different temperatures (RT = room temperature) and d) with different pH buffers. Thicknesses were all measured in dry state by ellipsometer and normalized to thicknesses before degrafting.

The synthesis of PMETAC brushes were conducted with the recently developed CuCRP, using Cu-tape as the catalyst source, because of its ability to create PMETAC

brushes with dry thicknesses > 100 nm measured by ellipsometer.^{24,25} Direct synthesis of strong polyelectrolyte brushes has been reported in many publications, but only limited thicknesses of ~ 70 nm have been achieved to date.^{26–28} Thicker brushes make it easier to characterize the morphology and provide better processability. The FTIR spectrum in Figure 4.2a of the resulting brush showed characteristic peaks as reported in the literature and hence proved its successful synthesis.^{29,30} The broad peak at 3400 cm^{-1} corresponds to the strong hydration of the PMETAC brush. The peaks at 1477 cm^{-1} , 1635 cm^{-1} and 3017 cm^{-1} correspond to the C-H in-plane vibration, amine asymmetric bending vibration, and asymmetric methyl stretching on the quaternary ammonium group, respectively.

First question is whether the effect of stress enhances hydrolysis of both the amide and siloxane bond or if only the siloxane bond is hydrolyzed.³¹ To test this, experiments were conducted on initiators with mono- functional siloxane links and multiple siloxane attachment sites to the surface since initiators with multiple attachment sites have been proved to increase the stability of the brushes.¹⁴ The siloxane layer thickness was controlled by the pressure used in the vapor deposition process of (3-aminopropyl)triethoxysilane (APTES). Thicknesses of the films were measured by ellipsometer under dry conditions. For consistency between samples, brushes were cut into pieces and individually subjected to degrafting conditions for a set time. The measured data were normalized by original thicknesses and shown in Figure 4.2. Figure 4.2b shows that with 14 nm APTES as the base the brush does not degraft, indicating the amide bond was not hydrolyzed in a 35 °C water bath after 24 h. Additionally, the aspect of multifunctionality and crosslinking of the siloxane bonds in APTES hindered their hydrolysis. This result was also observed by Ataman *et al.*

where no degrafting occurred for thick poly(poly(ethylene glycol)methyl ether methacrylate) brushes within 24 h with amide bond only initiators.¹⁴ Since the mono-functional initiator yielded such an unstable brush, APTES with 1.8 nm thickness was chosen for the initiator deposition process for subsequent investigation.

The stability of the PMETAC brush was then tested in water at different temperatures and pH. The results are shown in Figure 4.2c and 4.2d. The PMETAC brush at higher temperatures has faster degrafting kinetics and the resulting dry thickness is thinner. It is known that brushes have higher stretching forces acting on them at higher temperatures.^{32,33} This tension effect combined with thermodynamic enhancement of the hydrolysis reaction leads to removal of most of the brush at 50 °C. Compared to a brush on a curved surface, which has been shown to retain more than 50% of the brush after 100 h in an 85 °C bath, the degrafting rate here is more aggressive.²⁰ Disappearance of peaks at 3400 cm⁻¹ and 1635 cm⁻¹ suggests a decreased hydration of the brush. This phenomenon could be explained by the loss of material due to degrafting and partial counter-ion exchange between OH⁻ and Cl⁻ which leads to less dissociation.

pH has been shown to affect the degrafting of a polymer brush.^{8,9,13} Buffered water (pH 4 and 9) was then used to soak the brushes in order to investigate pH effects. The brushes showed no evident difference between acidic or basic conditions as shown in Figure 4.2e. This is similar to the results of Genzer *et al.*³⁴, who showed that strong PEBs lacking hydrolysis vulnerable groups such as ester functions, degrafted in equal measure at different pHs. Interestingly, brush thickness increased after 2 h of soaking in buffered water. This initial increase could be explained by counter-ion exchange between the buffering ions (phosphate) and the chloride ions. PEBs have been known to change their wetting energy with different counter-ions present. R uhe *et al.* were among the first who reported that there is a counter ion exchange between the PEB

layer and its surrounding solution.³⁵⁻⁴⁰ In the work of Huck *et al.* it was shown that fast counter-ion exchange could occur when a PMETAC brush was soaked in a salt solution.³⁰ The dry thickness could increase since the volume occupied by phosphate is larger than other smaller anions. This was also the reason that the resulting dry thickness is larger than the initial dry thickness. Furthermore, it could also be due to an increased stability of the structures resulting from the complexation step. In this case, a phosphate–ammonium complex formation could fortify the stability of the brush through an “ionic” pairing interaction such as sulfate–ammonium ion pairing.³⁰

The binding of the phosphates to the brushes after soaking in buffered solution for 24 h was confirmed by the FTIR spectra in Figure 4.2a. Compared to the original brushes, the brushes soaked in the buffered water showed an additional peak at 2850 cm^{-1} , which originated from the ammonium dibasic phosphate complex.⁴¹ Individually, the monobasic salt with peaks at 1099 cm^{-1} , 1334 cm^{-1} and 1651 cm^{-1} was observed on the brushes soaked at pH 4 and the dibasic phosphate salt with peaks at 1590 cm^{-1} was observed for pH 9 water-soaked brushes. Although the peaks corresponding to the different binding states could be observed under different conditions, the similarity of peaks in the 2800-3000 cm^{-1} region suggested that effect of binding to the polymer conformation did not change at different pH values. Peak at 2918 cm^{-1} which corresponding to the ethylene stretching of polymers showed stronger signal at acidic condition. Consider the binding state of phosphate, it could be expected that there were more phosphate binding in the brush at acidic condition and those binding led to increased dry thickness.

To test whether the brush would be more stable if it could relax enough laterally to reduce coulombic stress, we created line and space patterns on polymer brushes with selected lateral dimensions. All patterns were measured by AFM only in the dry state to minimize uncertainties caused by polymer compression during AFM contact.^{42,43}

Recent reports showed that the critical size for such an effect is $< 1 \mu\text{m}$ and the smallest resolution of 200 nm in this study is well within this range.^{21,42} Both TD and BU patterning methods created high-resolution structures; however, each process has their own benefits and drawbacks for this study. The TD method, with advanced lithography techniques, can create patterns with a perpendicular profile. In contrast, the BU method gives a brush with a curved profile, which is already relaxed.^{21,42} The

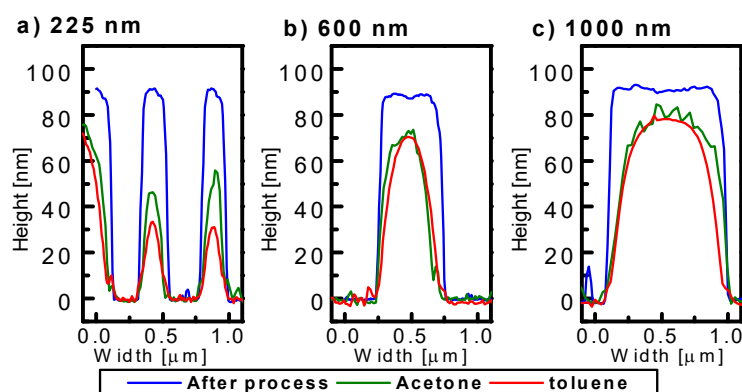


Figure 4.3 AFM scan cross-section images of top-down patterned PMMA brush.

Patterns with three different sizes [a) 225, b) 600, c) 1000 nm] are shown. Brushes were relaxed in acetone and toluene to show modification done by process.

TD brush with a perpendicular profile^{44,45} preserves the properties of the bulk brush before solvent immersion and the degrafting result should capture more dynamic information. However, the TD patterning method might create irreversible modifications on the brush structure like chain scission or crosslinking. Also the required patterning materials such as a photoresist might interact with the brushes. Therefore, we chose to investigate both methods together to compare our results. The process scheme is the same as shown in Scheme 2-1.

TD patterned brushes were created by a modified process based on the work of Henning *et al.*⁴⁶ A fluorinated polymer, CYTOP™ (Asahi Glass co.), was chosen to

act as a sacrificial layer to pattern the polymer brushes due to the ease of its removal from the organic materials. The process scheme is shown in Scheme 1. First, the process materials were coated in sequence on the polymer brush. Subsequent photolithography created the pattern on the photoresist and the following reactive ion etching transferred the pattern to the brush layer. Finally, hydrofluoroether, HFE-7300(3M™) was used to remove all the residual CYTOP™ from the brush. To test the effects caused by the process, neutral, non-degrafting PMMA brushes were patterned at first.

Figure 4.3 shows the AFM scans of both the patterned dry PMMA brush after CYTOP™ lift-off and after subsequent relaxation in acetone or toluene. First, it was observed that the pattern resolution could go down to 225 nm forming a perpendicular structure after removal of the process materials. This could not be achieved with normal photolithography processes due to the relaxation of the polymer in organic solvent. Further soaking in acetone/toluene was meant to test its stability since reactive ion etching (RIE) may still cause chemical changes on sidewall of patterns even though it is an anisotropic etching.^{47,48} We believe that such changes are the reason that the 225 nm pattern showed incomplete relaxation after acetone immersion. After solvent immersion, the brushes relaxed laterally and became lens-like shape as other bottom-up patterned brushes.^{21,49} The formation of lens-like shapes was due to the interaction between surface wetting and chain entropy, which reached the balance in dry state after relaxation in the solvent.²¹ In addition, all the patterns showed shrinking of the cross-sectional area after toluene immersion, which must be caused by the loss of edge materials. In Figure 4.4a we calculated the cross-sectional area for different patterns before and after solvent immersion and it showed the same difference

between different patterns. Such result confirmed that the RIE is the reason for

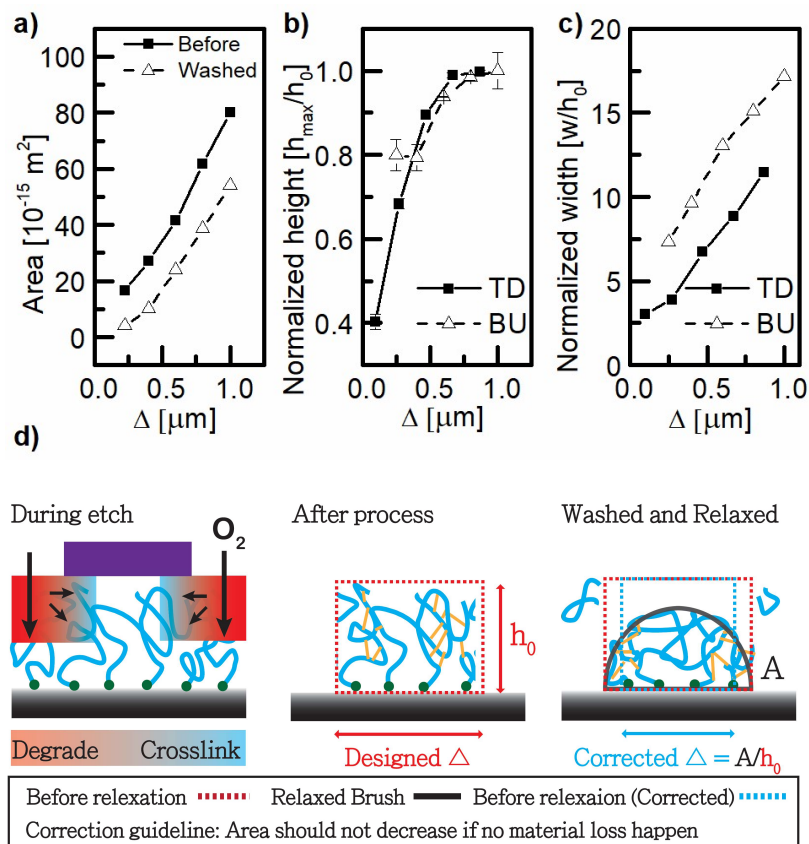


Figure 4.4 Comparison of AFM measured morphologies between TD and BU patterned PMMA brushes. a) Cross-sectional area of the patterns before and after toluene immersion. The area differences remain constant along different pattern sizes. Hence the correction process in 4d could be used to exclude process effect. The corrected Δ are then used for TD data in b), c). b) Normalized maximum height and c) width (aspect ratio) comparison between relaxed TD and BU patterned brushes for different pattern sizes. d) Schematic explanation for brush morphological evolution. Left: Etch modification on the brush. Middle: Brush morphology after process. Right: Relaxed brush morphology, the cross-sectional area was used to derive corrected Δ (Δ_c). It is considered that relaxed brushes were evolved from smaller patterns and material loss did not occur during relaxation.

material loss on TD patterned brushes.

A BU patterned PMMA brush was also created to compare the results (process as Scheme 2-1). Due to the material loss of the TD patterned brush, correction of the pattern size must be done to present meaningful comparison. The correction guideline is shown in Figure 4.4d. We considered that the relaxed brushes were evolved from the patterns with the same thickness but narrower pattern size. Such correction is based on the fact that PMMA brushes do not lose materials during the relaxation process. Based on the argument, the corrected pattern size was calculated by dividing the resulting area by the original thickness. The average decrease of 130 nm (65 nm on both sides) was used in all pattern corrections. Furthermore, since the PMMA brush was heated at 185 °C during the process (which is above its glass transition temperature) the decrease of the maximum thickness could be caused by the rearrangement of the polymer chains. A controlled experiment was done by first heating a PMMA brush at 185 °C on a hot plate and then soaking it in acetone. A 7 nm decrease of the PMMA brush thickness was observed (data not shown) before and after solvent immersion. Figure 4.4b and 4.4c compares TD and BU brushes with the normalized thickness and the width (aspect ratio) versus the pattern size. Direct dry brush morphologies comparison is possible because the normalized dry morphology is independent of the polymer dependent parameters. Factors like molecular weight, grafting density are all cancelled with each other and the normalized relation between pattern size and morphology is unique.²¹ Also by using the corrected pattern size for the TD patterned brushes the RIE effect was partly removed. The thickness of both patterned brushes were similar, but the widths at the same pattern size were different by about 300 nm. One reason why the TD brushes stretched less laterally is because of the damage done by the RIE to the chains at the very edge of the pattern. Another possibility is the crosslinking between polymer chains, which could also happen due to RIE treatment.⁵⁰⁻⁵² Crosslinking

could also explain why the 225 nm pattern relaxed incompletely in acetone. Although crosslinking was not obvious for PMMA brushes, it would later be more obvious for the patterned PMETAC brushes.

With the removal of the adjacent regions, it is expected that remaining polymer brushes are subjected to less pressure at the edges and any degrafting should be less. To investigate, how pattern size affects the stability of the PMETAC brush, TD and BU patterned brushes were degrafted in water for 24 h at different temperatures and the cross-sectional area ratio of the brushes. Cross-sectional area before/after degrafting were captured by AFM in the dry state to evaluate degrafting. In Figure 4.5, it can be seen that the degrafting trend of the BU brush fits the prediction but the TD patterned brush does not fit even with the corrected pattern size. Another difference observed was that the TD patterned brushes behaved inconsistently in their degrafting trend. Obvious difference was seen when comparing the AFM cross-sectional image of the 1 μm wide patterns, as shown in Figure 4.6. TD patterned PMETAC brushes after degrafting had a ridge like structure at the edge. Since this did not appear in the corresponding BU pattern, it can be assumed to be a result of the TD process. As pattern size shrank, the ridge structures became closer together and started to merge at around 500 nm (Figure 4.S3),

which implied that the modification of the brush structure caused by the plasma etching is greater than that of the patterned PMMA brush. At higher temperatures, those small patterns had no ridges could come to have ridges on the edge due to the increased instability of the polymer brush (Figure 4.S3, 35 °C 400 nm pattern). The increased stability of the brush suggested crosslinking also occurred. More comprehensive characterization on such sidewall crosslinking has been conducted and the result has been reported in chapter 3.

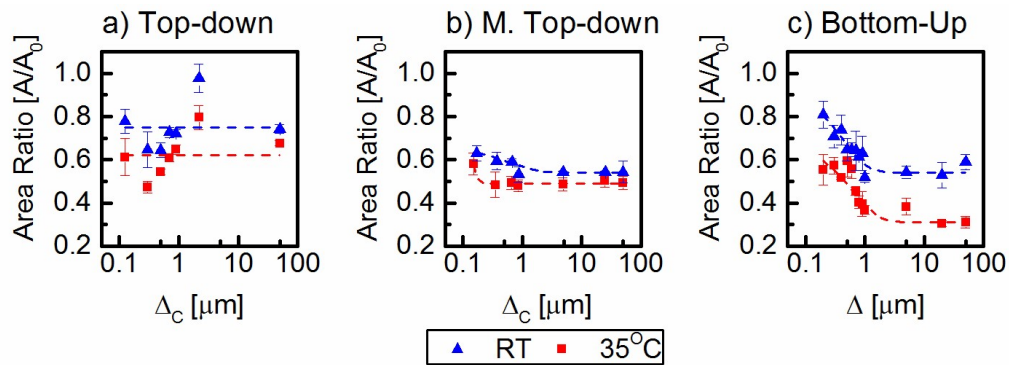


Figure 4.5 Characterization of degrafting condition of PMETAC brushes by comparing dry cross-sectional area ratio versus the pattern sizes for a) TD b) modified TD c) BU patterned brush after degrafting in water for 24 h. Area ratio was calculated by the cross-sectional area after degrafting/ cross-sectional area before degrafting.

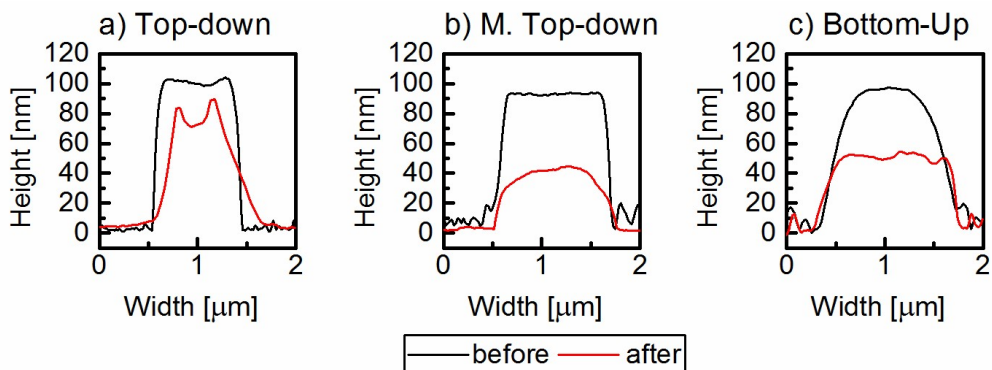


Figure 4.6 AFM dry cross-sectional image of the $1\mu\text{m}$ PMETAC brush pattern before and after degrafting at RT in water for different processes. a) TD b) Modified TD with different etching recipe c) BU patterned brush.

The unusual trend in TD patterned brush degrafting could be explained by considering possible results originating from the existence of sidewall crosslinking. First, water diffusion in the brushes and subsequent dissolution of the chains are

necessary for removal of the degrafted chains. With the sidewall crosslinking these two processes could be hindered since chains could have additional linking between each other, which results in increased stability. On the other hand, the stress relaxation which is the major reason for increased stability at narrower patterns is prevented by crosslinking. For those reasons, the stability between different patterns could be more similar to each other and thus the degrafting kinetics were similar between different pattern sizes.

To reduce the crosslinking of the brush at the edges, the RIE condition was tuned to make the effects of etching dominate any crosslinking. By increasing the etching pressure, the mean free path of the etchant gas is reduced correspondingly and enhance lateral etching.⁵³ It was expected that the degradation at the sidewall of the pattern would overwhelm the crosslinking. The results are shown in Figure 4.5 and 3.6. Not only did degrafting of the modified TD (M.TD) patterned brush show no ridge structures as observed in the bottom-up brush, but also the degrafting trend behaved similar to what was expected. Both of those phenomena suggested the reduction or absence of crosslinking at the edge. However, it could be noticed that at 35 °C the M.TD patterned brushes were more stable compared to BU patterned brushes for pattern sizes $\geq 1 \mu\text{m}$. It suggested that there was still partial crosslinking on the sidewall similar to those in the TD patterned brushes and it could still affect the stability of the brushes. At patterns with size $\leq 1 \mu\text{m}$, since reduced crosslinking allowed only partial stress relaxation and limited stability enhancement, the M.TD patterned brushes was less stable than BU patterned brushes at RT.

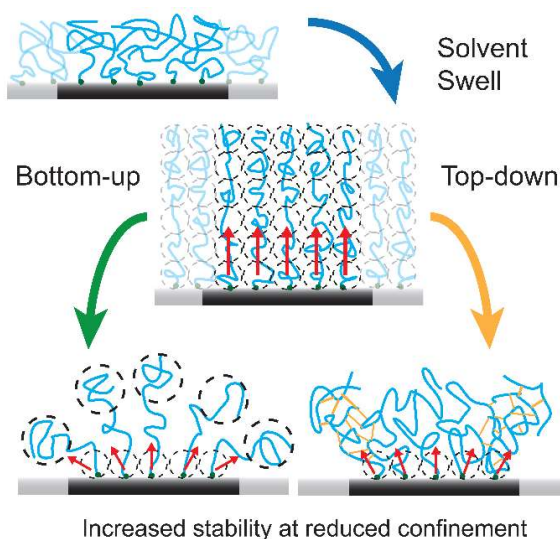


Figure 4.7 Scheme for the polymer brush relaxation under reduced lateral confinement.

Conclusions

We investigated the stability of thick, strong polyelectrolyte brushes under different conditions, which provide a new strategy to increase the stability of polymer brushes when the pattern size is reduced to nanoscale dimensions. Degrafting of the strong polyelectrolyte brushes could be enhanced by increasing immersion temperature, but it remained relatively stable under mild acidic and basic conditions compared to water. This was caused by binding of the phosphate counter-ions contained in the buffer through formation of complexation and ion pairing interaction. Etching during the TD patterning process caused crosslinking on the edge materials, which fortified the edge of PMETAC brushes. The crosslinking effect could be controlled by tuning the RIE process and the resulting brush has the same degradation trend as the bottom-up brush. Both BU patterned brushes and M.TD patterned brushes showed improved stability at smaller pattern sizes caused by enabled stress relaxation. We expect that both patterning processes could be applied to fulfill different requirements. The BU process is better for fundamental studies while the TD process provides enhanced stability and

is more convenient for industrial fabrication. The behavior of the patterned PMETAC under reduced lateral confinement is shown in Figure 4.7. The trends of degrafting on different pattern sizes should provide additional data for developing a theory to explain the degrafting phenomena and the force distribution within the patterned brush. Further studies that combine the effects of the grafting density, molecular weight, and pattern size brush behavior will be presented in chapter 5.

Acknowledgements

We would like to acknowledge the great opinions on etching condition from Cornell CNF staff Vince Genova and fruitful discussion with Ihsan Amin on CUCRP. Also we would like to thank prof. Kawakami Hiroyoshi and prof. Tanaka Manabu for sending Tsukasa to the group. This work made use of several facilities at Cornell University. 1) Cornell NanoScale Facility, a member of the National Nanotechnology Coordinated Infrastructure (NCI), which is supported by the National Science Foundation (Grant ECCS-1542081). 2) Cornell Center for Materials Research Shared Facilities, which are supported through the NSF MRSEC program (DMR-1120296). 3) Nanobiotechnology Center shared research facilities at Cornell. 4) The Center for Nanomaterials Engineering & Technology.

Supporting information

S1. Characterization of the polymer brushes

Polymer brushes were characterized by ellipsometry and atomic force microscopy (AFM). Thicknesses of the non-patterned polymer brushes were measured using a imaging ellipsometer – Nanofilm Ep3 with a 532 nm laser at 50-60° angle of

incidence. A Cauchy model (Cauchy layer/silicon substrate) was used to fit the data, in which the Cauchy layer was representative of the polymer brush. Surface topography was analyzed and using a Veeco Icon atomic force microscope. AppNANO ACCESS-NC tapping mode silicon cantilever were used to acquire topographic images in air at room temperature. Each lines were scanned for 2 times and the two cross-sectional images were taken in each scanning result to get in total 4 sets of data. Cross-sectional areas of each data were averaged and shown together with the statistical error in the figures. IR spectra were measured at ATR-mode using Thermo Scientific Nicolet iZ10 FTIR. Hydrogen nuclear magnetic resonance spectroscopy (NMR) spectra were recorded on Varian Gemini 400 MHz spectrometer with deuterium oxide, chemical shifts (δ) were reported in parts per million (ppm) relative to tetramethyl silane (TMS).

S2. Reaction condition selection of the PMETAC brushes

The polymerization of the brushes were conducted at different reducing agent concentration, the kinetics showed the similar trend as the PMETAC brush due to the similar reducing agent effect provided by the amino functional group.⁵⁴ However, we noticed that the inhomogeneity extent of the brush increased as we reduced the reducing agent concentration. Additional hydrazine has been proven to increase the polymerization rate of free polymer in CuCRP process⁵⁵. Because reaction was conducted with self-reducing monomer, there is already certain reducing ability existing and hence the reaction rate has achieved the maximum, further increase of reducing agent would only soil equilibrium and reduce the reaction rate. Such high reaction rate and poor mixing in the heterogeneous reaction should be the reason for increase of inhomogeneity. To ensure the quality of the brush, we pick medium hydrazine concentration as our reaction condition for the following experiment. In the literature it was reported that the by using methanol/ water mixture as atom transfer

radical polymerization (ATRP) medium for PMETAC would make resulting polymer losing 70% of the functional group. Based on the NMR spectrum shown in Figure 4.S1, the esterification was ~37% (calculated by the ratio of methyl groups on nitrogen atom) and this was similar to isopropyl alcohol /water mixture reported.⁵⁶ Less transesterification should be caused by limited amount of Cu catalyst present in the reaction medium. We hence still chose methanol as our reaction medium for its better solubility.

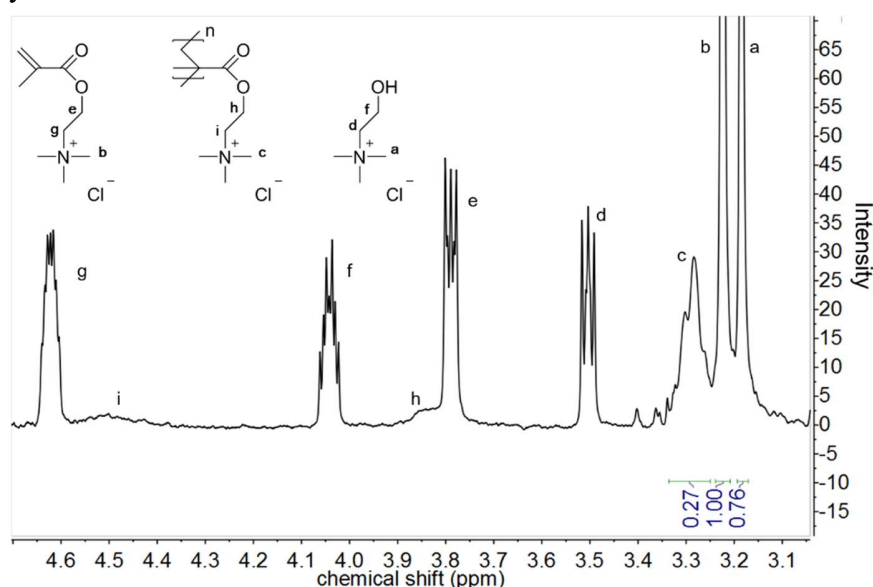


Figure 4.S1. NMR spectrum of the reaction solution of PMETAC brush (after polymerization and Copper purified).

S3. Size correction for the top-down / modified top-down patterned brushes

For top-down(TD) patterned polymer brushes, the cross-sectional areas of the patterns were used to correct the pattern sizes. In poly(methyl methacrylate) (PMMA), the pattern sizes were shrunk down both 130 nm for all the patterns. In terms of PMETAC brushes, due to the degrafting, it's hard to isolate process damage from cross-sectional area data and derive the correction size. Hence, we assumed that the

lateral penetration depths where reactive ion etching (RIE) induces structural modification are similar in PMMA and PMETAC. The shrinking size which was used to compensate the material loss in RIE process was approximated to be 130 nm for TD and modified TD patterned brushes. Considering the fact that etching rate of PMETAC is almost twice as fast as the etching rate of PMMA (in both SRIE/WRIE processes), the lateral penetration depth should have been deeper. However, with 130 nm as shrinking size the TD patterned brushes would have area ratio >1 after degrafting which is not reasonable. Thus, 100 nm was used for the correction of TD patterned PMETAC brushes and 130 nm was used for modified top-down (M. TD) patterned PMETAC brushes. The unmodified data are shown in Figure 4.S2.

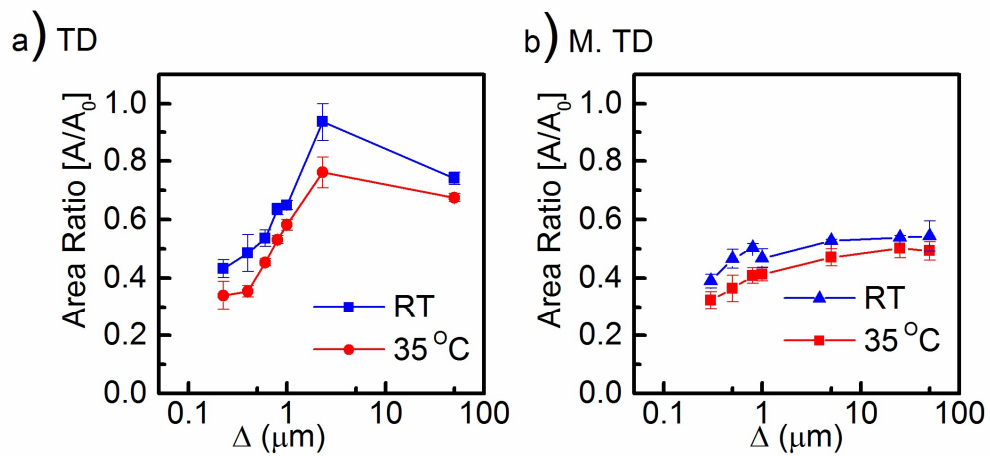


Figure 4.S2. Uncorrected degrafting trend for the TD and the M. TD patterned brushes.

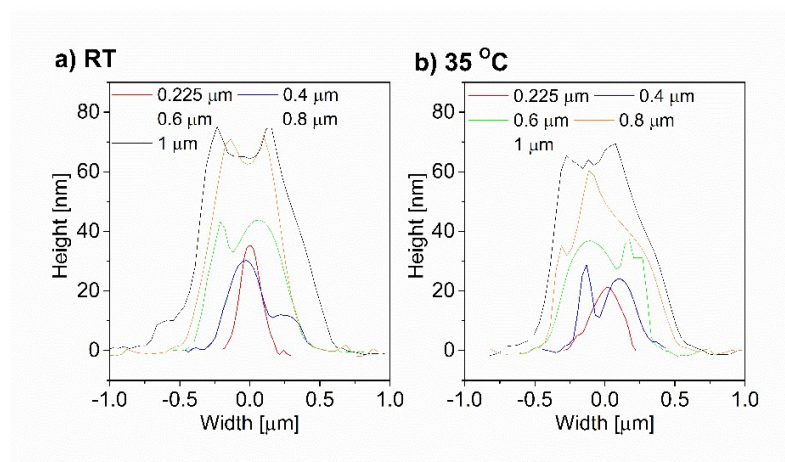


Figure 4.S3. Dry AFM cross-sectional images of the top-down patterned PMETAC brushes degrafting in water at a) room temperature (RT) b) 35 °C for 24h.

REFERENCES

- (1) Yang, W. J.; Neoh, K.-G.; Kang, E.-T.; Teo, S. L.-M.; Rittschof, D. Polymer Brush Coatings for Combating Marine Biofouling. *Prog. Polym. Sci.* **2014**, *39* (5), 1017–1042.
- (2) Bai, H.; Zhang, H.; He, Y.; Liu, J.; Zhang, B.; Wang, J. Enhanced Proton Conduction of Chitosan Membrane Enabled by Halloysite Nanotubes Bearing Sulfonate Polyelectrolyte Brushes. *J. Membr. Sci.* **2014**, *454*, 220–232.
- (3) de Groot, G. W.; Santonicola, M. G.; Sugihara, K.; Zambelli, T.; Reimhult, E.; Vörös, J.; Vancso, G. J. Switching Transport through Nanopores with PH-Responsive Polymer Brushes for Controlled Ion Permeability. *ACS Appl. Mater. Interfaces* **2013**, *5* (4), 1400–1407.

- (4) Li, Z.; Wang, H.; Song, X.; Yan, J.; Hu, H.; Yu, B. Dual-Responsive Polymer Brushes as an Electrochemical Logic Gate. *J. Electroanal. Chem.* **2014**, *719*, 7–13.
- (5) Tugulu, S.; Klok, H.-A. Stability and Nonfouling Properties of Poly(Poly(Ethylene Glycol) Methacrylate) Brushes under Cell Culture Conditions. *Biomacromolecules* **2008**, *9*(3), 906–912.
- (6) Zhu, Y.; Lv, B.; Zhang, P.; Ma, H. Swelling Induced Au–S Bond Breakage Is Determined by the Molecular Composition of Surface Tethered Copolymers—carboxylated Poly(OEGMA-r-HEMA). *Chem. Commun.* **2011**, *47*(35), 9855.
- (7) Zhang, Y.; Lv, B.; Lu, Z.; He, J.; Zhang, S.; Chen, H.; Ma, H. Predicting Au–S Bond Breakage from the Swelling Behavior of Surface Tethered Polyelectrolytes. *Soft Matter* **2011**, *7*(24), 11496–11500.
- (8) Paripovic, D.; Klok, H.-A. Improving the Stability in Aqueous Media of Polymer Brushes Grafted from Silicon Oxide Substrates by Surface-Initiated Atom Transfer Radical Polymerization. *Macromol. Chem. Phys.* **2011**, *212*(9), 950–958.
- (9) Borozenko, O.; Godin, R.; Lau, K. L.; Mah, W.; Cosa, G.; Skene, W. G.; Giasson, S. Monitoring in Real-Time the Degrafting of Covalently Attached

Fluorescent Polymer Brushes Grafted to Silica Substrates—Effects of PH and Salt. *Macromolecules* **2011**, *44* (20), 8177–8184.

- (10) Cimen, D.; Kursun, T. T.; Caykara, T. Synthesis and Stability of BODIPY-Based Fluorescent Polymer Brushes at Different PHs. *J. Polym. Sci. Part Polym. Chem.* **2014**, 3586–3596.
- (11) Alswieleh, A. M.; Cheng, N.; Canton, I.; Ustbas, B.; Xue, X.; Ladmiral, V.; Xia, S.; Ducker, R. E.; El Zubir, O.; Cartron, M. L.; et al. Zwitterionic Poly(Amino Acid Methacrylate) Brushes. *J. Am. Chem. Soc.* **2014**, *136* (26), 9404–9413.
- (12) Melzak, K. A.; Yu, K.; Bo, D.; Kizhakkedathu, J. N.; Toca-Herrera, J. L. Chain Length and Grafting Density Dependent Enhancement in the Hydrolysis of Ester-Linked Polymer Brushes. *Langmuir ACS J. Surf. Colloids* **2015**, *31* (23), 6463–6470.
- (13) Galvin, C. J.; Bain, E. D.; Henke, A.; Genzer, J. Instability of Surface-Grafted Weak Polyacid Brushes on Flat Substrates. *Macromolecules* **2015**, 150803081219001.
- (14) Ataman, N. C.; Klok, H.-A. Degrafting of Poly(Poly(Ethylene Glycol) Methacrylate) Brushes from Planar and Spherical Silicon Substrates. *Macromolecules* **2016**, *49* (23), 9035–9047.

- (15) Klok, H.-A.; Genzer, J. Expanding the Polymer Mechanochemistry Toolbox through Surface-Initiated Polymerization. *ACS Macro Lett.* **2015**, *4* (6), 636–639.
- (16) Sheiko, S. S.; Panyukov, S.; Rubinstein, M. Bond Tension in Tethered Macromolecules. *Macromolecules* **2011**, *44* (11), 4520–4529.
- (17) Tran, Y.; Auroy, P.; Lee, L.-T. Determination of the Structure of Polyelectrolyte Brushes. *Macromolecules* **1999**, *32* (26), 8952–8964.
- (18) Biesalski, M.; R uhe, J. Scaling Laws for the Swelling of Neutral and Charged Polymer Brushes in Good Solvents. *Macromolecules* **2002**, *35* (2), 499–507.
- (19) Dunlop, I. E.; Thomas, R. K.; Titmus, S.; Osborne, V.; Edmondson, S.; Huck, W. T. S.; Klein, J. Structure and Collapse of a Surface-Grown Strong Polyelectrolyte Brush on Sapphire. *Langmuir* **2012**, *28* (6), 3187–3193.
- (20) Enomoto, K.; Takahashi, S.; Iwase, T.; Yamashita, T.; Maekawa, Y. Degradation Manner of Polymer Grafts Chemically Attached on Thermally Stable Polymer Films: Swelling-Induced Detachment of Hydrophilic Grafts from Hydrophobic Polymer Substrates in Aqueous Media. *J. Mater. Chem.* **2011**, *21* (25), 9343.
- (21) Jonas, A. M.; Hu, Z.; Glinel, K.; Huck, W. T. S. Chain Entropy and Wetting Energy Control the Shape of Nanopatterned Polymer Brushes. *Macromolecules* **2008**, *41* (19), 6859–6863.

- (22) KOEPEL, R. R.; RUSSELL, A. J.; RAVIKUMAR, T. United States Patent Application: 0090074709 - METHODS, DEVICES AND SYSTEMS FOR BIOCIDAL SURFACE ACTIVITY. 20090074709, A1.
- (23) Ramakrishnan, A.; Dhamodharan, R.; Rhe, J. Controlled Growth of PMMA Brushes on Silicon Surfaces at Room Temperature. *Macromol. Rapid Commun.* **2002**, *23* (10–11), 612–616.
- (24) Zhang, T.; Du, Y.; Mller, F.; Amin, I.; Jordan, R. Surface-Initiated Cu(0) Mediated Controlled Radical Polymerization (SI-CuCRP) Using a Copper Plate. *Polym Chem* **2015**, *6* (14), 2726–2733.
- (25) Zhang, T.; Du, Y.; Kalbacova, J.; Schubel, R.; Rodriguez, R. D.; Chen, T.; Zahn, D. R. T.; Jordan, R. Wafer-Scale Synthesis of Defined Polymer Brushes under Ambient Conditions. *Polym Chem* **2015**, *6* (47), 8176–8183.
- (26) Osborne, V. L.; Jones, D. M.; Huck, W. T. S. Controlled Growth of Triblock Polyelectrolyte Brushes. *Chem. Commun.* **2002**, No. 17, 1838–1839.
- (27) Kobayashi, M.; Terada, M.; Terayama, Y.; Kikuchi, M.; Takahara, A. Direct Synthesis of Well-Defined Poly[2-(Methacryloyloxy)Ethyl]trimethylammonium Chloride] Brush via Surface-Initiated Atom Transfer Radical Polymerization in Fluoroalcohol. *Macromolecules* **2010**, *43* (20), 8409–8415.

- (28) Dong, R.; Molloy, R. P.; Lindau, M.; Ober, C. K. Direct Synthesis of Quaternized Polymer Brushes and Their Application for Guiding Neuronal Growth. *Biomacromolecules* **2010**, *11* (8), 2027–2032.
- (29) Yameen, B.; Ali, M.; Álvarez, M.; Neumann, R.; Ensinger, W.; Knoll, W.; Azzaroni, O. A Facile Route for the Preparation of Azide-Terminated Polymers. “Clicking” Polyelectrolyte Brushes on Planar Surfaces and Nanochannels. *Polym Chem* **2010**, *1* (2), 183–192.
- (30) Azzaroni, O.; Moya, S.; Farhan, T.; Brown, A. A.; Huck, W. T. S. Switching the Properties of Polyelectrolyte Brushes via “Hydrophobic Collapse.” *Macromolecules* **2005**, *38* (24), 10192–10199.
- (31) Schmidt, S. W.; Kersch, A.; Beyer, M. K.; Clausen-Schaumann, H. Mechanically Activated Rupture of Single Covalent Bonds: Evidence of Force Induced Bond Hydrolysis. *Phys. Chem. Chem. Phys.* **2011**, *13* (13), 5994–5999.
- (32) Auroy, P.; Auvray, L. Collapse-Stretching Transition for Polymer Brushes: Preferential Solvation. *Macromolecules* **1992**, *25* (16), 4134–4141.
- (33) Kent, M. S. A Quantitative Study of Tethered Chains in Various Solution Conditions Using Langmuir Diblock Copolymer Monolayers. *Macromol. Rapid Commun.* **2000**, *21* (6), 243–270.

- (34) Bain, E. D.; Dawes, K.; Özçam, A. E.; Hu, X.; Gorman, C. B.; Šrogl, J.; Genzer, J. Surface-Initiated Polymerization by Means of Novel, Stable, Non-Ester-Based Radical Initiator. *Macromolecules* **2012**, *45* (9), 3802–3815.
- (35) Zhang, H.; Rühle, J. Interaction of Strong Polyelectrolytes with Surface-Attached Polyelectrolyte Brushes–Polymer Brushes as Substrates for the Layer-by-Layer Deposition of Polyelectrolytes. *Macromolecules* **2003**, *36* (17), 6593–6598.
- (36) Manfred Schmidt. *Polyelectrolytes with Defined Molecular Architecture I*, Advances in Polymer Science; Springer Berlin Heidelberg: Berlin, Heidelberg, 2003; Vol. 164.
- (37) Konradi, R.; Rühle, J. Interaction of Poly(Methacrylic Acid) Brushes with Metal Ions: An Infrared Investigation. *Macromolecules* **2004**, *37* (18), 6954–6961.
- (38) Biesalski, M.; Johannsmann, D.; Rühle, J. Electrolyte-Induced Collapse of a Polyelectrolyte Brush. *J. Chem. Phys.* **2004**, *120* (18), 8807.
- (39) Zhang, H.; Rühle, J. Swelling of Poly(Methacrylic Acid) Brushes: Influence of Monovalent Salts in the Environment. *Macromolecules* **2005**, *38* (11), 4855–4860.
- (40) Konradi, R.; Rühle, J. Interaction of Poly(Methacrylic Acid) Brushes with Metal Ions: Swelling Properties. *Macromolecules* **2005**, *38* (10), 4345–4354.

- (41) Miller, F. A.; Wilkins, C. H. Infrared Spectra and Characteristic Frequencies of Inorganic Ions. *Anal. Chem.* **1952**, *24*(8), 1253–1294.
- (42) Lee, W.-K.; Patra, M.; Linse, P.; Zauscher, S. Scaling Behavior of Nanopatterned Polymer Brushes. *Small* **2007**, *3*(1), 63–66.
- (43) Kidoaki, S.; Ohya, S.; Nakayama, Y.; Matsuda, T. Thermoresponsive Structural Change of a Poly(*N*- Isopropylacrylamide) Graft Layer Measured with an Atomic Force Microscope. *Langmuir* **2001**, *17*(8), 2402–2407.
- (44) Rastogi, A.; Paik, M. Y.; Tanaka, M.; Ober, C. K. Direct Patterning of Intrinsically Electron Beam Sensitive Polymer Brushes. *ACS Nano* **2010**, *4*(2), 771–780.
- (45) Paik, M. Y.; Xu, Y.; Rastogi, A.; Tanaka, M.; Yi, Y.; Ober, C. K. Patterning of Polymer Brushes. A Direct Approach to Complex, Sub-Surface Structures. *Nano Lett.* **2010**, *10*(10), 3873–3879.
- (46) Chang, J.-F.; Gwinner, M. C.; Caironi, M.; Sakanoue, T.; Siringhaus, H. Conjugated-Polymer-Based Lateral Heterostructures Defined by High-Resolution Photolithography. *Adv. Funct. Mater.* **2010**, *20*(17), 2825–2832.
- (47) Oehrlein, G. S.; Chan, K. K.; Jaso, M. A.; Rubloff, G. W. Surface Analysis of Realistic Semiconductor Microstructures. *J. Vac. Sci. Technol. A* **1989**, *7*(3), 1030–1034.

- (48) Conard, T.; Franquet, A.; Vandervorst, W. Nano-Scale Feature Analysis Achieving High Effective Lateral Resolution with Micro-Scale Material Characterization Techniques: Application to Back-End Processing: Nano-Scale Feature Analysis. *Phys. Status Solidi A* **2015**, *212* (3), 506–511.
- (49) Dong, R.; Krishnan, S.; Baird, B. A.; Lindau, M.; Ober, C. K. Patterned Biofunctional Poly(Acrylic Acid) Brushes on Silicon Surfaces. *Biomacromolecules* **2007**, *8* (10), 3082–3092.
- (50) Claes, M.; Le, Q.; Kesters, E.; Lux, M.; Urionabarrenetxea, A.; Vereecke, G.; Mertens, P.; Carleer, R.; Adriaenssens, P. All-Wet Strip Approaches for Post-Etch Photoresist Layers After Low-K Patterning; ECS, 2007; Vol. 11, pp 177–187.
- (51) Ting, Y.-H.; Park, S.-M.; Liu, C.-C.; Liu, X.; Himpsel, F. J.; Nealey, P. F.; Wendt, A. E. Plasma Etch Removal of Poly(Methyl Methacrylate) in Block Copolymer Lithography. *J. Vac. Sci. Technol. B Microelectron. Nanometer Struct.* **2008**, *26* (5), 1684.
- (52) Ting, Y.-H.; Liu, C.-C.; Park, S.-M.; Jiang, H.; Nealey, P. F.; Wendt, A. E. Surface Roughening of Polystyrene and Poly(Methyl Methacrylate) in Ar/O₂ Plasma Etching. *Polymers* **2010**, *2* (4), 649–663.
- (53) Nojiri, K. *Dry Etching Technology for Semiconductors*; Springer International Publishing: Cham, 2015.

- (54) Dong, H.; Matyjaszewski, K. ARGET ATRP of 2-(Dimethylamino)Ethyl Methacrylate as an Intrinsic Reducing Agent. *Macromolecules* **2008**, *41* (19), 6868–6870.
- (55) Fleischmann, S.; Rosen, B. M.; Percec, V. SET-LRP of Acrylates in Air. *J. Polym. Sci. Part Polym. Chem.* **2010**, *48* (5), 1190–1196.
- (56) Visnevskij, C.; Makuska, R. SARA ATRP in Aqueous Solutions Containing Supplemental Redox Intermediate: Controlled Polymerization of [2-(Methacryloyloxy)Ethyl] Trimethylammonium Chloride. *Macromolecules* **2013**, *46* (12), 4764–4771.

CHAPTER 5

Entropic Death of Non-patterned and Nanostructured Polyelectrolyte Brushes*

ABSTRACT: The stability of non-patterned and nanostructured strong polyelectrolyte brushes (PEBs) is studied as a function of both brush character and the properties of a contacting liquid. High molecular weight PEBs of poly(4-methyl vinylpyridinium iodide) (PMeVP) are synthesized using surface-initiated radical-chain polymerization (SI-RCP). Nanopatterned brushes (NPBs) with pattern sizes ranging from 50 μm down to 200 nm are generated by patterning the initiator layer using deep-ultraviolet (DUV) photolithography followed by brush growth initiated from the patterned layer. Homogeneous PEBs with different degrees of charging and grafting densities are exposed to water and salt solutions with different temperatures for different periods of time. The degradation is monitored through dry-state ellipsometry and atomic force microscopy (AFM) measurements. Enhanced degrafting for more strongly swollen polymer brushes can be observed in agreement with an ‘entropic spring’ model. Based on the results of the non-patterned brushes the nanobrushes are exposed to water at different temperatures and external salt content for varying periods of time. Counterintuitively, the NPBs show increased degrafting for smaller patterns, which is attributed to different polymer chain dynamics for nano- and microbrushes. We investigate the influence of thermodynamic and kinetic parameters on the stability of (nanopatterned) PEBs and discuss the role of entanglements and formation of complexes in such films.

*This work was done in collaboration with Matthias Menzel, Dr. Kimberly Simancas, Dr. Oswald Prucker and Prof. Jürgen Rühle at University of Freiburg and Dr. Hong Xu at Cornell University

Introduction

Polyelectrolyte brushes are densely end-tethered linear polymer chains with charged subunits grafted on flat solid substrates.^{1,2,3,4} Because of the excluded volume and electrostatic repulsion between charged segments of the same type the chains must stretch away from the surface. By using different polymer compositions from charge neutral to charged polyelectrolyte (PEL), they can be used as antifouling^{5,6} coatings and transport-enhancing⁷, or stimuli-responsive^{8,9} materials. Polyelectrolytes are polymer chains that carry electrolyte groups on their repeat units, which dissociate in polar and/or protic solvents leaving charges on the polymer chain and releasing counterions into solution.¹⁰ A complete dissociation at all pH values is characteristic of strong PEBs, while the dissociation of weak PEBs is pH dependent.

The additional strong electrostatic interactions due to the charges are a reason for the unusual and versatile behavior of polyelectrolyte brushes (PEBs) compared to their neutral peers.¹¹ Thus if polymer brushes with similar structures are compared, while neutral polymer brushes can already stretch by up to 40% of their contour length, polyelectrolytes can stretch even more and stretched values of more than 65% of the contour length have been observed.¹² Such strong stretching leads to a significant loss of entropy and completely changes the properties of the layers, rendering PEBs as an attractive molecular architecture. They are often used for applications in the field of biochemistry as most organic molecules synthesized by living organisms carry electrolyte groups themselves. Thus PEBs have been used for the analysis and study of

proteins¹³, DNA¹⁴, vitamins¹⁵ and in gene¹⁵ and drug¹⁶ delivery. In addition they are also perfect candidates for applications in antifouling medical devices¹⁷, biosensing¹⁸, antibacterial coatings⁵, cell culture substrates¹⁹, stem cell expansion²⁰ and implant material²¹ because of their chemical versatility, which allows tuning of interfacial properties like hydrophilicity and surface energy.

Although there are many possible applications, stability of the PEBs is critical. Within the last decade there has been an increasing number of reports about degradation of polymer brushes.^{22,23,24,25,26,27,28,29,30,31,32} A first report of Tugulu *et al.* in 2008 described the delamination process of poly(polyethylene glycol) methacrylate (PPEGMA) brushes upon exposure to a cell culture medium.²² In another report by Borozenko *et al.*,²⁶ degrafting was described for poly(acrylic acid) brushes using total internal reflection fluorescence microscopy. They showed that the cleavage process starts at $\text{pH} \geq 9.5$ with an increased ionic strength of the buffer solution (10 mM NaCl). The majority of experimental reports agree that the chain failure and the chemical mechanism behind the loss of covalently tethered chains from the surface is facilitated by the solvent-induced stretching.^{22,25,26,33,34} However, very few studies have investigated the scaling behavior^{35,36,37} and stability³² ('entropic death') of strong PEBs that are subjected to very strong stretching of the polymer chains. The stretching reduces the possible conformations the chain can adopt.^{3,38} This means the polymer chain loses entropy and thus the overall free energy is increased according to Gibbs-Helmholtz theory.³⁹ Thus polymer brushes are inherently metastable where the supply of additional energy such as a mechanical activation can lead to chain fracture and degrafting.^{30,40}

The grafting density plays an important factor in the brush stability. An increasing number of chains per surface area leads to a larger excluded volume and therefore a larger tensile stress on chains. Both effects of grafting density and molecular weight have been investigated by Melzak *et al.*²⁹ They synthesized poly(*N,N*-dimethylacrylamide) (PDMA) brushes and monitored a faster degradation rate for both higher grafting densities and molecular weights. Also, the tensile stress on the polymer chains can be controlled by the lateral confinement of polymer brushes, e.g. by generating nanopatterns. The chains at the edge of the pattern can fan out and reach into the free space next to the grafted polymer area, which provides more space for the polymer chains close to the edge of the pattern and thus decrease the excluded volume and increase the brush's stability. In the case of nanopatterned polymer brushes (NPBs) with feature sizes close to that of the chain's contour length^{41,42,43} this edge effect ranges up to the center parts of the pattern. Such behavior leads to a unique scaling response in the micrometer scale and should provide significant lateral stress relaxation for all chains of an NPB. Chen *et al.*³² gave proof for this assumption. They fabricated strong polyelectrolyte nanostructured poly([(2-methacryloyloxy)ethyl]trimethylammonium chloride) (PMATEC) brushes using Cu(0)-mediated controlled radical polymerization (CuCRP) and monitored the stability of the brushes as a function of the pattern size. The results showed an increased brush stability with decreasing pattern size corresponding to less lateral confinement. Similarly, by giving more space to spherical polymer brushes through a decrease in the size of a substrate nanoparticle, Ataman *et al.*³¹ have shown that the stability of poly((polyethylene glycol methyl ether) methacrylate) brushes grafted on

nanoparticles can be increased. The results are interesting considering that the chain stretching level of strong PEBs in the osmotic brush regime is irrelevant to the grafting density.¹² Nevertheless, the exact relationship between grafting density and brush stability remains not well understood.

In addition, it is still not clear how degrafting takes place or where the polymer chains break. There are some theoretical reports on mechanical activation of tethered macromolecules by Sheiko and Rubinstein *et al.*⁴⁴ and Panyukov and Rubinstein *et al.*⁴⁵, who addressed the build-up of tensile stress within tethered macromolecules. They came to the conclusion that an end-grafted macromolecule will experience the largest tension in the surface linker that binds the polymer chain to the solid surface. This shows that PEBs are mechanically activated systems and drives interest in understanding the mechanisms of polymer brush degradation. However, it is an extremely complex phenomenon with regard to understanding its mechanochemistry and mechanical activation owing to the large number of contributing factors, such as ionic strength, charging of the backbone, screening of charges, solvent quality and temperature, hydrophilicity of the brush and, of course, the grafting density and molecular weight. Also it is noticed that are only few works discussed the effect of the chain dynamic and only the kinetics part of the brush degrafting was studied. Although it has been reported that the relaxation time of polymer brushes are strongly affected by their structural parameters⁴⁶, it has not shown much effect on the stability of polymer brushes in previous studies.

Motivated by this situation, the present experimental work investigates the thermodynamic stability and its kinetic aspects of high molecular weight PMeVP

brushes as a function of different extrinsic and intrinsic parameters. The growth by SI-RCP of high molecular weight polymer brushes on silicon is performed as reported previously^{47,48}, as was the nanopatterning by DUV photolithography to achieve bottom-up (BU) nanostructured PEBs.^{32,49} The brush layer thickness or rather the cross section integral is studied by ellipsometry and tapping mode AFM. The investigation enables a closer look on the impact of the chemical nature, the confinement, the environment and the polymer chain dynamics on the PEBs thermodynamic stability, which is important for the preservation of their function.

Results and Discussion

5.1. Homogeneous Polyelectrolyte Brush Layers

Synthesis of Polyelectrolyte Brushes. The PEBs were generated according to Biesalski and R  he⁵⁰ as shown in Figure 5.1. The first step is the immobilization of an azo-initiator with a dimethylchlorosilane headgroup on a flat silicon surface. In the next step a PVP brush was grown by thermal activation of the attached initiator via surface-initiated radical chain polymerization (SI-RCP) in bulk or DMF. SI-RCP enables the fabrication of densely grafted polymer brushes with a molecular weight of more than $10^6 \text{ g} \cdot \text{mol}^{-1}$ as termination by recombination or disproportion reactions are strongly prevented due to the fact that the growing polymer radicals cannot move in respect to each other.⁵² Accordingly, under many polymerization conditions the main termination mechanism of the chain growth reaction is transfer to monomer or solvent. Such a process leads to growth of polymer in solution, which is lost during extraction, but stops the growth of the surface-attached chain. At the same time polymer brush

parameters like molecular weight or grafting density can be easily controlled by changing the reaction time or monomer concentration similar to normal RCP.⁵² The supernatant solution was poured into excess of toluene to precipitate the non-attached polymer. The molecular weight of the non-bonded polymer could be determined by GPC or calculated from the dry brush thickness h through:

$$h = \frac{M_n * \Gamma}{\rho}, \quad 5.1$$

where Γ is the grafting density, M_n the molecular weight and ρ the density of the polymer brush or rather the polymer. Both methods, determination of M_n by GPC and calculation of Γ or determination of Γ by using the graft density of the initiator and the reaction time and calculating M_n using Equation 5.1, lead to comparable results.⁵³

Thus the molecular weight of the non-bonded polymer is taken as representative of that of the polymer brush. Subsequently the neutral PVP brush was quaternized using methyl iodide gaining the PEB PMeVP. The complete conversion of pyridine into

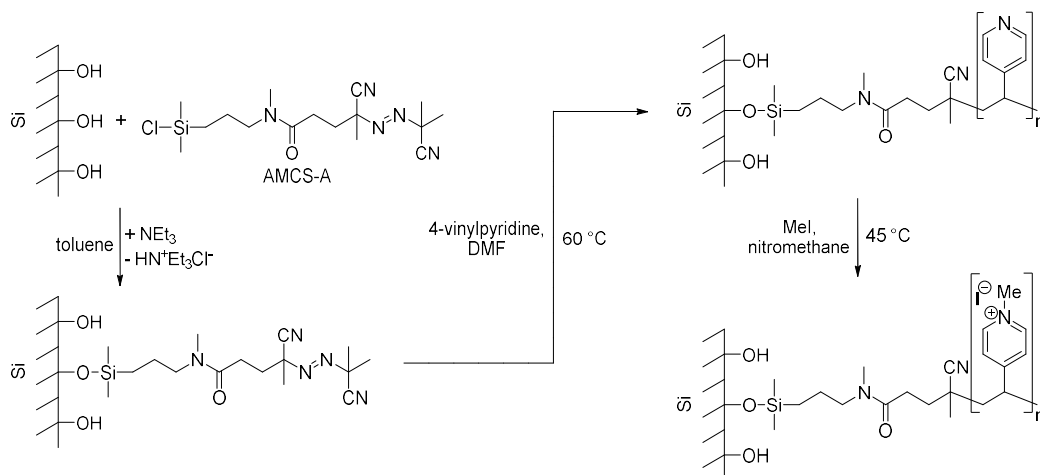


Figure 5.1: Synthesis of a cationic polyelectrolyte brush (poly[4-vinyl-N-methylpyridinium] iodide) by quaternization of the neutral poly(4-vinylpyridine) brush with methyl iodide in nitromethane.

pyridinium groups was monitored using FT-IR spectroscopy (see supporting information).

Thermodynamic stability of non-patterned PMeVP brushes. Strong PEBs are metastable systems. To study their stability in detail the influence of different brush parameters such as degree of charging, grafting density, solvent temperature or lateral confinement on the thermodynamic stability of the brushes must be monitored. One PEB was cut into several pieces and each piece was degraded for a certain period of time. Each piece yielded one data point. To determine the rate of degradation, the brush dry thickness was measured by ellipsometry for non-patterned polymer brushes before and after exposure to good solvents. From the observed values, the relative brush layer height h_{rel} was calculated as:

$$h_{\text{rel}} (\%) = 100 * \frac{h_i}{h_0}, \quad 5.2$$

where h_0 is the initial dry brush layer height and h_i the dry brush height after the exposure procedure. In the following, the reported results for the different exposure times correspond to individual samples cut from a single brush.

First of all, the influence of the degree of charging of the PEBs on the brush's thermodynamic stability is to be analyzed. This cannot not be done by analyzing the stability of PMeVP brushes with varying degrees of completion of the quaternization reaction since pure PVP brush does not swell completely in water like the polyelectrolyte (see supporting information). Thus, a water soluble copolymer based on poly(*N,N*-dimethylacrylamide) (PDMA) and PMeVP was used, as PDMA brushes show complete swelling in water and can thus form a suitable matrix component for

the copolymers.⁵⁴ For this, three PDMA-*co*-PMeVP brushes with different PMeVP content ($f = 0\%$; 73% ; and 100%) were synthesized (see supporting information) and exposed to water at $22\text{ }^{\circ}\text{C}$. The results are shown in Figure 5.2a. The results suggest that as the degree of charging in the brush increases, the stability of the layer is decreased. Similar to our finding, Galvin *et al.*³⁰ observed an increasing degradation rate depending on the degree of charging. They immersed weak polyacid brushes in buffer solutions with different pH. The degree of deprotonation and thus charging of the polymer increased with increasing pH. It was concluded that a faster degradation rate is obtained at higher pH.

The degrafting behavior can be understood, when looking at the swelling behavior of PEBs. For PEBs in the osmotic brush regime^{11,55}, the balance between the osmotic pressure and restoring force of stretched polymer chains determines the extent of brush swelling. Therefore, as the number of charged groups in the polymer chain increases, the brush thickness increases correspondingly to counteract the osmotic pressure. Due to the stronger osmotic pressure induced by the charged groups, PEBs stretch much more in water than neutral polymer brushes and, as a consequence, chain entropy decreases further. Thinking in terms of the Gibbs-Helmholtz Equation,³⁹ an entropy decrease leads to an increase in the energetic state of the polymer brush system which decreased the required energy to start the degrafting reaction. Therefore, the rate of the degrafting reaction increases as well as the speed of material loss with the degree of charging.

In addition to the degree of charging, the stretching of the PEB chains in solution can also be influenced by the external salt concentration.⁵⁶ To understand the effect of

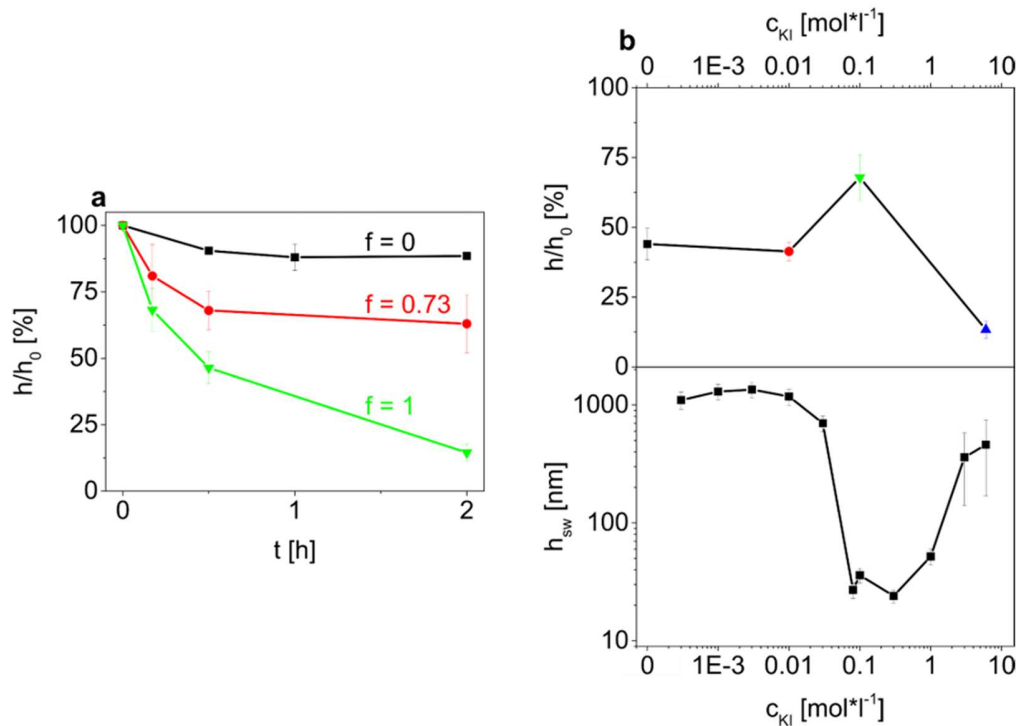


Figure 5.2: Degrafting behavior of PMeVP brushes at different degrees of charging and external salt concentrations. a) Relative dry thickness of three copolymer brushes based on PDMA and PMeVP of increasing degree of charging after exposure to water at 22 °C for different periods of time: ■ ($f = 0\%$; $\Gamma = 0.070 \mu\text{mol}\cdot\text{m}^{-2}$; $M_n = 480\cdot 10^3 \text{ g}\cdot\text{mol}^{-1}$; PDI = 1.84); ● ($f = 73\%$; $\Gamma = 0.135 \mu\text{mol}\cdot\text{m}^{-2}$; $M_n = 330\cdot 10^3 \text{ g}\cdot\text{mol}^{-1}$); and ▼ ($f = 100\%$; $\Gamma = 0.219 \mu\text{mol}\cdot\text{m}^{-2}$; $M_n = 210\cdot 10^3 \text{ g}\cdot\text{mol}^{-1}$; PDI = 1.59) b) Upper graph: Degrafting behavior monitored with the help of the relative dry thickness of PMeVP brushes ($\Gamma = 0.320 \mu\text{mol}\cdot\text{m}^{-2}$; $M_n = 330.000 \text{ g}\cdot\text{mol}^{-1}$) as a function of external salt concentration. The PEBs have been exposed to water with different KI salt concentrations at 24 °C for 24 h: ■ ($c = 0.1 \text{ mol}\cdot\text{l}^{-1}$), ● ($c = 0.01 \text{ mol}\cdot\text{l}^{-1}$), ▼ ($c = 0.1 \text{ mol}\cdot\text{l}^{-1}$) and ▲ ($c = 6.0 \text{ mol}\cdot\text{l}^{-1}$). Lower graph: Swollen brush layer thickness h_{sw} of a 20-nm-thick PMeVP brush on a LaSFN9 prism as a function of the KI salt concentration. [Reprint from ref. 56 with permission, Copyright 2004, American Institute of Physics]

potassium iodide solutions at 24 °C for 24 h. Potassium iodide was used to make sure that there is no exchange of the counter ions during the immersion procedure. The results shown in the upper graph of Figure 5.2b. It shows that brushes at low and highly concentrated salt solution degrade much faster than in medium salt solution which is in good agreement with the stretching level of PEBs. Biesalski *et al.*,⁵⁶ have investigated the electrolyte-induced structure change of PMeVP brushes and it was found that the swelling behavior strongly depends on the presence of external salt (see lower graph Figure 5.2b). Within a narrow concentration range between 0.01 and 0.08 mol·l⁻¹ they monitored a collapse of the brush to almost the dry thickness which corresponds to the increased stability shown here. It was also suggested that the strong dependence cannot be caused by electrostatic screening alone, but should also be attributed to the formation of charge-transfer complexes between the iodide ions and the pyridinium moieties of the PMeVP brush chains.^{57,58,59} These additional intermolecular interactions could also have a strong influence on the thermodynamic stabilities of the brushes as they significantly reduce the electrostatic repulsion within the brush layer. Furthermore, at higher salt concentration, the complex will be further charged and even assume the opposite charge sign in the presence of a sufficient excess of iodide ions which makes the brushes re-swell into the solution. Therefore, the stretching of the PEBs increases again at high salt concentrations, accompanied by a corresponding decrease of stability. The apparent slightly smaller dry brush thickness after immersion in 6 mol·l⁻¹ KI solution, washing and drying might be attributed to the uptake of iodide ions into the brush layer which leads to reduced dissolution of the brush and less swelling by the contacting humid air.⁵⁰ Such phenomena were

confirmed by the increase of the iodine content as evidenced in the XPS spectra.

Detailed information are presented in the supporting information.

For strong PEBs the force inducing swelling mainly depends on the ion osmotic pressure.¹¹ This means that the wet thickness of strong PEBs can be assumed to be more or less independent of temperature since the ion dissociation level of strong PEBs is not sensitive to temperature. This permits evaluation of the thermodynamics of the degrafting process with near constant chain stretching. To this, a PMeVP brush with grafting density of $0.08 \mu\text{mol}\cdot\text{m}^{-2}$ was exposed to water at different temperatures (ranging from 2 to 50 °C) for different periods of time. Figure 5.3 illustrates the dry brush layer thickness as a function of exposure time in water at different temperatures. These results show, for example, that at 50 °C the brush has lost 90% of its mass in only 10 min, while at 2 °C the loss of mass only amounts to 10% even after five hours of exposure. Similar behavior was reported by Chen *et al.*³² with poly(2-(methacryloyloxy)ethyl ammonium chloride) (PMETAC) brushes immersed in water at different temperatures. They also reported that at higher temperature the brushes became less stable.

To analyze the bond scission kinetics, a first order reaction kinetics was used to fit the data since neutral polymer brush degradation was found out to follow pseudo-first order kinetics.²⁹ The reaction rate was determined for every solvent temperature by the slope of the initial reaction rate obtained from the data in Figure 5.3a. The reaction rate coefficients for these temperatures are shown in Table 5.1.

T [°C]	2	14	24	30	50
k [s ⁻¹]	1.46*10 ⁻⁵	5.87*10 ⁻⁵	4.48*10 ⁻⁴	1.14*10 ⁻³	8.51*10 ⁻³

Table 5.1: Reaction rates of bond scission in 0.08 mol*mol⁻² PMeVP brushes in water at different temperatures.

Subsequently, its dependence of the reaction rate on the temperature was then plotted (see Figure 5.3b) and fit using the Arrhenius Equation:⁶⁰

$$k = A * \exp\left(-\frac{E_a}{RT}\right), \quad 5.3$$

where A is the pre-exponential factor, E_a is the reaction activation energy and R is the gas constant. E_a was then determined by the plotting of ln(k) as a function of -1/T and the slope gives E_a = 102 kJ*mol⁻¹. This value shows that the activation energy for degrafting, i.e. the breaking of a bond of the brush connecting it to the surface, is significantly lower than that of a conventional C-C bond. A similar value for the activation energy has been shown for chain hydrolysis in the work of Bershtein *et al.*⁶¹, who found that a mechanically activated hydrolyzed amide bond has an E_a = 84-104 kJ*mol⁻¹ and a siloxane bond has E_a = 79-96 kJ*mol⁻¹ in the presence of the moisture. Such correspondence suggests that the Si-O and/or C-N bonds are the

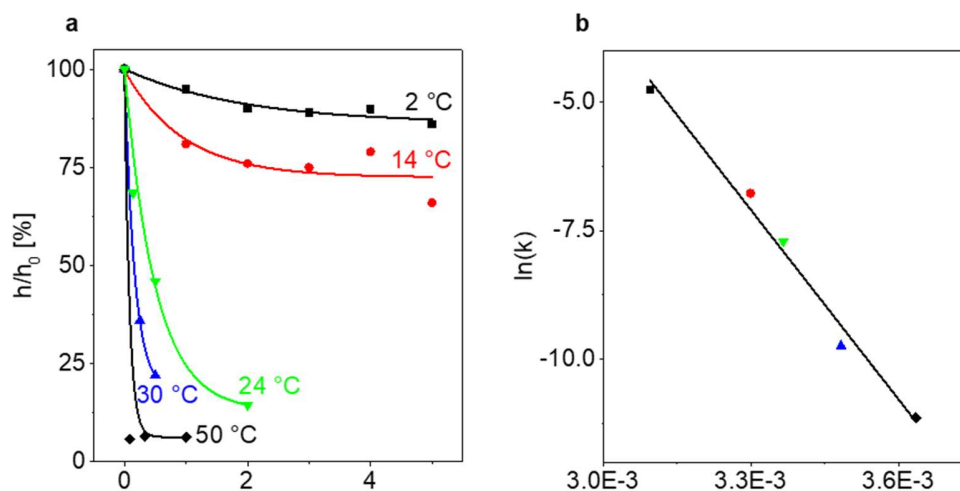


Figure 5.3: Degrafting behavior of PMeVP brushes at different solvent temperatures.

a) Relative dry layer thickness of PMeVP brushes ($h_0 = 78 \pm 6$ nm;

$\Gamma = 0.08 \mu\text{mol} \cdot \text{mol}^{-2}$; $M_n = 550 \cdot 10^3 \text{ g} \cdot \text{mol}^{-1}$; PDI = 2.50) as a function of the

exposure time in water at different temperatures: ■ (T = 2 °C); ● (T = 14 °C);

▼ (T = 24 °C); ▲ (T = 30 °C); and ◆ (T = 50 °C). The straight lines represent

exponential fits of the data. b) Corresponding Arrhenius plot of the reaction rate of the

thickness decrease in PMeVP brushes as a function of the temperature. The straight

lines represent a linear fit of the data.

origins for the degrafting which are in agreement with the literatures that the presence of nucleophiles enhances the degrafting process of polymer brushes.^{30,40,62}

It was reported that a tethered macromolecule experiences the largest tension in the surface linker that binds the polymer chain to the rigid surface^{44,45} which enhances the degrafting²⁹. Since the tension on the polymer brushes is directly related to the grafting density, a series of PMeVP brushes with graft densities ranging from 0.0069 to 0.1693 $\mu\text{mol} \cdot \text{m}^{-2}$ were exposed to water at 22 °C for different periods of time to determine the effect of grafting density on the stability of strong PEBs,. The results are

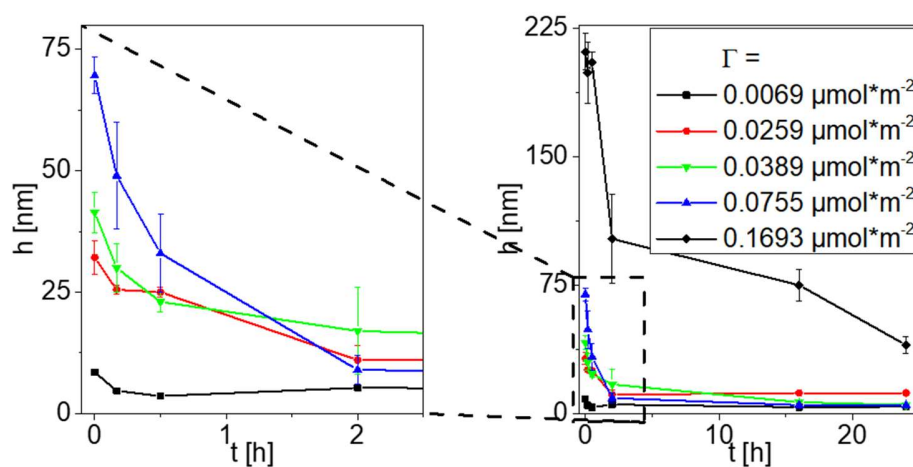


Figure 5.4: Degrafting behavior of strong polyelectrolyte PMeVP brushes

($M_n = 650 \cdot 10^3 \text{ g} \cdot \text{mol}^{-1}$; PDI = 1.67) with different grafting densities:

■ ($\Gamma = 0.0069 \text{ } \mu\text{mol} \cdot \text{m}^{-2}$); ● ($\Gamma = 0.0259 \text{ } \mu\text{mol} \cdot \text{m}^{-2}$); ▼ ($\Gamma = 0.0389 \text{ } \mu\text{mol} \cdot \text{m}^{-2}$);

▲ ($\Gamma = 0.0755 \text{ } \mu\text{mol} \cdot \text{m}^{-2}$); and ◆ ($\Gamma = 0.1693 \text{ } \mu\text{mol} \cdot \text{m}^{-2}$). a) PEBs have been to water

at 22 °C for different periods of time. The left graph is an enlarged cut-out of the right diagram.

shown in Figure 5.4. Since each brush had a different initial thickness, the absolute brush layer height is given instead of the relative one. In addition, note that in this graph the final thicknesses after each exposure time is given. The results indicate that for all grafting densities there is a strong dependence of the film thickness on exposure time. All brushes seemed to show the same degrafting behavior with a significant decrease of the brush height at the beginning and a slower degradation rate or even no degradation once a significant number of chains have been removed. Similar degrafting behavior could be observed by Malzak *et al.*²⁹ for PDMA brushes, who report that the rate of cleavage of polymer chains during a given experiment changed

by up to one order of magnitude to a lower rate as the reaction progressed.

Additionally, independent of the initial grafting density all our samples exhibited a similar stable polymer film layer thickness, where no further degrafting could be observed. We assume that the last remaining end-tethered polymer chains benefit from the gained free space and additional stabilizing interactions with the substrates surface (dipolar forces or hydrogen bonds) could play a role here.⁶³

22 °C for different periods of time. The left graph is an enlarged cut-out of the right diagram.

5.2. Nanopatterned Polyelectrolyte Brushes

Thermodynamic stability of nanostructured PMeVP. To investigate the influence of the lateral pressure on the degrafting in more detail, nanopatterned PEBs were generated and exposed to solvents. The nanopatterned polymer brushes (NPBs) were fabricated by a bottom-up process as reported before.³² The widths of the polymer chain grafted areas varied over a range from 0.2 to 50 μm to ensure to cover the point of transition from a nanobrush, where the whole pattern is affected by stress relaxation due to edge effects, to a microbrush, where only the chains at the edge of the pattern experience stress relaxation (see Figure 5.8a).^{49,41,43} To monitor the rate of degradation the cross section integrals A of all brush patterns were measured in the dry state using tapping mode AFM before and after exposure to solvents. An example is depicted in Figure 5.5a. The widening of the brush line after exposure to water is caused by relaxation of the brush chains at the periphery of the pattern and wetting of the substrate, which has been described in detail in a previous work.⁴⁹ From the

observed values, the relative cross section integrals A_{rel} of the brush patterns were calculated as

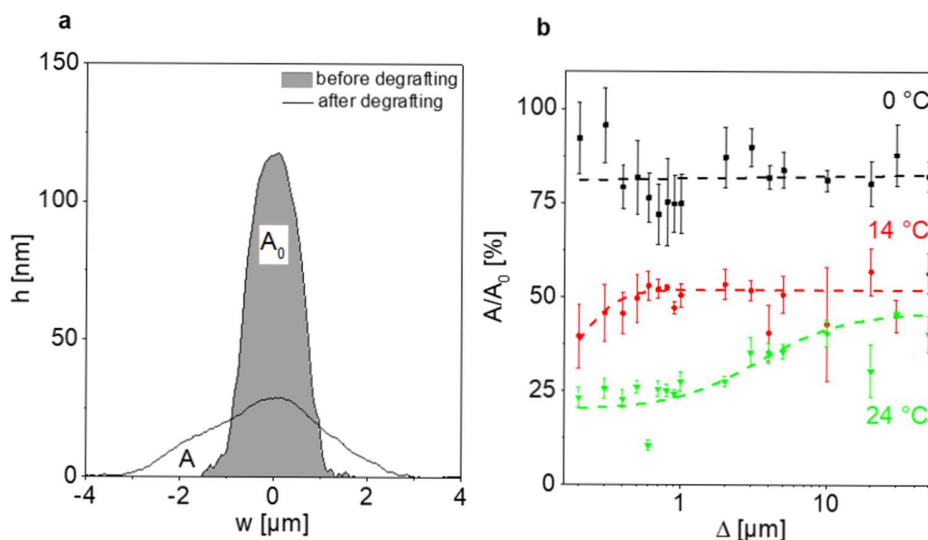


Figure 5.5: Degrafting behavior of nanostructured PMeVP brushes monitored using the relative dry cross section integral as a function of the pattern size. a) AFM height profiles illustrating the cross-sectional area of the PMeVP brush pattern line $\Delta = 1 \mu\text{m}$ before and after exposure to water at $14 \text{ }^\circ\text{C}$ for 3 h. b) Diagram showing the area ratio of the PMeVP nanobrushes ($\Gamma = 0.293 \mu\text{mol} \cdot \text{m}^{-2}$; $M_n = 340.000 \text{ g} \cdot \text{mol}^{-1}$) which were exposed to a good solvent (water) at different temperatures for different periods of time: \blacksquare ($t = 3 \text{ h}$); \blacksquare ($t = 3 \text{ h}$); and \blacksquare ($t = 0.5 \text{ h}$). The dashed lines are guides to the eye.

$$A_{rel} (\%) = 100 * \frac{A_i}{A_0}, \quad 5.4$$

where A_0 is the initial dry brush cross section integral and A_i the dry brush integral after the exposure procedure. Thus the value represents essentially the fraction of mass of the brush still left after degrafting, when it is assumed that the materials density of the brush remains unaffected by the degrafting process.

To investigate the influence of the pattern size on the thermodynamic stability of PMeVP brushes, the NPBs were exposed to water at different temperatures. The results shown in Figure 5.5b imply that smaller patterns are less stable and lose relatively more material under the given conditions. Additionally, it is obvious that this effect decreases with decreasing temperature. At low temperature both the degrafting rate is low and the dependence of the degrafting rate with the size of the pattern is also low. These results are in contrast to simple assumptions, where one would expect that a smaller pattern size allows a stronger stress relaxation due to the stronger influence of edge effects and thus an increased stability. The fact that the solvent temperature seems to have also a strong influence on the pattern size-stability relation indicates that both thermodynamic and kinetics (and chain dynamics) aspects need to be considered. To probe the interplay between thermodynamics and kinetics, additional experiments were conducted.

Since the solvent temperature has a strong impact on the degrafting-pattern size relation as the additional thermal energy influences the energy level of the chains, other factors like solvent quality or molecular weight may show similar results by tuning the chain stretching level. Therefore, we changed the solvent properties by adding potassium iodide. Based on the results with non-patterned PMeVP brushes mentioned before, we have chosen salt concentrations of 0.1 and 0.01 mol⁻¹ of potassium iodide to see how the brush stability as a function of pattern sizes reacts to the stretching level. The brushes were immersed in the different salt solutions for 24 h at 24 °C and the results are depicted in Figure 5.6a. They were in good agreement with the degrafting behavior at different temperatures shown in Figure 5.5b. Again, the same trend could be observed that the smaller patterns are less stable, whereas this effect decreases with decreasing degradation rate and stretching level. The match of

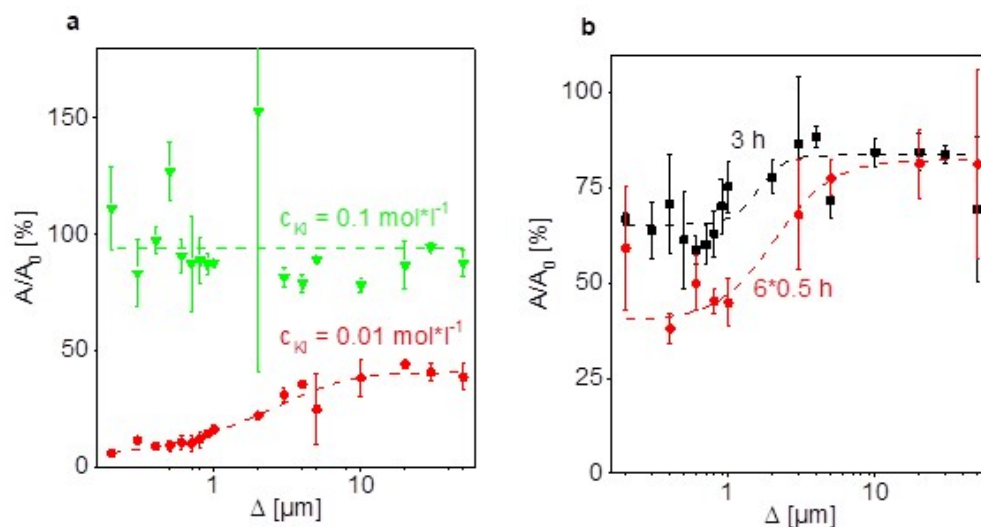


Figure 5.6: Degrafting behavior of nanostructured PMeVP brushes

($\Gamma = 0.239 \mu\text{mol}\cdot\text{m}^{-2}$; $M_n = 820.000 \text{ g}\cdot\text{mol}^{-1}$) monitored using the relative dry cross section integral as a function of the pattern size. a) The NPBs have been exposed to water with different KI salt concentrations at 24 °C for 24 h: ● ($c = 0.01 \text{ mol}\cdot\text{l}^{-1}$); and ▼ ($c = 0.1 \text{ mol}\cdot\text{l}^{-1}$). The dashed lines are guides to the eye. b) The NPBs have been exposed to water in different ways for overall 3 h at 0 °C: ■ (1*3 h); and ● (6*0.5 h). The dashed lines are guides to the eye.

the results between temperature and salt tests suggest that degrafting rate plays an important role in the trend of brush degrafting at different pattern sizes.

To explore how the kinetics of the degrafting plays a role in the degradation behavior, PMeVP nanobrushes were exposed to water at 0 °C in two different ways. The first sample was immersed continuously for 3 h and the second sample was also exposed for a total amount of 3 h, but after every 0.5 h step it was taken out and dried before re-immersion into water. As shown in Figure 5.6b, both NPBs showed a degrafting behavior dependent on the pattern size. Interestingly, for the PMeVP brush which was immersed in water continuously experienced weaker degradation, while the

sample exposed for the same time, but submitted to 6 immersion and reimmersion cycles showed not only an overall stronger degrafting behavior, but also a stronger size dependence. Similar to the experiments before, the difference in degrafting got stronger with smaller pattern sizes when the degrafting rate was higher.

Discussion

The experiments shown here demonstrate that polymer brushes are metastable systems composed of polymer chains in an entropically unfavorable stretched state ('entropic spring' model). The stretching of these entropic springs consisting of PEBs is strongly influenced by intrinsic parameters (molecular weight, degree of charging and grafting density of the polymer chains and pattern size = lateral confinement) and also extrinsic parameters (temperature, solvent quality, external salt concentration). As additional energy is supplied to the system, for example by exposure to a good solvent, this addition leads to breaking of chemical bonds and a loss of material for the surface-attached layer is observed. When the brush is swollen in a good solvent (i.e. water in the case of the PEB studied here) the chains become even more stretched and less chain conformations are available. The loss of entropy leads to a higher energetic state of the system, which can lead to degrafting of the chains. This phenomenon is also known as 'entropic death' of the chains constituting the brush. As more and more chains are cleaved off the elastic energy stored in the brush drops and the degrafting process is slowed until a point of equilibrium is reached, whereupon there is no further degrafting.

The tendency to degrafting can be mitigated or exacerbated by extrinsic parameters: By varying the degree of charging of the PEB chains the stability of the brush can be influenced. Charging of the polymer brush chain leads to a strong swelling of the brush layers ('osmotic pull') when immersed into a good solvent (water in the case of the PEB brushes studied here). Polymer brushes with a higher degree of charging show an overall stronger degrafting than those with a lower concentration of charged repeat units. Accordingly, any parameter which influences the charging will thus have a strong influence on the stability of the layers. Thus it is not surprising, that the swelling behavior also strongly depends on the external salt concentration, as high concentrations of salt leads to electrostatic screening.⁵⁶ The screening of the charges reduces the osmotic pull on the chain and thus improves the brush stability.

Another important extrinsic parameter is the temperature to which the brush is exposed. By heating the brushes, the more thermal energy is imparted into them, and the more readily the energy required for breaking the entropic spring can be reached. By determination of the degrafting rates at different temperatures the activation energy for bond scission can be calculated for PMeVP brushes ($\approx 100 \text{ kJ}\cdot\text{mol}^{-1}$). Although the exact value of this activation energy will depend quite strongly on the details of the parameters of the brush, this illustrates nicely under how much tension the polymer chains (or 'entropic springs') are.

However, the fact that the stability of the brush depends not only on such parameters, but also on how exactly it is treated, i.e. the contact time with solvent is of less importance than how many times the brush has been immersed, demonstrates clearly that thermodynamic parameters are not the only parameters which must be considered. In fact, polymer chain dynamic also plays a major role. When the brushes are immersed in water, then the rapid swelling process would apply tension on polymer chains even before their relaxation and disentanglement. Such process which

leads to a strong non-equilibrium situation on a short time scale and the tension could be amplified through entanglement points. It leads to a peak force which subsequently accelerates the degrafting procedure before the systems reaches a state of equilibrium. This phenomenon is illustrated in Figure 5.7a and we will it in the following sections ‘osmotic shock’. We assume that during this period, aspects like chain flexibility or entanglements would have a strong influence on force distribution and affect degrafting kinetic significantly.

When the brushes are patterned the polymer chains at the edge of the pattern can expand into the polymer free space next to the polymer grafted areas. Thus if the pattern size is in the length scale of the polymer chain contour length and below (NPBs) this affects the whole pattern and leads to reduced lateral confinement of all brush chains. In the end this situation is similar to reducing the grafting density and should decrease the lateral pressure and lead to an improved stability of the brushes from a thermodynamic point of view. However, the observed behavior of confined PMeVP brushes is surprisingly exactly opposite of these expectations. If the pattern size is reduced, under most conditions the stability of PMeVP brushes is not enhanced, but instead significantly reduced. It is observed that the faster the degrafting, the more pronounced is the difference of the degrafting rate between samples having larger or smaller pattern sizes. To understand this, we need to take a closer look at the dynamics of polymer chains. When PMeVP brushes are immersed in deionized water, water diffuses into the brush layer. This happens on a rather short time scale and leaves the PEB in a strong non-equilibrium state, which increases the lateral pressure on the polymer chains. This highly non-equilibrated state induces high pulling forces for a short time (chains are overstretched), accelerates the degrafting procedure so that steric effects can be neglected in first approximation. Since larger pattern sizes have a smaller surface/volume ratio, the amount of water flowing into the brush during

swelling is smaller in relation to the volume of the brush, which should have a strong effect on the ‘osmotic shock’. In addition, the time scale for swelling is shorter than the time scales of disentangling of entangled polymer brushes. As the PMeVP brushes have a very high molecular weight, they are highly entangled⁴⁶, which due to the surface-attachment show only rather slow disentanglement. While the chains are still entangled those physical crosslinks could lead to a distribution of the tensile stress from one chain on multiple chains as depicted in Figure 5.7b and thus slow down the degrafting process. When patterned brushes are viewed, as the pattern size decreases, the fraction of chains at the edge of the pattern which can fan out easily to the free spaces without any hindrance increases. This leads to a decreasing number of stabilizing entanglements per unit area.⁶⁴ So that even though the steric constraints are released, the degrafting becomes faster.

We cannot exclude a priori that no chemical bonds are generated between individual polymer molecules during growth of the chains through a chain transfer reaction to polymer. The probability of such a transfer reaction would strongly depend on the polymer concentration in the film which is higher with increasing grafting density and/or pattern size and is lowered if the tethered polymer chains are given a chance to ‘fan out’.⁶⁵ However, from the fact that eventually degrafting *does* occur, it can be concluded that the extent of such reactions will be limited. An anchoring of polymer chains leading to the generation of a (small) network connected through several anchor points at the surface would slow down a degrafting reaction to such an extent that the process would no longer be observed, which is not the case.

A second effect which leads to a stabilization of the brushes are interchain interactions. The stabilization effect between pyridinium moieties and iodide has been monitored in form of a reduced enthalpy during a mixing experiment⁶⁶, where iodide is the only halide ion which has a negative mixing enthalpy with PMeVP. Furthermore

the formation of charge-transfer complexes between iodide ions and pyridinium moieties suggest the possible existence of such interactions between the chains.⁵⁶ Even though polyelectrolyte chains with effective charges have interpolymer repulsion, this is not the case for strong PEBs where counterions are retained in the structure for electroneutrality.¹¹ To confirm our hypothesis, simulation based on Density-Functional Tight-Binding method (DFTB) was conducted to check the interaction between different components (see supporting information). Reduction of total energy by 1465.2 kJ*mol⁻¹ was observed for a mole of complex composed of three chains (each chain with 30 monomer units) when compared to the sum energy of three individual chains. The value, which equals to 4.2 times the C-C bond energy approximately, means that the system is more stable when more chains are present in the system. The result is highly suggestive of the existence of inter/intra-polymer interactions, which should be responsible for the hinderance of stress relaxation. The effect on the intermolecular interactions is illustrated in Figure 5.7c. The complex formation leads to reduced distances between the different polymer chains⁶⁷ and the formation of a weakly cross-linked supramolecular polymer, which hinders the stress-relaxation effects by nanopatterning.

To prove the developed model we conducted additional experiments with neutral, high molecular weight and charged, low molecular weight nanobrushes. Thus patterned, neutral PVP brushes with high molecular weight (= entangled) were generated. The PVP brushes were immersed in anhydrous DMF at 100 °C for 24 h. The results are shown in Figure 5.8. Because of the missing charges compared to PMeVP brushes a high temperature (T = 100 °C) was needed to induce visible degradation in case of the PVP brushes. Because of the slow degradation rate the chains have enough time for disentanglement. Thus the degrafting is dominated by thermodynamic aspects and the PVP brush sample showed an increased stability at

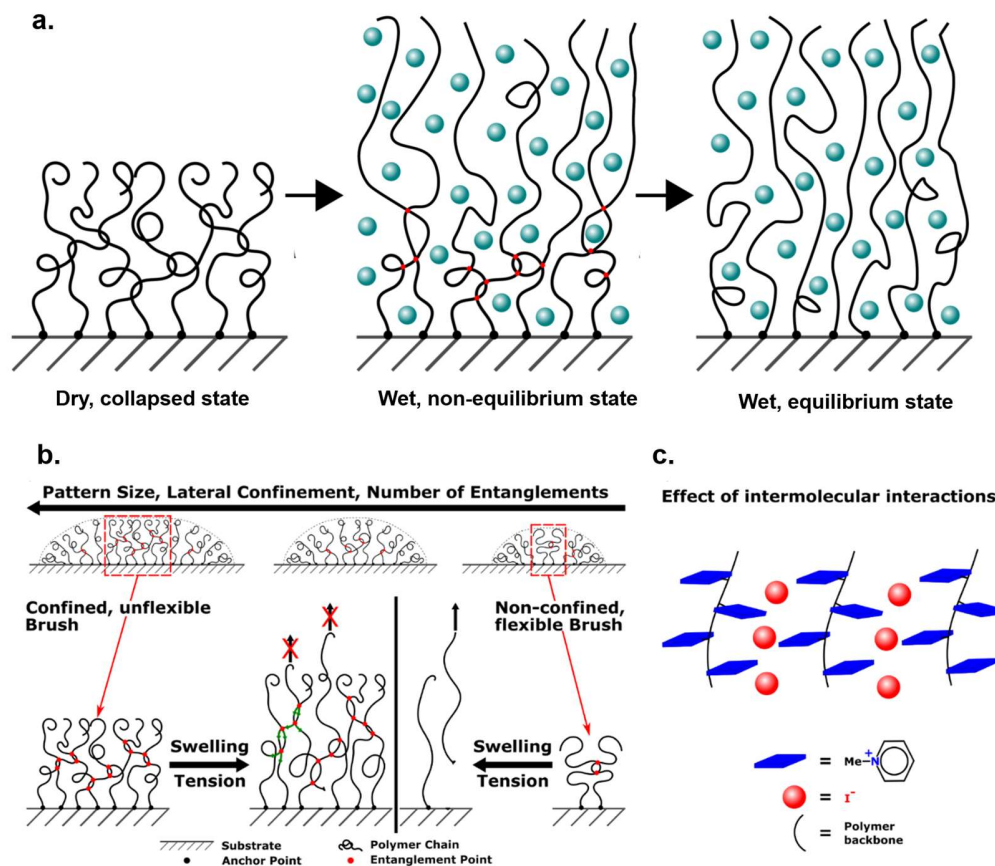


Figure 5.7: a) Sketch illustration the influence of the osmotic shock. b) Illustration depicting the number of entanglements as a function of the pattern size. No implication is made about the actual distribution of the entanglements in the film. The entanglements can distribute the pulling force on multiple polymer chains and entrap degraded polymer chains within the brush. c) Depiction of the influence of the pyridinium-iodide interactions on the intermolecular structure of the PEB chains.

smaller pattern sizes as predicted by the ‘entropic spring’ model (less lateral confinement = lower energy = more stable). Similar experiment with a second polymer brush (PtBuMA brush) shown in the supporting information exhibited the same behavior (i.e. smaller patterns are more stable).

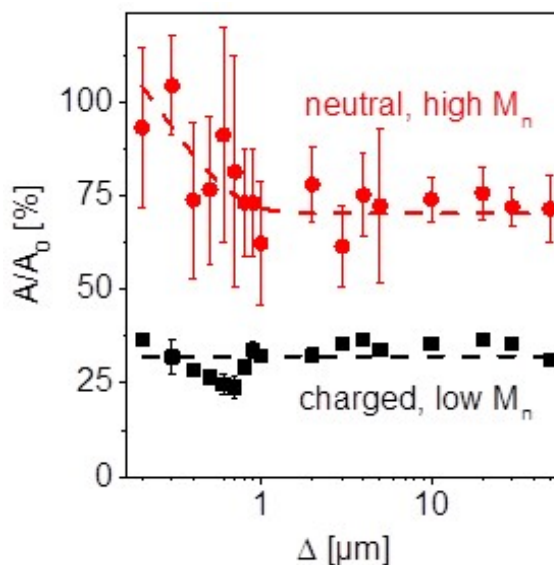


Figure 5.8: Degrafting behavior of high molecular weight, neutral PVP (RCP; $\Gamma = 0.239 \mu\text{mol}\cdot\text{m}^{-2}$; and $M_n = 560,000 \text{ g}\cdot\text{mol}^{-1}$) and low molecular weight, polyelectrolyte PMeVP (CuCRP; monofunctional silane initiator, expected $\Gamma = 1.27 \mu\text{mol}\cdot\text{m}^{-2}$; and $M_n = 73,132 \text{ g}\cdot\text{mol}^{-1}$) nanobrushes monitored using the relative dry cross section integral as a function of the pattern size. The NPBs have been exposed to good solvents at different temperatures for different periods of time: ■ (PMeVP; water; $T = 23 \text{ }^\circ\text{C}$; and $t = 3 \text{ h}$); ● (PVP; dry DMF; $T = 100 \text{ }^\circ\text{C}$; and $t = 48 \text{ h}$). The dashed lines are guides to the eye.

In a second set of experiments, low molecular weight (= not/less entangled), polyelectrolyte PMeVP brushes were synthesized. As shown in Figure 5.8, the sample showed uniform degrafting trends along the different pattern sizes. The observed increased stability at smaller pattern sizes contrasts strongly to the degrafting behavior of high molecular weight PMeVP brushes (see Figure 5.5b) and demonstrates the importance of molecular weight of the tethered chains on the stability. Similar

experiments with a second low molecular weight PMeVP sample shown in the supporting information exhibits the same behavior (i.e. smaller patterns are more stable).

Conclusion

The degrafting behavior of strong (nanopatterned) polyelectrolyte PMeVP brushes is due to a complex interaction of kinetic and thermodynamic effects. From a thermodynamic point of view the stability of polymer brushes depends strongly on intrinsic polymer brush properties such as the degree of charging, molecular weight, grafting density and pattern size. Additionally, extrinsic properties, i.e. parameters due to the properties of brush environment, like solvent quality and temperature strongly influence the stability. All of these parameters work in concert to increase or decrease the extension of the polymer chains and associated tension or release the ‘entropic springs’. This guides also the way for stabilization of PEL brushes. When the charges are screened e.g. at solution with higher salt concentration the stability of the brushes can be improved by orders of magnitude and degrafting is no longer an issue.

However, not only thermodynamic, but also kinetic effects such as how the brushes are immersed into the solvent (‘osmotic shock’) and intermolecular interactions such as entanglements can play a big role. These parameters influence the way that stress is imparted into the chains and how it is concentrated in certain chain segments or distributed among them. This can lead to the counterintuitive behavior observed in nanobrushes, where tethered chains in such small structures, which are prone to less stress from a thermodynamic point of view, degraft even faster than their microbrush peers. The complexity of the combination of kinetic and thermodynamic effects make a quantitative prediction of the degrafting behavior challenging and only qualitative

statements can be made so far. The recovered knowledge for controlling the polymer brush's stability broadens the range of possibilities for brush applications as it will help in finding the optimal brush properties and experimental conditions for a desired grafting density.

REFERENCES

1. Milner, S., Polymer brushes. *Science* **1991**, *251* (4996), 905-914.
2. Advincula, R. C.; Brittain, W. J.; Caster, K. C.; Rühle, J., *Polymer brushes*. Wiley Online Library: 2004.
3. Brittain, W. J.; Minko, S., A structural definition of polymer brushes. *Journal of Polymer Science Part A: Polymer Chemistry* **2007**, *45* (16), 3505-3512.
4. Chen, W.-L.; Cordero, R.; Tran, H.; Ober, C. K., 50th Anniversary Perspective: Polymer Brushes: Novel Surfaces for Future Materials. *Macromolecules* **2017**.
5. Yang, W. J.; Neoh, K.-G.; Kang, E.-T.; Teo, S. L.-M.; Rittschof, D., Polymer brush coatings for combating marine biofouling. *Progress in Polymer Science* **2014**, *39* (5), 1017-1042.
6. Yang, W.; Zhou, F., Polymer brushes for antibiofouling and lubrication. *Biosurface and Biotribology* **2017**.
7. Bai, H.; Zhang, H.; He, Y.; Liu, J.; Zhang, B.; Wang, J., Enhanced proton conduction of chitosan membrane enabled by halloysite nanotubes bearing sulfonate polyelectrolyte brushes. *Journal of Membrane Science* **2014**, *454*, 220-232.
8. de Groot, G. W.; Santonicola, M. G.; Sugihara, K.; Zambelli, T.; Reimhult, E.; Vörös, J. n.; Vancso, G. J., Switching transport through nanopores with pH-responsive

- polymer brushes for controlled ion permeability. *ACS Applied Materials & Interfaces* **2013**, *5* (4), 1400-1407.
9. Li, Z.; Wang, H.; Song, X.; Yan, J.; Hu, H.; Yu, B., Dual-responsive polymer brushes as an electrochemical logic gate. *Journal of Electroanalytical Chemistry* **2014**, *719*, 7-13.
 10. Dobrynin, A. V.; Rubinstein, M., Theory of polyelectrolytes in solutions and at surfaces. *Progress in Polymer Science* **2005**, *30* (11), 1049-1118.
 11. Pincus, P., Colloid stabilization with grafted polyelectrolytes. *Macromolecules* **1991**, *24* (10), 2912-2919.
 12. Biesalski, M.; Rhe, J., Scaling Laws for the Swelling of Neutral and Charged Polymer Brushes in Good Solvents. *Macromolecules* **2001**, *35* (2), 499-507.
 13. Bittrich, E.; Uhlmann, P.; Eichhorn, K.-J.; Hinrichs, K.; Aulich, D.; Furchner, A., Polymer Brushes, Hydrogels, Polyelectrolyte Multilayers: Stimuli-Responsivity and Control of Protein Adsorption. In *Ellipsometry of Functional Organic Surfaces and Films*, Hinrichs, K.; Eichhorn, K.-J., Eds. Springer Berlin Heidelberg: Berlin, Heidelberg, 2014; pp 79-105.
 14. Gu, P.; Liu, X.; Tian, Y.; Zhang, L.; Huang, Y.; Su, S.; Feng, X.; Fan, Q.; Huang, W., A novel visible detection strategy for lysozyme based on gold nanoparticles and conjugated polymer brush. *Sensors and Actuators B: chemical* **2017**, *246*, 78-84.
 15. Xue, C.; Cai, F.; Liu, H., Ultrasensitive Fluorescent Responses of Water-Soluble, Zwitterionic, Boronic Acid-Bearing, Regioregular Head-to-Tail

Polythiophene to Biological Species. *Chemistry-a European Journal* **2008**, *14* (5), 1648-1653.

16. Zou, H.; Wang, Z.; Feng, M., Nanocarriers with tunable surface properties to unblock bottlenecks in systemic drug and gene delivery. *Journal of Controlled Release* **2015**, *214*, 121-133.

17. Surman, F.; Riedel, T.; Bruns, M.; Kostina, N. Y.; Sedláková, Z.; Rodriguez-Emmenegger, C., Polymer Brushes Interfacing Blood as a Route Toward High Performance Blood Contacting Devices. *Macromolecular bioscience* **2015**, *15* (5), 636-646.

18. Welch, M.; Rastogi, A.; Ober, C., Polymer brushes for electrochemical biosensors. *Soft Matter* **2011**, *7* (2), 297-302.

19. Divandari, M.; Dehghani, E. S.; Spencer, N. D.; Ramakrishna, S. N.; Benetti, E. M., Understanding the effect of hydrophobic protecting blocks on the stability and biopassivity of polymer brushes in aqueous environments: A Tiramisu for cell-culture applications. *Polymer* **2016**, *98*, 470-480.

20. Tan, K. Y.; Lin, H.; Ramstedt, M.; Watt, F. M.; Huck, W. T.; Gautrot, J. E., Decoupling geometrical and chemical cues directing epidermal stem cell fate on polymer brush-based cell micro-patterns. *Integrative Biology* **2013**, *5* (6), 899-910.

21. Buzzacchera, I.; Vorobii, M.; Kostina, N. Y.; de los Santos Pereira, A.; Riedel, T.; Bruns, M.; Ogieglo, W.; Möller, M.; Wilson, C. J.; Rodriguez-Emmenegger, C., Polymer Brush-Functionalized Chitosan Hydrogels as Antifouling Implant Coatings. *Biomacromolecules* **2017**, *18* (6), 1983-1992.

22. Tugulu, S.; Klok, H.-A., Stability and nonfouling properties of poly (poly (ethylene glycol) methacrylate) brushes under cell culture conditions. *Biomacromolecules* **2008**, *9* (3), 906-912.
23. Zhu, Y.; Lv, B. e.; Zhang, P.; Ma, H., Swelling induced Au–S bond breakage is determined by the molecular composition of surface tethered copolymers—carboxylated poly (OEGMA-r-HEMA). *Chemical Communications* **2011**, *47* (35), 9855-9857.
24. Zhang, Y.; Lv, B. e.; Lu, Z.; He, J. a.; Zhang, S.; Chen, H.; Ma, H., Predicting Au–S bond breakage from the swelling behavior of surface tethered polyelectrolytes. *Soft Matter* **2011**, *7* (24), 11496-11500.
25. Paripovic, D.; Klok, H. A., Improving the Stability in Aqueous Media of Polymer Brushes Grafted from Silicon Oxide Substrates by Surface-Initiated Atom Transfer Radical Polymerization. *Macromolecular Chemistry and Physics* **2011**, *212* (9), 950-958.
26. Borozenko, O.; Godin, R.; Lau, K. L.; Mah, W.; Cosa, G.; Skene, W. G.; Giasson, S., Monitoring in Real-Time the Degrafting of Covalently Attached Fluorescent Polymer Brushes Grafted to Silica Substrates—Effects of pH and Salt. *Macromolecules* **2011**, *44* (20), 8177-8184.
27. Cimen, D.; Kursun, T. T.; Caykara, T., Synthesis and stability of BODIPY-based fluorescent polymer brushes at different pHs. *Journal of Polymer Science Part A: Polymer Chemistry* **2014**, *52* (24), 3586-3596.
28. Alswieleh, A. M.; Cheng, N.; Canton, I.; Ustbas, B.; Xue, X.; Ladmiral, V.; Xia, S.; Ducker, R. E.; El Zubir, O.; Cartron, M. L., Zwitterionic Poly (amino acid

- methacrylate) Brushes. *Journal of the American Chemical Society* **2014**, *136* (26), 9404-9413.
29. Melzak, K. A.; Yu, K.; Bo, D.; Kizhakkedathu, J. N.; Toca-Herrera, J. L., Chain length and grafting density dependent enhancement in the hydrolysis of ester-linked polymer brushes. *Langmuir* **2015**, *31* (23), 6463-6470.
30. Galvin, C. J.; Bain, E. D.; Henke, A.; Genzer, J., Instability of surface-grafted weak polyacid brushes on flat substrates. *Macromolecules* **2015**, *48* (16), 5677-5687.
31. Ataman, N. C.; Klok, H.-A., Degrafting of Poly (poly (ethylene glycol) methacrylate) Brushes from Planar and Spherical Silicon Substrates. *Macromolecules* **2016**, *49* (23), 9035-9047.
32. Chen, W.-L.; Menzel, M.; Watanabe, T.; Prucker, O.; Rühle, J.; Ober, C. K., Reduced lateral confinement and its effect on stability in patterned strong polyelectrolyte brushes. *Langmuir* **2017**, *33* (13), 3296-3303.
33. Klok, H.-A.; Genzer, J., Expanding the polymer mechanochemistry toolbox through surface-initiated polymerization. ACS Publications: 2015.
34. Quintana, R.; Gosa, M.; Jańczewski, D.; Kutnyanszky, E.; Vancso, G. J., Enhanced stability of low fouling zwitterionic polymer brushes in seawater with diblock architecture. *Langmuir* **2013**, *29* (34), 10859-10867.
35. Dunlop, I. E.; Thomas, R. K.; Titmus, S.; Osborne, V.; Edmondson, S.; Huck, W. T.; Klein, J., Structure and collapse of a surface-grown strong polyelectrolyte brush on sapphire. *Langmuir* **2012**, *28* (6), 3187-3193.
36. Tran, Y.; Auroy, P.; Lee, L., Determination of the structure of polyelectrolyte brushes. *Macromolecules* **1999**, *32* (26), 8952-8964.

37. Biesalski, M.; Johannsmann, D.; Rhe, J., Synthesis and swelling behavior of a weak polyacid brush. *The Journal of Chemical Physics* **2002**, *117* (10), 4988-4994.
38. Zhao, B.; Brittain, W. J., Polymer brushes: surface-immobilized macromolecules. *Progress in Polymer Science* **2000**, *25* (5), 677-710.
39. Atkins, P.; De Paula, J., *Elements of physical chemistry*. Oxford University Press, USA: 2013.
40. Schmidt, S. W.; Kersch, A.; Beyer, M. K.; Clausen-Schaumann, H., Mechanically activated rupture of single covalent bonds: evidence of force induced bond hydrolysis. *Physical Chemistry Chemical Physics* **2011**, *13* (13), 5994-5999.
41. Patra, M.; Linse, P., Simulation of Grafted Polymers on Nanopatterned Surfaces. *Nano Letters* **2006**, *6* (1), 133-137.
42. Lee, W.-K.; Patra, M.; Linse, P.; Zauscher, S., Scaling Behavior of Nanopatterned Polymer Brushes. *Small* **2007**, *3* (1), 63-66.
43. Jonas, A. M.; Hu, Z.; Glinel, K.; Huck, W. T., Chain entropy and wetting energy control the shape of nanopatterned polymer brushes. *Macromolecules* **2008**, *41* (19), 6859-6863.
44. Sheiko, S. S.; Panyukov, S.; Rubinstein, M., Bond Tension in Tethered Macromolecules. *Macromolecules* **2011**, *44* (11), 4520-4529.
45. Panyukov, S.; Zhulina, E. B.; Sheiko, S. S.; Randall, G. C.; Brock, J.; Rubinstein, M., Tension amplification in molecular brushes in solutions and on substrates. *The Journal of Physical Chemistry B* **2009**, *113* (12), 3750-3768.

46. Ruths, M.; Johannsmann, D.; Rhe, J.; Knoll, W., Repulsive forces and relaxation on compression of entangled, polydisperse polystyrene brushes. *Macromolecules* **2000**, *33* (10), 3860-3870.
47. Prucker, O.; Rhe, J., Synthesis of Poly(styrene) Monolayers Attached to High Surface Area Silica Gels through Self-Assembled Monolayers of Azo Initiators. *Macromolecules* **1998**, *31* (3), 592-601.
48. Biesalski, M.; Rhe, J., Preparation and characterization of a polyelectrolyte monolayer covalently attached to a planar solid surface. *Macromolecules* **1999**, *32* (7), 2309-2316.
49. Chen, W.-L.; Menzel, M.; Prucker, O.; Wang, E.; Ober, C. K.; Rhe, J., Morphology of Nanostructured Polymer Brushes Dependent on Production and Treatment. *Macromolecules* **2017**, *50* (12), 4715-4724.
50. Biesalski, M.; Rhe, J., Swelling of a Polyelectrolyte Brush in Humid Air. *Langmuir* **1999**, *16* (4), 1943-1950.
51. Dong, R.; Krishnan, S.; Baird, B. A.; Lindau, M.; Ober, C. K., Patterned biofunctional poly (acrylic acid) brushes on silicon surfaces. *Biomacromolecules* **2007**, *8* (10), 3082-3092.
52. Prucker, O.; Rhe, J., Mechanism of Radical Chain Polymerizations Initiated by Azo Compounds Covalently Bound to the Surface of Spherical Particles. *Macromolecules* **1998**, *31* (3), 602-613.
53. Konradi, R.; Rhe, J., Interaction of Poly(methacrylic acid) Brushes with Metal Ions: An Infrared Investigation. *Macromolecules* **2004**, *37* (18), 6954-6961.

54. Simancas, K., *Entropic Death of Polyelectrolyte Brushes: Chain Stretching, Bond Scission and Surfactant Complexation*. Der Andere Verlag: 2011.
55. Israels, R.; Leermakers, F.; Fleer, G.; Zhulina, E., Charged polymeric brushes: structure and scaling relations. *Macromolecules* **1994**, *27* (12), 3249-3261.
56. Biesalski, M.; Johannsmann, D.; Rhe, J., Electrolyte-induced collapse of a polyelectrolyte brush. *The Journal of Chemical Physics* **2004**, *120* (18), 8807-8814.
57. Fuoss, R. M.; Strauss, U. P., Polyelectrolytes. II. Poly-4-vinylpyridonium chloride and poly-4-vinyl-N-n-butylpyridonium bromide. *Journal of Polymer Science* **1948**, *3* (2), 246-263.
58. Strauss, U. P.; Gershfeld, N. L.; Spiera, H., Charge Reversal of Cationic Poly-4-vinylpyridine Derivatives in KBr Solutions I. *Journal of the American Chemical Society* **1954**, *76* (23), 5909-5911.
59. Beer, M.; Schmidt, M.; Muthukumar, M., The electrostatic expansion of linear polyelectrolytes: Effects of gegenions, co-ions, and hydrophobicity. *Macromolecules* **1997**, *30* (26), 8375-8385.
60. Arrhenius, S., ber die Reaktionsgeschwindigkeit bei der Inversion von Rohrzucker durch Suren. *Zeitschrift fr physikalische Chemie* **1889**, *4* (1), 226-248.
61. Bershtein, V.; Egorova, L.; Solov'ev, V., Disintegration of polymers by a hydrolytic mechanism. *Mechanics of Composite Materials* **1977**, *13* (5), 715-721.
62. Schmidt, S. W.; Pill, M. F.; Kersch, A.; Clausen-Schaumann, H.; Beyer, M. K., Mechanically induced silyl ester cleavage under acidic conditions investigated by AFM-based single-molecule force spectroscopy in the force-ramp mode. *Faraday discussions* **2014**, *170*, 357-367.

63. Jones, R.; Richards, R., *Polymers at surfaces and interfaces*. Cambridge University Press, Cambridge: 1999.
64. Hoy, R. S.; Grest, G. S., Entanglements of an end-grafted polymer brush in a polymeric matrix. *Macromolecules* **2007**, *40* (23), 8389-8395.
65. Koltzenburg, S.; Maskos, M.; Nuyken, O.; Mülhaupt, R., *Polymere: Synthese, Eigenschaften und Anwendungen*. Springer: 2014.
66. Luo, Z.; Wang, X.; Zhang, G., Ion-specific effect on dynamics of polyelectrolyte chains. *Physical Chemistry Chemical Physics* **2012**, *14* (19), 6812-6816.
67. Das, A.; Ghosh, S., Supramolecular Assemblies by Charge-Transfer Interactions between Donor and Acceptor Chromophores. *Angewandte Chemie International Edition* **2014**, *53* (8), 2038-2054.

CHAPTER 6

Toward a platform for comprehensive polymer brush characterization with neutron and laser scattering

Abstract

For further characterization of polymer brushes by neutron and laser scattering, two specific platforms were fabricated with both silicon and silicon dioxide. The platforms allow the anchoring of the polymer brushes on the sidewall of the trenches only which makes the scattering signals responsive to the change of the polymer brush morphologies. Such methods could increase the sensitivity of the characterization and make probing of more complicated structures possible. Poly(2-(dimethylamino)ethyl methacrylate) brushes were synthesized by atom transfer radical polymerization on the grating and the grafting densities were measured by cleaving them off directly from the surface. The polymer brushes grown on the sidewall have gradient profiles with a maximum thickness at the bottom of the grating which is due to the lack of confinement on the top. These platforms lay down the foundation for the future characterization.

Introduction

Polymer brushes have already demonstrated their application in many fields and their structures have been studied widely in different conditions as described in Chapter 1. However, studies focusing on the more complicated structures of polymer brushes are still in need. There have been already several examples in nature with complex brush structures. The local functionality of surface-attached biomolecules is determined by their morphologies. For example, proteoglycan is a brush composed of

a protein backbone with multiple polysaccharide sidechains. Its presence on the cellular surface plays an important role in cell migration, synaptogenesis, and structural plasticity.¹ Another example has been shown in the work of Paszek *et al.* that cell matrix-attached glycoproteins would influence transmembrane receptor spatial organization and function.² The mechanical deformation will promote local kinetic trap of integrin at the free area between glycoproteins. The local functionality of these surface-attached biomolecules is determined by their morphologies. One of the common characteristics in these examples are that the polymers are equipped with long and functional side chains and such polymer brushes are called molecular brushes (Bottle Brushes).

Molecular brushes can provide additional functional control over the original polymer brush architecture by the addition of the graft chains. By proper design, they could have more sophisticated 3-dimensional ordered structures which is especially important in material design nowadays. The structures of the brushes are determined by both the backbone and sidechain and this adds versatility to brush structures. Because of that, free molecular brushes have already been used by researchers in different fields. For instance, Wooley *et al.* synthesized the molecular brushes with dense side chains as E-beam resists. With the help of fluorinated end chains and solvent annealing, molecular brushes could have ~75% vertical stretching and shown well-defined 30 nm isolated line patterns.³⁻⁵ Other studies of self-assembly of the free molecular brushes also revealed various self-assembled morphologies⁶. Surface-grafted molecular brushes have also found their application in anti-fouling⁷⁻¹⁰, lubrication¹¹ and photolithography,^{3,12,13} since the orientation of the chains in

molecular brushes are confined both vertically and horizontally due to their neighboring chains. We believe that with the proper control molecular brushes could be a material with sophisticated 3D order that there with more potential applications to be discovered. Because there are few studies that focus on the fundamental properties of surface-tethered brushes,¹⁴ it is important for us to first develop a better way to characterize these surface-attached molecular brushes before further studies.

It is critical to characterize the polymer brushes in wet state since the tension applied on them is amplified and thus forms more ordered structures. As shown by Ryan *et al.*, laser scattering can provide important information for the change of the polymer morphology at the macroscopic scale and they could be used simultaneously with x-ray scattering to obtain nanoscopic information.¹⁵ Considering that the swelling degree of PEL brushes could be > 300 nm (similar to visible wavelengths), laser scattering could be a valuable technique for non-destructive, liquid phase characterization. On the other hand, neutron scattering is another technique that's useful for the characterization of nanostructures due to its non-damaging manner and small wavelength comparable with interatomic spacings.¹⁶ Recently it has been shown by Zhernenkov *et al.* that by using silicon diffraction gratings as substrates, the spin-coated poly(*N*-isopropylacrylamide) (PNIPAM) demonstrated effective alignment for the cultured fibroblast cells and such alignment could be controlled by changing the temperature.¹⁷ The characterization of the PNIPAM on the grating with neutron scattering reveal the potential of this method to reconstruct 3D profiles of the measured materials by combination of the data from specular and off-specular scattering. This inspired us to develop a platform, which has polymer brushes

anchored on the sidewall of the grating only. When having such platforms in the wet medium, the morphological change of the polymer brushes then controls the opening of the grating which could subsequently be captured by laser and neutron scattering. By using the grating, the response of the polymer brushes would be amplified and allow us to reveal more details in polymer brush structures.

Experimental Section

Materials 0.5 mm thick 100 mm both side polished quartz wafers (silicon dioxide) were purchased from Mark Optics Inc. 0.7 mm thick, 100 mm both side polished (100) silicon wafers were purchased from El-Cat Inc. Allylamine, anhydrous toluene, α -bromo-isobutyryl bromide (BIBB), chlorodimethylsilane, copper bromide(CuBr), dimethyl sulfoxide (DMSO), inhibitor remover (for removing hydroquinone and monomethyl ether hydroquinone), magnesium sulfate, (2-dimethylamino)ethyl methacrylate (DMAEMA), Pt on activated carbon (10 wt %), triethylamine, bipyridine, 2,2'-bipyridine, pyridine, sodium chloride, sodium phosphate monobasic monohydrate, were purchased from Sigma Aldrich and used without further purification unless stated otherwise. All the other solvents, chemicals were purchased from Fisher Scientific.

Synthesis of the PDMAEMA brushes.

The initiator synthesis and the deposition process on the silicon wafer were the same as described in chapter 3 (mono-functional silane initiator). Glass fibers were first cleaned in SC-1 solution (H_2O : NH_4OH 30% by weight: H_2O_2 30% = 5:1:1 (v/v)) at 70 °C for 15 min. After cleaning fibers were washed with copious water, acetone, isopropanol and then baked in oven at 110 °C for 2 hour to dehydrate. Subsequently, fibers were subject to plasma cleaning for 7 min and put into the same initiator

deposition solution in the Erlenmeyer flask as used for wafer in the glovebox for overnight. Fibers were then taken out from the Erlenmeyer flask and washed with toluene and methanol before nitrogen blow dry.

PDMAEMA monomer solution was first passed through inhibitor remover column to remove monomethyl ether hydroquinone. Then monomer (10mL, 68.2 mmol) was mixed with DMSO (10mL, 116 mmol) and injected in closed Schlenk flask with Argon bubbling for more than 30 minutes. CuBr (93 mg, 0.65 mmol), 2,2'-bipyridine (207 mg, 1.33 mmol) were taken in another 25 mL Schlenk flask equipped with a magnetic stir bar. Another Schlenk flask was equipped with initiator deposited substrates. The air in the both flask was evacuated and replaced with argon three times. The solvent mixture was then cannulated into the flask containing the ligand and copper salts. The reaction mixture was stirred at room temperature more than 30 minutes to ensure the dissolution of the monomer and the copper-ligand complex in the solvent. This solution was then transferred into the Schlenk flask containing the initiator-deposited substrates. Polymerization was carried out for a set reaction time at 60 °C. After polymerization, the substrates were removed from the flask and washed with ethanol and dried under a stream of nitrogen.

Measurement of the grafting density of the PDMAEMA brushes

The TBAF degrafting process is modified from published procedure.¹⁸ Wafer pieces/fibers with PDMAEMA brushes were put in Teflon dish containing solution of 0.04 M TBAF in THF. The dishes were then heated at 55 °C using a hot plate for 4 days. The solution was then filtered through 0.2 µm polytetrafluoroethylene (PTFE) filters and rotary evaporated to dry. It was then re-dissolved in dimethyl formamide (DMF) as a gel permeation chromatography (GPC) sample.

For HF degrafting, the PDMAEMA brushes were etched by THF diluted HF (25 %). After 8 h of immersion the wafers were removed from the HF bath which was then left in a fume hood to dry by evaporation. Free PDMAEMA was collected with ethanol and re-dissolved in DMF as GPC sample after vacuum drying.

The collected PDMAEMA was then subjected to DMF-solvent GPC analysis for molecular weight analysis and the resulting information was used to calculate the grafting density for the PDMAEMA brushes.

Fabrication of the transmissive platform

Silicon dioxide wafer was cleaned with hot piranha before deposition of each layers. Three thin films: Cr 5 nm/SiO₂ 250 nm/Cr 5 nm were deposited on it in the way described below:

Cr deposition was conducted in AJA Flagship system at 3 mTorr with 150 W DC source power and the substrate was biased with 30 W RF plasma and 0 reflected power. Deposition rate was 4 nm /min.

Plasma-enhanced chemical vapor deposition of SiO₂ was conducted in Oxford Plasmalab system 100 at 350 °C and 1800 mTorr. SiH₄=20 sccm, N₂O=2500 sccm, High frequency power=140 W. Resulting stress: - 162 Mpa compressive.

Bottom anti-reflective coating (BARC), DUV 42-P was then spin-coated and subject to post-application bake (PAB) at 205 °C for 1 min. UV210 was then also spin-coated and PAB at 135 °C for 1 min. Photolithography was conducted with ASML 300C DUV stepper to form pattern. Reactive ion etching (RIE) was then conducted with Oxford PlasmaLab 80+ RIE System to transfer pattern into BARC. Subsequently, Cr etch was conducted in Trion Minilock III etcher to remove top Cr in the exposed trenches. Patterns were then transferred into SiO₂ by RIE in Oxford Plasmalab system

100 etcher. The residual photolithographic materials were then removed in Gasonics Aura 1000 to have the final platform.

Fabrication of the reflective platform

A silicon wafer was cleaned with hot piranha and the photolithography was conducted as used for the fabrication of the transmissive platform. RIE was then conducted on Unaxis SLR 770 to transfer pattern into the silicon. Residual photolithographic materials were then removed by RIE in Oxford PlasmaLab 80+ RIE System. SiO₂ was then conformally deposited with Oxford ALD FlexAL at 110 °C, 80 mTorr with the help of plasma to have a required sacrificial layer (used trisdimethylaminosilane, rate = 0.827 nm/cycle). SiO₂ on top and bottom of the trenches were then removed by RIE with CHF₃/O₂ gas mixture in Oxford PlasmaLab 80+ RIE System and the substrates were then cleaned with O₂ RIE in the same system. Deposition of the Cr was conducted on CVC SC4500 E-gun Evaporation system with deposition rate ~ 0.5 nm/sec probed by QCM. Temperature of the substrate was monitored, and it was always below 25 °C during the process at 3x10⁻⁶ torr. Lift-off was conducted by immersing samples in the HF or the buffered oxide etch for a given time. The samples were then washed with copious of water to remove residual etchant. After drying in 110 °C oven for 10 minutes, samples were then subject to plasma clean in a Harrick Plasma Cleaner for 7 minutes before being put into the solution for initiator deposition. The following cleaning and polymer brushes synthesis procedures were the same as previously described.

Etching conditions:

Oxford PlasmaLab 80+:

For etch of BARC: Ar= 42.5 sccm, O₂=7.5 sccm, 40 W, 15 mTorr.

For etch of SiO₂: CHF₃= 50 sccm, O₂=2 sccm, 240 W, 40 mTorr.

For cleaning: O₂=50 sccm, 150 W, 60 mTorr.

Oxford Plasmalab system 100: CH₂F₂=20 sccm, He=80 sccm, Inductively coupled plasma power(ICP): 3000 W, RIE power=60 W, 40 mTorr, 10 °C.

Unaxis SLR 770:

Plasma lighting: C₄F₈=2 sccm, SF₆=2 sccm, Ar=40 sccm, O₂=10 sccm, ICP=700 W, RIE power=35 W, 8 mTorr, 5 sec.

Etch: C₄F₈=56 sccm, SF₆=24 sccm, Ar=40 sccm, O₂=10 sccm, ICP=700 W, RIE power=12 W, 8 mTorr.

Trion Minilock III: Ar=3 sccm, Cl₂=21 sccm, O₂=9 sccm. ICP=300 W, RIE power=50 W, 20 °C, 30 mTorr.

Characterization:

Scanning electron microscope (SEM) pictures were taken at ZEISS ultra/supra SEM. Thickness of the PDMAEMA brushes were measure with Woollam VASE spectroscopic ellipsometer with Cauchy model. Gel permeation chromatography was conducted in water GPC with Waters 410 differential refractive index detector while DMF was used as eluent.

Results and discussion

Synthesis and grafting density determination of PDMAEMA brushes

Our first subject polymer is poly(2-(dimethylamino)ethyl methacrylate) (PDMAEMA) whose morphology could be tuned by changing the pH value in the medium and addition of different counterions.^{19,20} To have a systematic comparison, the PDMAEMA brushes must have controlled thickness and grafting density. Atom transfer radical polymerization (ATRP) is applied to synthesize the PDMAEMA brushes. With the control of the polymerization time, PDMAEMA brushes up to ~120

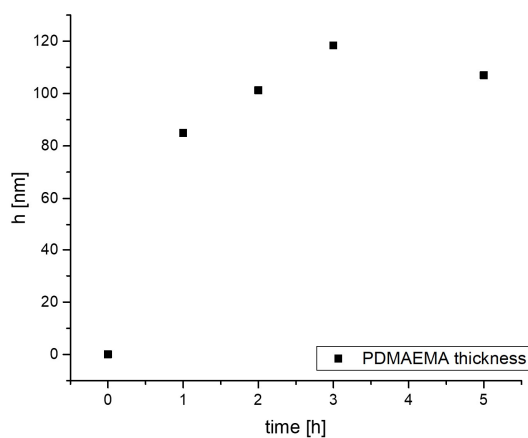


Figure 6.1. PDMAEMA brushes dry thickness as function of polymerization time.

nm could be grown on the silicon wafer. As shown in Figure 6.1, the polymerization reaction reached its end at ~ 2-3 hours. Further polymerization time cannot increase the thickness of the polymer brushes. The grafting density of PDMAEMA brushes were measured by first growing brushes on wafer and glass fiber²¹ in order to have enough of polymer for the GPC analysis. Since it has already been proven in theory that the kinetics of the polymerization are different between the bulk and surface-initiated conditions, measurement of the polymer directly cleaved from the polymer brushes is necessary to measure its molecular weight and grafting density.²² Here we would like to first test if the glass fiber with large diameter (13 μm), which has been proven to have similar dry polymer brush thickness to the one grown on the wafer, would also have the same grafting density.²¹

In the first few trials, tetrabutylammonium fluoride (TBAF) was used to degraft the PDMAEMA brushes for it is a safer compound to handle compared to HF.¹⁸ Following the published recipe, PDMAEMA brushes were put in 0.05 M TBAF solution in THF at 55°C.²² However, even after 4 days there was still residual brush present on the silicon wafer as confirmed by the naked eye. In the following

concentrating step, the THF was removed from the solution through use of a rotavap down to 1 ml to have enough polymer mass. Nevertheless, the solution became too viscous and the GPC measurement did not show any signal. It is possible that the viscous solution containing PDMAEMA/TBAF had already been filtered out in the filter of GPC before passing through the column or they aggregated somewhere in the column. One or the other, it showed that TBAF is not a proper compound for PDMAEMA lift-off. PDMAEMA brushes were then cleaved by HF immersion and the polymers were successfully collected by ethanol after HF evaporation. The GPC measurement showed clear signal of the polymer in IR detector. The grafting density is calculated with equation 5.1 by assuming that the polymer brushes have the same density as in the melt state. Two sets of samples polymerized with different times (2/3 hours) were made. Their thickness, grafting density and dispersity are presented in table 6.1. The grafting density, thickness and Mw/Mn all increased with increasing polymerization time. However, the grafting density and Mw/Mn are quite different between the polymers grown on fiber and wafer. The dispersities are greater on polymers from the wafer than from fiber, which tells that even though the fiber has a larger diameter compared to the thickness of the brushes (10^3 times), they could still feel the additional free space and better achieve equilibrium on fibers compared to on wafer.²² It proved the necessity to use exactly the same substrate and HF to measure the grafting density of the PDMAEMA brushes.

Polymerization time	Dry Thickness	Fiber	Wafer
2 hours	94.563 nm	0.920734/1.02	0.693064/1.08
3 hours	122.518 nm	1.356491/1.043	1.422949/1.22

Table 6.1. Measured parameters of two different samples with PDMAEMA brushes. Values reported are grating density (chains/ nm^2) / PDI.

Fabrication of transmission platform

To fabricate the platform which allows the laser to penetrate and result in transmissive scattering, the substrate we chose was fused silica wafer. The fabrication process is shown in Figure 6.2. The desired pattern sizes are 300-400 nm 1:1 line:space with depth 250 - 600 nm. With the presence of the thin chromium film on top and bottom of the grating, the chemical orthogonality is created between sidewall and flat area which has no available functional group for ATRP silane initiator

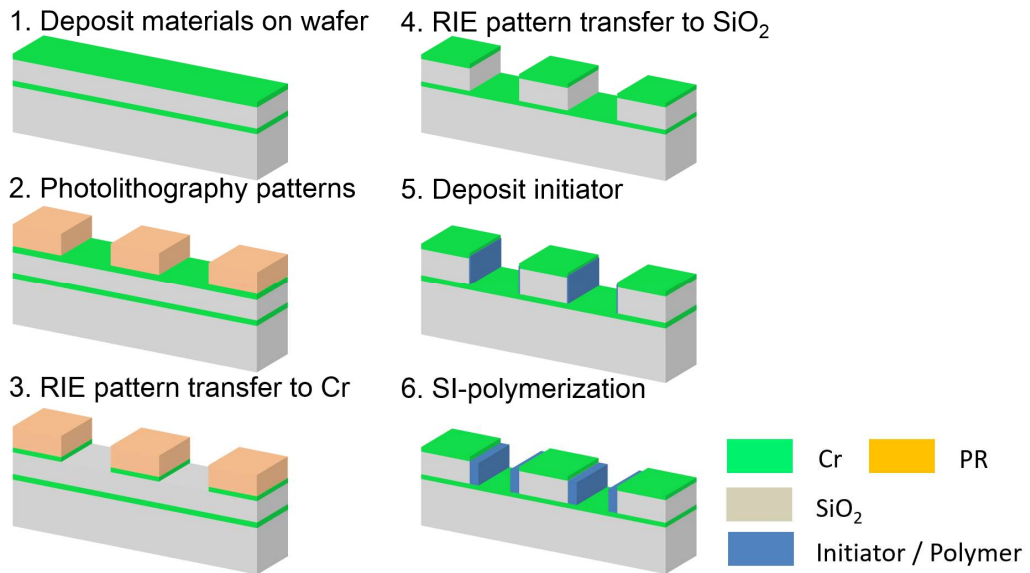


Figure 6.2. fabrication process of the transmission platform.

anchoring. The Cr film thickness is chosen to be 5 nm to keep it transparent. There were 3 important problems that had been solved before successful fabrication of the desired platform with photolithography.

- 1) Particles/contamination on the surface
- 2) Thin film stress
- 3) Stitch lines

Due to the high pattern density of the design, the problem 1) could cause light projection out of focus plane even if the particles are of nm level. Problem 2) leads to

the bending of the substrate and also makes proper focusing difficult. To solve these two problems, we first reduced the numerical aperture in the photolithography tool (ASML 300C DUV stepper) which then increased the tolerance of proper focusing. Second, between each film deposition process the substrate is cleaned thoroughly with hot piranha and the backside is cleaned also before the photolithography process. Thin film stress on the final layer combination is balanced by proper control of the chromium residual stress with plasma bias during the sputtering deposition which in the end makes substrate flat. Problem 3) on the other hand is part of the nature of the projection photolithography and it is eliminated by exposing patterns 4 times with constant offset between each other. By doing so the stich line becomes distributed within the pattern and cannot be observed again with bare eyes (also not observed under AFM/ EM). Pictures of different defected platforms and final improved one are shown in Figure 6.3. The diffraction grating-induced color change on the surface is clearly observed. A green laser pen (wavelength, $\lambda \sim 532$ nm) was then used to test if the presence of the chromium interrupts the pattern of the diffraction. The optical setting and diffraction result are shown in Figure 6.4. The aperture was set so the light focused on single spot. In theory, the diffraction grating has the following equation:

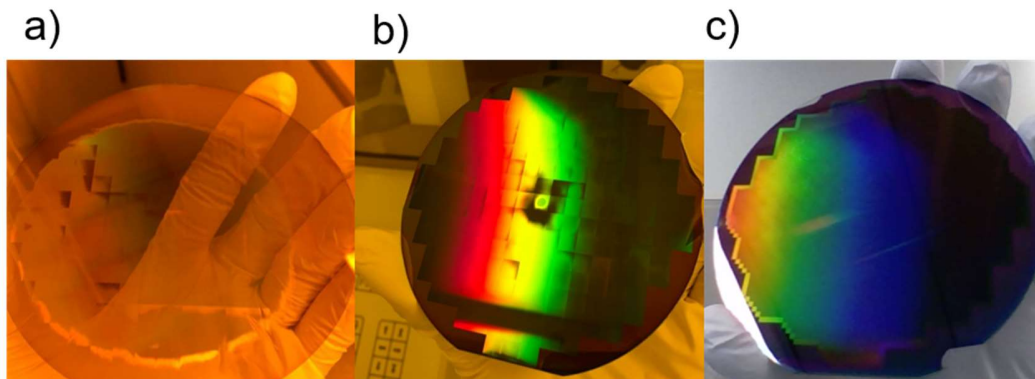


Figure 6.3. Pictures of the platforms. a) platform with substrate bending, only part of the wafer was exposure properly. b) platform with particles and stitch line. c) platform with all improving process conducted.

$$n\lambda = d\sin\theta \quad (6.1)$$

Here n is the integral number (1,2,....) which defines the order of diffracted light. d is the distance between the slit on the grating. θ , angle of emergence is the angle between transmissive light and diffracted light. For the grating used here ($d = 600$ nm), the first order diffracted lights have $\theta = 62.46^\circ$ and the higher order lights could not be resolved. This is observed that after passing through the platform, the laser was diffracted into only 3 beams on the blocking paper. This showed that a thin, transparent Cr layer on the surface does not interrupt the formation of the clear diffraction pattern and this platform could be used for subsequent polymer brush characterization.

Fabrication of reflective platform.

Neutron scattering provides a way to characterize the materials in a non-destructive manner and different rules are needed to be followed to have better characterization results. Since the characterization will be conducted in liquid, the scattering from the

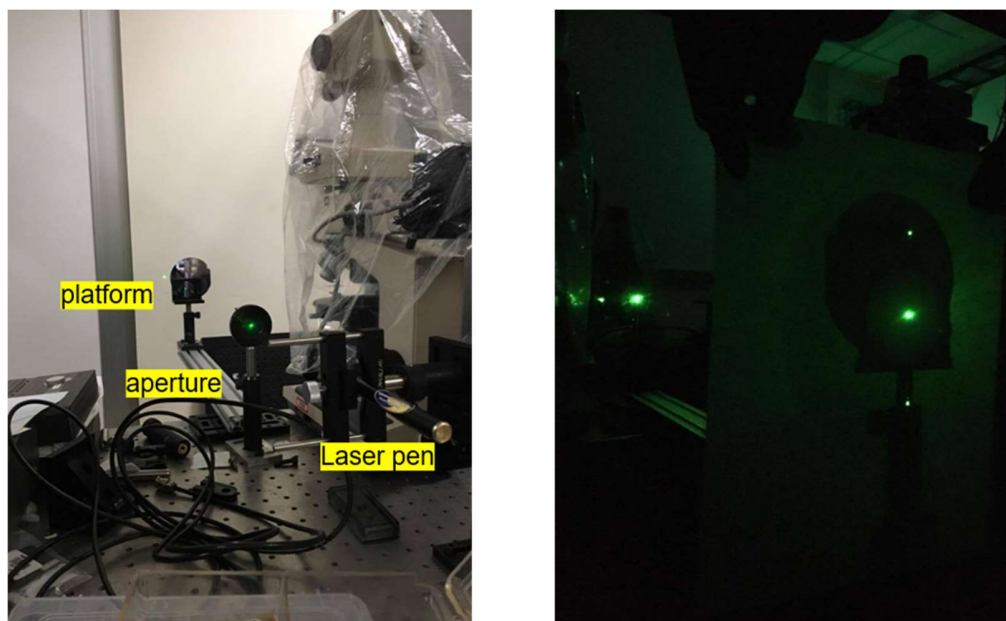


Figure 6.4. Optical characterization setup and the resulting diffraction signals.

back of the platform is preferred since it can reduce the interruption from liquid to a minimum by both reducing the number of interfaces and incoherent scattering. The substrate chosen for the platform is therefore of the utmost importance since it occupies a big fraction in the path of the neutron beam. Silicon is then chosen since it has a single crystalline structure in commercially available wafers and good scattering interactions with neutrons. These properties make it a good substrate for detection because it is almost transparent to neutron beams. The values of the neutron scattering related parameters of the substrates are shown in table 6.2. Silicon dioxide has higher noise from both higher incoherent scattering cross-section and grain boundaries in polycrystalline and therefore is not an ideal material for neutron scattering. When mixing the pure and deuterated water, the SLD could be tuned to any value between 7.66 to -0.561. When SLD of the medium is tuned to the value of silicon (so called ‘contrast match’), it could highlight the material with different SLD in the neutron measurement and provide more detail information in molecular level.²³ It is expected

that the structure of the different components of the polymer brushes could be highlighted by using proper SLD with medium.

	Density (g/cm³)	SLD (10⁻⁶/Å²)	Incoherent scattering cross section (1/cm)
Si	2.33	2.072	0.00019
SiO₂	2.2	3.475	0.005
Cr	7.19	3.027	0.152
H₂O	1	-0.561	5.621
D₂O	1.33	7.66	0.166
PDMAEMA	1.318	1.3637	5.4571

Table 6.2. Values for neutron scattering-related parameters of the substrates. SLD: scattering length density.

To have single crystalline Si grating, Si could not be post-deposited on the wafer surface like the process in Figure 6.2. A top-down process had to be developed to fabricate the platform. On the other hand, since there is no method to perfectly deposit thin films on top and bottom of the trenches, a sacrificial layer based on silicon dioxide is needed on the sidewall of the trenches to make sure the sidewalls are free of any residual chromium. The developed process is shown in figure 6.5. Atomic layer deposition(ALD) technique is selected for its layer-by-layer depositing mechanism allowing it to create precise, conformal layer on the grating.²⁴ After deposition of thin silicon dioxide on the grating, the reactive ion etching process (RIE) is selected to remove only the top and bottom materials to achieve selectivity between sidewall and flat surface on the grating. After depositing thin chromium layers, the lift-off process

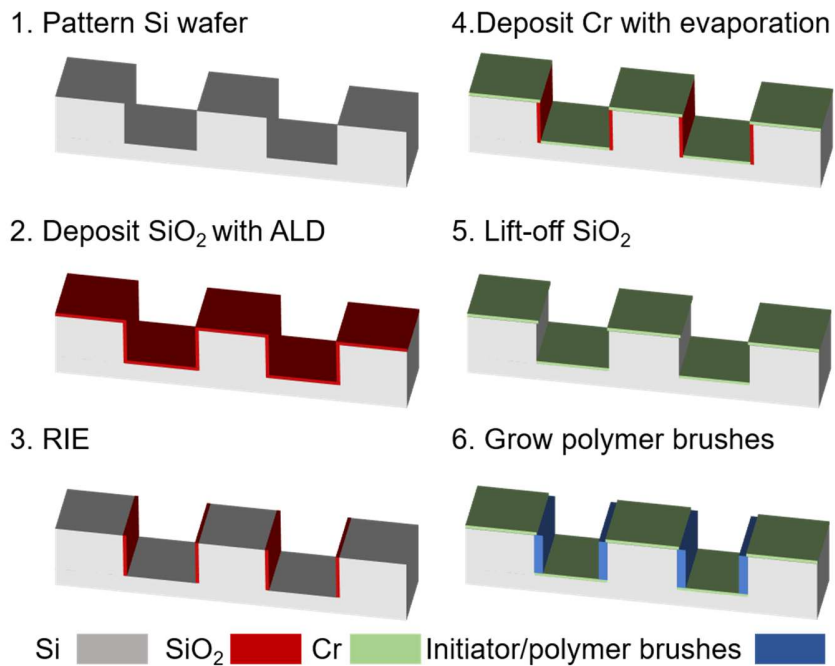
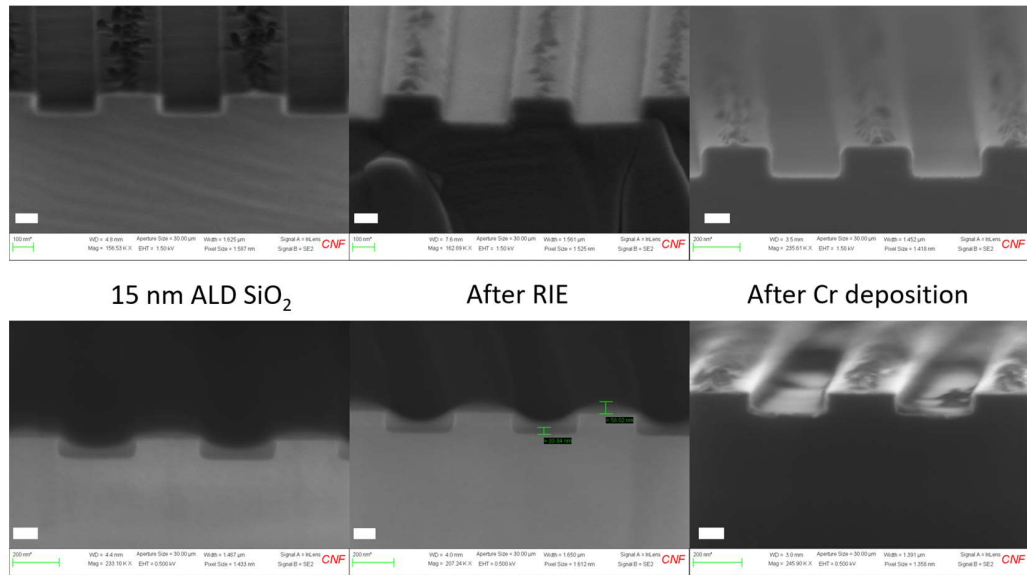


Figure 6.5. fabrication process of reflective platform on silicon. ALD: atomic layer deposition. RIE: reactive ion etching.

with hydrofluoric acid could remove undesired chromium on the sidewall and the required grating is obtained for the growth of sidewall-only polymer brushes.

The ALD formed silicon dioxide is tuned to have low density which facilitates the lift-off. The target chromium film thickness is still 5 nm for preservation of the grating original dimension. Etch rate was measured by etching ALD SiO₂ on bare Si wafer to be 0.827 nm/sec. Different SiO₂ thicknesses (5/15 nm) were used for the first test and etching with corresponding time to remove SiO₂. PDMAEMA polymer brushes were



15 nm ALD SiO₂ After RIE After Cr deposition

15 nm SiO₂/Polymer brushes 5 nm SiO₂/Polymer brushes No SiO₂/Polymer brushes

Figure 6.6 SEM pictures of the platform during the fabrication process.

Top row: Grating with 15 nm ALD SiO₂ layer / after RIE treatment/ after Cr deposition.

Bottom row: Polymer brushes grown grating with from 15 nm SiO₂ sacrificial layer/ 5 nm SiO₂ sacrificial layer/ no sacrificial layer.

Scale bar: 100 nm.

then synthesized on the grating after lift-off with 10 min HF immersion. The cross-sectional scanning electron microscope (SEM) images are shown in Figure 6.6

ALD successfully deposited SiO₂ conformally on the grating and subsequently both the top and bottom SiO₂ layers were removed by anisotropic RIE treatment. It was found out that few dirt-like materials aggregated to the top of the grating are residues of the lithographic materials. Those residues could be removed with longer RIE treatment. Unexpected results showed after synthesis of PDMAEMA brushes that the polymer brushes were grown on all surfaces of the grating. Nevertheless, the

control sample fabricated with only grating with Cr deposition showed no brushes on the top and bottom surfaces and shorter brushes on the sidewall compared to the ones with sacrificial layer. This result means that 1) the Cr on the sidewall is detrimental to the polymer brush synthesis as expected, 2) 5 nm of the Cr is enough to prevent the formation of the polymer brushes. The only problem left was, why were there brushes grown on the samples with the sacrificial layer?

Through more detailed inspection, we noticed that the residual photolithographic materials disappeared in the samples with sacrificial layers. We then suspected that the HF lift-off process also took away 5 nm Cr by penetrating through its porous structure and reached native SiO₂. This is confirmed by SEM inspection which showed that no

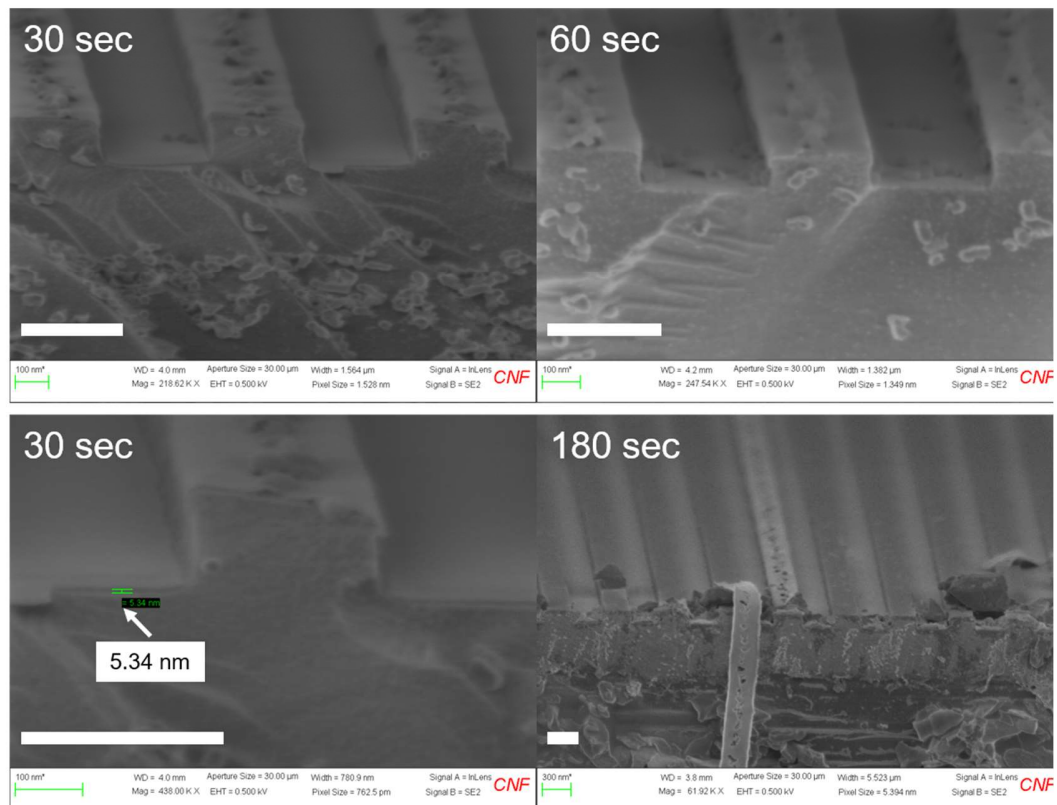


Figure 6.7. SEM images of the grating (10 nm SiO₂/ 5 nm Cr) after etching with BOE 30:1. The etch time is displayed within the figure. Scale bar: 300 nm.

photolithographic residual was on the initiator deposited grating (initiator deposited sample after HF lift-off). To solve this problem, we then use buffered oxide etch (BOE) 30:1 solution which has slower oxide etch rate compared to HF. Since the etchant needs enough time to diffuse through Cr and make etching happen, site-specific etching is possible by controlling the etch time. We then fabricated the sample with the same process but with 10 nm SiO₂ and 5 nm Cr. The SEM pictures of this grating after etching with BOE for different times are shown in Figure 6.7. Clearly, after 180 sec BOE etch, the top layer is peeled off of the grating due to the removal of the native oxide. On the other hand, the samples with 30/ 60 sec etch time preserved the photolithographic residues on the surface, which means that the etchant had not penetrated through the top Cr and into the bottom native oxide. In addition, a Cr thickness was confirmed to be 5 nm for 30 sec etched sample. Even though the Cr layer seems to recede a bit on the 60 sec etched sample, both 30 sec and 60 sec etched gratings were used to synthesize PDMAEMA brushes with the same condition and the results are shown in Figure 6.8. Both gratings showed that the PDMAEMA only anchored on the sidewall of the grating and have the maximum thickness at the bottom of the grating. This is reasonable for the fact that the confinement is no longer existing

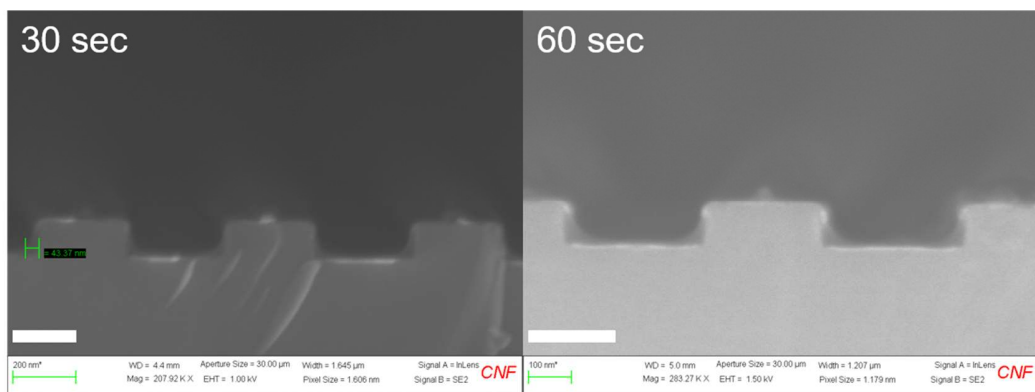


Figure 6.8. SEM images of the grating with PDMAEMA brushes grown on the gratings in Figure 6.7. Scale bar: 200 nm.

on the top of the polymer brushes which makes them like the patterned polymer brushes as studied in chapter 3. Without the lateral confinement (on the top of the grating in this case) the polymer chains feel no steric repulsion and therefore the stretching level of the polymer chains decreases from the bottom to top of the grating so as the thickness of the polymer brushes.

Further improvement had been tried by using thicker Cr (> 10 nm) which should completely prevent the penetration of the BOE into the native oxide. The result with the grating made of the same process but with 10 nm SiO₂ and 15 nm Cr is shown in Figure 6.9. Even though thicker did prevent the penetration of the BOE, it sacrifices the structure integrity by leaving the SiO₂ ‘hat’ on the top of the grating which is bad for the later scattering experiments. It was then determined that 10 nm SiO₂ and 5 nm Cr should still be used for the fabrication of the grating.

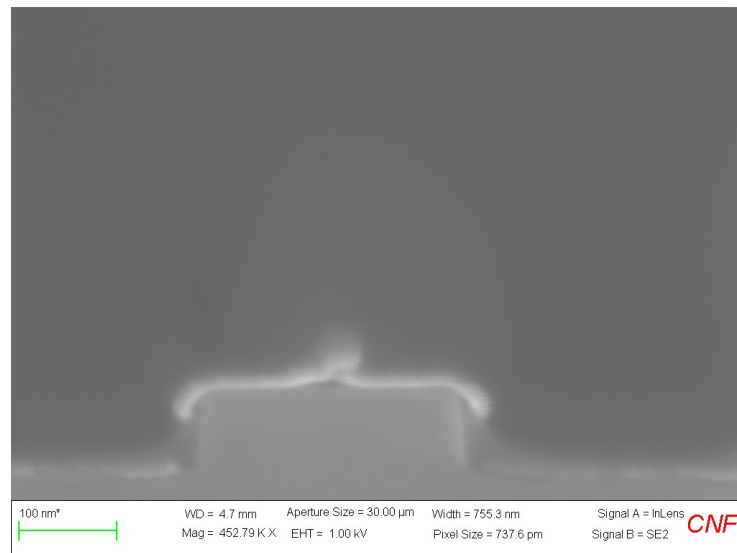


Figure 6.9. SEM images of the PDMAEMA brushes grown on grating made of 10 nm SiO₂ and 15 nm Cr

Conclusion

In conclusion, here we demonstrated the successful fabrication of both transmission and reflective grating with polymer brushes anchored on the sidewall only. These gratings would make it possible for the neutron/laser scattering characterization responding to the change of the brush in a liquid environment and reveal further details in the structure/dynamic of polymer brushes. It is then expected that not only cationic, but also anionic/zwitterionic polymer brush characterization will soon become available after the preliminary characterization which is still required to finalize the setup of the experiment instruments. The synthesis of the polymer brushes with ATRP and characterization of the grafting density has been also explored and this will help fabrication of the well characterized samples. In the future, this will be used to reveal the structure grafted molecular brushes which has more delicate 3D structures.

REFERENCES

- (1) Bandtlow, C. E.; Zimmermann, D. R. Proteoglycans in the Developing Brain: New Conceptual Insights for Old Proteins. *Physiol. Rev.* **2000**, *80* (4), 1267–1290.
- (2) Paszek, M. J.; DuFort, C. C.; Rossier, O.; Bainer, R.; Mouw, J. K.; Godula, K.; Hudak, J. E.; Lakins, J. N.; Wijekoon, A. C.; Cassereau, L.; et al. The Cancer Glycocalyx Mechanically Primes Integrin-Mediated Growth and Survival. *Nature* **2014**, *511* (7509), 319–325.
- (3) Sun, G.; Cho, S.; Clark, C.; Verkhoturov, S. V.; Eller, M. J.; Li, A.; Pavía-Jiménez, A.; Schweikert, E. A.; Thackeray, J. W.; Trefonas, P.; et al. Nanoscopic Cylindrical Dual Concentric and Lengthwise Block Brush Terpolymers as

- Covalent Preassembled High-Resolution and High-Sensitivity Negative-Tone Photoresist Materials. *J. Am. Chem. Soc.* **2013**, *135* (11), 4203–4206.
- (4) Trefonas, P.; Thackeray, J. W.; Sun, G.; Cho, S.; Clark, C.; Verkhoturov, S. V.; Eller, M. J.; Li, A.; Pavia-Sanders, A.; Schweikert, E. A.; et al. Bottom-up/Top-down, High-Resolution, High-Throughput Lithography Using Vertically Assembled Block Bottle Brush Polymers. *J. MicroNanolithography MEMS MOEMS* **2013**, *12* (4), 043006–043006.
- (5) Cho, S.; Yang, F.; Sun, G.; Eller, M. J.; Clark, C.; Schweikert, E. A.; Thackeray, J. W.; Trefonas, P.; Wooley, K. L. Directing Self-Assembly of Nanoscopic Cylindrical Diblock Brush Terpolymers into Films with Desired Spatial Orientations: Expansion of Chemical Composition Scope. *Macromol. Rapid Commun.* **2014**, *35* (4), 437–441.
- (6) Verduzco, R.; Li, X.; Pesek, S. L.; Stein, G. E. Structure, Function, Self-Assembly, and Applications of Bottlebrush Copolymers. *Chem Soc Rev* **2015**, *44* (8), 2405–2420.
- (7) Zheng, X.; Zhang, C.; Bai, L.; Liu, S.; Tan, L.; Wang, Y. Antifouling Property of Monothiol-Terminated Bottle-Brush Poly(Methylacrylic Acid)-Graft-Poly(2-Methyl-2-Oxazoline) Copolymer on Gold Surfaces. *J Mater Chem B* **2015**, *3* (9), 1921–1930.
- (8) Glinel, K.; Jonas, A. M.; Jouenne, T.; Leprince, J.; Galas, L.; Huck, W. T. S. Antibacterial and Antifouling Polymer Brushes Incorporating Antimicrobial Peptide. *Bioconjug. Chem.* **2009**, *20* (1), 71–77.

- (9) Fan, X.; Lin, L.; Messersmith, P. B. Cell Fouling Resistance of Polymer Brushes Grafted from Ti Substrates by Surface-Initiated Polymerization: Effect of Ethylene Glycol Side Chain Length. *Biomacromolecules* **2006**, *7* (8), 2443–2448.
- (10) Nagasaki, Y. Construction of a Densely Poly (Ethylene Glycol)-Chain-Tethered Surface and Its Performance. *Polym. J.* **2011**, *43* (12), 949–958.
- (11) Liu, X.; Dedinaite, A.; Rutland, M.; Thormann, E.; Visnevskij, C.; Makuska, R.; Claesson, P. M. Electrostatically Anchored Branched Brush Layers. *Langmuir* **2012**, *28* (44), 15537–15547.
- (12) Sun, G.; Cho, S.; Yang, F.; He, X.; Pavia-Sanders, A.; Clark, C.; Raymond, J. E.; Verkhoturov, S. V.; Schweikert, E. A.; Thackeray, J. W.; et al. Advanced Photoresist Technologies by Intricate Molecular Brush Architectures: Diblock Brush Terpolymer-Based Positive-Tone Photoresist Materials. *J. Polym. Sci. Part Polym. Chem.* **2015**, *53* (2), 193–199.
- (13) Trefonas, P.; Thackeray, J. W.; Sun, G.; Cho, S.; Clark, C.; Verkhoturov, S. V.; Eller, M. J.; Li, A.; Pavia-Jiménez, A.; Schweikert, E. A.; et al. Bottom-up/Top-down High Resolution, High Throughput Lithography Using Vertically Assembled Block Bottle Brush Polymers; Somervell, M. H., Ed.; 2013; p 86820H.
- (14) Yang, F.; Cho, S.; Sun, G.; Verkhoturov, S. V.; Thackeray, J. W.; Trefonas, P.; Wooley, K. L.; Schweikert, E. A. Nanodomain Analysis with Cluster-SIMS: Application to the Characterization of Macromolecular Brush Architecture: Nanodomain Analysis w/ Cluster-SIMS: Macromolecular Brush Architecture. *Surf. Interface Anal.* **2015**, *47* (11), 1051–1055.

- (15) Swann, J. M. G.; Bras, W.; Howse, J. R.; Topham, P. D.; Ryan, A. J. Quantifying Hydrogel Response Using Laser Light Scattering. *Soft Matter* **2010**, *6* (4), 743–749.
- (16) Penfold, J.; Thomas, R. K. Neutron Reflectivity and Small Angle Neutron Scattering: An Introduction and Perspective on Recent Progress. *Curr. Opin. Colloid Interface Sci.* **2014**, *19* (3), 198–206.
- (17) Zhernenkov, M.; Ashkar, R.; Feng, H.; Akintewe, O. O.; Gallant, N. D.; Toomey, R.; Ankner, J. F.; Pynn, R. Thermoresponsive PNIPAM Coatings on Nanostructured Gratings for Cell Alignment and Release. *ACS Appl. Mater. Interfaces* **2015**, *7* (22), 11857–11862.
- (18) Patil, R. R.; Turgman-Cohen, S.; Šrogl, J.; Kiserow, D.; Genzer, J. On-Demand Degrafting and the Study of Molecular Weight and Grafting Density of Poly(Methyl Methacrylate) Brushes on Flat Silica Substrates. *Langmuir* **2015**, *31* (8), 2372–2381.
- (19) Rauch, S.; Uhlmann, P.; Eichhorn, K.-J. In Situ Spectroscopic Ellipsometry of PH-Responsive Polymer Brushes on Gold Substrates. *Anal. Bioanal. Chem.* **2013**, *405* (28), 9061–9069.
- (20) Wang, T.; Long, Y.; Liu, L.; Wang, X.; Craig, V. S. J.; Zhang, G.; Liu, G. Cation-Specific Conformational Behavior of Polyelectrolyte Brushes: From Aqueous to Nonaqueous Solvent. *Langmuir* **2014**, *30* (43), 12850–12859.
- (21) Morse, A. J.; Edmondson, S.; Dupin, D.; Armes, S. P.; Zhang, Z.; Leggett, G. J.; Thompson, R. L.; Lewis, A. L. Biocompatible Polymer Brushes Grown from

Model Quartz Fibres: Synthesis, Characterisation and in Situ Determination of Frictional Coefficient. *Soft Matter* **2010**, *6* (7), 1571.

- (22) Turgman-Cohen, S.; Genzer, J. Computer Simulation of Concurrent Bulk- and Surface-Initiated Living Polymerization. *Macromolecules* **2012**, *45* (4), 2128–2137.
- (23) Kilbey II, S. M.; Ankner, J. F. Neutron Reflectivity as a Tool to Understand Polyelectrolyte Brushes. *Curr. Opin. Colloid Interface Sci.* **2012**, *17* (2), 83–89.
- (24) Johnson, R. W.; Hultqvist, A.; Bent, S. F. A Brief Review of Atomic Layer Deposition: From Fundamentals to Applications. *Mater. Today* **2014**, *17* (5), 236–246.

CHAPTER 7

Summary and Outlook

7.1 Patterned polymer brushes

Patterned polymer brushes have been described thoroughly in Chapters 3/4/5 in terms of their morphologies and their stability in patterned form. The studies on neutral polymer brushes demonstrate that the surface energy and solvent treatment could be used as a knob to control the brush morphology while the morphology of the polyelectrolyte brushes are determined in large part by their stability. With the combination of these new knobs, a new morphology fitting a particular requirement could then be designed and reveal more potential features of polymer brushes as an engineering material for functional platforms. Nevertheless, there are still other types of polymer brushes which have not been investigated in a patterned form yet. For example, weak polyelectrolyte brushes have their dissociation level affected by the condition of the medium which subsequently determines the stretching level of the chains. Zwitterionic polymer brushes have interesting swelling behavior. Due to the presence of the ion pair interactions, they swell more strongly in a salted solvent and shrink in a salt free aqueous solution which is completely different from the behavior of polyelectrolytes with a single charge. These polymer brushes could provide more complicated functionality due to the presence of these side chains. Together with the platform developed in the Chapter 6, the 3D structure of these complicated polymer brushes could be resolved, and it could provide complementary information on the lateral structure other than patterned polymer brushes. Since it is still unknown to people if the change of lateral confinement could lead to modification of the internal

*The work in 7.2 on liquid crystal elastomer was done in collaboration with David Ditter, prof. Rudolf Zentel at Johannes Gutenberg-University Mainz.

properties of these polymer brushes, further fundamental studies would be useful and help people to design more polymer brushes with complex functionality.

7.2 Extended application of CYTOP patterning process

In chapter 2, CYTOP-based orthogonal patterning processing has proven its versatility in both top-down and bottom-up approaches. This process features the use of a fluorinated polymer, CYTOP, as sacrificial layer which allows the commercial lithographic material above to preserve its performance and to be lifted-off through use of an orthogonal solvent, hydrofluoroether. By collaborating with other research groups, we have extended our patterning capabilities to enable two different applications: liquid crystal patterning as a microelectromechanical system (MEMS) and patterning of an immunobiosensor.

Liquid crystal elastomer (LCE) has been studied for years due to the unique properties benefitting from a combination of the elastomer and liquid crystals. By controlling the phase transition between a pre-aligned anisotropic (nematic/semectic) phase and an isotropic phase through designed stimuli, the shape of the LCE based object could be tuned to produce reversible actuation.¹ However, integration of the LCE into devices is still a challenge for the difficulty in preserving alignment until the end of the process, in other words, the patterning process has to maintain structural integrity.² Direct patterning by crosslinking an LCE locally with light exposure results in poor pattern formation since LCE does not have the same finely-tuned interfacial properties as photoresists.³ Although intact LCE patterns could be fabricated with direct imprint methods⁴, such methods require additional instruments/process time and material design. Patterning LCE with the orthogonal process, on the

other hand has advantages that it can both prevent damage and provide large scale production.

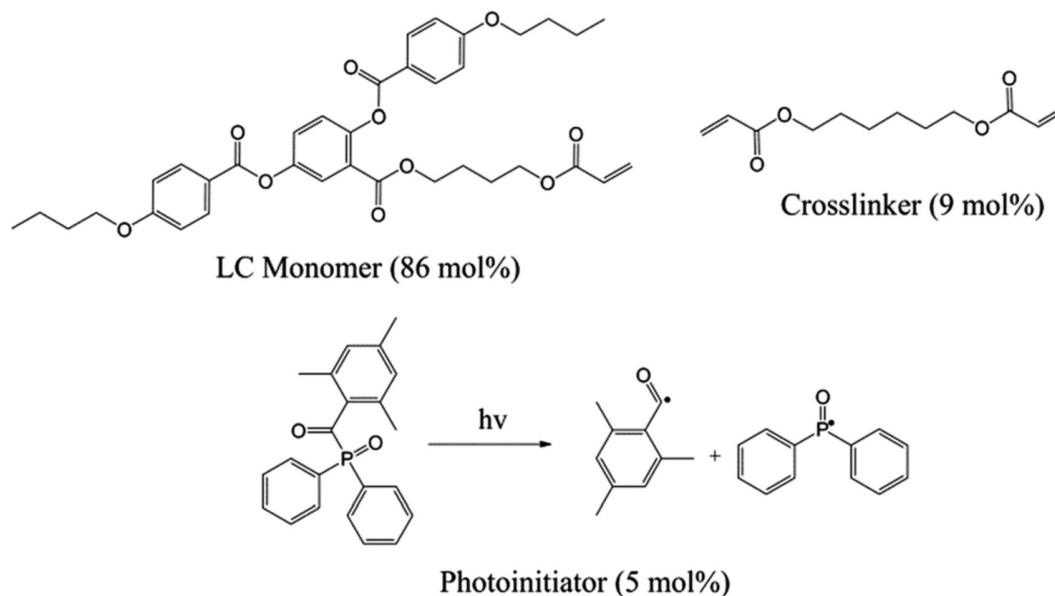


Figure 7.1 LCE formulation used as patterning subject.

The patterning target was a LCE (structure shown in Figure 7.1a) on a photoalignment layer and a hydrophilic poly(acrylic acid) (PAA) as a sacrificial layer. This specific LCE formulation was optimized by our collaborator at the University of Mainz with up to 70 % actuation reported.⁵ All materials could be spin-coated on the silicon substrate which is a standard process for its manufacture. When soaking the films into the water, PAA sacrificial layer is dissolved and LCE is then released as free film. This free film then could conduct actuation movement under thermal stimulation since the pre-aligned LCE would have a phase transition from liquid crystal to the isotropic state. The LCE has its glass transition temperature at 40 °C and a liquid crystal phase exists between 70 °C to 120 °C.

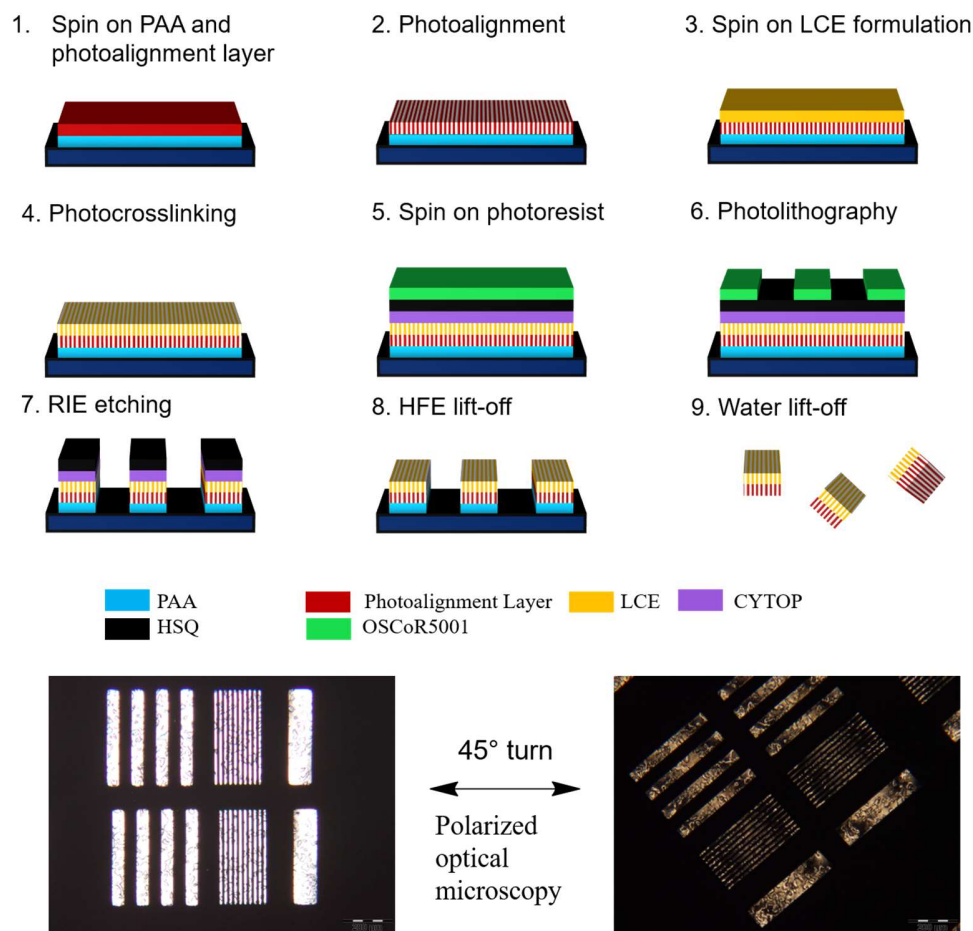


Figure 7.2 Fabrication process and result for the patterned LCE free films. RIE: reactive ion etching. (First CF_4 for HSQ and O_2 for LCE + PAA). Reproduced from ref. with permission from Royal Society of Chemistry.

Since the film contains both organic material and a water-soluble sacrificial layer, normal photoresists based on organic solvent deposition and water developer could not properly pattern the film without damage to the polymers. Fluorinated photoresists have orthogonal solubility to the film but it has limited maximum thickness ($\sim 1.3 \mu\text{m}$) and poor etch resistance. Those disadvantages make it unable to pattern thick organic materials. Previously during the development of the patterning process, it has been

found that hydrogen silsesquioxane (HSQ) could form a continuous film with only limited cracking on the CYTOP. Such a finding then allowed us to use a photoresist/HSQ/CYTOP/patterning subject multilayer combination to pattern a thick organic film $> 10 \mu\text{m}$. The fabrication process is shown in Figure 7.2 and details could be found in our published paper.⁶ The patterns still preserve the alignment as observed under a polarized light microscope that the image changes from bright to dark while rotating the sample by 45° .

Since the alignment direction defined in the photoalignment step is preserved until the end of the process, this patterning process could easily produce patterns with various actuations through simply changing the direction of the pattern relative to the alignment. As shown in Figure 7.3, upon heating, the phase transition would induce residual stress in the direction of the aligned phase (director) and the direction of the bending could be controlled. The most interesting results could be observed when the director is 45° to the direction of the pattern that the tilted bending motion leads to the formation of the helix. These programmed actuations are fully reversible and made completely with industrial nanofabrication techniques, which showed the potential of large-scale integration of LCE in MEMS devices. One can imagine more LCE based application like artificial iris⁷, muscle⁴ and cilia⁸ could be integrated together with other functional parts to reach more comprehensive functions. Although the best resolution obtained was $1.5 \mu\text{m}$ line on 3500 nm thick film with the contact aligner, with further optimization, it should be able to pattern even thicker film down to at least 500 nm line using projection photolithography. This work has been published in *Journal of Materials Chemistry C*.⁶

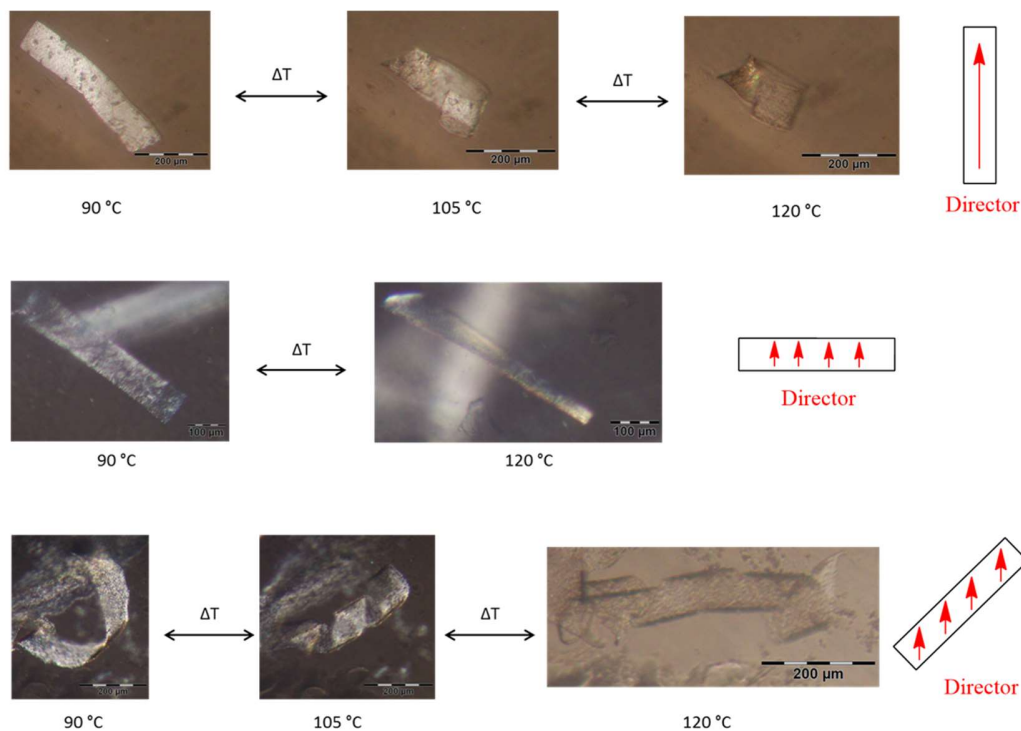


Figure 7.3 Thermal actuation motion of patterned LCE ($100 \times 500 \mu\text{m}^2$ stripe) with different director alignments. Top: head-tail bending. Middle: side bending. Bottom: helix twisting. Reproduced with permission from Royal Society of Chemistry.

On the other hand, *Welch et al.* in 2014 have developed a immunobiosensor based on patterned polymer brushes on gold which demonstrated extremely high sensitivity (2pM) for the specific antibody.⁹ This design benefited from the excellent properties of poly(oligo(ethylene glycol) methacrylate) (POEGMA) polymer brushes in terms of both preventing non-specific adsorption and anchoring functional hapten groups.¹⁰ With that in mind, we would like to improve this sensor by using colorimetric detection because the electrochemical signal in original design is not as intuitive and require electric set-up for the reading. To enable economic calorimetric design, we chose Rose

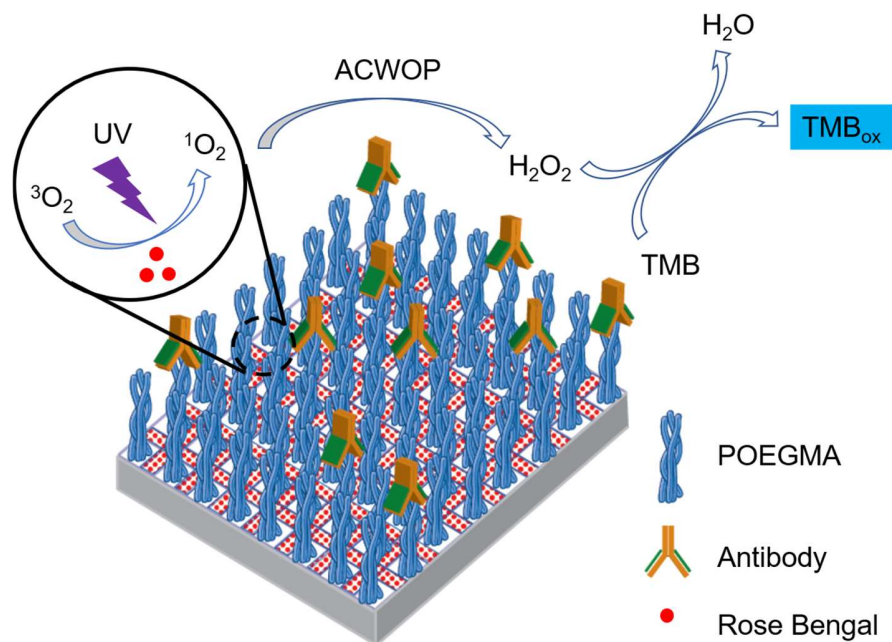


Figure 7.4. Detection mechanism for the proposed immunosensor. Under UV light exposure, singlet oxygen is formed under catalyzation of Rose Bengal. Singlet oxygen then form hydrogen peroxide through ACWOP. Hydrogen peroxide subsequently oxides TMB to its oxidized state which has blue color for colorimetric readout. TMB: 3,3',5,5' tetramethylbenzidine.

Bengal rather than $[\text{Ru}(\text{4-vinyl-4'-methyl-2,2'-bipyridine})_3]^{+2}$ as photosensitizer for its high quantum yield (0.75)¹¹, low price and ease of anchoring. The detection mechanism is based on antibody catalyzed water oxidation pathway (ACWOP)¹² which is the same as previous work in our group as shown in Figure 7.4.

The dimension requirement for the sensor is well above the micron level (150 μm line pattern) which could be easily achieved with 365 nm UV photolithography. Unlike previous work, the orthogonal resists should be suitable for such dimensions.

To have the desired patterned functional surface, it needs to have two components separately deposited on the assigned areas. The bottom-up patterning process suits this application better for the resulting structural integrity. Since we already know that the monolayer made of silane compounds is unable to completely block all the reactive sites on the silicon substrates, deposition of the second chemical species must be conducted while patterning material (like the photoresist) is still present on the surface or the mixed chemical species will show up in the pre-defined area. A diffusion problem could be prevented by either vapor deposition or liquid deposition with limited time as proven in Chapter 2. However, the test results are still discouraging for the OSCoR4000 and OSCoR5001 fluorinated photoresists. For the OSCoR4000, the solubility changes from hydrophobic to hydrophilic upon UV light exposure and it makes poor pattern formation on the hydrophilic surface due to strong adhesion. If starting with a hydrophobic surface, then the following plasma cleaning process for creating the reactive site then makes the resist layer reactive to the silane coupling agent and creates initiator deposited resist residue which could not be removed. OSCoR5001 also has similar problems, which could also be found in other commercial photoresists.

The CYTOP bottom-up patterning process like what's previously described in Chapter 2 was then applied to fabricate the functional surface. The fabrication process and results are shown in Figure 7.5. The 3-aminopropyldimethylethoxysilane (APDMES) must be deposited before polymerization since it could also react with the hydroxy group on the POEGMA polymer brushes. However, it turned out that the Rose Bengal could still adsorb on the surface with POEGMA polymer brushes even

though the amount is limited. This happened because an esterification reaction used for anchoring Rose Bengal on an amine could also anchor it on a hydroxy group.

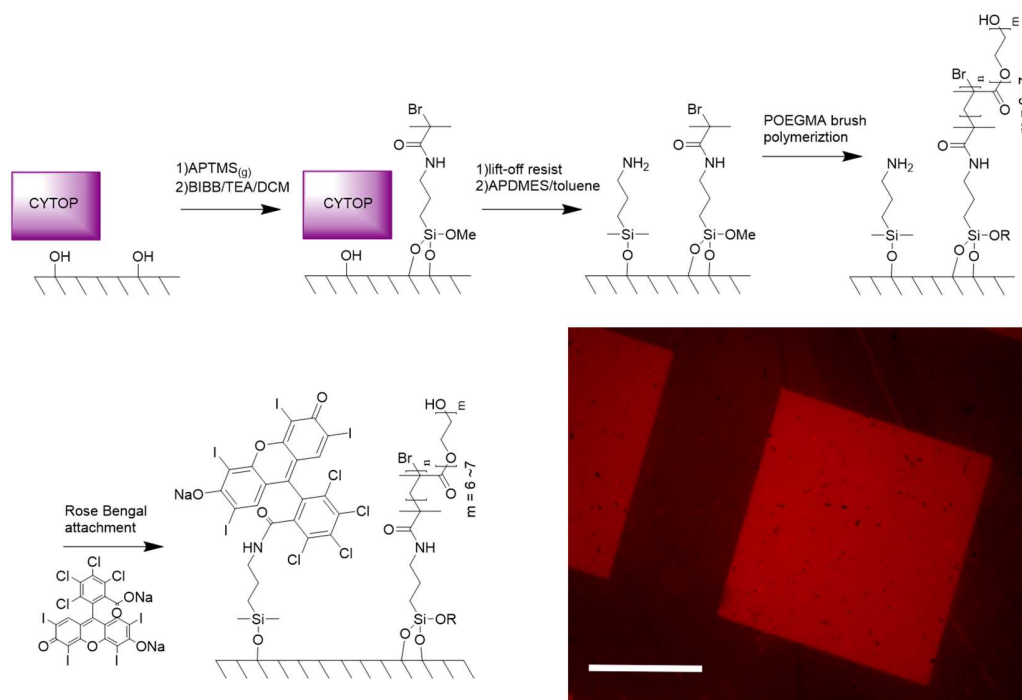


Figure 7.5. Process flow for the fabrication of the biosensor platform and the picture of the platform taken with fluorescent microscope.

To create more defined patterns, in the future other chemically orthogonal reactions should be selected to anchor the compounds on the surface. For example, 3-mercaptopropyltrimethoxysilane could be used instead of the APDMES to be the anchoring group, which could be reacted by a thiol-ene click reaction. Another problem showed up that the Rose Bengal monolayer on the surface is not enough to trigger enough signal. Such problems may be further solved by using polymer brushes on the surface to provide more surface area for the anchoring of the Rose Bengal. If the thickness of the polymer brushes is high enough, the amount of the Rose Bengal could be increased to more 100 times to the amount grafted on the surface and this

should be enough to create detectable signal. With the orthogonal anchoring chemistry for the functional groups and polymer brushes for Rose Bengal anchoring, this platform could be more applicable for fabrication and provide easy detection by colorimetric methods. In conclusion, a CYTOP patterning process could be easily extended to other fields and enable better complex platform fabrication.

7.3 Polyelectrolyte Cushions for Supported Biologically Complex Planar Cell Plasma Membranes

In this study¹³ we have demonstrated that by using a strong PEB, PMETAC, the formation of a supported lipid bilayer (SLB) could happen naturally due to the electrostatic interaction.¹³ However, the formed lipid bilayer had a fraction of membrane protein to be immobile on it. On the one hand, the cytosolic portion of the protein may be dragged/entangled by the chains of the PEB which then prevents its movement. If that's the case, there should be an optimal brush configuration that would allow SLB and protein lying on it to have the best mobility/functionality. As described in the literatures, roughness, hydrophilicity, grafting density and chain length all affect the properties of the SLB in different ways.¹⁴⁻¹⁶ It will be interesting to figure out the optimal configuration for the strong PEB before moving forward to more complicated studies.

On the other hand, it is also possible that the negative charged part of the protein was attracted on the SLB and made protein immobile. If so, the best strategy is to remove/reduce the positive charge on the PEB which could reduce the electrostatic attraction. However, since a strong positive charge is necessary for the spontaneous vesicle rupture this is not available. To solve the dilemma, we could fabricate photo-

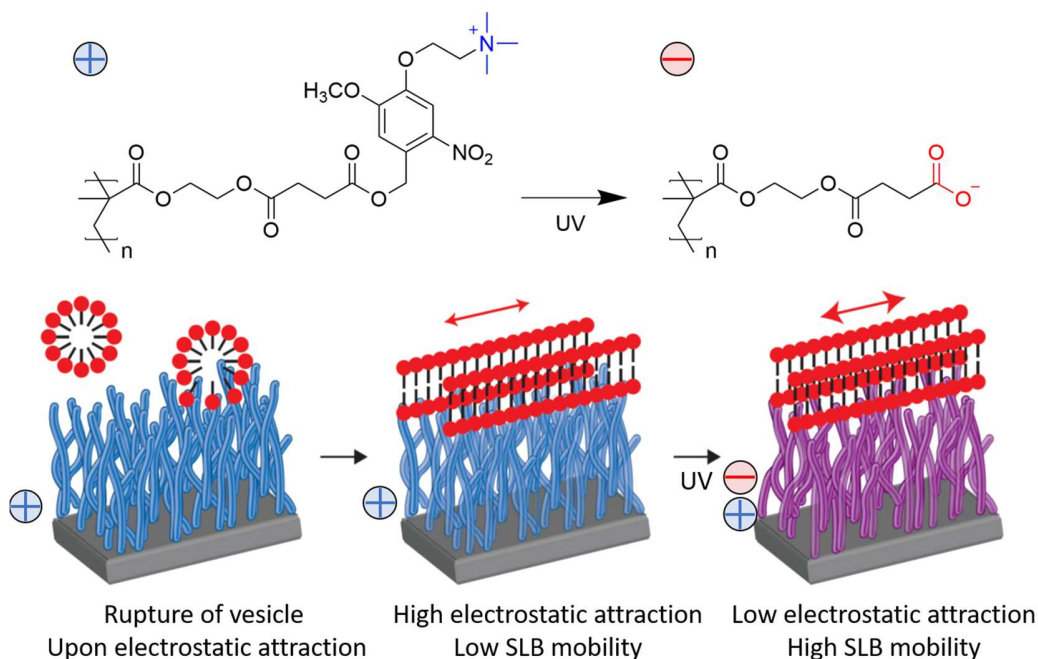


Figure 7.6. Proposed design for the photo-cleavable polymer brushes as SLB cushion. Top: chemical structures of the polymer brushes before and after photoreaction. Bottom: Schematic expression for the evolution of SLB on polymer brush cushion. With proper control of the UV exposure the resulting zwitterionic polymer brushes could be a base for high mobile SLB and membrane protein.

switchable PEBs with structures similar to previous publications in our group.¹⁷ The structure of such a PEB is shown in Figure 7.6. This special PEB with o-nitrobenzyl-containing photo-cleaving cationic unit part could transform into an anionic PEB under UV exposure. By controlling the amount of UV exposure, the ratio of the cationic/anionic groups could be properly controlled at will, which leads to the formation of zwitterionic polymer brushes. It is expected that after the spontaneous rupture induced by electrostatic attraction, subsequent UV exposure could reduce the amount of net charge in the PEB and thus decrease the dragging attraction. This effect

is significant even though the extent of hydration in the zwitterionic brushes is less than cationic/anionic PEB due to the presence of inter/intra-polymer complexes¹⁸. The diffusivity of the SLB could be at the level of $1 \mu\text{m}^2 \text{s}^{-1}$ when zwitterionic polymer brushes are used as cushion^{15,19} which is at the same level of the freely diffusing lipid bilayer.²⁰ If necessary, the UV light could also be cast from the backside with incidence above the critical angle. In such way light propagation will be in the form of an evanescent wave which is surface limited. With finely tuned control of the layer structure is also possible by forming diblock copolymer brushes with different charges on top and bottom. This platform could help to form a damage free, highly mobile lipid bilayer which is of utmost importance for the study of membrane activity.

REFERENCES

1. Ohm, C., Brehmer, M. & Zentel, R. Liquid Crystalline Elastomers as Actuators and Sensors. *Adv. Mater.* **22**, 3366–3387 (2010).
2. Sánchez-Ferrer, A., Torras, N. & Esteve, J. Integration of Liquid-Crystalline Elastomers in MEMS/MOEMS. in *Liquid Crystalline Polymers* (eds. Thakur, V. K. & Kessler, M. R.) 553–582 (Springer International Publishing, 2016). doi:10.1007/978-3-319-22894-5_19
3. Van, M.-P., Bastiaansen, C. W. M. & Broer, D. J. Polarization-Selective Patterning in an Anisotropic Smectic B Film. *Adv. Opt. Mater.* **4**, 677–681 (2016).

4. Buguin, A., Li, M.-H., Silberzan, P., Ladoux, B. & Keller, P. Micro-Actuators: When Artificial Muscles Made of Nematic Liquid Crystal Elastomers Meet Soft Lithography. *J. Am. Chem. Soc.* **128**, 1088–1089 (2006).
5. Ohm, C., Serra, C. & Zentel, R. A Continuous Flow Synthesis of Micrometer-Sized Actuators from Liquid Crystalline Elastomers. *Adv. Mater.* **21**, 4859–4862 (2009).
6. Ditter, D. *et al.* MEMS analogous micro-patterning of thermotropic nematic liquid crystalline elastomer films using a fluorinated photoresist and a hard mask process. *J. Mater. Chem. C* **5**, 12635–12644 (2017).
7. Schuhloden, S. *et al.* Iris-Like Tunable Aperture Employing Liquid-Crystal Elastomers. *Adv. Mater.* **26**, 7247–7251 (2014).
8. van Oosten, C. L., Bastiaansen, C. W. M. & Broer, D. J. Printed artificial cilia from liquid-crystal network actuators modularly driven by light. *Nat. Mater.* **8**, 677–682 (2009).
9. Welch, M. E. *et al.* Generalized Platform for Antibody Detection using the Antibody Catalyzed Water Oxidation Pathway. *J. Am. Chem. Soc.* **136**, 1879–1883 (2014).
10. Harder, P., Grunze, M., Dahint, R., Whitesides, G. M. & Laibinis, P. E. Molecular Conformation in Oligo(ethylene glycol)-Terminated Self-Assembled Monolayers on Gold and Silver Surfaces Determines Their Ability To Resist Protein Adsorption. *J. Phys. Chem. B* **102**, 426–436 (1998).
11. DeRosa, M. Photosensitized singlet oxygen and its applications. *Coord. Chem. Rev.* **233–234**, 351–371 (2002).

12. Wentworth Jr., P. Antibody Catalysis of the Oxidation of Water. *Science* **293**, 1806–1811 (2001).
13. Liu, H.-Y., Chen, W.-L., Ober, C. K. & Daniel, S. Biologically Complex Planar Cell Plasma Membranes Supported on Polyelectrolyte Cushions Enhance Transmembrane Protein Mobility and Retain Native Orientation. *Langmuir* (2017). doi:10.1021/acs.langmuir.7b02945
14. Renner, L., Pompe, T., Lemaitre, R., Drechsel, D. & Werner, C. Controlled enhancement of transmembrane enzyme activity in polymer cushioned supported bilayer membranes. *Soft Matter* **6**, 5382 (2010).
15. Santonicola, M. G., Memesa, M., Meszyńska, A., Ma, Y. & Vancso, G. J. Surface-grafted zwitterionic polymers as platforms for functional supported phospholipid membranes. *Soft Matter* **8**, 1556–1562 (2012).
16. Smith, E. A. *et al.* Lipid Bilayers on Polyacrylamide Brushes for Inclusion of Membrane Proteins. *Langmuir* **21**, 9644–9650 (2005).
17. Xu, Y., Hoshi, Y. & Ober, C. K. Photo-switchable polyelectrolyte brush for dual protein patterning. *J. Mater. Chem.* **21**, 13789 (2011).
18. Galvin, C. J., Dimitriou, M. D., Satija, S. K. & Genzer, J. Swelling of Polyelectrolyte and Poly-zwitterion Brushes by Humid Vapors. *J. Am. Chem. Soc.* **136**, 12737–12745 (2014).
19. Blakeston, A. C. *et al.* New Poly(amino acid methacrylate) Brush Supports the Formation of Well-Defined Lipid Membranes. *Langmuir* **31**, 3668–3677 (2015).
20. Jacobson, K. Lateral diffusion in membranes. *Cell Motil.* **3**, 367–373 (1983).